DISSERTATION

"EFFECTS OF PRINCIPAL STRESS ROTATION AND INTERMEDIATE PRINCIPAL STRESS CHANGES ON THE DRAINED MONOTONIC AND UNDRAINED CYCLIC BEHAVIOR OF CLEAN AND NONPLASTIC SILTY OTTAWA SANDS FORMED UNDERWATER"

Submitted by

Erdem Onur Tastan

Department of Civil and Environmental Engineering

In partial fulfillment of the requirements

For the Degree of Doctor of Philosophy

Colorado State University

Fort Collins, Colorado

Spring 2009

COLORADO STATE UNIVERSITY

January 12, 2009

WE HEREBY RECOMMEND THAT THE DISSERTATION PREPARED UNDER OUR SUPERVISION BY ERDEM ONUR TASTAN ENTITLED EFFECTS OF PRINCIPAL STRESS ROTATION AND INTERMEDIATE PRINCIPAL STRESS CHANGES ON THE DRAINED MONOTONIC AND UNDRAINED CYCLIC BEHAVIOR OF CLEAN AND NONPLASTIC SILTY OTTAWA SANDS FORMED UNDERWATER BE ACCEPTED AS FULFILLING IN PART REQUIREMENTS FOR THE DEGREE OF DOCTOR OF PHILOSOPHY.

Committee on Graduate Work

Charles D. Shackelford

Paul Heyliger

João Antonio Hool Carvalho

Advisor

Luis Garcia

Department Head/Director

ABSTRACT OF DISSERTATION

EFFECTS OF PRINCIPAL STRESS ROTATION AND INTERMEDIATE PRINCIPAL STRESS CHANGES ON THE DRAINED MONOTONIC AND UNDRAINED CYCLIC BEHAVIOR OF CLEAN AND NONPLASTIC SILTY OTTAWA SANDS FORMED UNDERWATER

A state-of-the-art dynamic hollow cylinder apparatus was used to systematically study the effect of drained changes in the major principal stress direction (α, taken from the vertical) and intermediate principal stress coefficient (b) on the (1) drained static and (2) undrained cyclic stress-strain responses, and (3) liquefaction resistance of clean and nonplastic (NP) silty Ottawa sands formed underwater. A modified slurry deposition method was developed to reconstitute HC clean and NP silty Ottawa sand specimens in a way that resembles the actual field deposition of these soils underwater. Using a new density gradient mold developed during this study, the maximum local deviations of relative density (D_R) and fines content (FC) from their global averages were determined to be as small as (or lower) than the deviations obtained for similar reconstitution methods typically used for solid triaxial specimens.

Drained increases in α and/or b at constant mean normal effective stress and octahedral deviator stress were shown to induce strains as large as those induced during anisotropic-K_0 consolidation, with the NP silty Ottawa sand typically yielding larger strains than the clean Ottawa sand at similar states.

As α increased, the sands exhibited weaker undrained cyclic responses. However, the relative effect of α on soil response appears to be less significant for Ottawa sands with NP silt content between 11 % and 15 %. Increase in b improved

the liquefaction resistance of the sands. However, when both α and b were greater than zero, their combined effect typically decreased the liquefaction resistance of the sand, suggesting that α may play a more dominant role on the undrained response of the sand than b. Undrained instability was observed in many tests carried out on anisotropically consolidated specimens subjected or not to α and/or b changes. Occurrence of undrained instability depends upon the cyclic stress ratio, α, b, D_R and FC of the soil.

The results of this study indicate that liquefaction analyses based on axisymmetric parameters may be unconservative for most types of geotechnical applications since axisymmetric conditions do not account for the effect of α on the liquefaction resistance of the soil. Appropriate evaluation of the liquefaction potential of a soil requires consideration of both α and b, although the major controlling mechanism might be associated with the mechanical response imparted by drained principal stress rotation. The results obtained in this study may be used to develop new or improve and calibrate current constitutive models that address soil anisotropy and more realistic loading conditions in geotechnical analyses. Typical applications of such advanced models include geotechnical analyses of slope stability, design of foundations, dams, embankments, pavement subgrades, and retaining structures, particularly those involving tailings, hydraulic fills, and alluvial or marine deposits of sands with fines formed underwater.

ERDEM ONUR TASTAN
Civil and Environmental Engineering
Colorado State University
Fort Collins, CO 80523
Spring 2009

ACKNOWLEDGEMENTS

I would like to first thank my advisor Antonio Carraro for his invaluable guidance, and support throughout the course of my studies at Colorado State University. I would also like to thank my PhD exam committee members, Charles D. Shackelford, Paul Heyliger and Dennis Harry, for their participation and valuable inputs in shaping this research.

This research has required a tremendous technical support from Joe Willmetti and Wykeham Farrance personnel, and I am really grateful for their help in troubleshooting.

I would also like to thank my coworkers Gabriel Iltis, Rodrigo Silveira, Jesse Dunham, Jesus Seda, Micah Smidt, Gretchen Bohnhoff and Gustavo Vienna for their encouragement and friendship. Special thanks also go to my friend Ugur Ayturk for his input and help.

Last but not the least, I would like to thank my parents and brother for their continuous support and love.

TABLE OF CONTENTS

LIST OF TABLES

LIST OF FIGURES

1. INTRODUCTION

Soil structure anisotropy is affected by (i) the mode of deposition (the geological and environmental conditions where soil deposition takes place) and the prevalent particle shapes and sizes of the soil (inherent anisotropy), and (ii) the stress history experienced by the soil after deposition (induced anisotropy) (Oda 1993).

Triaxial (TX) tests are usually employed to evaluate the mechanical response of geomaterials. However, laboratory simulation of stress paths such as the ones imposed by (1) wave loads on off-shore foundation soils (Ishihara et al. 1983, Ishihara et al.1985), (2) multi-stage constructed embankments (Hight et al.1983, Zdravkovic and Jardine 2001), (3) traffic loads on pavements (Brown and Richardson 2004), (4) earthquakes (Peacock and Seed 1968), and (5) shallow foundations on soil elements located away from the centerline of the footing require taking into account the effect of intermediate principal stress (σ_2) and major principal stress direction (α) with respect to the vertical. The effect of σ_2 is usually taken into account through the intermediate principal stress coefficient

$$b = \frac{\sigma_2 - \sigma_3}{\sigma_1 - \sigma_3} \tag{1.1}$$

where σ_1 and σ_3 are the major and minor principal stresses, respectively.

Laboratory simulation of the five aforementioned loading conditions requires appropriate testing apparatuses and procedures that allow independent control of b

and α. The widely-used TX apparatus is inherently limited to simulation of stress states with b equal to either 0 or 1 and α equal to either 0° or 90°. Thus, TX testing is not a convenient protocol to impose b between 0 and 1 and α between 0° and 90°. Extensive research has been conducted to design more versatile testing equipment such as the directional shear cell, simple shear, true TX and hollow cylinder (HC) apparatuses so that any b between 0 and 1 and any α between 0 and 90° can be applied to soil elements (Arthur et al. 1980, Hight et al. 1983, Saada 1988, O'Kelly and Naughton 2005). The specific details associated with each one of the testing protocols cited above are discussed by Sayao and Vaid (1989), who concluded that HC testing is the most versatile protocol to study anisotropic soil behavior. In HC testing, fluid pressures both inside (p_i) and outside (p_o) the HC specimen cavity are applied in addition to axial (W) and torsional (T) boundary loads. As a result, a completely generalized stress state, with $0 < b < 1$ and $0° < \alpha < 90°$ can be imposed within the HC specimen wall.

The objective of this research is to evaluate the undrained cyclic behavior of sands with and without small amounts of NP silt under generalized stress conditions using a modern HC testing apparatus. As part of the study, a slurry deposition (SD) technique was developed for the preparation of HC specimens of sands with or without fines that (1) produces uniform, saturated specimens, (2) eliminates segregation, and (3) replicates the fabric and stress-strain response of sand deposits formed underwater.

The goals of this study include:

1) To investigate systematically the effect of α and b on the undrained cyclic behavior and drained response of SD specimens of Ottawa sands with and without nonplastic (NP) silt.
2) To discuss the impact of generalized stress conditions on the cyclic response of sandy soils under a foundation element.

1.1 SCOPE

This study aims to shed light on the undrained cyclic anisotropic behavior of clean sands and sands with about 15 % of NP silt. An appropriate specimen preparation method was developed to simulate the inherent anisotropy of these materials when deposited under water. The stress conditions studied included α = 0, 30, 60° and b = 0, 0.5, 0.8. The study characterizes the behavior of clean sands and sands NP silt by systematically varying the stress conditions discussed above. Even though this approach may not directly relate to some common geotechnical applications, the results are invaluable to systematically determine the effect of α, b, and fines content on the behavior of sands formed under water.

1.2 MANUSCRIPT ORGANIZATION

This manuscript has five chapters in addition to the Introduction. In Chapter 2, a detailed background on soil anisotropy, testing and specimen preparation methods available, and liquefaction phenomenon based on a comprehensive literature is provided. Other similar studies, their methodologies and shortcomings are also discussed in Chapter 2. Chapter 3 includes the description of the state-of-the-art HC apparatus and materials used, and details of the HC specimen preparation and testing protocol developed during the research. Considering the issues with the commonly used soil testing and specimen preparation methods mentioned in Chapter 2, Chapter 3 describes the unique approach used in this study to address the inherent and induced anisotropy of sandy soils when tested under cyclic loads. In Chapter 4, the results of the study are presented for both clean sands and sands with NP silt. Chapter 4 also includes the comparison of the results of this study with other studies whenever appropriate. In Chapter 5, the conclusions of this study along with the practical implications are discussed. Chapter 6 summarizes the contents of this study and proposes topics for further research to expand the database generated in this study.

2. LITERATURE REVIEW

2.1 SOIL ANISOTROPY

Soils are anisotropic materials. Environmental and geological conditions during the deposition of the soils, along with the particle shapes, sizes, and void structure are some factors constituting the natural anisotropy of the soil. The fabric of the soil may later be disturbed (further anisotropy) with application of loads and, thus, plastic strains. Casagrande and Carillo (1944) first distinguished these two sources of anisotropy as inherent and induced anisotropies. Inherent anisotropy is impacted by the particle shapes and depositional conditions and is independent from strains. Induced anisotropy is the reconfiguration of the soil fabric to withstand the applied loads.

Oda (1972a) assessed the initial fabric (inherent anisotropy) of sands and its effect to the mechanical behavior. He used four different sands with different roundness. The specimens were prepared using two specimen preparation methods, tapping method (tapping the side of the mold) and plunging method (plunge the hand hammer on the sand in the mold). Then, he solidified the specimens using the polyester resin, and sliced at different planes. For elongated particles, tapping method caused the particles on the vertical plane to have their longer axes align with the horizontal, while on the horizontal axis, the particles were more randomly oriented. For the spherical grains, no preferred orientation was observed at any plane. Plunging method oriented the longer axes of non-spherical particles in the vertical direction on the vertical plane. Then, he concluded that the orientation depended on the particle shape and the method of compaction. The nature of the contacts developed between the sand grains also impacts the initial fabric of the specimen. Oda (1985) elaborated on the nature of particle contacts and defined S_Z / S_X to quantitatively describe the distribution of particle contact normals, where S_Z, S_x were projected contact areas on z (vertical), and x (horizontal) planes, respectively. The larger S_Z / S_X ratio indicated larger mobilized strength and dilatancy rate. Wong and Arthur (1985) studied the inherent and induced anisotropy of sand, and concluded that even at appreciable strains, the inherent anisotropy of the sand could survive. However, according to Oda et al. (1985), after post peak was reached, the contacts between the particles and structure of the voids could radically change which would destroy the inherent anisotropy. Nevertheless, the inherent anisotropy of soils influences their mechanical behavior no matter if the inherent anisotropy survives during plastic strains or not.

When a load is applied to a soil deposit, the initial fabric (inherently anisotropic or not) resists the load initially. However, as the load increases, deformation takes place and soil grains roll and slide over one another. During this process, the nature of contact normals and the void structure of the soil change. Oda et al (1985) studied these changes, and concluded that further anisotropy was induced in the soil structure to resist the loads applied. They mentioned that the particle contact normals aligned themselves parallel to the direction of the larger principal stress, and, in a way, formed load resisting columns. According to them, at the same time, the voids between the grains also interconnected and formed columns that were also parallel to the major principal stress (induced anisotropy). As the peak stress was achieved, these void and contact normal columns started breaking down and the soil fabric was altered. They also mentioned that if the principal stresses acted in a direction different than vertical, these aforementioned columns still tended to align with the principal stresses.

In summary, the anisotropies associated with soils, inherent and induced anisotropy, are influenced by the particle shape, depositional conditions and the nature of the applied loads.

2.2 EFFECT OF PRINCIPAL STRESS ROTATION AND INTERMEDIATE PRINCIPAL STRESS ON THE CYCLIC BEHAVIOR OF SANDY SOILS

Many researchers have used the HC apparatus to investigate the cyclic behavior of sandy soils. However, the boundary conditions in these studies varied greatly, and the primary focus was on regenerating simple shear conditions rather than systematically investigating the effect of principal stress rotation and intermediate principal stress on the cyclic behavior of sands. In this section, a brief summary of these studies are given along with the effect of principal stress rotation or intermediate principal stress on the cyclic resistance of sandy soils.

Ishibashi and Sherif (1974) used torsional simple shear testing apparatus, where they tested "donut-like" sand specimens subjected to cyclically varying torque loads. During shearing, the specimen was laterally confined by keeping the outer cell pressure chamber sealed. With these stress conditions, they claimed to reproduce the simple shear conditions that take place under level ground deposits during an earthquake. Principal stress rotation was limited to a jump rotation between -45° and +45° and the effect of b was not considered.

Tatsuoka et al. (1986) designed a torsional hollow cylinder testing apparatus that could cyclically shear the specimens under undrained simple shear conditions by preventing any axial strain development and inner cell volume change. These boundary conditions eliminated changes in the inner and outer radii during shearing. They reported that the direction of the major principal strain increment discontinuously varies between -45° and +45° to the vertical. However, they also mentioned that, at large strains, the strain increments were almost plastic and the principal stress direction tended to coincide with the directions of the principal strain increments. In other words, the major principal stress direction was also close to 45°. The effect of continuous principal stress rotation was observed only at small strains below 0.2 %. Above this strain level, the effect of continuous principal stress rotation was negligible. Although they indicated that principal stress rotation was done in a continuous manner, their results suggested that the principal stresses were rotated from +45° to -45° rather abruptly. They also did not report on variations of b during cyclic shearing.

Koester (1992) investigated the liquefaction of resistance of alluvial soils including sands with fines, by using cyclic triaxial and cyclic torsional simple shear tests. He also did not evaluate the effect of α or b on the liquefaction resistance of the sandy soils tested.

Yamashita and Toki (1993) conducted undrained cyclic TX and torsional HC tests on sand specimens prepared by multiple sieving pluviation method, vibration method and centrifugal force method. In their cyclic torsional HC tests, the vertical loading ram was fixed and only the torque was cyclically applied. The major principal stress rotation was not varied in a controlled manner and was somewhere between 0° or 90° from the vertical. They found that the cyclic strengths obtained from cyclic TX tests and torsional HC tests were not equal and the difference may be more pronounced depending on the sample preparation technique.

Chaudhary et al. (2002) studied the effect of major principal rotation on the response of sands (anisotropy) under cyclic loading. Specimens were reconstituted using air pluviation, water pluviation and dry rodding. They consolidated the specimens isotropically to $p' = 98.1$ kPa and sheared under drained conditions with constant $p' = 98.1$ kPa and $b = 0.5$ at major principal directions of 0° (90°), 22.5° (-67.5°), and 45° (-45°) from the vertical. The major principal stress direction was reversed to the value given in parentheses after each half cycle. Anisotropy was observed in the stress-strain response of air pluviated and water pluviated specimens. Dry rodding erased the anisotropy of the soil fabric. The shear modulus and the damping ratio response of sand were independent of the major principal stress rotation during cyclic loading.

Drnevich (1972) combined the resonant column torsional shear testing with quasi-static (or cyclic) testing in his apparatus. Therefore, he could measure shear strains in the range of 0.001 % to 0.1 %. He applied torsional vibration to the top of the specimen through an electromagnetic torsional oscillator to monitor the cyclic shear behavior of sands at very low strain rates. For some tests, he combined this torsional vibration with the application of quasi-static cyclic shearing at the frequency of 0.1 Hz. The principal stress rotation in these tests was a jump rotation between -45° and

+45°, and he did not investigate the effect of either α or b on the cyclic behavior of sands.

Towhata and Ishihara (1985) used a HC testing apparatus to investigate the effect of continuous principal stress rotation on the undrained behavior of sands. They adapted the stress paths given in Fig. 2.1 and concluded that, even under constant deviator stress, continuous principal stress rotation results in large pore pressure development. They also concluded that the liquefaction resistance of sand that has undergone continuous principal stress rotation between -45° and +45° was lower than the liquefaction resistance of sand subjected to typical cyclic torsional shear test where the principal stresses do not rotate continuously but instead rotate abruptly between -45° and +45°. The drawback in their study was that α and b were correlated due to having equal inner and outer cell pressures. This resulted in a combined effect of α and b.

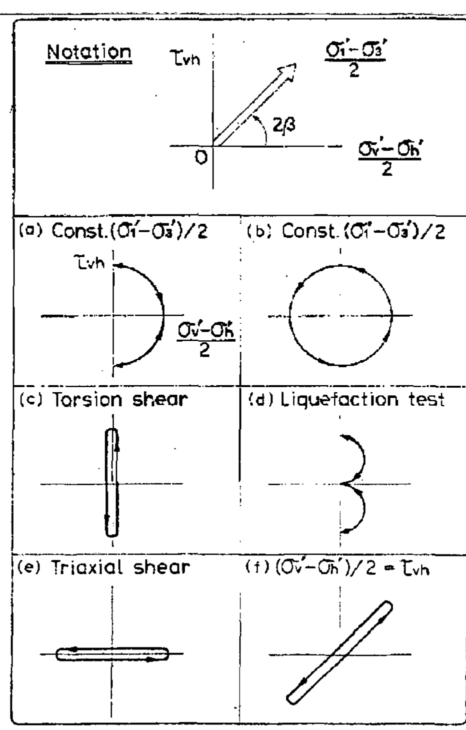

Figure 2.1. Stress paths followed by Towhata and Ishihara (1985). $\beta = \alpha$

Altun et al. (2005) used a cyclic torsional simple shear apparatus similar to the one used by Towhata and Ishihara (1985). They investigated the cyclic undrained behavior of sandy, and silty soils. Their testing program did not include investigation of the effect of neither α and b on the cyclic behavior of sandy or silty soils.

Shibuya et al. (2003) investigated the effect of α and b on the monotonic and cyclic behavior of sands. Specimens were reconstituted using wet pluviation and consolidated isotropically to $p' = 200$ kPa. They adapted stress paths in which α and b were cycled at constant $(\sigma_1 - \sigma_3) / 2$. The effects of α and b are separated by means of the stress paths given in Fig. 2.2.

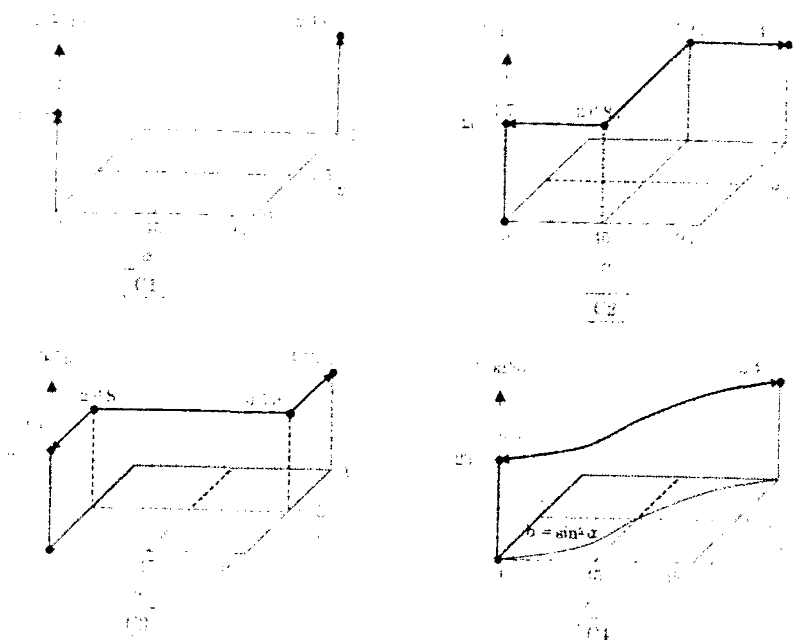

Figure 2.2. Stress paths followed by Shibuya et al. 2003

The pore pressure response of the sand subjected to these stress paths showed that large pore pressures are generated due to continuous principal stress rotation at constant $(\sigma_1 - \sigma_3) / 2$. Changes in b also caused changes in excess pore pressures, but the changes were not as significant as the ones created by the continuous principal stress rotation. They also observed that wet pluviated sand specimens may experience strains and generate excess pore pressure due to changes in α and b even at constant $(\sigma_1 - \sigma_3) / 2$. Partial liquefaction occurred after five cycles of stress paths shown in Fig. 2.2.

Most of the undrained cyclic shear tests conducted on HC specimens as given above involved principal stress rotations between -45° and +45°. Additionally, the rotation was not continuous but rather an instantaneous (or jump) rotation was imposed between -45° and +45°. Ishihara and his coworkers partially overcame this limitation by continuously rotating the principal stress directions. Except for Shibuya et al. (2003), none of the researchers mentioned above investigated the effect of intermediate principal stress on the cyclic behavior of sandy soils. In summary, there is a lack of systematic research on the effect of principal stress rotation and intermediate principal stress on the cyclic behavior of sandy soils.

2.3 HOLLOW CYLINDER TESTING

As discussed earlier, soil structure anisotropy is affected by the mode of deposition and the prevalent particle shapes and sizes of the soil (inherent anisotropy), and by the stress history experienced by the soil after deposition (induced anisotropy) (Oda 1993).

Induced anisotropy may develop following soil deposition due to applied loads such as (1) cyclic loads imposed by earthquakes, traffic, and sea waves (Ishihara et al 1983; Ishihara et al. 1984; Ishihara et al. 1985; Miura et al. 1986), or (2) incremental static loads under embankments, building foundations, dams, etc. Therefore, the nature of the applied stress history also impacts soil behavior. The stress tensor $\tilde{\sigma}$ for a soil element under any structure or any loading condition has six independent components (tensor symmetry). The components of $\tilde{\sigma}$ in polar coordinates (z, r, and θ in Fig. 2.3a) can be expressed as follows:

$$\tilde{\sigma} = \begin{bmatrix} \sigma_{zz} & \sigma_{zr} & \sigma_{z\theta} \\ \sigma_{rz} & \sigma_{rr} & \sigma_{r\theta} \\ \sigma_{\theta z} & \sigma_{\theta r} & \sigma_{\theta\theta} \end{bmatrix}$$

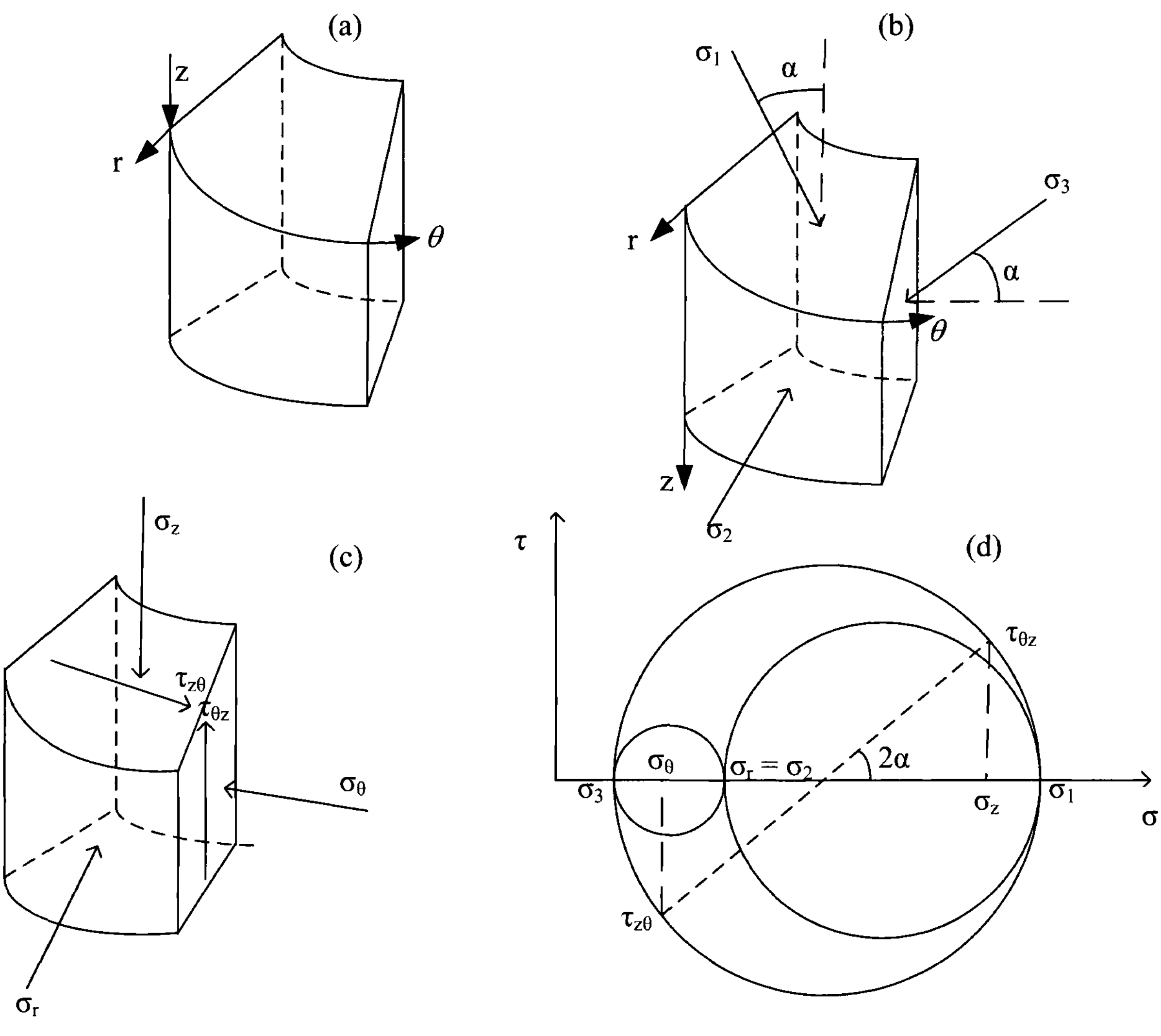

Figure 2.3 Description of stress state: (a) polar coordinates, (b) principal stresses, (c) three normal and one shear stress configuration, (d) Mohr circle for the configuration in (c).

$\tilde{\sigma}$ also can be expressed in terms of principal stresses along the principal directions 1-2-3.

$$\tilde{\sigma} = \begin{bmatrix} \sigma_1 & 0 & 0 \\ 0 & \sigma_2 & 0 \\ 0 & 0 & \sigma_3 \end{bmatrix}$$

$\tilde{\sigma}$ has three independent principal stress components. However, the principal stress directions, 1, 2, and 3 may not necessarily be aligned with the z, r, and θ directions. Thus, the exact representation of a stress tensor requires defining both the directions and magnitudes of the three principal stresses. The exact analysis would require obtaining angles α (angle between 1-z), β (angle between 2-r), and γ (angle between 3-θ). However, the common approach in HC testing is to assume that the intermediate principal stress does not rotate while σ_1 and σ_3 rotate through the same angle, generally referred as α, from the vertical and horizontal directions (Fig. 2.3b), i.e., there are shear stresses and normal stresses on two planes and only a normal stress on the third plane (Fig. 2.3c). The Mohr's circle representation of this stress state is given in Fig. 2.3d. Some practical examples of this stress state in the field include the stress conditions imposed by (1) wave loads on the foundation soils of off-shore structures (Ishihara et al. 1983, Ishihara et al.1985), (2) loads on soil elements under multi-stage constructed embankments (Zdravkovic and Jardine 2001), (3) rolling wheel loads on pavements (Brown and Richardson 2004), and (4) earthquake loads (Peacock and Seed 1968). The effect of σ_2 is usually taken into account by the intermediate principal stress ratio:

$$b = \frac{\sigma_2 - \sigma_3}{\sigma_1 - \sigma_3} \tag{2.1}$$

The widely used TX testing protocol can be conveniently used only for $b = 0$ and 1 or $\alpha = 0°$ and 90°. Therefore, the TX testing is not convenient for b between 0 and 1 and α between 0° and 90°. In an effort to simulate realistic field stress conditions that incorporate ranges of b between 0 and 1 and α between 0° and 90°, different laboratory equipment such as true TX, simple shear, directional shear cell, and HC (also referred to as torsional shear) were developed (Arthur et al. 1980, Hight et al. 1983, Saada 1988, Kelly and Naughton 2005). Brief descriptions of these methods are given below.

<u>True Triaxial Testing:</u>

The true TX test (TTT) involves application of three separate normal stresses on the six faces of a cubical specimen, and it allows independent variation of each principal stress magnitude and, thus, b. TTT does not allow rotation of principal stresses.

<u>Simple Shear Testing:</u>

The simple shear test (SST) was originally designed to shear specimens under plane strain conditions. The SST also allows principal stress rotations between 0° and 90°. However, there are limitations as to how much principal stress rotation can be simulated. The most widely used SST apparatuses are the Cambridge type (originally developed by Roscoe 1953) and the model developed by the Norwegian Geotechnical Institute (NGI) (originally developed by Bjerrum and Landva 1966). Both test methods involve placing the specimen between two horizontal platens and moving one platen relative to another creating simple shear conditions (Fig. 2.4). The NGI apparatus (Fig. 2.4a) uses cylindrical specimens, while the Cambridge apparatus (Fig. 2.4b) requires cubical specimens.

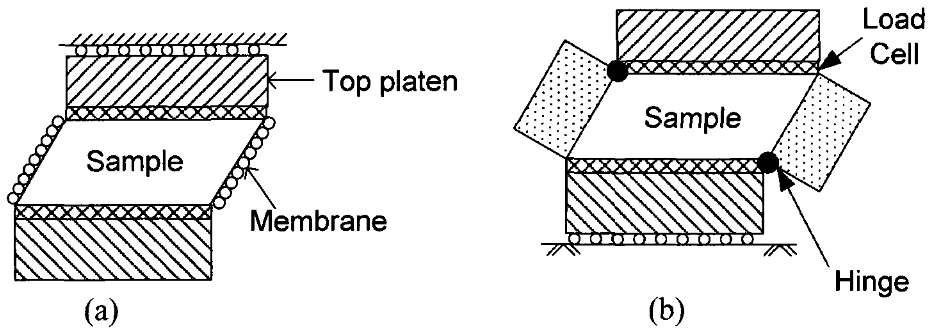

Figure 2.4. Simple shear test: (a) NGI type, (b) Cambridge type (Budhu 1988).

The NGI apparatus does not have vertical walls on the two sides of the specimen, unlike the Cambridge apparatus, which has hinged walls on the side of the specimen. The basic measurements taken during these tests are the average vertical and horizontal stresses and the displacements in the vertical and horizontal planes. The lateral stress can be measured in the NGI apparatus if a strain gage is installed on the reinforcement mesh attached to the membrane on the vertical wall of the specimen. However, Budhu (1988) claimed that these measured stresses were neither equal to the radial stresses nor to σ_2, which made it impossible to determine the stress tensor. Boulanger (1995) added that the measurement of an average lateral stress could only qualitatively replicate the ideal stress conditions. Furthermore, the NGI apparatus lacks the complementary shear stress component on the vertical walls of the specimen, and this causes significant stress and strain nonuniformities (Bhatia et al. 1985, Budhu and Britto 1987, Boulanger et al. 1995). In the Cambridge apparatus, the specimen is forced to deform more uniformly due to the platens on the vertical walls of the specimen. However, the lack of complementary shear stress still persists (Bhatia et al. 1985). Nonuniform slippage, difficulty in measuring K_o and variations in the octahedral stress are other problems associated with both types of simple shear test apparatuses (Prevost and Hoeg 1976).

The SST has the advantage of simulating principal stress rotation unlike the axisymmetric and true TX tests. However, the extent of the principal stress rotation is limited. Arthur et al. (1980) mentioned that there are zero extension lines in simple shear testing and for any dilatancy angle (ψ), having fixed zero extension lines implies fixing the major principal strain rate direction and, thus, the major principal stress direction. He defined the possible major principal stress rotation as ($\pi/4-\Delta\psi/2$). For sands, the change in the dilatancy angle is about -10 to 30 degrees even for small strains (1-2 %). According to this, the major principal stress rotation can be between 30 and 50°. Similarly, Budhu (1988) showed that principal stress rotation for shear strains up to 5% can range between 23° and 40° and between 33° to 41° for shear strains larger than 5 %.

Since the SST is designed to generate plane strain conditions, a fixed value of b must be used during the test.

<u>Directional Shear Testing:</u>

In the directional shear cell, controlled changes in principal stress directions are applied under plane strain conditions (Fig. 2.5). Shear stresses and normal stresses are applied on four sides of the cubical specimen through layers of rubber (Arthur et al. 1977). Due to the elastic deformation nature of rubber up to strains as high as 300%, Arthur et al. (1977) claimed that the shear stress distribution on the side of the specimen is generally uniform even if the initial cubical geometry changes as the sample strains.

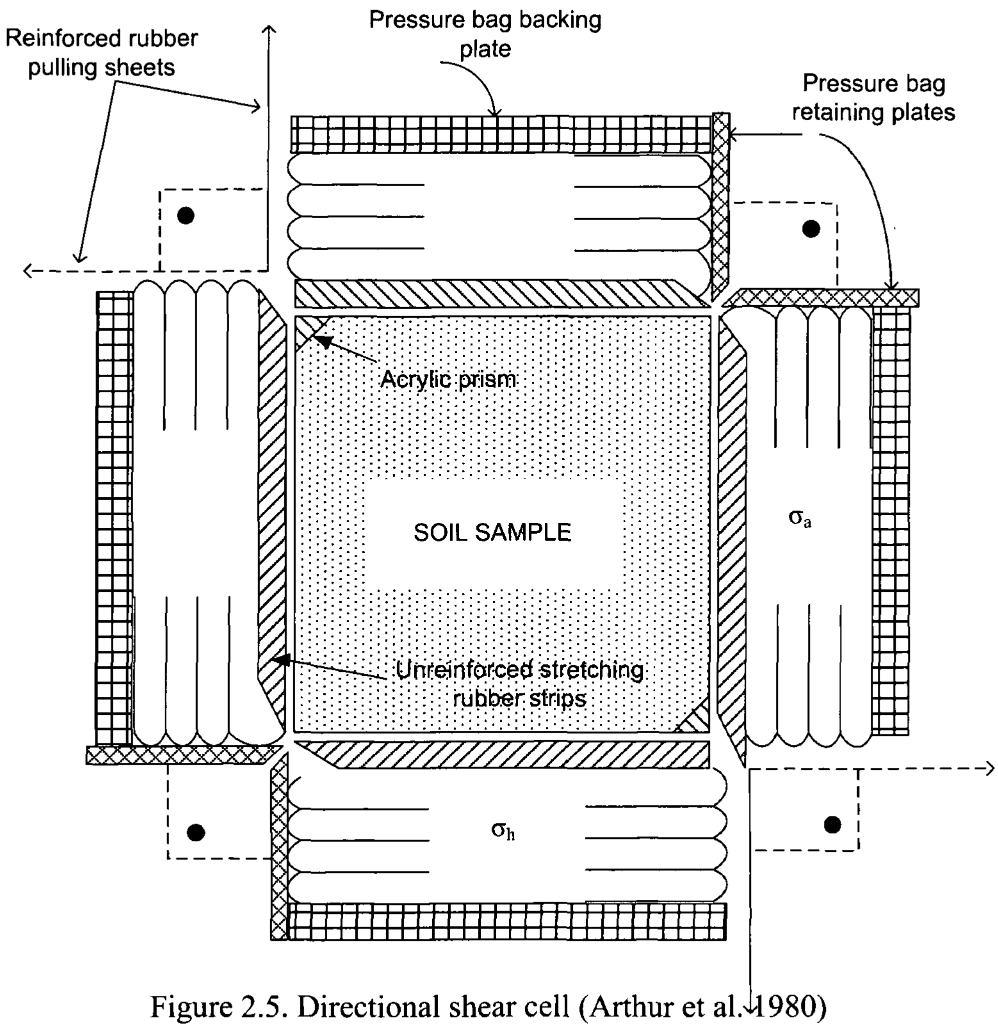

Figure 2.5. Directional shear cell (Arthur et al. 1980)

Due to the stress conditions imposed by the apparatus, principal stresses can be rotated freely (Arthur et al. 1977, Arthur et al. 1980, Sture et al. 1987). The major limitations of the apparatus are: (1) saturated material can not be tested, (2) operator error might be involved in setting up of the apparatus, (3) relatively small shear stresses can be applied between 50 kPa and 90 kPa (Arthur et al. 1980, Sture et al. 1987), and (4) *b* can not be changed.

Hollow Cylinder Testing:

Another way to experimentally evaluate the anisotropic behavior of soils consists of applying a combination of axial and torsional stresses to HC soil specimens. In addition to the axial and torsional stresses, fluid pressures inside the hollow cavity and outside the specimen are typically applied so that a completely generalized stress state can be imposed on soil elements within the wall of hollow specimens. In HC testing, (1) any combination of α and b parameter can be imposed (Fig. 2.6), thus allowing the stress and strain tensors to be determined, and (2) the pore pressure can be measured at any stage (i.e., undrained or drained conditions can be used). Typical values of α and b for simple boundary conditions such as those imposed in simple shear, directional shear cell, TX compression, and TX extension are presented in Fig. 2.6 which also shows possible stress paths for varying α and b and some other testing methods available in the literature. Considering all these advantages, HC testing offers significantly more versatility than other conventional testing equipment (Saada 1988, Sayao and Vaid 1989). A chronological list of early studies on HC testing is provided in Table 2.1.

The simultaneous application of vertical (i.e. axial) and horizontal (i.e. radial and circumferential) normal stresses as well as torsional shear stresses on horizontal planes brings about complicated stress and strain distributions in HC specimens (if compared to stress-strain distributions in conventional solid TX specimens). The uniformity of the stress and strain distributions in HC specimens is discussed later in Section 2.4.

Table 2.1.Researchers who worked with hollow cylinder (HC) specimens (expanded from Koester 1992)

#	Reference	Year	Specimen Dimensions (mm) H	R_0	R_i	Soil Type	Control Restrictions	Applications	Specimen Preparation Method	Uniformity Check
1	Cooling and Smith	1936	19-38	50.8	41.3	Clay	$F_z = P_o = P_i = 0$	Undrained shear strength	Kneading - remoulded specimens	NO
2	Norton	1938	50.8	11.1	7.9	Clay	$F_z = P_o = P_i = 0$	Torsional deformability of ceramic clays	No info	NO
3	Geuze and Kie	1953	80	19	13	Clay	$F_z = P_o = P_i = 0$	Undrained creep	Kneading - remoulded specimens	NO
4	Kirkpatrick	1957	152.4	50.8	31.8	Sand	$F_z = T_h = 0$	σ_2 effect on failure condition	No info	NO
5	Haythornthwaite	1960	?	?	?	Silt	$P_o = P_i$	σ_2 effect on failure condition	Tamping in 3 layers followed by hydrostatic pressure application	NO
6	Whitman and Luscher	1962	76/127	25/19	12.7	Sand	$T_h = 0; \varepsilon_z = 0$	Soil-structure interaction at failure	No info	NO
7	Wu et al.	1963	127	50.8	38.1	Clay and Sand	$T_h = 0$	σ_2 effect on failure condition	No info	NO
8	Broms and Ratnam	1963	114.3	76.2	38.1	Clay	$T_h = 0$	3-D consolidation effects on strength	Compaction	In terms of water content
9	Broms and Casbarian	1965	254	63.5	38.1	Clay	----	σ_2 and α effects on strength	Compaction	NO
10	Broms and Jamal	1965	304.8	76.2	38.1	Sand	$T_h = 0$	Validity of $\sigma_r = \sigma_\theta$	Low Dr - WP + rodding High Dr - WP + vibration	NO
11	Esrig and Bemben	1965	203.2	50.8	38.1	Sand	$T_h = 0$	σ_2 and ε_2 effects on strength	WP	NO
12	Suklje and Drnovsek	1965	80	32	20	Clay	$T_h = 0; \sigma_z = 0$	Deformability under plane stress	No info	NO
14	Saada and Baah	1967	151.1	35.1	25.4	Clay	$P_o = P_i$	Influence of anisotropy	One-dimensional slurry consolidation	NO
16	Lomise et al.	1969	180	155	125	Clay	$P_o = P_i$	Drained creep under 3-D stress state	No info	NO
17	Jamal	1970	203	51	12.5-38	Sand	$P_o = P_i$	Extension behavior of solid and hollow cylinder specimens	WP + Tamping	NO
18	Barden and Proctor	1971	152.4	50.8	19.1	Sand	$T_h = 0$	Drained shear strength of granular material	No info	NO
19	Bishop et al.	1971	19.1	76.2	50.8	Clay	$\varepsilon_2 = 0$	Residual strength in ring shear torsion	Kneading - remoulded specimens Coring&trimming-undisturbed specimens	NO
20	Frydman et al.	1971	203.2	50.8	25.4	Sand	$T_h = 0$	End restraint; membrane penetration	Low Dr- AP High Dr - WP	NO
21	Drnevich	1972	100	25	20	Sand	$P_o = P_i$	Torsional resonant column test	Low Dr - WP High Dr - AP	NO
22	Arnold and Mitchell	1973	142	76	51	Sand	$T_h = 0$	3-D stress effect on strength	AP + Tamping	NO

Table 2.1. Researchers who worked with hollow cylin der (HC) specimens (expanded from Koester 1992) Contd.

#	Reference	Year	Specimen Dimensions (mm)			Soil Type	Control Restrictions	Applications	Specimen Preparation Method	Uniformity Check
			H	R_0	R_i					
23	Ishibashi and Sherif	1974	13 to 25	50.8	25.4	Sand	$P_o = P_i$	Liquefaction characteristics	WP	NO
24	Tseng	1974	?	72.8	35.7	Sand	$P_o = P_i$	Liquefaction , solid versus hollow specimens	Compaction	NO
25	Ishihara and Yasuda	1975	70	50	30	Sand	$P_o = P_i$; $\varepsilon_2 = 0$	Liquefaction of sands, irregular excitation	AP	NO
26	Lade	1975	50	110	90	Sand	$P_o = P_i$	α effect on stress-strain behavior	No info	NO
27	Al-Hussaini	1981	101.6	76.2	50.8	Clay and Clayey Sand	$\varepsilon'_z = 0$	Tensile properties of compacted soils	Compaction	NO
28	Cheng	1981	76.2	101.6	76.2	Clay	$F_z = P_o = P_i = 0$	Strain rate effects in torsion	One-dimensional slurry consolidation	NO
29	Dusseault	1981	200-240	50.8	25.4	Dense Oil Sand	$T_h = 0$	Tunneling and pressuremeter paths	Trimming and coring	NO
30	Lade	1981	400	110	90	Sand	$P_o = P_i$	Influence of specimen height		NO
31	Saada and Shook	1981	140-152	35.6	25.4	Clay	$P_o = P_i$	Slow cyclic and large shear strain behavior	One-dimensional slurry consolidation	NO
32	Fukushima and Tatsuoka	1982	200	50	30	Sand	$P_o = P_i$	Deformation and strength behavior	AP	NO
33	Symes et al.	1982	254	127.5	101.5	Sand	----	α and b effects on strain response	WP	NO
34	Tatsuoka et al.	1982	100-200	100	60	Sand	$P_o = P_i$, $\varepsilon_z = 0$	Cyclic undrained stress-strain, dense sands	AP & MT & Static moist compaction	NO
35	Donaghe and Gilbert	1983	203.2	50.8	35.6	Sand	$P_o = P_i$	Principal stress rotation; liquefaction	MT	NO
36	Hight et al.	1983	254	127.5	101.5	Sand	----	Specimen dimensions, α and b effects on stress- strain	WP	NO
37	Ishihara and Towhata	1983	104	50	30	Sand	$P_o = P_i$	Wave loading; principal stress rotation; pore pressures	AP	NO
38	Ishihara and Yamazaki	1984	101	50	30	Sand	$P_o = P_i$	Liquefaction in seabed deposits due to wave loads	AP	NO
39	Macky and Saada	1984	108-152	25-35	18-25	Clay	$P_o = P_i$	Dynamics of anisotropic clays, large strains	One-dimensional slurry consolidation	NO
40	Symes et al.	1984	254	127	101.6	Sand	----	Undrained anisotropy and principal stress rotation	WP	NO
41	Tatsuoka et al.	1984	100	50	30	Sand	$P_o = P_i$	Specimen preparation methods, cyclic undrained strength	AP, MT, wet-vibration, WP	NO
42	Ishibashi et al.	1985	142	35.5	25.4	Sand	$P_o = P_i$	Liquefaction characteristics	AP + Tamping	NO

Table 2.1. Researchers who worked with hollow cylinder (HC) specimens (expanded from Koester 1992) Contd.

#	Reference	Year	Specimen Dimensions (mm) H	R_0	R_i	Soil Type	Control Restrictions	Applications	Specimen Preparation Method	Uniformity Check
43	Symes et al.	1985	254	127.5	101.5	Sand	---	Liquefaction under principal stress rotation	WP	NO
44	Ishihara et al.	1985	100	50	30	Sand	$P_o = P_i$	Liquefaction of K0-consolidated sand under cyclic principal stress rotation and lateral constraint	AP	NO
45	Towhata and Ishihara	1985	100	50	30	Sand	$P_o = P_i$	Undrained strength under cyclic rotation of principal stresses	AP	NO
46	Tatsuoka et al.	1986	100	50	30	Sand	$P_o = P_i$	Sample preparation methods, cyclic undrained strength	AP, MT, wet-vibration, WP	NO
47	Alarcon et al.	1986	203	35.5	19	Sand	$P_o = P_i$	Stress and strain for $\gamma > 10^{-2}$ %	AP	NO
48	Miura et al.	1986	200	50	30	Sand	----	α effect on stress-strain and strength	AP	NO
49	Tatsuoka et al.	1986	200	50	30	Sand	----	Failure and deformation of sand in torsion	AP	NO
50	Anderson et al.	1988	150	75	12.5	Clay	$T_h = 0$	Pressuremeter paths; undrained creep	One-dimensional slurry consolidation	NO
51	Chen	1988	254	127	101.6	Sand	$T_h = 0$	Stress path effects on Monterey No.0/30 sand	AP + Tamping	NO
52	Saada	1988	127-177	35.5	25.5	Sand and Clay	---	Evaluation of the hollow cylinder testing method	Trimming and coring for clays AP for sands	NO
53	Tatsuoka et al.	1989	200	50	30	Sand	$\varepsilon_z = 0$	Simple shear testing using HC	AP	NO
54	Pradel et al.	1990	193	50	30	Sand	----	Yielding and flow under principal stress rotation	AP	NO
55	Talesnick and Frydman	1991	120	35.5	25	Clay	$P_o = P_i$	Comparison against NGI-type direct simple shear	Trimming and coring of undisturbed specimens	NO
56	Dakoulas et al.	1992	203	69.9	50.1	Sand	$P_o = P_i$	Experimental calibration of constitutive model	MT	NO
57	Koester	1992	203	127.0	102	Silty sand	$P_o = P_i$	Cyclic strength, and pore pressure response	AP, MT	NO
58	Yamashita and Toki	1993	100	50.0	30	Sand	$\varepsilon_z = 0$	Effect of fabric anisotropy on cyclic undrained strength	AP through sieves, AP through a funnel and vibration, centrifugal force method	NO
59	Vaid and Sayao	1995	300	75.0	50	Sand	----	Loading behavior under multiaxial stresses	WP	NO
60	Sayao and Vaid	1996	300	75.0	50	Sand	----	Effect of b on deformation response	WP	NO
61	Zdravkovic	1996	203	127.0	102	Silt	----	Anisotropic behavior of silt	SD	NO
62	Zdravkovic&Jardine	1997	254	127.0	101.6	Silt	---	Stiffness characteristics under general stress conditions	SD	NO

Table 2.1. Researchers who worked with hollow cylinder (HC) specimens (expanded from Koester 1992) Contd.

#	Reference	Year	Specimen Dimensions (mm)			Soil Type	Control Restrictions	Applications	Specimen Preparation Method	Uniformity Check
			H	R_0	R_i					
63	Nakata et al.	1998	200	50.0	30	Sand	----	Effect of α on undrained behavior	AP	NO
64	Lade and Kirkgard	2000	250	110	90	Clay	$P_o = P_i$	α and b effects on cross-anisotropic behavior	Trimming of undisturbed specimens	NO
65	Toyota et al.	2001	160	40	25	Clay	----	Stress-strain behavior of clays under 3-D stress conditions	One-dimensional slurry consolidation	NO
66	Zdravkovic&Jardine	2001	254	127.0	101.6	Silt	----	Effect of rotating principal stresses during consolidation	SD	NO
67	Lee et al.	2002	230	49	39	Mudstone	$P_o = P_i$	Stress-strain behavior of a mudstone	Drilling	NO
68	Sivathayalan and Vaid	2002	300	76	51	Sand	----	Influence of initial state and α on undrained response	WP	NO
69	Uthayakumar and Vaid	2002	300	76	51	Sand	----	Static liquefaction under multiaxial loading	WP + Vibration	NO
70	Chaudhary et al.	2002	100	50	30	Sand	----	Effect of initial fabric and shearing direction on cyclic deformation	AP, WP, dry rodding	NO
71	Shibuya et al.	2003	254	127.5	101.5	Sand	----	Four-dimensional local boundary surfaces	WP	NO
72	Rolo	2003	254	127	102	Clayey Sand	----	Anisotropic behavior of loose clayey sands	SD	In terms of fines content
73	Chaudhary et al.	2004	200	50	30	Sand	----	Quasi-Elastic stiffness parameters in HC and TX testing	AP	NO
74	Naughton and O'Kelly	2004	200	50	35.5	Sand	----	Induced anisotropy	WP	NO
75	Brown and Richardson	2004	500	140	112	Sand and granulated crushed slate	----	Cyclic loading behavior of dry granular material	AP	NO
76	Lin and Penumadu	2005	230	25.4	17.8	Clay	----	Effect of principal stress rotation on Kaolin clay behavior	One-dimensional slurry consolidation	In terms of water content
77	Lin and Penumadu	2005	230	25.4	17.8	Clay	----	Strain localization in combined axial-torsional loading	One-dimensional slurry consolidation	NO
78	Silvestri et al.	2005	100	50-63.5	19-25	Clay	----	Expansion tests in clay using HC apparatus	Cutting with the technique of electroosmosis	NO
79	O'Kelly and Naughton	2005	200	50	35.5	Sand	----	Development of a hollow cylinder apparatus	WP	NO
80	O'Kelly and Naughton	2005	200	50	35.5	Sand	----	Engineering properties of wet pluviated HC specimens	WP	NO
81	Altun et al.	2005	200	50	30	Silty sand	$P_o = P_i$	Effect of fines content on liquefaction resistance	AP	NO
82	Yang et al.	2007	314	100	75	Sand	----	Anisotropic behavior in rotational shear	AP	NO

F_z = axial load, P_o & P_i = outer and inner cell pressures, T_h = torque, ε_z = axial strain, ε_2 = intermediate principal strain, σ_z = axial stress, AP = air pluviation, MT= moist tamping, SD= slurry deposition

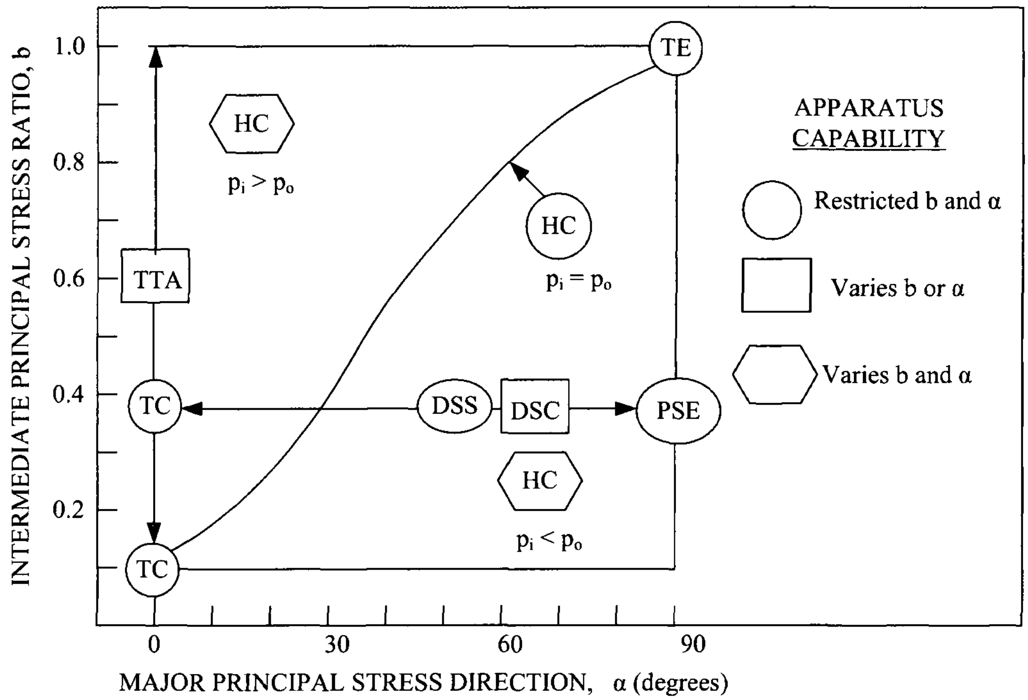

Figure 2.6.Major principal stress rotation (α) and *b* variations for different testing methods where HC = hollow cylinder, DSC = directional shear cell, PSC = plane strain compression, PSE = plane strain extension, TC = triaxial compression, TE= triaxial extension, DSS= direct simple shear, TTA= true triaxial (Ladd 1990).

Typical boundary conditions used in HC testing are shown in Fig. 2.7a. Even though the actual distributions of stresses and strains can be approximated by using linear elasticity, location-dependent equations for stresses and strains are not easy to solve. Analyzing test results based on these equations is not an easy task due to stress and strain nonuniformities. However, the appropriate selection of specimen geometry may significantly reduce the variations in stresses and strains over the entire specimen allowing the use of average stress and strain values (Hight et al. 1983).

According to the applied loads and pressures shown in Fig. 2.7a, Eqs. 2.2-2.9 can be derived using linear elasticity and assuming that the work done by external force, torque, and pressures is equal to the work done by the stresses and strains induced in the specimen:

Average vertical (or axial) stress: $\sigma_z = \dfrac{W}{\pi \cdot (r_o^2 - r_i^2)} + \dfrac{p_o r_o^2 - p_i r_i^2}{r_o^2 - r_i^2}$ (2.2)

Average radial stress: $\sigma_r = \dfrac{p_0 r_0 + p_i r_i}{r_0 + r_i}$ (2.3)

Average circumferential stress: $\sigma_\theta = \dfrac{p_0 r_0 - p_i r_i}{r_0 - r_i}$ (2.4)

Average shear stress: $\tau_{z\theta} = \dfrac{3 \cdot T}{2\pi \cdot (r_0^3 - r_i^3)}$ (2.5)

Average vertical (or axial) strain: $\varepsilon_z = \dfrac{\Delta H}{H}$ (2.6)

Average radial strain $\varepsilon_r = -\dfrac{l_0 - l_i}{r_0 - r_i}$ (2.7)

Average circumferential strain: $\varepsilon_\theta = -\dfrac{l_0 + l_i}{r_0 + r_i}$ (2.8)

Average shear strain: $\gamma_{z\theta} = \dfrac{2\theta \cdot (r_0^3 - r_i^3)}{3H \cdot (r_0^2 - r_i^2)}$ (2.9)

where W = vertical load; T = torque about vertical axis; p_i = inner cell pressure; p_o= outer cell pressure; r_i and r_o = inner and outer HC specimen radii, respectively; H = specimen height; ΔH = change in specimen height; l_i and l_o = displacements at the inner and outer surfaces of the HC specimen, respectively; and θ = rotation angle (Fig. 2.7a). The stress components defined in Eqs. 2.2 -2.5 are schematically illustrated in Fig. 2.7b.

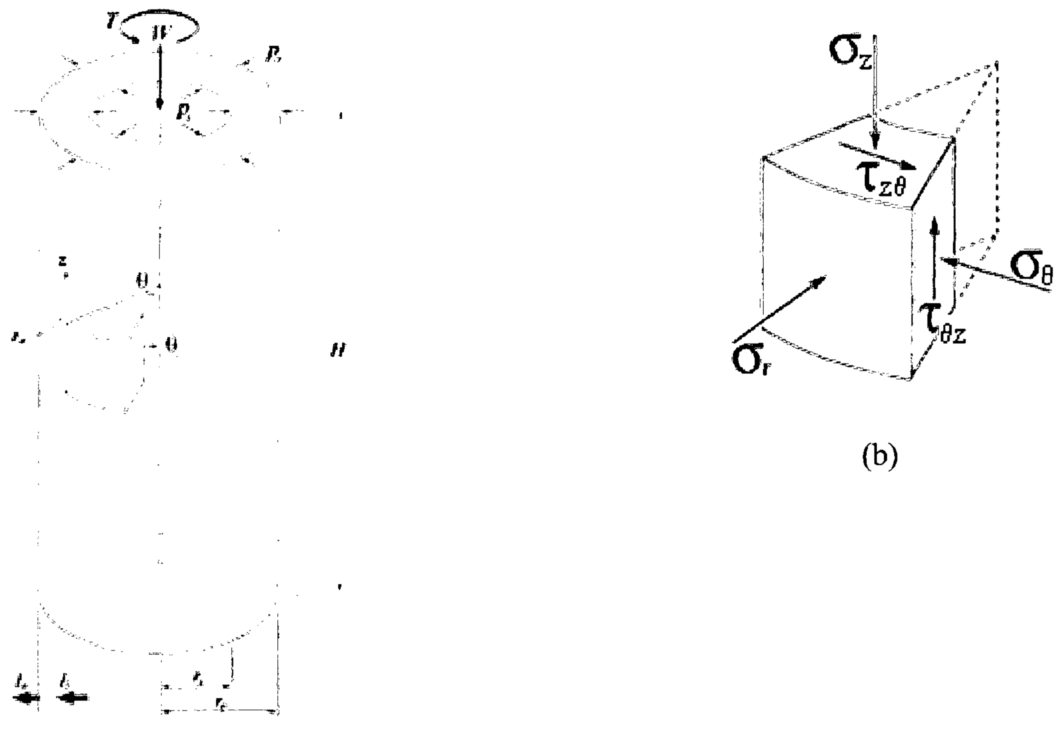

Figure 2.7.(a) Typical geometry and loading of hollow cylinder specimens, (b) stress components on a soil element in the wall of a HC specimen (Hight et al. 1983).

The average vertical and circumferential stresses are derived using equilibrium equations, and the average axial and shear strains are obtained through strain compatability. Therefore, the average axial stress, circumferential stress, axial strain, and shear strain are independent of the constitutive properties of the material tested (Hight et al.1983). The average radial stress (Eq. 2.3) is calculated based on the linear elastic behavior assumption. The average radial and circumferential strains are calculated based on the assumption that the radial displacement varies linearly across the wall of the specimen (Hight et al. 1983). To validate the assumption of linear variation of radial displacement, the use of equal inner and outer cell pressures, p_i and p_o, respectively, has been suggested (Saada 1988, Hight et al. 1983).

Eqs. 2.2-2.9 describe the stresses and strains that can be directly obtained by measuring W, T, p_o, p_i, H, ΔH l_o, l_i, r_o, r_i, and θ. The principal stresses prior to the application of shear stresses are $\sigma_1 = \sigma_z$ and $\sigma_2 = \sigma_3 = \sigma_\theta = \sigma_r$. Determination of the principal stresses and principal stress rotations after application of shear stresses requires one additional step, as outlined below in Eqs. 2.10-2.12:

Major principal stress: $$\sigma_1 = \frac{\sigma_z + \sigma_\theta}{2} + \sqrt{\left(\frac{\sigma_z - \sigma_\theta}{2}\right)^2 + \tau_{z\theta}^{\;2}} \tag{2.10}$$

Intermediate principal stress: $$\sigma_2 = \sigma_r \tag{2.11}$$

Minor principal stress: $$\sigma_3 = \frac{\sigma_z + \sigma_\theta}{2} - \sqrt{\left(\frac{\sigma_z - \sigma_\theta}{2}\right)^2 + \tau_{z\theta}^{\;2}} \tag{2.12}$$

Derivation of Eqs.2.10-2.12 can be easily done based on the Mohr circles of stresses. The Mohr circle for the stress conditions given in Fig. 2.7b is depicted in Fig. 2.3d. The largest circle is defined by σ_z, σ_θ and $\tau_{z\theta}$. The intermediate principal stress (σ_2) allows identification of the second point of the smallest Mohr circle. The second largest Mohr circle is inside the largest one and tangent to both other circles. The radius of the largest Mohr circle of stress is equal to

$$r = \sqrt{\tau^2{}_{z\theta} + \left(\frac{\sigma_z - \sigma_\theta}{2}\right)^2} \tag{2.13}$$

The major principal stress σ_1 corresponds to the largest intercept of the largest Mohr circle with the normal stress-axis, which can be determined using Eq. 2.10. The smallest intercept of the Mohr's circle with the normal stress-axis defines the minor principal stress σ_3 (Eq. 2.12). According to Eq. 2.11, the intermediate principal stress is equal to the radial stress as no shear stresses are applied to the vertical outer surface of the HC specimen. If equal p_i and p_o are used, σ_2 becomes equal to p_i and p_o (Eq. 2.3). The angle α between the major principal stress direction and the vertical also can be determined from the Mohr circle geometry (Fig. 2.3d) and is defined as:

$$\alpha = \frac{1}{2}\tan^{-1}\left(\frac{2\tau_{z\theta}}{\sigma_z - \sigma_\theta}\right) \tag{2.14}$$

Application of equal inner and outer cell pressures creates a correlation between α and b through Eq. 2.9 which does not allow independent controls α and b as

$$b = \sin^2(\alpha) \tag{2.15}$$

The stress formulations presented above do not consider the effect of membrane forces. Tatsuoka et al. (1986a) specified corrections for all stress components due to the inner and outer membrane forces. They used the theory of elasticity and assumed that membranes maintained their right cylinder shape during torsion. By assuming a Poisson's ratio (υ) of 0.5, they derived the following equations for the stress corrections due to membrane forces,

$$\Delta\sigma_z = -\frac{4}{3}\frac{E_m t_m}{r_0^2 - r_i^2}\left[r_0\{(2\varepsilon_z)_o + (\varepsilon_\theta)_o\} + r_i\{(2\varepsilon_z)_i + (\varepsilon_\theta)_i\}\right] \tag{2.16}$$

$$\Delta\sigma_r = -\frac{2}{3}\frac{E_m t_m}{r_0 + r_i}\left[\{(\varepsilon_z)_o + 2(\varepsilon_\theta)_o\} - \{(\varepsilon_z)_i + 2(\varepsilon_\theta)_i\}\right] \tag{2.17}$$

$$\Delta\sigma_\theta = -\frac{2}{3}\frac{E_m t_m}{r_0 - r_i}\left[\{(\varepsilon_z)_o + 2(\varepsilon_\theta)_o\} + \{(\varepsilon_z)_i + 2(\varepsilon_\theta)_i\}\right] \tag{2.18}$$

$$\Delta\tau_{z\theta} = -2E_m t_m \frac{(r_0^3 + r_i^3)}{(r_0^3 - r_i^3)(r_0 + r_i)}\gamma_{z\theta} \tag{2.19}$$

where E_m = Young's modulus, t_m = membrane thickness. The subscripts for the strain components describe whether the strain component is for the outer or the inner membrane. For example $(\varepsilon_z)_o$ represents the average axial strain for the outer membrane. For practical purposes, strains developed in the inner and outer membranes can be assumed to be the same, which reduces Eqs. 2.16-2.19 to,

$$\Delta\sigma_z = -\frac{4}{3}\frac{E_m t_m}{r_0 - r_i}(2\varepsilon_z + \varepsilon_\theta) \tag{2.20}$$

$$\Delta\sigma_r = -\frac{8}{3}\frac{E_m t_m}{r_0 - r_i}(\varepsilon_\theta) \tag{2.22}$$

$$\Delta\sigma_\theta = -\frac{4}{3}\frac{E_m t_m}{r_0 - r_i}(\varepsilon_z + 2\varepsilon_\theta) \tag{2.23}$$

$$\Delta\tau_{z\theta} = -2E_m t_m \frac{(r_0^3 + r_i^3)}{(r_0^3 - r_i^3)(r_0 + r_i)}\gamma_{z\theta} \tag{2.24}$$

Strain components in Eqs. 2.20-2.23 are the accumulated strains, i.e., the strains developed during all previous stages (saturation, consolidation etc). Tatsuoka et al. (1986a) assumed a Young's modulus of 1470 kPa for the membranes and added these correction factors to the stresses calculated in Eqs. 2.2-2.5. Koester (1992) used a correction factor due to membrane forces only for the shear stress component. The correction consisted of calculating the torque carried by the membranes by using Eq. 2.25,

$$\Delta T = \frac{G\theta\pi}{2L}\left(r_0^4 - r_i^4\right) \tag{2.25}$$

where G = shear modulus, L = length of the specimen, θ = rotation angle in radians. He used the shear modulus of 435 kPa (E = 1304 kPa with υ = 0.5) and (1) calculated the net torque on the specimen by subtracting ΔT from the applied torque, (2) determined the shear stress by using Eq. 2.5 and the net torque, and (3) added the shear stress correction, for the membrane forces (Eq. 2.24), to the calculated shear stress (Step 2). This way he determined the shear stress on the specimen that was free from the membrane forces effect. However, with this procedure, he considered the effect of membranes twice. Even then, the correction he obtained for shear stress was only 0.345 kPa at 1 % shear strain.

2.4 NON-UNIFORMITIES ASSOCIATED WITH HOLLOW CYLINDER SPECIMENS

Stress and strain non-uniformities have been reported as one of the most critical concerns related to HC testing (Arthur et al. 1980, Saada and Townsend 1981). Non uniformities develop due to (1) end restraints, and (2) specimen curvature (Hight et al. 1983).

Radial frictional forces are generated at the ends of the specimen, when the specimen dilates or contracts. Generation of these forces (i) develops additional circumferential stresses and bending moments, which, in turn, invalidates the equality of the radial stress to the intermediate principal stress, and (ii) causes non-uniformity in axial stress (Rolo, 2003). The end restraint effect can be reduced by having smoother surfaces on the top and bottom platens so that the friction between the sample and the platens is minimal in the radial direction. However, it should be noted that full friction is required in the circumferential direction to transmit torque to the specimen through the platen vanes. End restraint effects become less pronounced away from the platens since the generated radial frictional forces are self-equilibrating (Saada 1988). For tall specimens, the central portion of the specimen is likely to be free from the end restrain effects. Saada (1988) proposed the following criterion for the specimen height to reduce the end restraint effect;

$$H \geq 5.44 \cdot \sqrt{r_o - r_i} \tag{2.26}$$

where H = height, r_o and r_i = outer and inner radii, respectively. Vaid et al. (1990) suggested that the height should be 1.8 to 2.2 times the external diameter, r_o. The hollow cylinder apparatus (HCA) at Colorado State University (CSU) can test specimens with the following geometry: H = 200 mm, r_o = 50 mm and r_i = 30 mm, which meets the height requirements proposed by the previous researchers.

Even without the end restraint effect, stress non-uniformities may still develop across the HC specimen wall due to a gradient between p_o and p_i or a torque applied. The gradient between p_o and p_i causes variations in σ_r and σ_θ across the specimen wall. Application of torque results in shear stress variations across the specimen wall (Hight et al. 1983). Data analysis for HC testing usually involves average stresses and strains over the volume of the specimen or the area of the cross-section. However, the variation across the wall should be considered to assure a reliable stress-strain analysis. Hight et al. (1983) conducted elastic and elastoplastic finite element study to quantify the stress and strain non-uniformities for HC specimens. The level of non uniformity due to curvature was evaluated based on the parameter β_3 defined as:

$$\beta_3 = \frac{1}{r_o - r_i}\frac{1}{S_L}\int_{R_i}^{R_o}\left|S(r) - S_{av}\right|dr \tag{2.27}$$

where, S = distribution of the stress (or strain) component analyzed, S_{av} = the real average value of the stress (or strain) component, and S_L = stress (or strain) level, which was $(\tau_{z\theta})_{ave}$ for $\tau_{z\theta}$ and ½ $((\sigma_r)_{ave}+(\sigma_\theta)_{ave})$ for σ_r and σ_θ. They suggested that if $\beta_3 < 0.11$ for σ_r and σ_θ, the stress non-uniformity was acceptable. Their assumption of uniform $\tau_{z\theta}$ across the wall, for the limiting elasto-plastic behavior, implicitly required $\beta_3 = 0$ according to Eq.2.27. The magnitude of β_3 depended on the sample geometry, stress path followed, and the material constitutive law. In order to reduce β_3, Hight et al. (1983) attempted to optimize the geometry for their HC testing apparatus. First, they examined the variation of σ_r and σ_θ with respect to r_i/r_o by using a linear elastic analysis (Fig. 2.8).

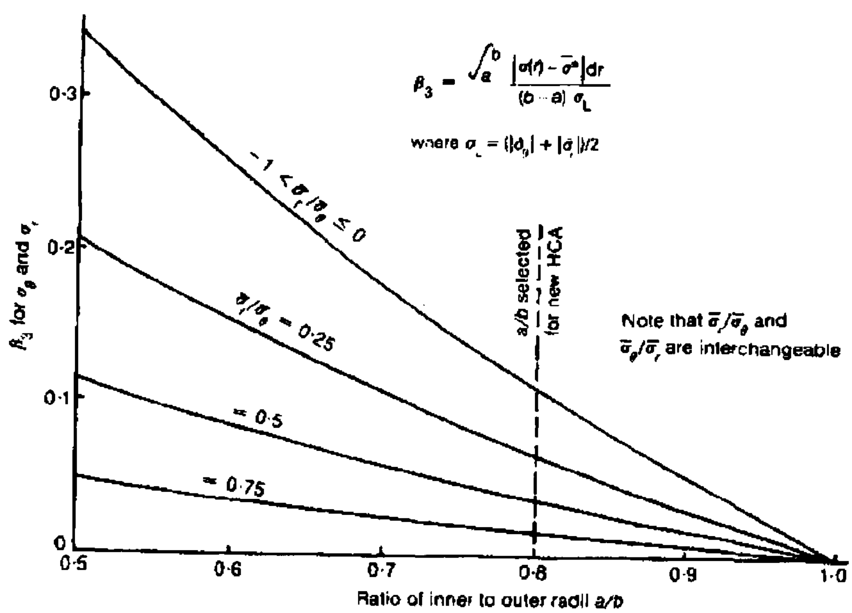

Figure 2.8. The change in β_3 as a function of r_i/r_o - Note a = r_i, b = r_o (after Hight et al. 1983)

For the loading ranges they were interested in, the ratio of r_i/r_o=0.8 was assumed to be suitable. The wall thickness for HC sand specimens was decided considering the following:

(a) The ratio of wall thickness to the maximum particle size should be large enough to ensure that failure mechanisms are not constrained.

(b) The density should be uniform across the wall.

(c) Sample volume should be large compared to potential volume change due to membrane penetration.

(d) The wall thickness should be large enough so that the internal instrumentation disturbance would be minimal.

According to Fig. 2.8, the smaller wall thickness reduces β_3 for σ_r and σ_θ. However, considering the aforementioned constraints, Hight et al. (1983) decided to have a wall thickness of 25.4 mm. Their next step was to establish r_o. They mentioned that the increase in p_o- p_i increase the non-uniformities for σ_r and σ_θ. For a given level of σ_r- σ_θ, the required (p_o-p_i) decreased as r_o increased. However, the improvement in uniformity was not significant for r_o>125 mm (Fig. 2.9). Therefore, they decided to have r_o =127 mm.

As mentioned previously, larger specimen heights can reduce end restraint effects. Hight et al. (1983) conducted a linear elastic finite element analysis on a HC specimen with dimensions r_o = 125mm, r_i = 100 mm and H = 250 mm for the end restraint and no-end restraint cases. They determined that over the central gage length of 125 mm, stresses due to end restraint case were at most 10% different than the stresses for the no-end-restraint case. Therefore, they decided to adopt a specimen height of 250 mm.

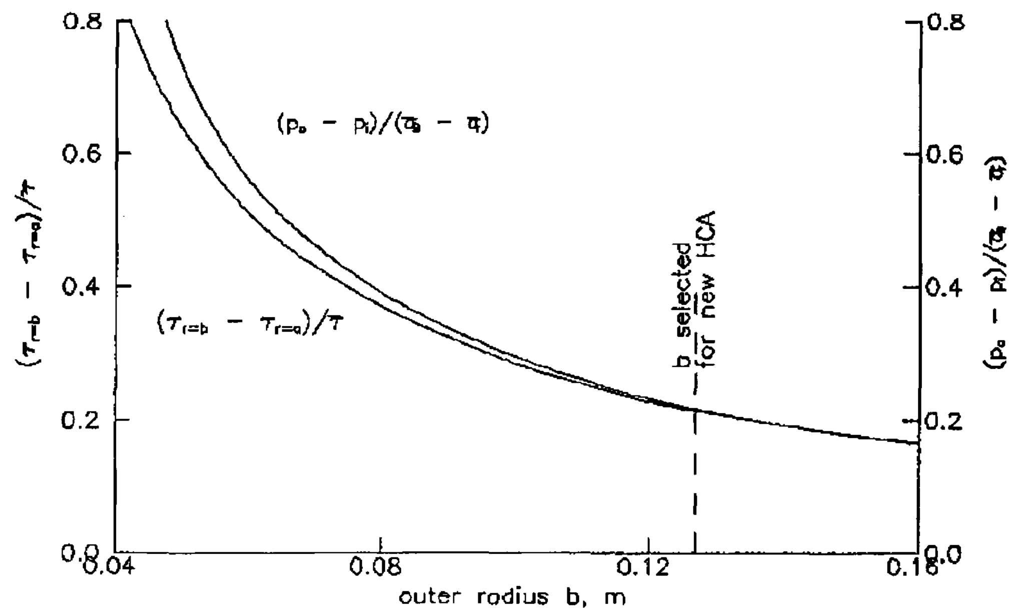

Figure 2.9. Effect of r_o (b in the figure) on shear stress non uniformity for 25.4 mm wall thickness

As a final measure to reduce the non-uniformities for the geometry they adopted, Hight et al. (1983) proposed the following condition to be met for all the stress paths,

$$0.9 < \frac{p_o}{p_i} < 1.2 \tag{2.28}$$

Vaid et al. (1990) conducted a linear elastic finite element analysis for a specimen with dimensions $r_o = 76$ mm, $r_i = 51$ mm, and H = 302 mm. They explored the stress paths where α varied between 0 and 90° and b varied between 0 and 1. They indicated that the behavior of frictional material primarily depended on the stress ratio, $R = \sigma'_1/\sigma'_3$, and, thus, evaluated the non uniformities in terms of R instead of σ_r and/or σ_θ. Furthermore, they proposed an alternative measure of non uniformity as follows:

$$\beta_R = \frac{R_{max} - R_{min}}{R_{av}} \tag{2.29}$$

where $R_{max} = \left(\frac{\sigma'_1}{\sigma'_3}\right)_{max}$, $R_{min} = \left(\frac{\sigma'_1}{\sigma'_3}\right)_{min}$, $R_{av} = \left(\frac{\sigma'_1}{\sigma'_3}\right)_{av}$ across the HC specimen wall.

The non-uniformity was assumed to be acceptable if $\beta_R \leq 0.2$, which corresponds to a maximum 10% variation in R across the specimen wall. They compared the non uniformities predicted by B_R and B_3 for r_0 = 76 mm and r_i = 51 mm at the stress states (1) p' = 300 kPa, R = 3, b = 0, α = 45°, and (2) p' = 300 kPa, R = 3, b = 0.5, α = 0°. For these stress states, they showed that B_R obtained through a linear elastic analysis predicted significant non uniformities, while B_3 predicted a uniform stress distribution. Their comprehensive analysis over the possible ranges of α and b showed that for any given R, the largest non uniformities occur around b = 1, α = 0°, and b = 0, α = 90°. More importantly, they also observed significant non uniformities around α = 45° even when $p_o = p_i$. An increase in R was also shown to increase these non-uniformities. In their study, the mean normal effective stress had a negligible effect on the stress non uniformities. Vaid et al. (1990) argued that linear elastic analysis overpredicted the non uniformities and yielded conservative results. Sayao and Vaid (1991) investigated the effect of specimen geometry, and stress path on the stress non uniformities using elastic finite element analysis. The comments regarding the effect of α and b on the non uniformity were similar to the ones made by Vaid et al. (1990). However, the specimen geometry effect on the non-uniformity was more detailed. They determined that, as the wall thickness increased, the stress non-uniformities also increased no matter what non uniformity parameter (β_3 or β_R) was used (Fig. 2.10). However, specifying a minimum wall thickness was again necessary due to similar constraints mentioned by Hight et al. (1983). Sayao and Vaid (1991) suggested that the wall thickness should be between 20 and 26 mm. Larger r_i reduced the non uniformity based on β_R. However, the improvement in uniformity was not significant as r_i becomes larger than 40-50 mm (Fig. 2.11). Furthermore, for larger r_i, p_o-p_i required to get a certain R increase, was shown to be really small and experimental control of such small p_o-p_i was reported to be difficult.

Sayao and Vaid (1991) proposed the following criteria for the HC specimen geometry to reduce the stress non uniformities,

(a) *wall thickness between 20 and 26 mm (20 mm for dynamic hollow* cylinder apparatus (HCA) at CSU),

(b) $0.65 \le r_i / r_o \le 0.82$ (0.60 for HCA at CSU), and

(c) $1.8 < H / 2r_o < 2.2$ (2.0 for HCA at CSU).

The evaluation of the HC geometries adopted by different researchers is given in Fig. 2.12. The boxed regions indicate the acceptable regions for the HC geometry. However, it should be remembered that the criteria set by Sayao and Vaid (1991) are based on a linear elastic behavior assumption and produce conservative results in terms of stress nonuniformity. If non-linear soil behavior is taken into account, the non-uniformities may be less than what Sayao and Vaid (1991) had determined. This was shown later by Wijewickreme and Vaid (1991), who conducted finite element analysis using both linear elastic and incremental elastic hyperbolic models.

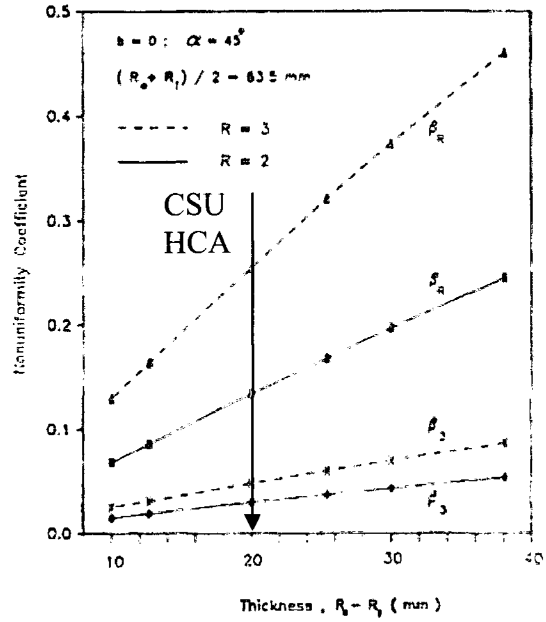

Figure 2.10. Effect of wall thickness on the non-uniformity according to elastic finite element analysis (Sayao and Vaid 1991)

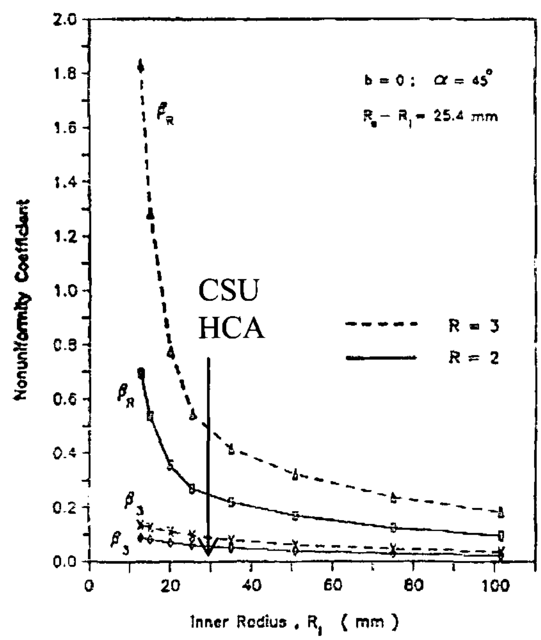

Figure 2.11. Effect of inner radius on the non-uniformity according to elastic finite element analysis (Sayao and Vaid 1991)

They concluded that linear elastic model significantly overestimated the non uniformities, and stressed that according to linear elastic model, increase in R always increased the non uniformity. On the other hand, the incremental elastic hyperbolic model predicted that an increase in R increased the non uniformity up to a certain point. Beyond that point, the increase in R did not significantly affect the stress non uniformity. This difference was attributed to the fact that the incremental elastic hyperbolic model takes into account stiffness degradation and stress redistribution as failure is approached. Additionally, Wijewickreme and Vaid (1991) mentioned that the relative density of sand specimens also may affect the stress non uniformities. They showed based on limited data that dense specimens may have more significant non uniformities than loose specimens.

In summary, linear elastic analysis seems to overestimate stress non uniformities compared to more realistic elastoplastic or incremental elastic hyperbolic models. Establishing an HC specimen geometry based on results of linear elastic analysis remains on the conservative side. Therefore, following the criteria for the HC specimen geometry suggested by Sayao and Vaid (1991) may be a more reasonable approach. The HC specimen geometry for the dynamic hollow cylinder apparatus (HCA) at CSU meets their first and third criteria. The ratio $r_i/r_o = 0.6$ is slightly below the required range for the second criterion. Thus, the geometry of the CSU HCA can be assumed to be appropriate.

As mentioned previuosly, the selected α, b and R (or stress path) affect the non-uniformities. Linear elastic models predict significant non uniformities when $b = 1$, $\alpha = 0$; $b = 0$, $\alpha = 90$; b = all values, $\alpha = 45$; and when $R > 1.5$ (Naughton and O'Kelly 2007) , whereas elastoplastic and incremental elastic hyperbolic models predict less uniformities when $\alpha = 45$ (Hight et al.1983, Wijewickreme and Vaid 1991).

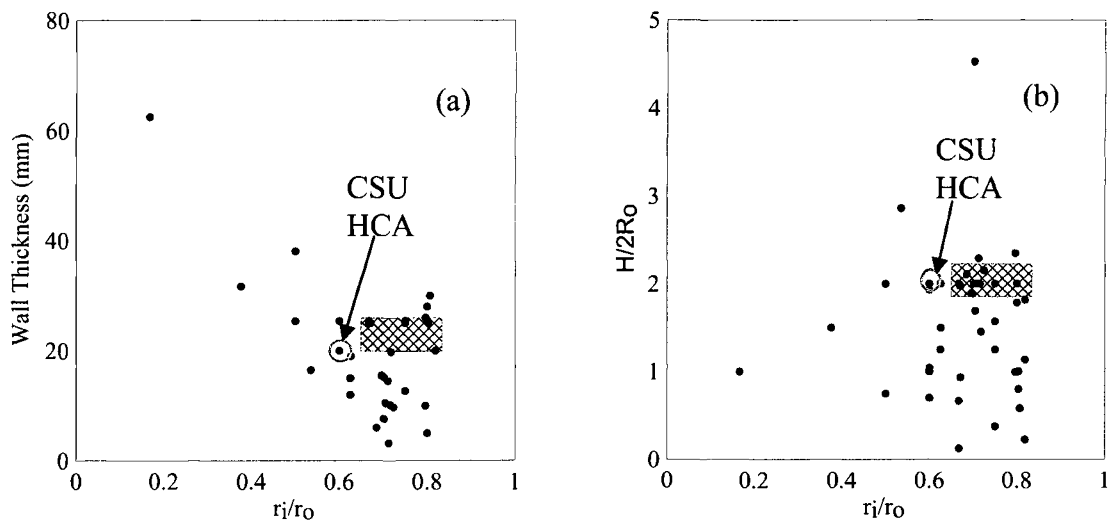

Figure 2.12. Geometry requirements for HC specimens suggested by Sayao and Vaid (1991) (a) first and second criteria combined, and (b) second and third criteria combined

The models that take the stiffness degradation into account do not necessarily indicate larger stress non uniformities when $R \geq 2$. Consequently, avoiding α and b combinations of b = 1, α = 0; b = 0, α = 90; and α = 45 can help keep the stress non uniformities within reasonable levels.

2.5. SPECIMEN PREPARATION

The reconstitution method used to prepare sand specimens in the laboratory significantly affects the structure and thus the mechanical behavior of the sand (Mulilis et al. 1977, Miura and Toki 1982, Tatsuoka et al.1986, Vaid et al. 1999, Hoeg et al. 2000, Ghionna and Porcino 2006, Yamamuro and Wood 2004). For this reason, the selected specimen reconstitution method should attempt to reproduce the in situ soil fabric as closely as possible so that the mechanical response of the reconstituted specimen would be as similar as possible to its in situ behavior at a given soil state. For example, laboratory pluviation methods through air or water may be appropriate to simulate natural eolian or alluvial clean sand deposits (Oda 1972, Vaid and Sayao 1995, Naughton and O'Kelly 2004), respectively.

The selected specimen reconstitution method should also (1) ensure specimen uniformity in terms of both density and fabric distribution, (2) ensure test result repeatability, and (3) facilitate saturation (Carraro and Prezzi 2008).

Various reconstitution techniques are summarized next for both solid and HC sand specimens. Studies evaluating the effects of different specimen reconstitution techniques on the behavior of HC specimens are not as common as studies that focus on the behavior of solid specimens. In any event, the fabric induced by a given solid specimen reconstitution method might be expected to be similar to the fabric imparted by the same method during reconstitution of HC specimens.

2.5.1. Solid Specimen Reconstitution and Uniformity

Similarly to HC testing, MT, AP, WP, and SD are the most widely used protocols to reconstitute solid specimens of sands with or without fines. MT involves tamping of moist sand layers in a mold. If the same compaction effort is applied to all layers, the top layers may have a lower relative density (D_R) than the lower layers (Ladd 1978). To minimize potential density gradients across the specimen height, a varying compaction effort may be applied to individual layers (Ladd 1978). Yet, MT may still lead to considerable density variations along the specimen height even if the compaction effort is varied (Mulilis et al. 1977, Frost and Park 2003). Furthermore, MT clean and silty sand specimens were shown to exhibit contractive behavior while their undisturbed counterparts showed dilative response (Vaid et al. 1999, Hoeg et al.

2000). Another problem associated with MT is the potential bulking of fines due to water tension, which causes large deformations during saturation (Kuerbis and Vaid 1988). Despite the aforementioned limitations, MT may impart no particle segregation to specimens of clean, well-graded sands or silty sands (Hoeg et al. 2000) and allows specimen reconstitution under a wide D_R range.

AP consists of pluviating dry sand from a controlled height and is most suitable to simulate the fabric of eolian deposits of uniform sand or silt (Kuerbis and Vaid 1988). AP produces an orthotropic fabric in which the longer axis of sand particles tends to be oriented along the horizontal direction (Yamashita and Toki 1993). AP sand specimens are generally uniform in terms of their local D_R distribution across specimen height (Kuerbis and Vaid 1988). Conversely, AP specimens of well-graded sands can be prone to segregation, especially for sands with high fines content (FC) (Kuerbis and Vaid 1988). Vaid and Negussey (1984) attributed the segregation to the lower deposition velocities attained by small particles and the corresponding larger deposition velocity of larger particles. Furthermore, AP silty sand specimens can be prone to bulking of fines and become meta-stable, thus experiencing deformations as large as those experienced by MT silty sand specimens (Tatsuoka et al. 1986, Kuerbis and Vaid 1988). Long saturation is another AP issue since the initial pore pressure coefficient B (Skempton 1954) at zero back pressure (BP) may be as low as 0.1 – 0.2. Thus, achieving a B value of 0.98 or higher may require application of large BPs over long periods of time.

WP involves deposition of dry clean sand into a mold previously filled with de-aired (DA) water. To expedite saturation, wet sand deposition has been suggested

(Yamamuro and Wood 2004). WP simulates the fabric of alluvial and marine deposits (Oda et al. 1978, Ghionna and Porcino 2002). Undisturbed and WP specimens of clean or silty sands were shown to exhibit similar undrained behavior (Vaid et al. 1999, Ghionna and Porcino 2006). WP produces uniform clean sand specimens (Kuerbis and Vaid 1988, Vaid et al. 1999, Ghionna and Porcino 2006). To achieve denser WP specimens, subsequent densification typically achieved by tapping on the side of the mold may be required. WP does not require control of particle drop height and flow and produces specimens with high initial degree of saturation. Despite these advantages, WP causes segregation of clean well-graded or silty sands (Kuerbis and Vaid 1988). To overcome the intrinsic segregation issue of the WP method, Kuerbis and Vaid (1988) proposed an alternative slurry-deposition (SD) method in which sand-fines slurries that are previously homogenized in a mixing tube are deposited in a fairly homogenous state. The procedure involves (1) homogenizing the sand-fines slurry (prepared with DA water) in a mixing tube, (2) placing the mixing tube filled with the slurry into a mold, and (3) carefully transferring the slurry from the mixing tube into the mold. In addition to eliminating particle segregation, SD presents all the desirable advantages of the WP method and has been validated for sands with nonplastic (Kuerbis and Vaid 1988, Yamamuro and Wood 2004) and plastic (Carraro and Prezzi 2008) fines.

The aforementioned research on solid TX specimens indicates that SD and WP are the most appropriate specimen reconstitution methods for deposits of sands with and without fines, respectively, formed underwater. This is because these methods (1) allow close replication of the actual in situ fabric, inherent anisotropy, and stress-strain response (Ghionna and Porcino 2006) of alluvial and off shore soildeposits, hydraulic fills and tailings dams, (2) produce uniform specimens with highly repeatable behavior, and (3) impart a high initial degree of saturation to the specimens (Carraro and Prezzi 2008).

For poorly-graded sands, WP and SD produce similar TX responses in monotonic compression or extension (Kuerbis and Vaid 1988). However, the stress-strain behavior of well–graded or silty sand specimens formed by WP differs from the behavior of SD specimens (Kuerbis and Vaid 1988). Additionally, WP causes particle segregation of clean well-graded and silty sands. Thus, SD stands out as the most effective method to produce uniform, saturated, repeatable specimens of well-graded sand or sands with fines that can exhibit similar behavior to their undisturbed counterparts obtained from field deposits formed underwater.

2.5.2 Hollow Cylinder Test Specimens

The effect of varying the type of specimen reconstitution method on the behavior of HC specimens of clean or silty sands has not been extensively studied as the behavior of their solid counterparts.

Tatsuoka et al. (1986) conducted undrained cyclic TX tests on solid specimens and torsional shear (TS) tests on HC specimens of sand prepared by four different methods: AP, MT, wet-vibration (MT followed by vibration), and water-vibration (WP followed by vibration). They concluded that the liquefaction resistance of specimens prepared by different methods varied significantly. AP specimens were the weakest for both solid and HC geometries, similarly to what Mulilis et al. (1977) and Ghionna and Porcino (2006) observed for solid specimens. Wet-vibrated MT specimens were the strongest for the solid specimens, but not for the HC specimens. This suggests that, the selected specimen reconstitution technique plays an important role on the cyclic response of sands regardless of specimen geometry.

Yamashita and Toki (1993) used multiple-sieve AP, AP with subsequent vibration, and centrifugal force (CF) methods to reconstitute solid TX and HC specimens. The CF method was intended to produce a fabric that was opposite to the fabric created by the multiple-sieve AP. Undrained cyclic TX on solid and HC specimens and cyclic TS tests on HC specimens (with α= 45°) were conducted. They reported differences in the cyclic resistances of HC specimens due to specimen reconstitution technique, although the difference was not as significant as that observed for solid specimens. Multiple-sieve AP produced the weakest fabric whereas the CF method created the strongest fabric based on cyclic TX tests on solid specimens. However, there was not a consistent trend on which specimen reconstitution method among the three methods employed would produce the highest cyclic TS shear strength for the three soil types considered.

Chaudhary et al. (2002) conducted a similar comparative study on the differences in the monotonic shear moduli of AP, WP, and dry-rodded (used for breaking the preferred particle orientations) HC clean sand specimens. At small strains, anisotropy was most pronounced for the AP specimens. They also observed that AP resulted in the stiffest moduli, which is contradictory to the weaker AP fabrics reported by other researchers.

The limited amount of comparative studies on HC specimen response suggests that the selected specimen reconstitution technique may affect the fabric and mechanical response of HC specimens. Additionally, the selection of an HC specimen reconstitution method should be based upon the field conditions that are to be simulated and the degree of specimen uniformity and reproducibility induced by the selected method. Consequently, WP and SD methods may be the most appropriate HC specimen reconstitution methods to simulate the fabric and mechanical response of alluvial deposits of sands with or without fines, as reported by various researchers (Sivathayalan and Vaid 2002, Rolo 2003, O'Kelly and Naughton 2005). Sayao and Vaid (1989) tested WP HC specimens of clean medium Ottawa sand (ASTM C 109) to evaluate the drained behavior of sand specimens subjected to generalized stress conditions. As part of their study, the inherent anisotropy was studied by monitoring the response of specimens subjected to isotropic stress increments ranging from 50 kPa to 300 kPa. They showed that the general relationship between the normal strain components during isotropic loading was $\varepsilon_r = \varepsilon_\theta > \varepsilon_z$, as WP specimens exhibited higher deformability in the horizontal direction than in the vertical (deposition) direction.

O'Kelly and Naughton (2005) also used WP to prepare uniform, medium HC clean sand specimens and study their inherent anisotropy. Their specimen reconstitution method involved (1) filling the annulus formed between the inner and outer molds with water, and (2) depositing saturated sand from a flask into the annulus. The final global void ratio (e) obtained with the method was within 2.6% of its target value. Three specimens prepared at identical e were subjected to the same isotropic mean effective stress (p') increase from 50 to 200 kPa to assess the method repeatability. Analysis of the stress-strain response of these three specimens showed that the major (ε_1), intermediate (ε_2), and minor (ε_3) principal strain variations as a function of p' were similar for all three specimens. Inherent specimen anisotropy was evaluated by conducting isotropic consolidation stages to mean effective stresses equal to 100 and 200 kPa. The strains on the ε_2-ε_3 plane were greater than the strains on the ε_1-ε_3 and ε_1-ε_2 planes by one order of magnitude. The observed anisotropy was described as a cross-anisotropy on the ε_2-ε_3 plane, which was attributed to the greater effect of densification due to tapping in the axial direction than in the horizontal direction. They also found that the level of inherent anisotropy decreases as D_R increases. O'Kelly and Naughton (2005) did not evaluate the uniformity of their specimens. Segregation was not an issue since they did not test sands with fines.

Among all the HC studies reviewed by the authors, only four studies were conducted on sands with fines (Al-Hussaini 1981, Koester 1992, Rolo 2003, Altun et al. 2005). Zdravkovic and Jardine and their co-workers used SD to reconstitutesilt specimens (Zdravkovic 1996, Zdravkovic and Jardine 1997, Zdravkovic and Jardine 2001).

Rolo (2003) conducted a series of HC tests on SD specimens of Ham River sand with Kaolin clay. His method consisted of (1) mixing sand, clay and water in a mixer, (2) transferring the mixture through a funnel that extended to the bottom of the annulus formed between the inner and outer molds, (3) raising the funnel as the slurry fills the annulus, and (4) allowing the specimen to settle for 6 h. Based on qualitative, visual inspection of specimens through a Perspex mold and quantitative FC evaluation of three 15 % clayey sand specimens, he reported that segregation was not observed and the FC distribution was uniform across the specimen height.

None of the aforementioned studies appear to have carried out a systematic evaluation to evaluate the uniformity of HC specimens in terms of density (or void ratio) variations, particularly in the case of HC specimens of sands with fines.

2.6 LIQUEFACTION

Liquefaction can be described as the loss of strength and excessive strain development due to excess pore pressure generation under undrained loading. Early liquefaction studies focused on sandy soils (Seed and Lee 1966, Lee and Seed 1967, Seed and Peacock 1971, Castro 1975). However, liquefaction of sands containing fines and silty soils were also observed during the 1964 Niigata, Japan, 1985 Chile and 1999 Adapazari, Turkey earthquakes.

Soil liquefaction is usually modeled according to one of the following two mechanisms: undrained instability (*UI*), or flow liquefaction as used in earlier studies, and cyclic mobility (Casagrande 1971).

Undrained instability (*UI*) is associated with the sudden loss of strength causing excessive deformation in the soil when the shear stress is larger than the undrained shear strength mobilized either at phase transformation (PT) or at critical state (CS). Undrained instability is usually associated with loose soil deposits (Castro 1975) and may be initiated by either static or cyclic loads (Kramer 1996). *UI* can happen in a very short time and cause significant deformations as in the case of Sheffield Dam or Lower San Fernando Dam (Kramer 1996). The large deformations are driven by the initial static shear stresses applied to the soil mass.

Cyclic mobility (CM) is the phenomenon that takes place during cyclic loading such as that imposed by earthquakes. Cyclic mobility occurs when the shear stress in the soil mass is less than the undrained shear strength mobilized at PT or CS. The deformation occurs in an incremental manner rather than suddenly. Cyclic mobility may be observed even in the densest soil deposits (Castro 1975)

2.6.1. Undrained Instability

According to the CS framework, soil elements consolidated to different initial mean effective stresses would reach, at large strains, the same critical state line (CSL) on the mean effective mean stress (p') vs. octahedral deviator stress (q) plane (Fig. 2.13) where p' and q are defined as follows:

$$p' = \frac{\sigma_1' + \sigma'_2 + \sigma_3'}{3} \tag{2.30}$$

$$q = \sqrt{\frac{1}{2}\left\{(\sigma_1 - \sigma_2)^2 + (\sigma_1 - \sigma_3)^2 + (\sigma_2 - \sigma_3)^2\right\}} \tag{2.31}$$

For the axi-symmetrical (triaxial) case, when $\sigma'_2 = \sigma'_3$, p' and q reduce to Eq.2.32 and 2.33, respectively, and the slope of the CSL is denoted as M ($= q/p'$).

$$p' = \frac{\sigma_1' + 2\sigma_3'}{2} \tag{2.32}$$

$$q = \sigma_1 - \sigma_3 \tag{2.33}$$

The isotropically consolidated samples A, B, C, D and E in Fig. 2.13a are assumed to have the same initial void ratio (or specific volume), but different p' before undrained TX compression. Samples C, D, and E initially show a contractive behavior (positive excess pore pressure build up). The contractive behavior up to the point marked by the X ends up with irreversible, sudden and large deformations accompanied by large excess pore pressure generation. Point X denotes the onset of static liquefaction (Ishihara et al. 1975) and represents the maximum local value of q for the first segment of the stress path. The locus of all points marked by X form the undrained instability surface (*UIL*) (Murthy et al. 2007) or flow liquefaction surface (Kramer 1996) in Fig. 2.13b. The soil state at this stage can be referred to as undrained instability state (UIS) since large deformations are triggered once this state is achieved (Murthy et al. 2007). As the stress path reaches the critical state line (CSL), the soil may mobilize the CS strength or exhibit additional dilative behavior. Samples D and E mobilize the critical state strength as soon as the stress path reaches the CSL. However, Sample C undergoes a change in behavior (from contractive to dilative) and an "elbow" shape is observed in the stress path. The point, where the change in behavior takes place, is referred to as the phase transformation (PT) point (Ishihara et al. 1975). The local minimum strength and PT typically take place at different locations. Alarcon-Guzman et al. (1988) focused on the minimum strength after UI and called that the quasi-steady state (QSS) strength of the soil. They also observed a small increase in pore pressure before the shear strength starts increasing.

Murthy et al. (2007) experimentally evaluated these states and concluded that the local minimum undrained strength at QSS and the minimum p' at PT do not happen necessarily at the same time. The increase in pore pressure observed by Alarcon-Guzman et al. (1988) after achieving the QSS strength is in agreement with this conclusion in that, the minimum strength is achieved right before there is a small increase in pore pressure, i.e. the smallest p'. The QSS occurs before PT and the difference between the two can be seen when axial strains are considered (Murthy et al. 2007). Due to their proximity, the distinction between the two may not be clear.

But, the undrained strength at QSS and at PT are virtually the same for practical purposes (Murthy et al. 2007).

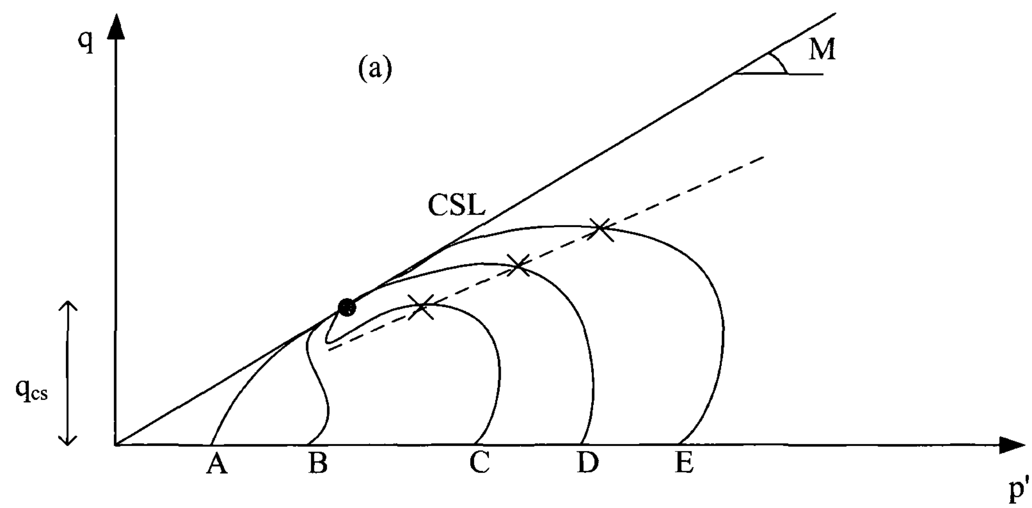

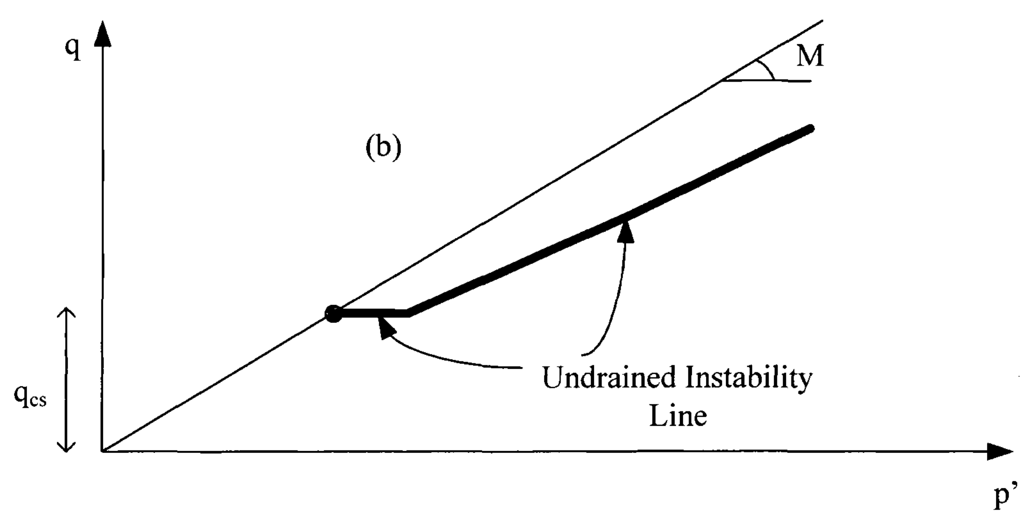

Figure 2.13. a) Undrained behavior of five specimens at the same void ratio under different effective isotropic consolidation stresses, b) Undrained Instability Line (*UIL*) (modified after Kramer 1996)

Samples A and B exhibit dilative behavior before they reach the CSL. Samples A and B do not show a strain softening response and develop strain hardening response due to the negative pore pressure generation as the strain increases. Considering the response of samples C, the local minimum undrained strength can happen at PT (q_{PT}). If the soil does not exhibit QSS behavior, then the minimum undrained strength will occur at critical state (q_{CS}) (Samples D and E).

In summary, UI may occur if the stress conditions fall into the shaded region in Figure 2.14a, which is defined by the UIL and either the q_{CS} or q_{PT}. Flow liquefaction in this region can be triggered by both cyclic and static loads (Kramer 1996).

Cyclic mobility may occur for stress combinations that fall into the region shown in Fig. 2.14b. Depending on the magnitude of the cyclic deviator stress applied and the initial static shear stress, the behavior of the soil may vary. Kramer (1996) defined three possible CM cases as shown in Fig.2.15.

The first case is when $q_{static} - q_{cyc} > 0$ (no stress reversals) and $q_{static} + q_{cyc} < q_{CS}$ (CS-strength not exceeded). In this case, the stress state never reaches the *UIS* and, with each loading cycle, the excess pore pressure generated during that cycle shifts the stress path to the left until the stress path reaches the CSL. At this point, the stress path moves up and down along the CSL. The stress path does not cross the *UIL* and excessive deformations are not likely to be observed. However, the drop in the mean effective stress and stiffness due to the pore pressure generation may cause some strain development in the soil.

For the second case (Fig. 2.15b), the stress conditions are $q_{static} - q_{cyc} > 0$ (no stress reversals) and $q_{static} + q_{cyc} > q_{CS}$ (CS strength may be exceeded briefly). In this case, the stress path may reach the *UIL* after a certain number of cycles. As soon as the *UIL* is reached, large strains may develop during a moment of instability. In the last case, (Fig. 2.15c), where $q_{static} - q_{cyc} < 0$ (stress reversals) and $q_{static} + q_{cyc} < q_{CS}$ (CS strength not exceeded), compressive and tensile loading are imposed.

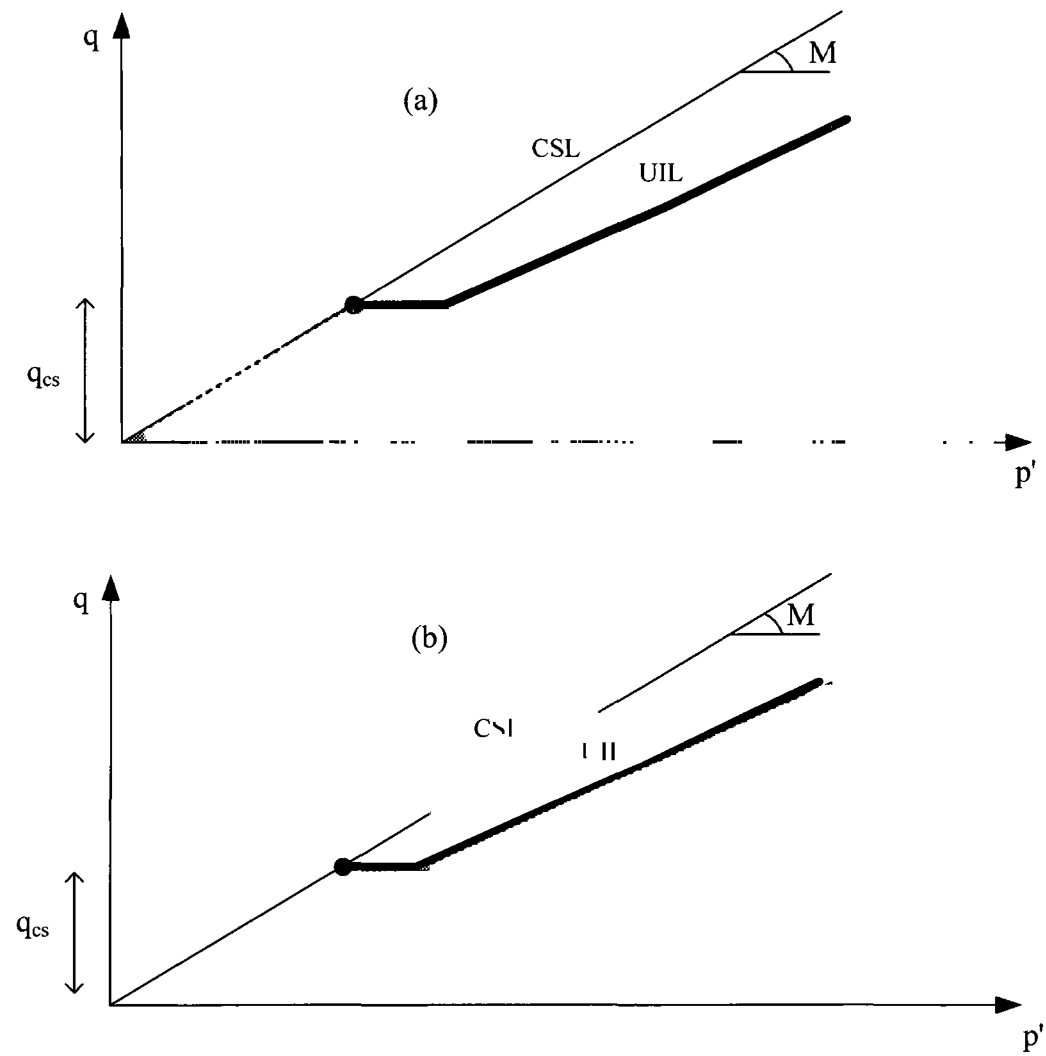

Figure 2. 14. Region prone to (a) undrained instability, and (b) cyclic mobility (modified after Kramer 1996)

Mohamad and Dobry (1986) and Castro and Poulos (1977) mentioned that for triaxial conditions, stress reversals increase the rate of pore pressure build-up and, thus, the stress path moves to the left relatively quickly. When the stress path reaches the CSL, it follows the darker solid line given in Fig. 2.15c, going through the origin twice for each cycle. In other words, zero effective mean stress may happen twice during one cycle. Kramer (1996) mentioned that when the mean effective stress becomes zero, the specimen does not have zero strength, since it will remain dilative until the critical-state strength is mobilized.

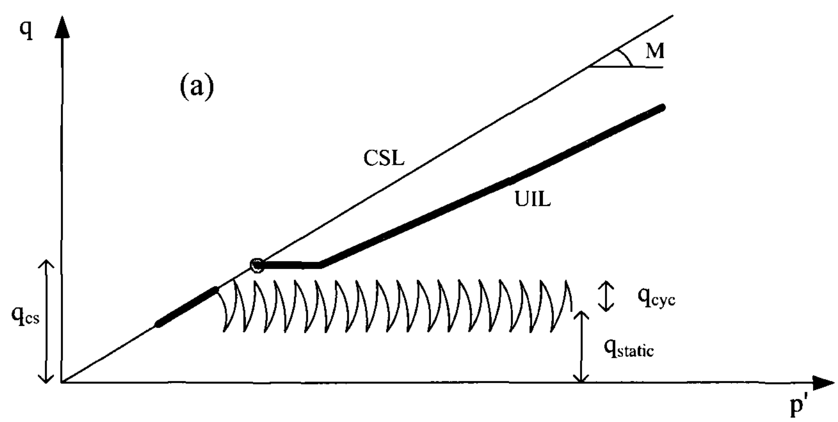

Figure 2.15a. The cyclic mobility when there is no stress reversals, and undrained strength is not exceeded

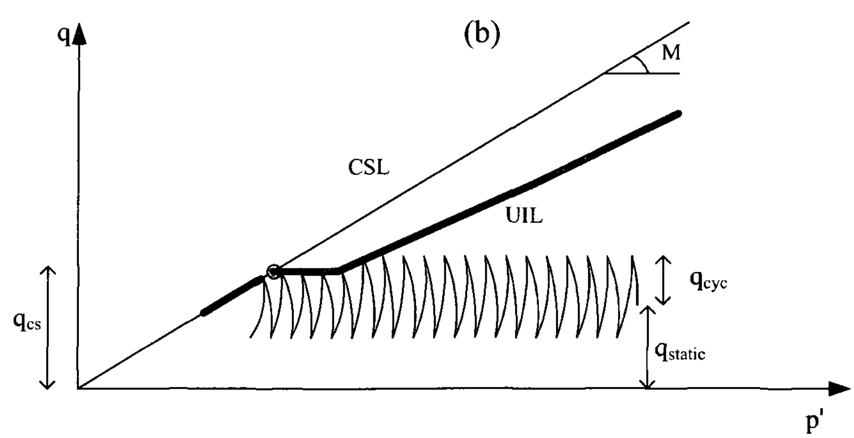

Figure 2.15b. The cyclic mobility when there is no stress reversals and steady state strength is exceeded briefly.

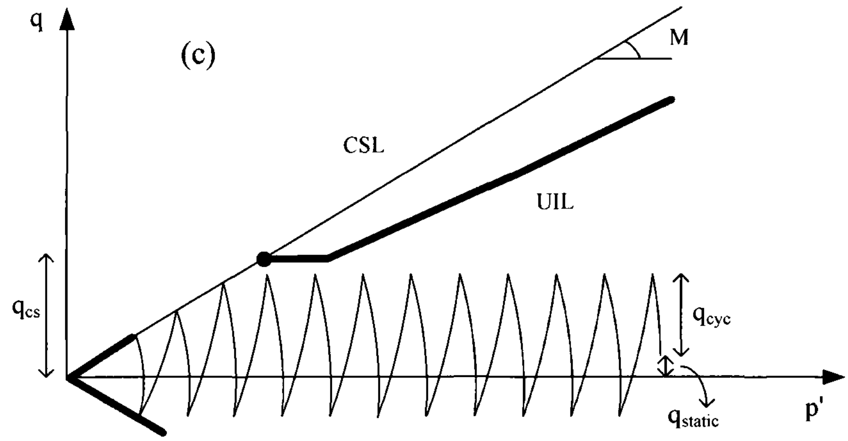

Figure 2.15c. The cyclic mobility when there is no shear stress reversals and steady state strength is not exceeded .

The assumption of FL and CM implicitly assumes that the monotonic undrained shear strength parameters such as q_{CS} and the *UIL* can be used to determine the cyclic behavior of soils. This assumption was shown to be valid with a series of undrained monotonic and cyclic tests (Vaid and Chern 1985, Mohamad and Dobry 1986, Alarcon-Guzman et al. 1988). The three mechanisms given in Fig. 2.15 indicate the importance of the initial static shear stresses prior to the cyclic stage. If the initial static shear stress is large, the soil state is close to the *UIS*, and development of temporary unstable behavior becomes more likely. Thus, the magnitude of both the cyclic shear stress and initial shear stress must be taken into account to properly evaluate the liquefaction response of soils.

2.6.2 Evaluation of Liquefaction Resistance under Cyclic Loads

The resistance of soils against liquefaction induced by cyclic loading usually has been evaluated in the laboratory by using cyclic triaxial (CT) and cyclic simple shear (CSS) tests. Although not as common, cyclic HC tests (sometimes referred to as torsional shear tests in the literature) also have been used to assess the liquefaction resistance of soils. CT and CSS tests were developed to simulate the simplified field stress conditions for level-ground scenarios such as those shown in Fig. 2.16. According to Fig.2.16a, for a soil element below level ground, K_0 conditions may be used to model anisotropic soil consolidation. The stress conditions in Fig.2.16a imply alignment of major and principal stresses in the vertical and horizontal directions, respectively. The effect of the change in the intermediate principal stress σ_2 is not considered for the conditions given in Fig.2.16a. Soil deposition for the element shown in Fig.2.16a may be approximated in the laboratory by an initial anisotropic consolidation stage with K_0 conditions. According to this simplified approach, horizontal shear waves propagate upward from the bedrock during an earthquake, and (1) generate shear stresses in the soil element above the bedrock, and (2) cyclically rotate the major and minor principal stresses every time the shear stress direction reverses. The shear stress direction changes continuously during the event of an earthquake (Fig. 2.16). The shear stress magnitude also varies during an earthquake. However, in the laboratory, the time history of the shear stress imposed during an earthquake is typically approximated by a series of uniform stress cycles (Kramer 1996). This approximation may involve application of a uniform cyclic shear stress magnitude of 0.65 τ_{max}, where τ_{max} is the maximum recorded shear stress during an earthquake, during an equivalent number of cycles that is determined in such a way that the seismic loading in the field and the uniform cyclic loading in the laboratory would generate the same excess pore pressure. For example, the simulation of an earthquake with a moment magnitude (M_w) of 7.5 would require 20 cycles (N_{eq}) of uniform loading in the lab (Kramer 1996).

Seed and Lee (1966) conducted a series of CT tests with the assumption that the CT test closely replicates the simplified stress conditions in the field as shown in Fig. 2.16a. The CT test involves the application of a varying cyclic deviator stress, σ_d, on the isotropically or anisotropically-consolidated specimens. However, anisotropic consolidation would be preferred over isotropic consolidation to better simulate the K_0 conditions given in Fig. 2.16a. During the cyclic stage of a CT test, the maximum shear stresses develop at a plane inclined by 45° from the horizontal in the specimen. The compressional deviator stress forces the major principal stress to be aligned in the vertical direction. As the deviator stress direction reverses, the major principal stress instantaneously reorients to the horizontal direction when q becomes negative. The maximum shear stress still remains at a plane 45° from the horizontal. Therefore, the stress conditions at the plane 45° from the horizontal are assumed to be close to the stress conditions of a soil element under a level ground during an earthquake. However, there are several significant limitations of this approach:

1. The major and minor principal stresses rotation is limited to a jump rotation of 90° during stress reversals ($q = 0$)
2. Only two planes (planes at 45° from horizontal) in the specimen are loaded with the maximum shear stress. Other potentially weaker planes in the specimen cannot be loaded with the maximum shear stresses. In other words, anisotropy in the soil cannot be properly assessed.
3. The effect of the intermediate principal stress σ_2, quantified by the parameter b, cannot be taken into account since the specimens are tested under axi-symmetric conditions.

Cyclic simple shear (CSS) test is an extension of the simple shear test described earlier. Application of horizontal cyclic shear stresses is intended to simulate earthquake loading on the soil element in the field. In general, CSS allows a closer replication of the field loading conditions than CT by partially eliminating the first and second limitations of CT. However, the CSS test also has some limitations such as:

1. In most CSS apparatuses, there are no complementary shear stresses on the vertical plane, which causes significant stress non uniformities in the specimens.
2. The major and minor principal stress rotations can cover a wider range than CT tests. Yet, they still cannot cover the full range of principal stress rotations experienced by a soil element in the field during cyclic loading.
3. Similar to CT tests, the effect of intermediate principal stress cannot be fully investigated, since CSS tests were designed to impose plane strain conditions where b is between 0.3 and 0.5.
4. Undrained CSS testing is complicated; the pore pressure response of the specimens cannot be investigated as easily as it would be with CT testing.

As mentioned previously, CT and CSS tests are conducted to simulate the simplified field stress conditions for a level ground (Fig. 2.16a). However, these two tests fail to simulate the deposition conditions for a soil element under a sloped ground, Fig. 2.16b. For the sloped ground conditions, initial static shear stress acts upon the soil element following the deposition, and the major and minor principal stresses are not in vertical and horizontal directions, respectively. Ishihara (1983) showed that during an earthquake shaking, two shear stresses components act simultaneously, tangential horizontal shear stresses and the normal stress difference $(\sigma_v - \sigma_h) / 2$. According to him, this simultenous application of shear stresses happens in such a way that initial principal stress rotation due to sloped ground conditions remains constant during ground shaking. He also added that this type of stress configuration may be valid not only for sloped ground conditions, but also under the foundations of superstructures.

Considering a circular footing resting on a saturated sand deposit (Fig. 2.17), a soil element at 1-m depth would have approximately 20 kPa (σ_1) overburden stress, and 8 kPa horizontal stress ($\sigma_2 = \sigma_3$) assuming $K_0 = 0.4$ and $\gamma_{sat} = 20$ kN/m^3. For this case, the additional stresses imposed by the footing load may be approximated using Eq.2.34 – 37 given by Das (1997) for an elastic medium,

$$\Delta\sigma_z = q(A' + B') \tag{2.34}$$

$$\Delta\sigma_r = q(2\upsilon A' + C + (1 - 2\upsilon)F) \tag{2.35}$$

$$\Delta\sigma_\theta = \sigma_2 = q(2\upsilon A' - D + (1 - 2\upsilon)E) \tag{2.36}$$

$$\Delta\tau_{rz} = \tau_{zr} = qG \tag{2.37}$$

where υ = poisson's ratio for the sand deposit (assumed to be 0.45), q = footing pressure, and A', B', C, D, E, F, and G are functions of s/b and z/b (Fig.2.15). If z/b = 1, these stress components are calculated as in Table 2.2 as a function of s/b.

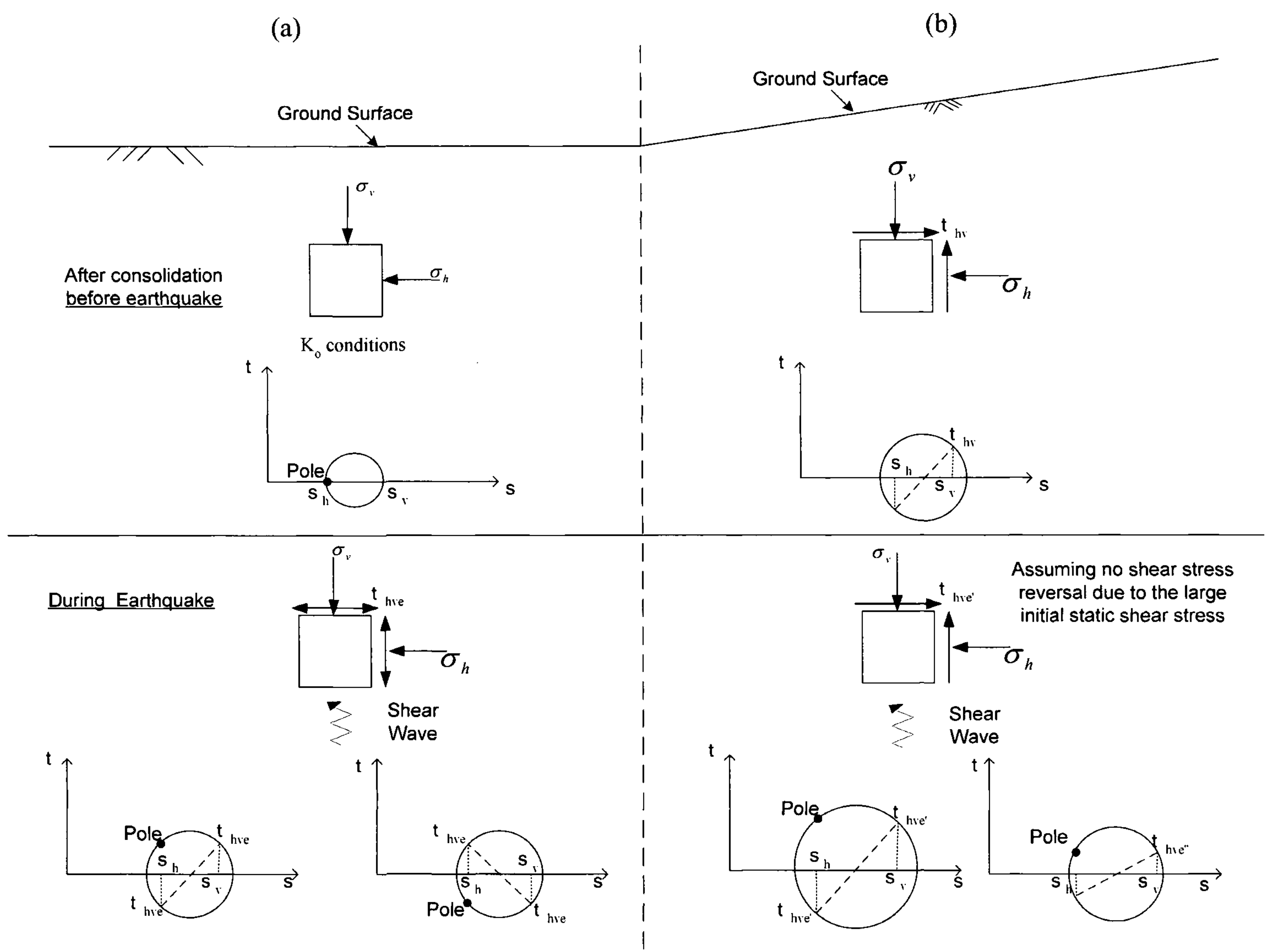

Figure 2.16. Simplified field stress conditions after deposition and during an earthquake

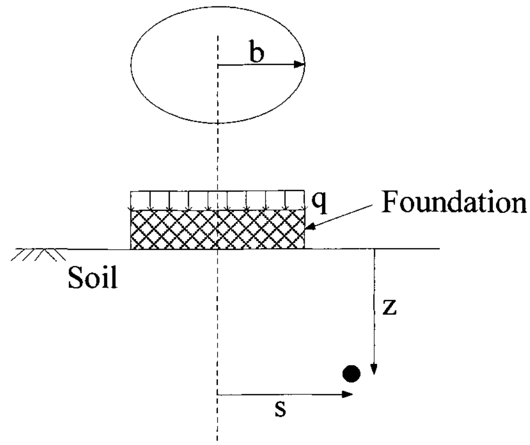

Figure 2.17. Circular footing resting on a saturated sand deposit.

Table 2. 2.Stresses induced due to a circular footing loaded with q = 100 kPa

	Stresses created due to addition of a circular footing loaded with q = 100 kPa				
	s/b = 0	s/b = 0.4	s/b = 0.6	s/b = 1	s/b = 2
$\Delta\sigma_z$ (kPa)	64.6	59.1	52.5	33.2	4.2
$\Delta\sigma_r$ (kPa)	10.1	10.4	11.4	13.9	10.0
$\Delta\sigma_\theta$ (kPa)	10.1	8.9	7.8	4.7	0.9
$\Delta\tau_{rz}$ (kPa)	0.0	10.3	14.6	18.2	6.4

Table 2.3 shows the final stress state after the footing load is taken into account. Under the centerline of the footing, the stress state is axi-symmetric, i.e. α and b are zero. However, α and b increase as the distance from the centerline increases. For this stress state, addition of cyclic earthquake loadings would further (1) change the shear stresses at any point in the ground, and (2) rotate the principal stresses.

Table 2.3.Final stress conditions on soil elements below a circular footing

	Final stress state on soil elements under the footing due to surcharge and footing loads				
	s/b = 0	s/b = 0.4	s/b = 0.6	s/b = 1	s/b = 2
$\sigma_{z\text{-}f}$ (kPa)	89.6	84.1	77.5	58.2	29.2
$\sigma_{r\text{-}f}$ (kPa)	18.1	18.4	19.4	21.9	18.0
$\sigma_{\theta\text{-}f}$ (kPa)	18.1	16.9	15.8	12.7	8.9
$\tau_{rz\text{-}f}$ (kPa)	0.0	10.3	14.6	18.2	6.4
α	0.0	8.5	12.6	19.3	19.7
b	0.00	0.02	0.06	0.20	0.45

Therefore, for a realistic simulation of this real field application, α and b should be considered in the laboratory testing. At this point, one might argue that major principal stress decreases away from the centerline, although α and b increase, and, thus, more critical location is below the centerline. Many researchers have shown that the undrained shear strength of the sandy soils decreases with the increase in α (Broms and Casparian 1965, Symes et al. 1984, Uthayakumar and Vaid 1998, Sivathayalan and Vaid 2002). Therefore, the more critical location may be away from the centerline, even though the major principal stress magnitude is less compared to the one below the centerline.

With CT and CSS tests, the sloped ground conditions and even the simplified circular footing case on level ground can not be simulated. Considering this inadequacy and also the inherent limitations of CT and CSS tests, cyclic HC tests have gained more popularity for the investigation of the effect of cyclic loads on the soil behavior (Ishihara and Yamazaki 1983, Tatsuoka et al. 1984, Ishihara et al. 1985, Tatsuoka et al. 1986, Koester 1992, Altun et al. 2005). With cyclic HC testing, circumferential shear stresses can be developed in the specimen by applying a torque at the bottom or top of the specimen.

Principal stress rotations can be simulated prior to or during the cyclic loading through the independent application of torque, i.e., shear stress application. The stress conditions generated in the specimen, i.e., σ_1, σ_2, σ_3 and α are by far more versatile compared to CT and CSS. The shear stress developed in the specimen is assumed to be constant across the wall thickness and the height of the specimen over the middle part of the specimen, which assists addressing the anisotropy in the specimen during cyclic loading. Therefore, cyclic HC testing is a versatile testing method to more realistically simulate field stress conditions.

The onset of liquefaction for CT, CSS, and cyclic HC tests has been commonly characterized by either cyclic stress or cyclic strain approach[1]. Only the cyclic stress approach is discussed hereafter. According to this approach, a uniform cyclic deviator stress is applied on the specimen with a certain frequency (Seed and Lee 1966) and the specimen response is determined. The cyclic stress approach, in simple terms, involves finding the cyclic resistance of the soil in the laboratory and comparing it to the cyclic stresses observed in the field during an earthquake. Based on CT tests, Seed and Lee (1966) concluded that the following factors influenced the cyclic resistance of sands:

1) Initial confining pressure
2) Cyclic deviator stress magnitude
3) Relative density of the specimen
4) The number of deviator stress cycles.

In addition to these four factors, initial shear stresses in the specimen after the consolidation, quantified by K_0, (Ishibashi and Sherif 1974), the fabric in the specimen induced by the specimen preparation method (Mulilis et al. 1977, Tatsuoka et al. 1986),

[1] The cyclic strain approach involves applying uniform shear strain cycles on the specimen.

the stress-strain history and the type and the gradation of the soil (Mulilis et al.1977) were shown to impact the cyclic behavior of sandy soils. Seed and Lee (1966) also investigated the effect of the cyclic loading frequency for the range of 1/6 to 4 Hz, and concluded that the frequency effects on the cyclic behavior can be ignored when compared to the effect of the aforementioned factors.

According to the cyclic stress approach, the liquefied state of the soil, for a given p' and uniform deviator stress cycles, occurs when (1) the double amplitude (DAM) strain reaches the failure strain, or (2) induced excess pore pressure, Δu, is equal to the initial effective mean stress, p'. The first state criterion requires a failure strain to be defined (5 % DAM, 10 % DAM, 20 % DAM etc.). The second state criterion requires monitoring the pore pressure response throughout the cyclic undrained test. According to this criterion, the soils are expected to develop zero effective stress when the excess pore pressure equals to the initial p'. Lee and Seed (1967) observed that the loose soils usually exhibit very large strains at virtually the same time as the excess pore pressure reaches p'. In other words, the developments of the large strain and large excess pore pressure are almost coincident. Therefore, for loose soils, two state criteria indicate the same number of cycles for the liquefied state. However, dense sands may undergo as large strains as predefined failure strain, when p' is always greater than the excess pore pressure.

Regardless of the liquefaction definition used, the purpose is to find the number of cycles to reach the liquefied state. Then, in order to obtain the liquefaction resistance of the soil, the same soil with the same D_R is tested again under a different cyclic deviator stress. After testing the soil under about four different cyclic deviator stresses, the measured number of cycles that constituted the liquefied state, are plotted versus the cyclic deviator stress magnitude. Based on this plot, the cyclic stress state that brings the soil to the liquefied state for a predetermined number of cycles (20 for the simulated earthquake with a $M_w = 7.5$) is considered to be the cyclic resistance of the soil.

As mentioned before, the cyclic stress approach requires conducting different tests with different cyclic deviator stress magnitudes at the same p'. In an effort to represent the stress state in one term that considers both cyclic deviator stress magnitude and p', Seed and Peacock (1971) defined cyclic stress ratios (CSR) for CT and CSS testing conditions as follows:

1) The maximum ratio of the shear stress developed to the normal stress $\left(\dfrac{\tau}{\sigma'_N}\right)$,
2) The maximum ratio of the change in shear stress on any plane to the normal stress on the same plane $\left(\dfrac{\Delta\tau}{\sigma'_N}\right)$,
3) The ratio of maximum shear stress induced to the mean principal stress on the sample before cyclic loading $(\tau_{\max} / p')$, and
4) The ratio of the maximum change in the shear stress on any plane during cyclic loading to the mean principal stress before cyclic loading $(\Delta\tau_{\max} / p')$.

Later, Ishibashi and Sherif (1974), who conducted cyclic HC tests, added two more possible definitions for CSR as $(\tau_{oct,\max} / \sigma_{oct})$ and $\Delta\tau_{\max} / [(1/2)(\sigma_1 + \sigma_3)]$. Among all these definitions, $(\Delta\tau_{\max} / p')$ seems to be applicable for all CT, CSS and cyclic HC testing conditions and allows comparing the results from different tests. Furthermore, for

DHC testing, Ishibashi and Sherif (1974) showed that by using $CSR = (\Delta\tau_{\max} / p')$, the effect of K_0 can be considered implicitly. The definition of $CSR = (\Delta\tau / p')$ is equivalent of $(\sigma_d / 2p')$ for CT test conditions, and $(\Delta\tau_{\max} / p')$ for both CSS and cyclic HC tests. However, keeping all other factors equal, $CSR = (\Delta\tau_{\max} / p')$ measured at failure may not be equal for CT, CSS and cyclic HC tests. Ishihara and Yasuda (1975) claimed that if $(\Delta\tau / p')$ is used as a CSR, CT and cyclic HC tests may yield similar cyclic strengths. However, Tatsuoka et al. (1986) found out that this may not always be true. They observed that for dense Sengenyama Sand, the cyclic strengths obtained as $(\sigma_d / 2p')$ from the CT test and $(\Delta\tau_{\max} / p')$ from the cyclic HC test were not the same. Yamashita and Toki (1993) added that the specimen preparation method also impacts cyclic resistance differences between CT and cyclic HC tests when $(\Delta\tau_{\max} / p')$ is the reference. Bhatia et al. (1985) compiled CT, CSS and cyclic HC test results in the literature, and claimed that even when $CSR = (\Delta\tau_{\max} / p')$ is used as a reference, sandy specimens exhibit different liquefaction resistances when tested with different testing methods. Although they observed a large scatter in liquefaction resistance data obtained from even the same testing methods, they claimed that soils exhibited the largest liquefaction resistance under the CT testing, the smallest liquefaction resistance under the CSS testing, and liquefaction resistance of somewhere in between under the cyclic HC testing. Therefore, using $(\Delta\tau_{\max} / p')$ may not indicate similar liquefaction resistances obtained in CT, CSS or cyclic HC tests, even though using this ratio is the most generic way of representing the cyclic test results. Consequently, a superior testing method of cylic HC testing should be conducted instead of conducting CT or CSS due to the aforementioned limitations of the latter two. $\Delta\tau_{max}$ can be defined as in Eq. 2.38 for HC testing, and does not take into account the effect of σ_2:

$$\Delta\tau_{max} = \frac{\sigma_1 - \sigma_3}{2} \tag{2.38}$$

The octahedral deviator stress q (Eq. 2.39) better represents the three dimensional deviatoric stress state:

$$q = \sqrt{\frac{1}{2}\left((\sigma_1 - \sigma_3)^2 + (\sigma_1 - \sigma_2)^2 + (\sigma_2 - \sigma_3)^2\right)} \tag{2.39}$$

Combining Eqs. 1.1 and 2.39, q can be written in terms of *b*, as given in Eq. 2.40.

$$q = \sqrt{(b^2 - b + 1)}(\sigma_1 - \sigma_3) \tag{2.40}$$

As mentioned previously, one of the significant components of the cyclic stress approach is the definition of the failure strain. The earliest cyclic strength tests were CT tests, and the strain component of concern was the axial strain (Seed and Lee 1966, Lee and Seed 1967). Tatsuoka et al. (1986) conducted both CT and HC tests. They defined the initiation of liquefaction at 2 %, 5 %, and 10 % DAM axial strain for CT tests, and at 3 %, 7.5 %, and 15 % DAM shear strain for DHC tests. Cyclic simple shear conditions were simulated in their cyclic HC tests. Yamashita and Toki (1993) similarly adapted failure strains of 5% DAM axial strain for CT tests, and 7.5% DAM shear strain for cycli HC tests. Both Tatsuoka et al. (1986) and Yamashita and Toki (1993) did not investigate the principal stress rotation during the cyclic loading, therefore the strain components of concern were simply shear strains. More recently, Koester (1992) and Altun et al. (2005) conducted cyclic HC tests to simulate cyclic simple shear as well. Altun et al. (2005) defined liquefaction at 10% DAM shear strain. However, as the principal stresses are rotated during cyclic loading, a strain component that reflects the three dimensional stress state should be used. For example, Ishihara et al. (1985) used the 2.5 % single amplitude deviator strain, ε_1-ε_3, to define the initiation of liquefaction under principal stress rotation. The deviator strain definition used by Ishihara et al. (1985) is more reasonable than using axial strain or shear strain for a generalized stress state during cyclic loading. However, this definition still lacks the intermediate principal strain effects. Therefore, the use of a more general strain component such as the deviatoric strain (ε_q) defined as in Eq. 2.41 is may be more appropriate to evaluate liquefaction under the most generalized stress state during cyclic loading,

$$\varepsilon_q = \frac{2}{\sqrt{6}}\sqrt{(\varepsilon_1 - \varepsilon_3)^2 + (\varepsilon_2 - \varepsilon_3)^2 + (\varepsilon_1 - \varepsilon_2)^2} \tag{2.41}$$

3. EXPERIMENTAL PROGRAM

3.1. DYNAMIC HOLLOW CYLINDER APPARATUS

Advanced testing of geomaterials requires accurate control of loads or deformations. Recent advances in the manufacturing of testing equipment have eliminated the role of the operator in modern systems. Most tests are conducted via closed loop control mechanisms, which may involve servo hydraulic or servo pneumatic systems.

The closed-loop control system of the dynamic HC apparatus used in this study has five main components: (1) HC software, (2) high-speed data acquisition system (DAS), (3) servo valves, (4) vertical and horizontal actuators, and (5) load, pressure and displacement transducers. Air pressure is used as the pressure source for the HC apparatus. The supplied air pressure level is maintained at 950 kPa. If the volume of air used becomes too large, especially for cyclic loading with a frequency of 1 Hz, the pressure level may drop below 950 kPa. To overcome this shortcoming, a pressure booster was used, which amplifies the air pressure up to 950 kPa and keeps it steady even for 1 Hz cyclic loading.

When active, the HC software sends a signal to the DAS with the required transducer load or pressure levels. Then, the DAS activates the servo valves where the amount of released pressurized air is controlled (Fig. 3.1). The air pressure released by the servo valves is used to activate the actuators or used to apply boundary pressures. Then, the applied loads or pressures are measured by the load or pressure transducers. The difference between the measured output and the requested input is registered as error. At this point, the closed-loop control system reduces the error to a minimum as follows: (1) the DAS calculates the error, and sends a signal to the appropriate servo valve to readjust the supplied air pressure, (2) the servo valve corrects the amount of pressurized air going into the actuator, and (3) another reading is obtained by the transducer. This cycle is repeated until the error is minimal and takes place at speeds that can not be observed by the operator (servo actuator frequency up to 70 Hz are used). In order to optimize this process over a wide range of applications, a three term auto controller with proportional (P), integral (I), and derivative (D) elements is used. The variation of each controller or their combination along with the speed and power of the servo valves allow running many different types of tests.

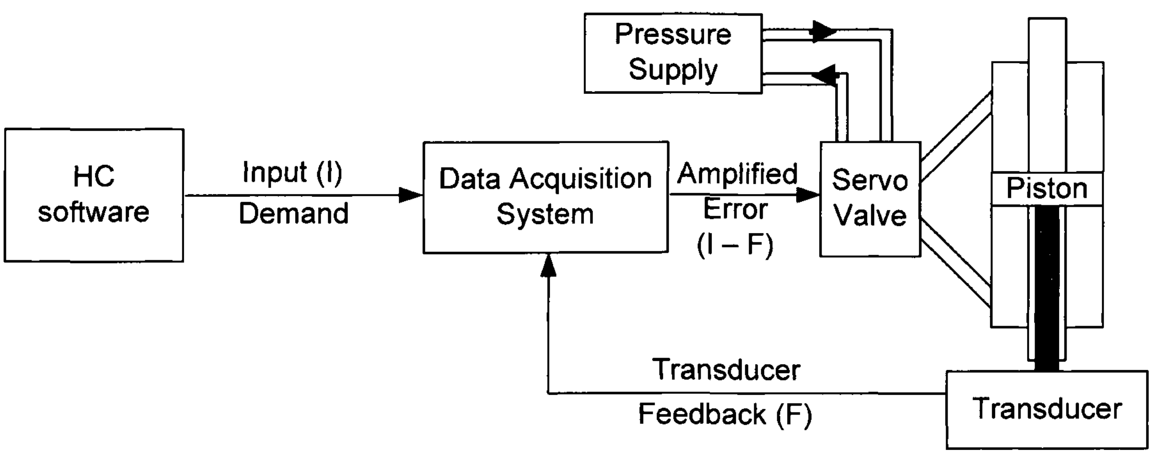

Figure 3.1 Closed-loop control system of the HC apparatus.

Even though the system can conduct various types of tests, there may still be some issues such as:

1) Pressure supply flow / charge rate limiting the velocity and, thus, the upper frequency limit of the actuator. Fig. 3.2 shows the largest force attainable at a given frequency for a sinusoidal loading.

2) Flow force / capacity ratio, which can cause mechanical/supply pressure noise, when high, especially in stiff load frames.

3) Frame stiffness, which can be reduced to lower the supply pressure noise, but then the system has difficulty in adapting to rapidly changing conditions such as sudden specimen failure.

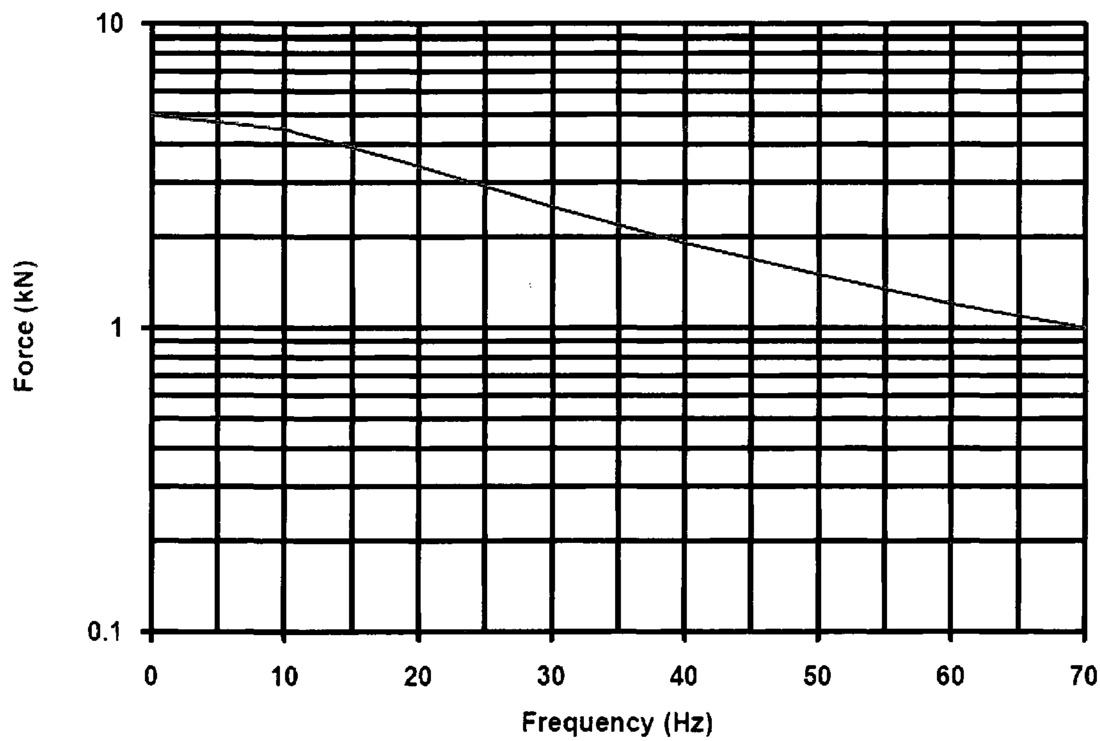

Figure 3.2. Maximum possible load amplitude for a sinusoidal loading as a function of frequency (Wykeham Farrance Manual, 2004)

The servo valves apply small currents to open and close the control spool of the valves and, thus, control the flow of air pressure. With servo valves, large rates of work can be done simply by controlling the electrical current input, since servo valves have very high power amplification.

The DAS provides servo-feedback loading control electronics and timing functionality, and acquires data from transducers. The current number of available transducer input channels in the system is 19. The DAS has a data acquisition resolution of 20 bit, data acquisition speed of 5 kHz, and data transfer rate of 20 Mb/s. The closed-loop control system is conducted by the DAS through PID values before a test starts. As soon as a test is initiated (saturation stage), the system is mainly controlled by the computer. Five channels are used to conduct the HC tests. These channels are used for the following parameters: (1) outer cell pressure (OP), (2) inner cell pressure (IP), (3) back pressure (BP), (4) vertical actuator position, and (5) horizontal actuator position, which are all independently controlled by the DAS and HC software. In the pre-test mode (specimen preparation stage), these parameters can be manually changed by the operator using the digital control panel provided in the HC software. Once the test starts, the closed loop control system manipulates these parameters to obtain the required target stress parameters.

The vertical actuator is coupled with the bottom pedestal of the specimen and can either push or pull the specimen in the vertical direction. The stroke available for the vertical actuator is 50 mm. The set-up of the system allows control of axial strains (in the vertical direction) of up to 18 % (for 200 mm high specimens). The span covered by the vertical actuator is measured by a displacement transducer with 0.1-mm resolution (Table 3.1). The vertical actuator motion is controlled by one of the servo valves.

The horizontal actuator also is mechanically coupled with the bottom pedestal of the specimen, and can rotate the bottom of the specimen by 90°. This rotation corresponds to a 100-mm displacement of the horizontal actuator. The horizontal actuator resolution is 0.1 mm displacement or 0.09° rotation at the base of the specimen (Table 3.1). The vertical and horizontal actuators can be controlled independently.

The internal load cell is mechanically attached to the top cap of the specimen and also to three internal steel rods that are fixed to the machine base (Fig. 3.3). During the test, the load cell is submerged in the cell water, and operates free from the effects of water pressure. Thus, when the cell pressure is varied, the load cell reading is not affected by cell pressure changes. When the specimen is formed and one of the actuators moves either in the vertical or horizontal direction, the load cell reads the load transmitted by the specimen in response to the actuator motion. The load cell can read both the vertical load and the torque applied to the specimen. The limit and resolution of the load cell are 10 kN and 1 N for the vertical load, respectively, while they are 300 N.m and 0.1 N.m for the torque, respectively.

As mentioned previously, the servo valves supply the air pressures for the OP, IP and BP. The supplied pressures are measured by pressure transducers after the pressurized air leaves the servo valve. Then, the pressurized air enters into the air-water interface (A/W) that is submerged in a water-filled chamber (Fig. 3.3). As the air pressure increases, the A/W interface transmits the pressure to the water with negligible losses. The system has three A/W interfaces (outer cell, inner cell, and back pressure lines) and they perform independently. The pressure transferred by each A/W interface is measured by a separate pressure transducer located between the servo valve and the A/W interface on the air line.

One additional pressure transducer measures the specimen pore water pressure nearby the base of the specimen. These pressure transducers are capable of measuring pressures as high as 1000 kPa and have a resolution of 1 kPa (Table 3.1). The pressure transducer readings were thoroughly checked with a standard pressure transducer calibrated with a dead weight tester by placing the transducers in line with the standard transducer. All pressure transducers are zeroed at the mid-height of the specimen before each test as follows: (1) air pressure is reduced to the lowest value by using the digital control panel in the HC software, and zeroed at that value, (2) the tubing that connects the A/W interface to the cell chamber, where the specimen is installed, is flushed with de-aired (DA) water, (2) the end of the tubing is sealed and held at the mid-height of the specimen, (3) pressure is increased to 7 kPa and the transducer reading is zeroed. Pressure offset of 7 kPa obtained by means of zeroing the transducer accounts for the elevation head difference between the outlet (water side) of the A/W interface and the mid-height of the specimen.

The IP and BP lines are connected to two volume change transducers with capacity of 100 ml and resolution of 0.1 ml (Table 3.1) so that volume changes of both the inner cell cavity and specimen volume changes can be measured throughout the test. The volume change transducers have two internal chambers inside them that are separated by belloframs. As water goes into one of the chambers, the linear variable differential transformer (LVDT) attached to the bellofram moves accordingly, and the LVDT displacement is converted to a volume reading. In order to eliminate gravity effects due to the internal piston weights, the volume change transducers are placed in the horizontal direction so that, the LVDT moves horizontally (Fig. 3.3). DA water can be diverted into either one of the two internal chambers using a three-way valve. Thus, the LVDT can move in two opposite directions so that, despite their 100-ml capacity, the volume change measurements can be made indefinitely for as long as the direction of the LVDT movements are changed as they get close to the LVDT limits. The membranes in the A/W interfaces are half inflated at the beginning of each test to allow for both expansion and contraction of the specimen and inner cell during the tests. The flow of water into or out of the specimen also happens in the same manner. However, there is a solenoid valve on the BP line between the volume change transducer and the specimen that may be used block the water flow upon a simple command from the HC software.

Accuracies for all transducers used in the HC apparatus are given in Table 3.1. Accuracies were determined as the ratio of the maximum deviation between the measured value and the actual values for a given calibration curve. Each transducer was checked with a special set up for their operational range rather than their capacity. Some error may arise due to the nature of the set up that may increase the accuracy (more error) for the transducer considered. Therefore, the accuracies reported in Table 3.1 may be considered conservative for the instruments used.

Table 3.1 Transducers used in the dynamic HC apparatus and their properties.

Component	Capacity	Resolution	Accuracy* (%)
Vertical Actuator Displacement Transducer	50 mm	0.1 mm	2
Horizontal Actuator Displacement Transducer	100 mm (90°)	0.1 mm (0.09°)	4
Load Cell, Vertical Load	10 kN	1 N	1
Load Cell, Torque	300 Nm	0.1 Nm	2
Pressure Transducers	1000 kPa	1 kPa	1
Volume Change Transducers	100 ml	0.1 ml	1

*Accuracy: The ratio of the error between the actual value and the measured value to the maximum value checked.

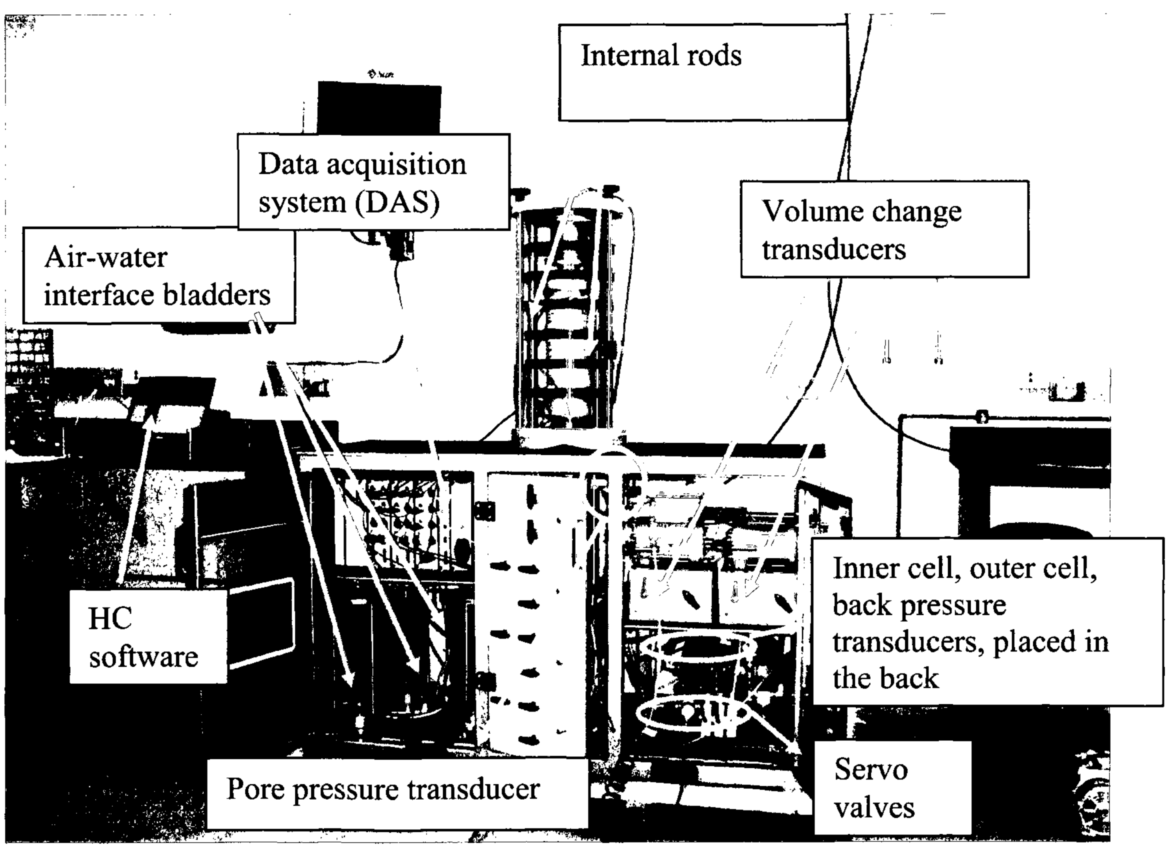

Figure 3.3.Dynamic HC apparatus and its components

3.2 MATERIALS

The sand used in this study is a commercial silica sand produced by U.S. Silica Inc. (Ottawa, IL) commonly known as graded Ottawa sand (ASTM C 778). Ottawa sand has round to subround particles and its basic index properties and grain size distribution are given in Table 3.2 and Fig. 3.4, respectively.

Table 3.2. Properties of the sand and silt used.

	Ottawa sand	Silt
Mean grain size, D_{50}(mm)	0.40	0.02
Coefficient of uniformity, C_u	1.67	7.5
Specific gravity, G_s	2.65	2.65
e_{max} (ASTM D 4254-Method B)	0.495[a]	N/A
e_{min} (ASTM D 4253-Method 1A)	0.767[a]	N/A
USCS Classification	SP	ML
SiO_2 (%)	99.7[b]	99.8[b]
Fe_2O_3 (%)	0.02[b]	0.04[b]
Al_2O_3 (%)	0.06[b]	0.05[b]

[a]Carraro (2004), N/A = not available
[b]U.S. Silica (2007)

The NP silt used in this study (#106 Sil-Co-Sil) is also produced by U.S. Silica, Inc. and its basic properties are provided in Table 3.2. The grain size distribution of the NP silt is given in Fig. 3.2, which also includes the grain size distribution curves for the materials tested by determined by Carraro (2004). Fig. 3.4 indicates that the soil samples used in both studies are identical in terms of their grain size distributions.

Quartz is the major mineralogical constituent of both Ottawa sand and NP silt materials tested.

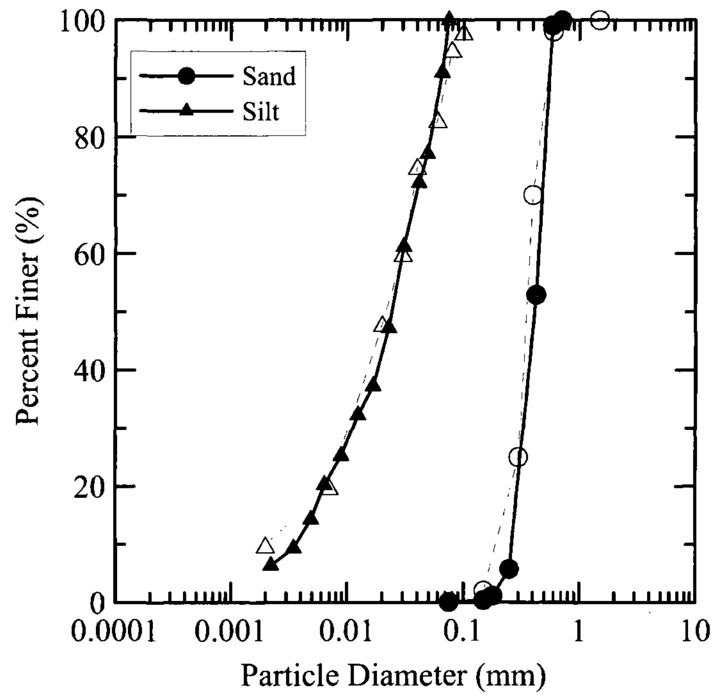

Figure 3.4. Particle size distribution curves for sand and silt tested (samples tested by Carraro (2004) are shown with open symbols).

3.3. DETERMINATION OF MAXIMUM VOID RATIO BY SLURRY DEPOSITION METHOD

As mentioned in section 2, relative density is one of the factors that affect the cyclic resistance of coarse grained soils such as clean sands and gravels as well as transitional soils such as silty and clayey sands. Accurate determination of the relative density requires measuring the minimum and maximum void ratios using appropriate procedures. The method used to determine e_{min} and e_{max} should reproduce the field deposition conditions considered. The method described in ASTM D 4253 allows using wet methods to determine e_{min}, which may simulate the maximum density conditions in alluvial deposits. However, e_{max} measured using dry samples as specified by ASTM D 4254 may not be appropriate to evaluate the e_{max} of soil deposits formed underwater. To overcome this shortcoming, the SD method of e_{max} determination described by Carraro and Prezzi (2008) was used to determine e_{max} in this study.

The SD maximum void ratio was obtained by allowing sand or silty sand to settle in an assembly of acrylic collar and mold filled by the slurry of sand-silt-water. The acrylic mold and collar have the inner diameter of 45 mm, and heights of 45 mm and 48 mm, respectively. The mold is sealed at the bottom by a smooth aluminum plate. The collar is placed on the mold and adhesive tape is used to seal the mold-collar connection. The assembly of plate, mold and collar is placed on a rubber mat to minimize the impact during final placement of the entire assembly on the counter top. Dry sand and silt are thoroughly mixed. The amounts of sand and fines required to fill the mold are tentatively determined based on the maximum void ratio of the clean sand and the target fines content. The mold is filled with de-aired water and the dry, homogeneous mixture of sand and silt is slowly pluviated into the water in the mold. Then, more de-aired water is added to fill the collar, and a rubber stopper with a valve is placed on the collar (Fig. 3.5). The slurry is mixed by turning the whole assembly upside down several times. Then, the assembly is gently placed on the rubber mat; valve is opened and more water is added to eliminate air bubbles. This procedure is repeated until all visible air bubbles are eliminated.

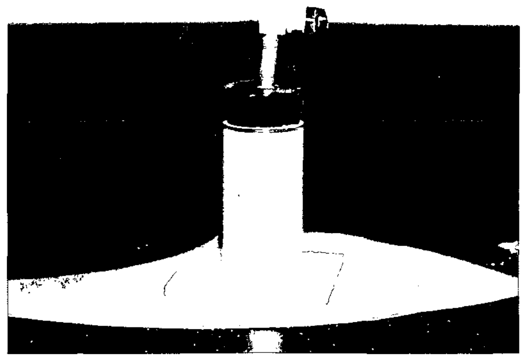

Figure 3.5. Assembly used to determine the slurry deposition e_{max}

After the slurry is homogenized and the air bubbles are removed, the assembly of aluminum plate-mold-collar-valve is placed on the rubber mat and the mixture is allowed to settle in the mold for 20 minutes. Then, the valve on the rubber stopper is opened, and the rubber stopper is gently removed. The excess fines slurry (in the case of silty sands) or clean water (clean sand) that remains in the collar is removed by applying a small suction. At this stage, the homogeneous mixture of sand and silt with a thin layer of silt on top should not exceed the mold height by more 2-3 mm. The amount of sand and silt used at the beginning may be adjusted in subsequent determinations to achieve this condition. Next, the adhesive tape between the collar and mold is removed and the collar is carefully taken away. Using a spatula, the material above the mold is trimmed in two strikes from the center to the mold edge. Finally, the fines content and the void ratio of the homogenous sand-silt mixture in the mold are determined by (1) placing the saturated sample of sand and silt in the oven for 24 h, (2) weighing the dry mixture of sand and silt, (3) sieving the mixture through the No. 200 sieve, and (4) collecting and weighing the material retained on the No. 200 sieve (sand). Details of the method are provided in Carraro and Prezzi (2008). The results of the SD e_{max} determinations carried out in this study are compared with the e_{max} obtained with ASTM D 4254 (method B) and discussed later in section 4.

3.4 PREPARATION OF HOLLOW CYLINDER SPECIMENS

In this study, an alternative version of the SD method of reconstitution of solid TX specimens of sands with fines proposed by Carraro and Prezzi (2008) was developed to reconstitute homogenous HC specimens of clean and NP silty Ottawa sands with a high initial degree of saturation. The HC specimens formed had nominal outer diameter, inner diameter and height equal to 100 mm, 60 mm, and 200 mm, respectively.

Briefly, the proposed SD technique consists of (1) forming a slurry by mixing DA water with a homogenous dry mixture of sand with or without fines, (2) transferring the slurry into the annulus between two polycarbonate concentric mixing tubes (CMTs) with length and thickness of 711mm and 3mm, respectively (the outer diameter of the inner and outer tubes were 70 mm and 95 mm, respectively), (3) placing the CMTs filled withthe saturated homogenous slurry into the annulus space between the inner and outer HC molds, and (4) carefully raising the CMTs to allow the slurry to deposit inside the HC mold annulus. By minimizing as much as possible the disturbance imparted by tube withdrawal, this procedure can produce loose specimens of clean and NP silty sands with D_R of around 25%. Denser specimens can be prepared by tapping the sides of the outer mold. The detailed steps of the proposed method are described below.

Installation of the HC base pedestal, top cap, membranes and mold:

1) The inner membrane is folded into the groove of the inner surface of the HC base pedestal and secured with three o-rings (Fig. 3.6a).

2) The 59-mm-diameter inner mold is set inside the base pedestal cavity, and the inner membrane is pulled up around the inner mold.
3) The base pedestal with the inner membrane and mold is fastened to the axial actuator base platen.The outer membrane is placed on the base pedestal outer surface and secured with two o-rings.
4) The outer mold is set around the base pedestal and leveled. The outer membrane is stretched along the inner side of the outer mold and folded over the outer top surface of the outer mold. Two o-rings are placed on the outer membrane to temporarily secure it to the outer mold top.
5) Themold collar is placed on the outer mold top, and the collar-outer mold interface is temporarily sealed with an additional membrane. Two o-rings are placed over this membrane on the outer collar surface (Fig. 3.6b).
6) The pore water pressure (PWP) lines are connected to the base pedestal and fully saturated by flushing DA water (upwards) through them.

Sealing of the bottom of the CMTs:

7) The two CMTs are temporarily sealed at the bottom by a plastic cap and the annulus at the bottom of the CMTs is filled with DA water. The thickness of this DA water layer is 60 mm for clean sand and 70 mm for the NP silty sand samples.
8) The CMTs are left in a freezer room at -5°C for at least 12 h to freeze the DA water layer and form an ice plugat the bottom of the CMTs.

Mixing of sand with or without fines and DA water:

9) The required amounts of dry sand and fines are determined based on the target D_R and FC of the mixture. Then, the dry materials are thoroughly mixed.

10) The annulus between the CMTs is filled up to its mid height with DA water at 5 °C.

11) Using a funnel, the dry sand (with or without fines) is slowly pluviated into the CMTsannulus already partially filled with DA water. Additional DA water may be added so that the annulus between the CMTs is completely filled with the sand slurry.

12) A rubber stopper, which has two valves attached to it, is placed on the upper open end of the CMTs; the valves are closed off.

13) The CMTs with the sand slurry are turned upside down and rotated around their long axes several times to homogenize the slurry. After each turn and rotation of the CMTs, the sand slurry is allowed to settle for two minutes so that any air bubbles that remain in the slurry can move to the CMTs top. Additional DA water may be added at this stage through the two rubber stopper valves to remove any remaining air bubbles. This step is repeated until all visible air bubbles are removed. Total mixing time typically takesaround 10-15 minutes. Longer mixing times may lead to melting orpremature collapse of the bottom ice plug.

Slurry deposition in the HC mold:

14) Approximately one third of the annular space between the inner and outer molds is filled with DA water at about 30 °C to expedite melting of the bottom ice plug. Water temperatures higher than 50°C should be avoided as this may deform the rubber membranes.

15) The plastic cap that helps keep both the bottom ice plug in place and the slurry inside the CMTs is quickly removed after the slurry is thoroughly homogenized for the last time and is in uniform suspension in the CMTs.

16) Next, the CMTs with the slurry are immediately placed on the base pedestal inside the annulus between the inner and outer molds (Fig. 3.6c). During this process, the bottom ice plug temporarily seals the bottom of the CMTs.

17) The CMTs are then left in place for about 45 minutes, during which water at 30°C may be occasionally added to the gap between the CMTs and the inner and outer molds. This waiting time along with the continuous supply of warm water completely melts the bottom ice plug.

18) After the bottom ice plug melts, the two rubber stopper valves are opened. Then, the CMTs are raised slowly and simultaneously. This allows the slurry to deposit into the annulus between the inner and outer molds. While raising the CMTs, great attention is paid to avoid (1) interrupting the raising procedure, even if briefly, (2) tilting the CMTs, and (3) vibrating the CMTs. Once the CMTs are completely removed, the slurry fills the entire annular space between the inner and outer molds and between the inner mold and the collar.

19) If denser specimens are to be formed, the outer mold sides may be tapped. In this study, tapping was conducted with the plastic handle of a screwdriver. In this process, the bottom pedestal drainage line was opened and the mold was tapped six times for clean sands and nine times for NP silty sands at the mid-height of the specimen. This tapping pattern produced medium-dense clean and NP silty sand specimens with D_R around 40-60%.

20) The slurry fraction that remains in the collar (above the specimen top), which typically has a higher FC than the rest of the specimen, is removed through application of a small suction using a rubber tubing attached to a plastic water bottle.

21) The collar is removed and the specimen top is gently leveled off with a long spatula. The inner and outer rubber membrane sections that extend above the specimen top are thoroughly cleaned at this stage.

22) The top cap is not placed directly on the specimen top since the top cap weight and any potential disturbance caused by securing the membrane to the top cap may significantly alter the density and uniformity of the specimen top. Instead, a triangular plastic holder (TPH) specifically designed for this purpose is used to accurately center and firmly keep the top cap in place at the desired height (Fig. 3.6d). The TPH with the top cap can be clamped and fixed at any vertical location by sliding the TPH vertically along the three steel rods of the HC apparatus, which are originally designed to hold the internal load cell. This allows the steel rods to carry temporarily the weights of the top cap and TPH rather than the specimen. The TPH, which is firmly clamped to the top cap at this point, is slowly guided down the steel rods until the top cap vanes penetrate into the specimen top and the cap is in full contact with the specimen top (Fig. 3.6d).

23) The clean, top sections of the inner and outer membranes are rolled over the top cap and secured by o-rings.

24) The BP lines are attached to the top cap and a 20-kPa vacuum is applied to the specimen top through the BP line. As long as 1 h may be required at this stage for

complete equilibrium of the applied vacuum throughout the height of the NP silty sand specimens.

25) The inner mold, outer mold and TPH are removed (in this order). Removing the inner mold may cause a drop in the vacuum level in the specimen. If the vacuum drops to 15 kPa, inner mold removal is halted and time is allowed to restore the vacuum to 20 kPa, before inner mold removal can proceed.

26) The load cell, which rests on the three vertical steel rod tops inside the chamber, is attached to the top cap by raising the vertical actuator to the appropriate level. The four screws that connect the load cell to the top cap are fastened at this time. This step is carried out with extreme care so that negligible compressive or tensile loads are applied to the specimen. This can be easily accomplished by monitoring the vertical load cell readings on the HC software.

27) The outer diameter and height of the specimen are measured by using a pi tape, and a caliper, respectively, both with resolution of 0.01 mm.

28) The cell chamber is set around the specimen, locked, and filled with DA water. The inner and outer cell pressures are gradually increased to 20 kPa while the suction is simultaneously decreased to maintain a constant 20-kPa effective stress level at the beginning of the test. Then, testing can proceed as per conventional HC protocol.

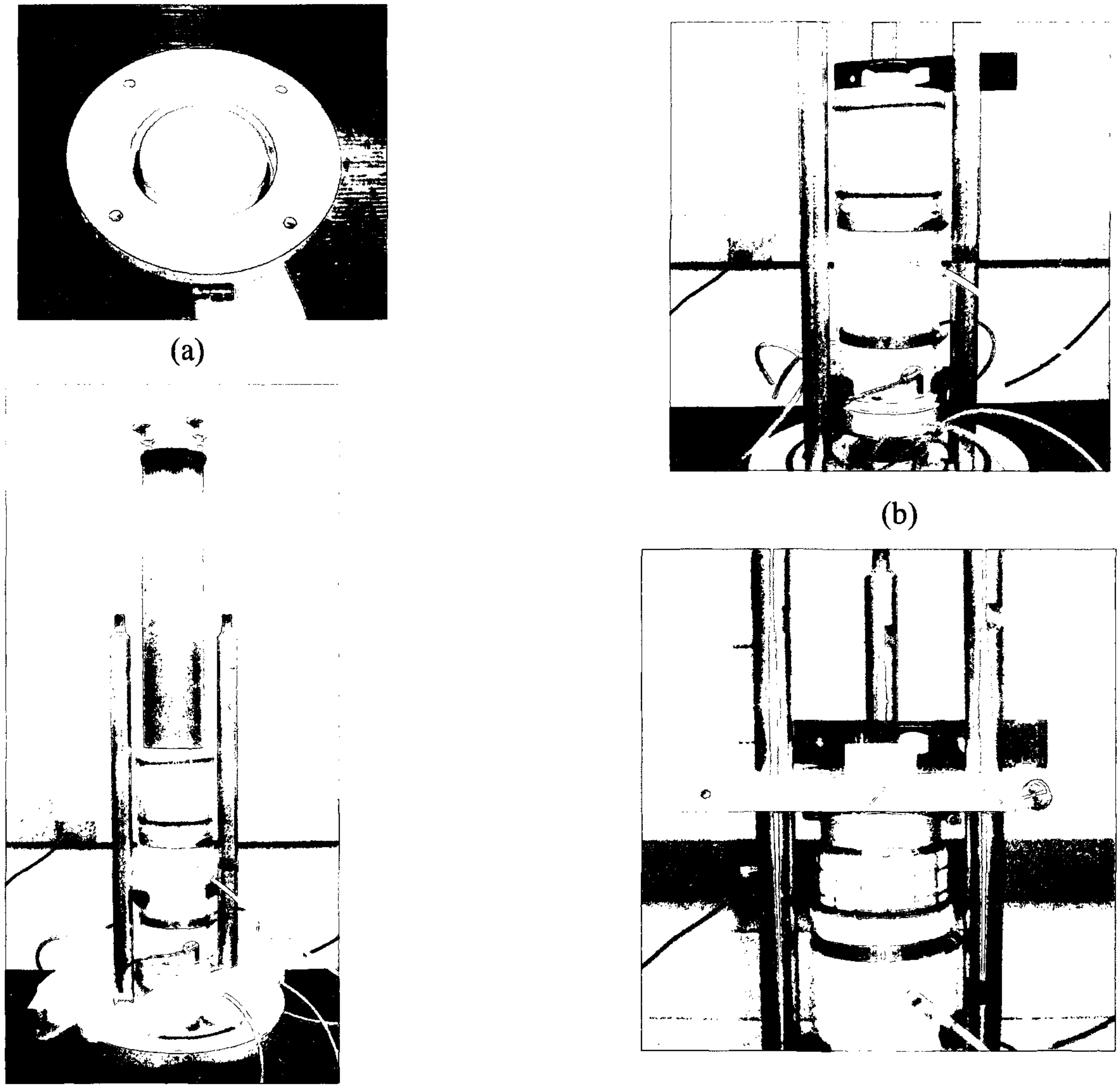

(a) (b) (c) (d)

Figure 3.6. (a) Base pedestal with the inner membrane and o-rings, (b) Additional membrane and o-rings to seal the outside of the outer mold and collar, (c) Sand slurry in the HC concentric tubes, and (d) Placement of the top cap on the specimen top with the help of the triangular plastic holder.

3.5 EVALUATION OF HOLLOW CYLINDER SPECIMEN UNIFORMITY

Like solid specimens, HC specimens may not be uniform in terms of their D_R and FC distributions across the specimen. As discussed previously, this may depend to a large degree upon the specimen reconstitution method used. The uniformity of the SD specimens tested in this study (both in terms of D_R and FC distributions) was assessed systematically by (1) horizontally slicing the reconstituted specimens using a special density gradient mold (DGM) specifically designed for this purpose (Fig. 3.7), and (2) determining the D_R and FC for each slice. The gelatin technique proposed by Emery et al. (1972) was used to solidify the HC specimens subjected to uniformity testing prior to slicing. In this approach, a 3%gelatin solution is used as the pore fluid of the specimen (Emery et al. 1972, Kuerbis and Vaid 1988, Carraro and Prezzi 2008). To allow slicing of various HC specimen layers, a DGM with five 40-mm-long aluminum rings was designed and fabricated. This five-ring stack forms the outer mold boundary that will contain the HC specimens subjected to uniformity tests. Five 40-mm-long solid aluminum disks also were fabricated. This five-disk stack constitutes the inner mold boundary and serves as a replacement for the conventional HC inner mold. An additional collar set including a 60-mm-long outer ring and 60-mm-long inner disk is used to replace the conventional collar and allow the specimen to be reconstituted with a longer initial height before the specimen is leveled off to its desired height of 200 mm. The HC specimens subjected to uniformity tests were prepared in the DGM in a very similar manner to that described previously for the regular HC specimens, except that: (1) the pore water fluid consisted of a 3% gelatin solution at 78 °C, (2) the bottom ice plug used in the CMTs was replaced by a 70-mm-thick gelatin plug (made of solidified 3% gelatin solution), (3) about one third of the annulus between the stacked outer rings and the inner solid disks was filled with the 3% gelatin solution at about 90-95°C, (4) the slurry was homogenized by turning the CMTs upside down and rotating them around their axis for only 10 minutes to minimize early hardening of the gelatin – a typical 3% gelatin solution solidifies in about 1 h (Emery et al. 1972), and (5) the time allowed for slurry deposition inside the CMTs (before the CMTs are raised) is limited to 5 minutes to prevent the slurry from becoming too viscous due to gelatin hardening.

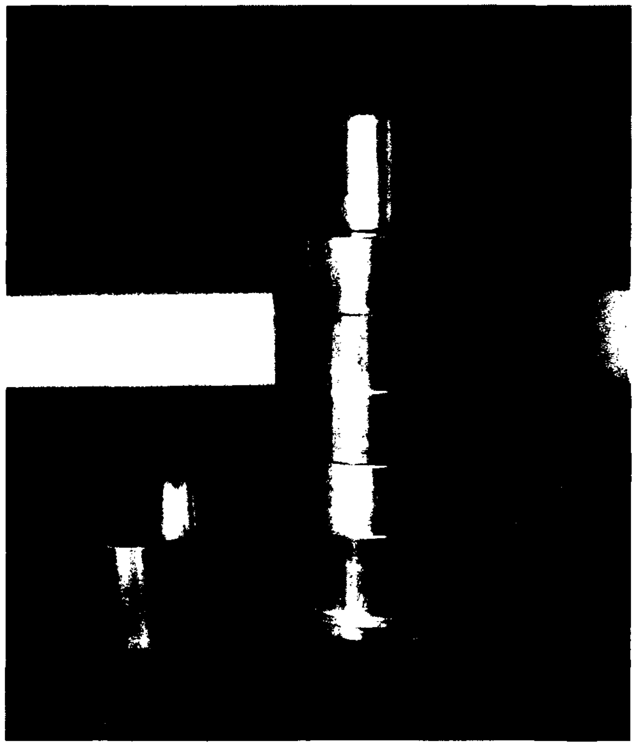

Figure 3.7. Specimen density gradient mold with collar outer ring removed.

Then, the HC gelatin specimen formed inside the DGM isplaced in a controlled-temperature room at 1°C for at least 12 h for specimen solidification. Once specimen solidification is completed, the four vertical rods that connect and keep the inner disks and the outer rings in place (Fig. 3.7) are removed and the HC gelatin specimen is sliced into five layers with a 0.2-mm-thick wire saw. Next, the slice FCs are determined by washing the soil in each slice with hot water through the No. 200 sieve and collecting both the retaining and passing fractions separately. The retained material is taken as the coarse sand fraction, whereas the material passing the No. 200 sieve constitutes the slice fines fraction. Neglecting the gelatin mass present in each slice is expected to alter the layer FC by no more than 0.5% for the specimens tested. The D_R of each layer is also determined at this step.

3.6 HOLLOW CYLINDER TESTING

The HC testing protocol followed in this study included five main stages: (1) de-aired water flushing, (2) back pressure saturation, (3) anisotropic consolidation, (4) alpha rotation and b change, and (5) undrained cyclic loading. Each stage is described separately below.

3.6.1 De-aired water flushing

After the HC specimens were reconstituted according to the method described in section 3.4, de-aired (DA) water was flushed through the specimen from the pore pressure lines at the base pedestal to the BP lines at the top cap. The maximum hydraulic gradient used during DA water flushing was approximately 3. The amount of DA water flushed was at least 3 times the volume of voids of the specimen.

3.6.2 Back pressure saturation

The BP saturation stage of HC specimens was conducted as follows:

1) The inner cell pressure (p_i) and the outer cell pressure (p_o) were simultaneously increased by 50 kPa in one or ten minutes for clean or silty sand, respectively, under undrained conditions. Then, an additional one- minute or ten-minute period for silty sand was allowed for the pressures to stabilize. The Skempton's pore pressure coefficient (Skempton 1954) B $(= \Delta u / \Delta p)$ was determined by measuring both the excess pore pressure increment Δu due to the corresponding

increment in the mean total stress $\Delta p\left(=\dfrac{\Delta\sigma_1+\Delta\sigma_2+\Delta\sigma_3}{3}\right)$, which at this stage is simply equal to the isotropic increment in both inner and outer cell pressures ($\Delta p = \Delta p_i = \Delta p_o$, since $\Delta\sigma_1 = \Delta\sigma_2 = \Delta\sigma_3$)

2) The BP was increased by 50 kPa in one minute or ten minutes for silty sand and another minute (ten minutes for silty sand) was allowed for the pressures to stabilize. Then, the BP valve was opened so that the BP could be applied to the specimen. Next, p_i and p_o were increased again by 50 kPa and the B-value was determined as before. This procedure was repeated until B was equal to at least 0.98. The level of BP typically required to obtain $B > 0.98$ was 400-450 kPa.

The saturation scheme outlined above was used to determine the variation of B as a function of BP. Thirteen clean sand specimens, and one of the silty sand specimens were saturated in this manner (manual saturation mode). For the remaining of the specimens, a different protocol was used. In alternative protocol, p_i and p_o and BP were increased simultaneously to 570, 570, and 550 kPa (ramp pressure mode), respectively, when the BP valve is open (drained conditions). The time elapsed during this pressure increment was 2 h for clean sand specimens, and 8 h for silty sand specimens. Then, the BP valve was closed, and under undrained conditions, p_i and p_o were incremented by 50 kPa (in one minute for clean sand specimens, and 10 minutes for silty sand specimens). The pore pressure increase Δu in response to the cell pressure increase was measured at this time. Finally, the B-value was determined as before. The B-values of the specimens saturated using this ramping protocol was no less than 0.98.

3.6.3 Anisotropic consolidation

An initial anisotropic consolidation stage was conducted on the HC specimens to simulate K_0 deposition in the field. During this stage, the specimens were consolidated to a mean effective stress $p' \left(= \dfrac{\sigma_1' + \sigma_2' + \sigma_3'}{3} \right)$ of 100 kPa and a stress ratio $K = \sigma_3' / \sigma_1'$ that produced approximately K_o conditions (zero lateral strains). In HC specimens, there are two normal strain components on the horizontal plane, namely the radial and circumferential strains, ε_r and ε_θ, respectively. Following the definition of K_o conditions, both of these strain components should be zero. However, this cannot be easily achieved, since there is no physical lateral constraint involved. Therefore, K was selected in such a way that anisotropic consolidation would produce ε_r and ε_θ that are close to zero as it will be discussed in section 4.2. The target stress parameters leading to this approximately zero lateral strain requirement, p' = 100 kPa and K were applied in a period of 8 h, which is long enough to allow full dissipation of excess pore pressures during consolidation. After the target stress conditions were achieved, the specimens were allowed to creep until $\Delta\varepsilon_p \leq 0.05\%$ /day (Zdravkovic and Jardine 2001).

3.6.4 α and b Increase Stages

After anisotropic consolidation was completed, the selected values of α and b were increased in 8 h under constant p' and K. Next, the HC specimens were allowed to creep until $\Delta\varepsilon_p \leq 0.05\% / day$. In the field, α and b may be imposed on soil elements along with an increase in p' and q depending upon the analysis and/or application in consideration. However, during the stage of α and/or b increase, p' and K were kept constant to systematically evaluate the effect of α and b on the drained behavior of the HC specimens tested.

3.6.5 Undrained Cyclic Loading

The specimens were cyclically sheared under undrained conditions at constant *p*, *b*, and α. The maximum shear stress, $\Delta\tau_{max} = (\sigma_1^{'} - \sigma_3^{'})/2$, was applied cyclically to the specimen in a sine wave form. The starting point of the sine wave was $(\sigma_1^{'} - \sigma_3^{'})/2$ at the end of α and/or *b* increase stage (Point A in Fig. 3.8). The undrained cyclic loading may be represented as a series of Mohr circles that grow and shrink around the same initial mean stress. The initial Mohr circle denoted by A defines the starting stress state prior to cyclic loading. The Mohr circle becomes largest at B, where the specimen experiences the largest shear (or deviator) stress. Then, the Mohr circle becomes smaller until point C is reached and then starts growing again between C and D. At point D, the Mohr circle is equal to the one at A.

Typical variation of octahedral deviator stress during undrained cyclic loading is shown in Fig. 3.9 for one of clean sand specimens tested. Variation of q in one cycle is parallel to what is shown in Fig. 3.8.

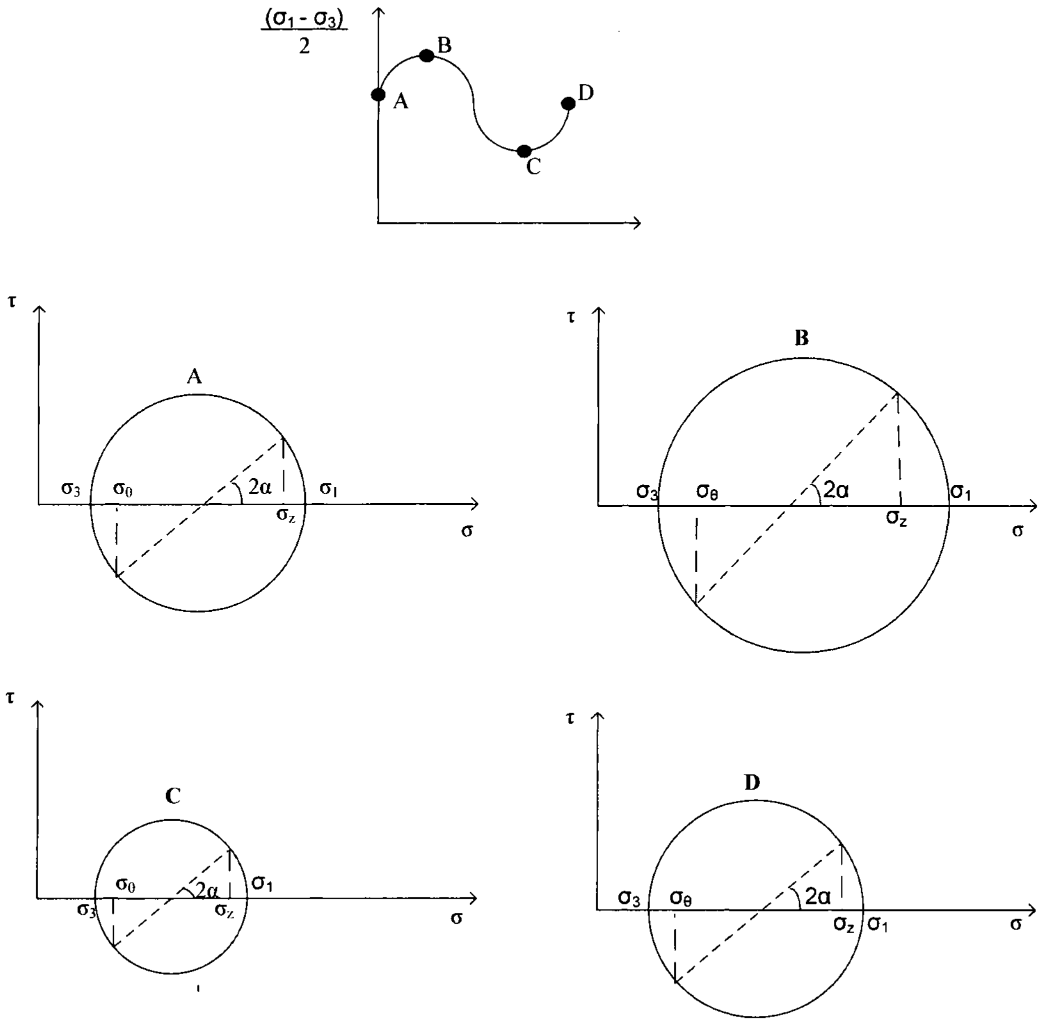

Figure 3.8.Mohr circle representation of the cyclic loading stage.

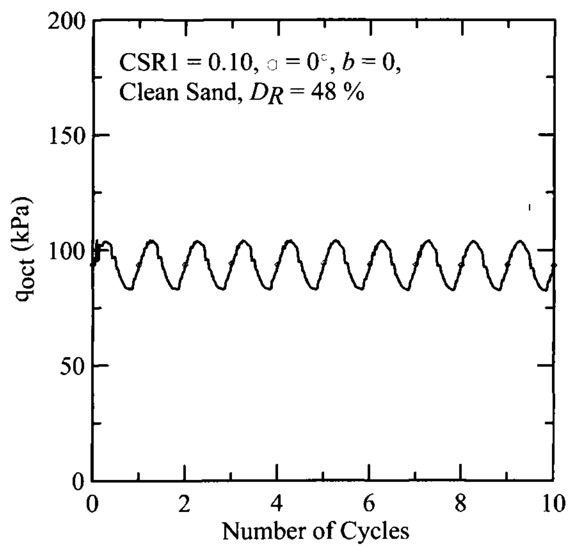

Figure 3.9.Typical variation of q during undrained cyclic loading

4. RESULTS

4.1 MAXIMUM VOID RATIO

The effect of fines on e_{max} of Ottawa sand was investigated for the fines content (FC) range of 0 to 22% by using slurry deposition (SD) method. The results are depicted in Fig. 4.1, which also includes e_{max} and e_{min} that were obtained according to ASTM D 4254 ($e_{max\text{-}ASTM}$) and ASTM D 4253 ($e_{min\text{-}ASTM}$) for the same sand and silt, respectively, by Carraro and Prezzi (2008).

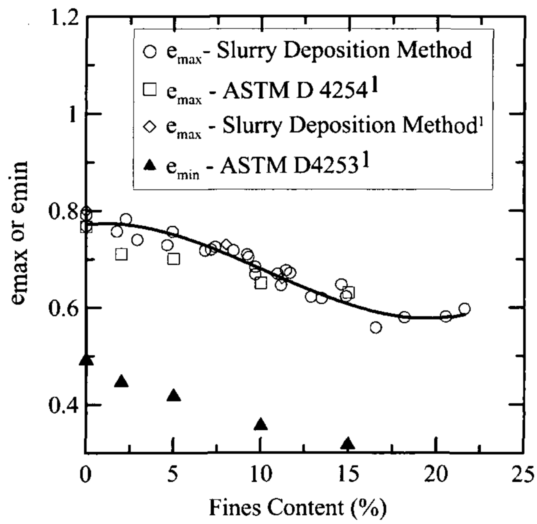

Figure 4.1.The variation of e_{max} as a function of fines content
[1]Determined by Carraro and Prezzi (2008).

According to Fig. 4.1, e_{max} decreases as the FC increases when FC < 19% regardless of the method used to determine e_{max}. When FC < 10%, ASTM D 4254 underestimates e_{max} compared to e_{max} obtained by the slurry deposition method ($e_{max\text{-}SD}$). When FC>16-17%,

$e_{max\text{-}SD}$ does not decrease as the FC increases. A decrease in $e_{min\text{-}ASTM}$ with an increase in the FC is also evident in Fig. 4.1. The measured FC as a function of the initial FC used to prepare the sand-silt mixture is shown in Fig. 4.2.

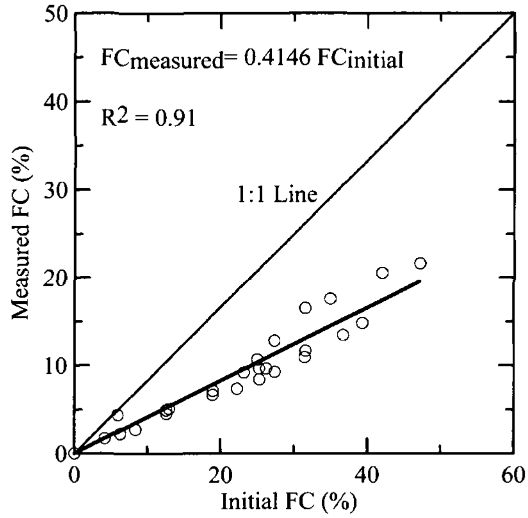

Figure 4.2.Measured FC versus initial FC for maximum void ratio tests.

An addition of fines to a loose sand specimen (D_R = 40% or e = 0.658) would affect the D_R, as shown in Fig. 5.3, where the D_R was calculated using both $e_{max\text{-}ASTM}$ and $e_{max\text{-}SD}$ along with $e_{min\text{-}ASTM}$. An increase in the FC, at a constant void ratio, significantly reduces the D_R of sand-silt mixture, similar to what Polito and Martin (2003) reported. They also reported that after a certain limiting FC, the D_R starts increasing again as the FC increases. A maximum FC = 15 % in Fig. 4.3 may be less than the limiting FC that Polito and Martin (2003) described, since the increase in D_R as the FC exceeds the limiting FC is not evident in Fig. 4.3. Another observation from Fig. 4.3 is a large difference between the D_R determined according to $e_{max\text{-}SD}$ and $e_{max\text{-}ASTM}$. If $e_{max\text{-}ASTM}$ is used for the D_R calculation, a silty sand specimen with a FC = 10% and e = 0.658 is physically impossible (D_R < 0); however, the D_R is 32 % if $e_{max\text{-SD}}$ is used in the calculation..

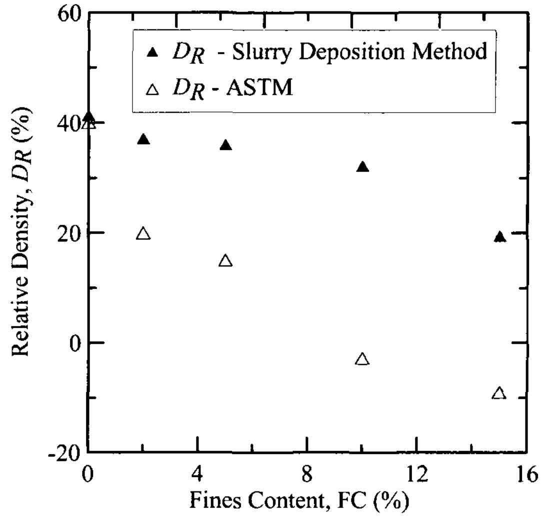

Figure 4.3.Variation of D_R, calculated based on $e_{max\text{-}ASTM}$, $e_{max\text{-}SD}$ and $e_{min\text{-}ASTM}$ at e = 0.658, as a function of FC

Even though D_R calculated according to $e_{max\text{-}ASTM}$ are shown to be significantly different than D_R calculated according to $e_{max\text{-}SD}$, relative densities were calculated based on $e_{max\text{-}ASTM}$, since: (1) the slurry deposition method to determine the maximum void ratio still needs to be improved, (2) using $e_{max\text{-}ASTM}$ allows comparing the results of this study with other studies that used the same materials.

4.2. HOLLOW CYLINDER SPECIMEN UNIFORMITY

The D_R of each HC specimen slice was evaluated based on the $e_{\max}$ and $e_{\min}$ determined according to ASTM D4254 Method B and ASTM D4253 Method 1A, respectively (Carraro and Prezzi 2008). Local D_R variations across the HC specimen height are shown in Fig. 4.4a for one medium-dense (MS1) and three loose (LS1, LS2 and LS3) clean sand specimens. The average global D_R of the LS1, LS2 and LS3 specimens are 26 %, 26 % and 25 %, respectively. The maximum difference among the global D_R values measured for each of the three loose specimens is not larger than 1.1%, which shows the high reproducibility in terms of global D_R that can be obtained with the proposed method for specimens in their loosest state. Maximum variations between the local and the average global D_R values are 3.4 %, 6.1 % and 4.0 % for the LS1, LS2 and LS3 specimens, respectively. Fig.4.4a also shows the local D_R variation for a medium-dense HC specimen (MS1) formed by the densification procedure described previously. For the MS1 specimen, the average D_R and maximum local deviation from the average D_R were 35 % and -5.5 %, respectively.

To the author's knowledge, systematic evaluations of maximum local D_R deviations from the overall average D_R of HC clean sand specimens have not been reported in the literature. However, for solid WP specimens, Vaid et al. (1999) claimed that a maximum local D_R deviation of +/- 2-3 % from the average was acceptable. For their MT specimens, they measured a +/- 10 % variation from the average D_R. Similarly, Ghionna and Porcino (2006) reported a maximum local D_R variation of + 6.5 % from the average D_R for solid WP specimens. Kuerbis and Vaid (1988) reported maximum local D_R variations of -5.8 % and +5.2 % from the global average D_R for solid WP and SD specimens, respectively. Based on the typical D_R variations reported for solid specimens, the maximum local variations for the HC specimens prepared with the proposed method might also be considered acceptable, especially given the additional difficulties associated with HC specimen reconstitution. Specimens LS1, LS2 and LS3 were prepared at the loosest state possible to be achieved with the proposed method (D_R around 25%).

The D_R and FC variations for two loose NP silty sand HC specimens are shown in Fig. 4.4b. The first loose NP silty sand specimen (LSS1) had average D_R of 30% and FC of 13%. The maximum local deviation from the average D_R and FC values were 4.1 % and 0.7 %, respectively. Tapping nine times with the plastic handle of a screwdriver at the mid-height of the second NP silty sand specimen (LSS2) was attempted to increase the specimen D_R. These results are also shown in Fig. 4.4b. TheLSS2 specimen had average global D_R of 29% and FC of 13%, and maximum D_R and *FC* deviations from the average equal to -7.1%and 0.3%, respectively. Fig. 4.4b results indicate that tapping at the mid-height of the NP silty sand specimen does not increase its $_R$ as in the case of the clean sand specimens. Lack of densification through tapping may be attributed to the single top drainage of the DGM specimen. Additionally, since the FC of the LSS2 specimen was 13%, its hydraulic conductivity may not be sufficiently high to allow densification under the relatively low energy imparted by the tapping procedure employed. Carraro and Prezzi (2008) evaluated the uniformity of a solid SD clayey sand specimen in terms of FC and D_R. The maximum local FC variation from the average FC of 4.8 % was 0.1 %, whereas the maximum local D_R variation from the average D_R of 54 % was +/- 2 %. Kuerbis and Vaid (1988) also evaluated the uniformity of a solid SD silty sand specimen by showing the grain size distribution curves for four slices of their specimen. They claimed that no significant segregation occurred since the curves were virtually identical. However, they did not present the FC or D_R distributions for their specimen. Rolo (2003) reported a maximum local FC variation of 0.3 % from the average value of 15 % for his SD HC specimens of Ham River with 15 % of Kaolin clay.

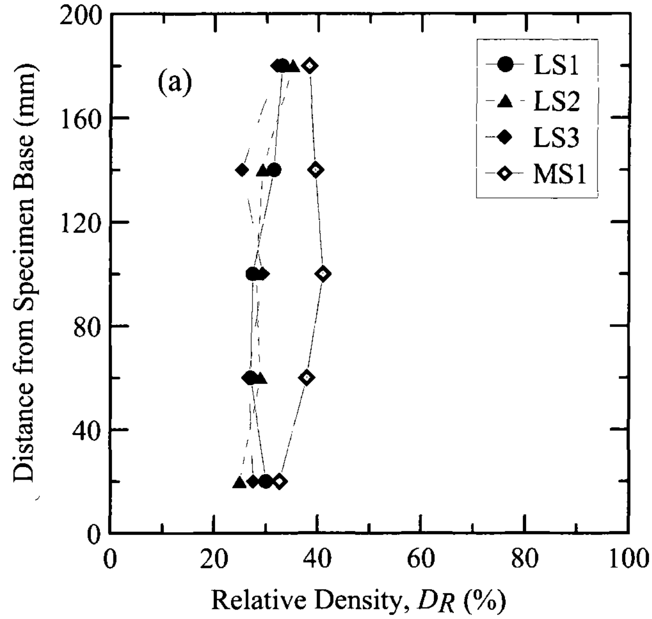

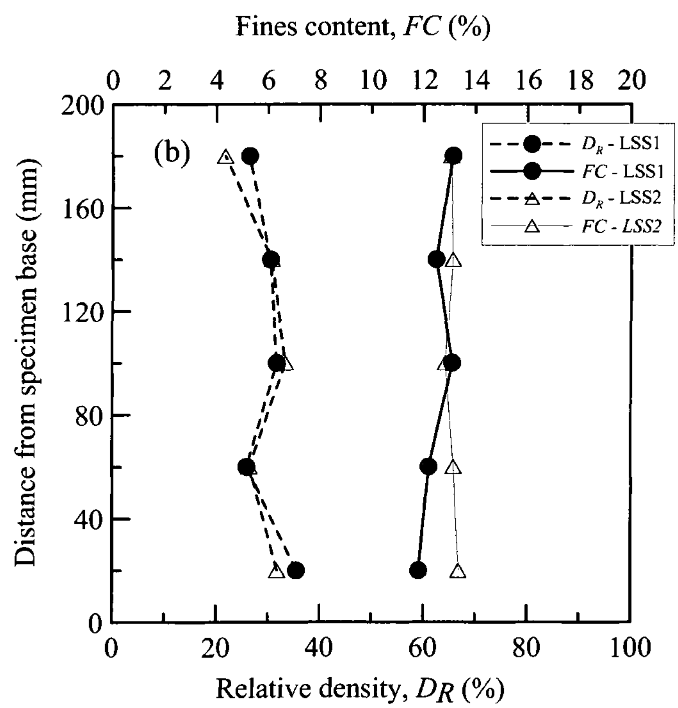

Figure 4.4. Uniformity evaluation of hollow cylinder specimens of (a) clean sand and (b) nonplastic silty sand.

Based on the results reported above and the maximum local FC variations from the global average FC reported by Carraro and Prezzi (2008) for solid SD specimens and by Rolo (2003) for HC SD specimens, the FC variation observed in this study for the NP silty sand HC specimens is small, which reinforces the applicability of the proposed method for the reconstitution of SD HC specimens of sands with fines.

The maximum local D_R variations from the average D_R for the HC NP silty sand specimens are similar to those observed for HC clean sand specimens for the D_R ranges and procedures used in this study. This indicates the suitability of the proposed SD method for HC specimen reconstitution of both clean and NP silty sands.

4.3. HOLLOW CYLINDER TEST RESULTS

4.3.1 Saturation of Hollow Cylinder Specimens

The HC specimens were BP saturated as described in section 3.5.2. Thirteen tests on clean Ottawa sand and one test on NP Ottawa silty sand were conducted using the manual saturation protocol as described in section 3.5.2. The remaining specimens were saturated using the ramping saturation protocol (defined in section 3.5.2). The typical variation of the Skempton's pore pressure coefficient B (Skempton 1954) with increasing BP for various HC specimens subjected to manual saturation is shown in Fig. 4.5. The initial B values obtained prior to BP saturation (i.e., when BP = 0 kPa) were equal to approximately 0.6 for clean sands (only one specimen is an outlier for the trend) and 0.5 for NP silty sands. These initial B value range was significantly higher than the typical initial B value range that can be achieved with MT or AP, as discussed by Carraro and Prezzi (2008). The B values after BP saturation were equal to or greater than 0.98 for all specimens tested, which is consistent with the B values reported for solid specimen reconstitution using a similar SD method (Carraro and Prezzi 2008) for the same soils tested. The B values obtained at the end of the saturation are given in Table 4.1 and 4.2 for clean and NP silty Ottawa sand specimens, respectively. Fig. 4.5 indicates that a BP > 450 kPa was typically required to saturate the HC specimens of clean and NP silty Ottawa sands tested in this study. Complete specimen saturation might not have been able to be achieved if other reconstitutions methods such as MT and AP had been used during specimen preparation.

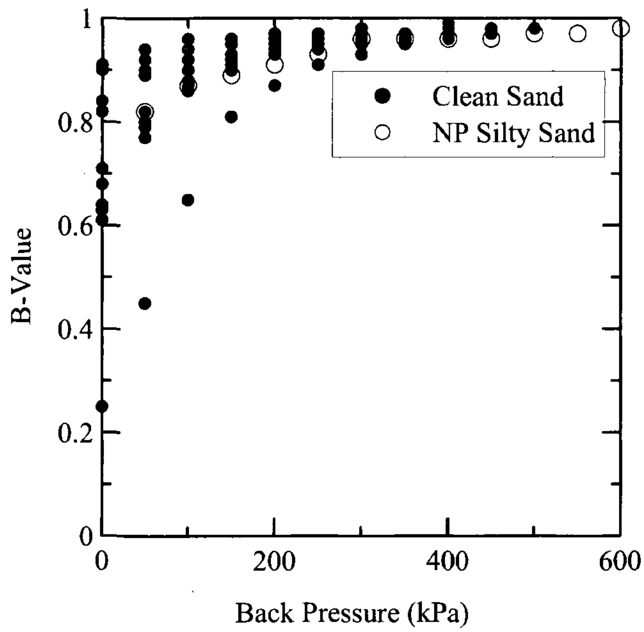

Figure 4.5 Variation of Skempton's pore pressure coefficient B as a function of back pressure.

Table 4.1. Stress conditions and relative density at the end of various testing stages for clean sand specimens

Test #	α (deg)	*b*	*CSR*	Saturation Mode	Skempton's B value after BP Saturation	Relative Density (%)		
						Initial	End of Anisotropic Consolidation	End of α and/or b Stage
1	0	0	0.60	Manual	0.98	46	48	-
2	0	0	0.30	Manual	0.99	50	53	-
3	0	0	0.20	Manual	0.98	39	42	-
4	0	0	0.14	Manual	0.98	40	43	-
5	0	0	0.10	Manual	0.98	47	48	-
6	30	0	0.10	Manual	0.98	38	40	41
7	30	0	0.08	Manual	0.98	37	40	41
8	30	0	0.06	Manual	0.98	46	48	49
9	60	0	0.10	Manual	0.98	38	39	43
10	60	0	0.08	Manual	0.98	44	48	50
11	60	0	0.06	Manual	0.98	46	48	50
12	0	0.5	0.52	Ramp	0.98	40	42	43
13	0	0.5	0.48	Ramp	0.98	49	51	51
14	0	0.5	0.40	Ramp	0.98	47	50	52
15	0	0.5	0.26	Manual	0.98	40	41	41
16	0	0.5	0.09	Manual	0.98	51	54	55
17	0	0.8	0.55	Ramp	0.98	46	49	51
18	0	0.8	0.37	Ramp	0.98	43	44	45
19	0	0.8	0.24	Ramp	0.98	41	43	44
20	0	0.8	0.09	Ramp	0.98	50	52	55
21	30	0.5	0.17	Ramp	0.98	41	44	45
22	30	0.5	0.10	Ramp	0.98	52	56	58
23	30	0.5	0.07	Ramp	0.98	43	45	47
24	30	0.8	0.20	Ramp	0.98	50	51	53
25	30	0.8	0.15	Ramp	0.98	52	53	55
26	30	0.8	0.09	Ramp	0.98	49	51	53
27	60	0.5	0.09	Ramp	0.98	49	51	54
28	60	0.5	0.07	Ramp	0.98	51	55	57
29	60	0.5	0.05	Ramp	0.98	41	45	49
30	60	0.8	0.09	Ramp	0.98	41	45	47
31	60	0.8	0.06	Ramp	0.98	45	48	51
32	60	0.8	0.07	Ramp	0.98	45	48	51
			Mean =		0.98	45	47	49
			COV (%) =		0.18	10	10	10
			Minimum=		0.98	37	39	41
			Maximum=		0.99	52	56	58

Table 4.2. Stress conditions and relative density at the end of various testing stages for NP silty sand specimens.

Test #	α (deg)	b	CSR	FC (%)	Saturation Mode	Skempton's B value after BP Saturation	Relative Density (%)		
							Initial	End of Anisotropic Consolidation	End of α and/or b Stage
1	0	0	0.20	15	Ramp	0.98	54	59	59
2	0	0	0.30	15	Manual	0.98	55	61	61
3	0	0	0.10	15	Ramp	0.98	54	59	59
4	30	0	0.10	14	Ramp	0.98	53	57	58
5	30	0	0.24	13	Ramp	0.98	36	41	43
6	30	0	0.30	16	Ramp	0.98	39	45	46
7	30	0	0.20	13	Ramp	0.98	48	58	60
8	60	0	0.10	14	Ramp	0.98	48	53	57
9	60	0	0.20	11	Ramp	0.98	47	53	57
10	60	0	0.28	14	Ramp	0.98	43	47	51
11	0	0.5	0.17	13	Ramp	0.98	35	42	43
12	0	0.5	0.26	12	Ramp	0.98	46	51	53
13	0	0.8	0.18	13	Ramp	0.98	47	51	53
14	0	0.8	0.27	14	Ramp	0.98	59	64	66
15	0	0.5	0.14	13	Ramp	0.98	41	46	47
16	0	0.8	0.46	13	Ramp	0.98	34	39	41
			Mean =	14		0.98	46	52	53
			COV (%) =	9		0.00	17	15	14
			Minimum=	11		0.98	34	39	41
			Maximum=	16		0.98	59	64	66

4.3.2 Anisotropic Consolidation Behavior of Slurry Deposited Ottawa Sand with and without NP Silt

Back pressure saturated clean and NP silty sand specimens were anisotropically consolidated under K_0 conditions. A trial and error procedure was conducted to find $K = \left(\sigma_3^{'} / \sigma_1^{'}\right)$ with which p' was increased to 100 kPa so that K_0 conditions (zero radial and circumferential strains) prevail during the anisotropic consolidation of clean sand. The ideal approach to find the optimum K that produces K_0 conditions is to run a series of tests utilizing different K. However, this would be impractical considering the purposes of this study. Therefore, instead of running one test for each K, one test with several K was conducted. Jaky's (1944) equation (K_0 = 1-sinϕ) yields K = 0.51 for clean sand (Φ_c =

29.5°) and K = 0.44 for NP silty sand with FC = 15 % (ϕ_c = 34.4°). In an effort to determine K that produces the least radial and circumferential strain rates (change in strain by time), p' = 100 kPa was reached in three steps by using three different K in the following order: 0.45, 0.50 and 0.47. The range of K was determined based on Jaky's (1944) aforementioned equation. Stress path followed and strains developed due to the stress path are given in Fig. 4.6a, and Fig. 4.6b, respectively, where the stress path is defined in terms of octahedral deviator stress, q. The octahedral deviator stress, q, reduces to $(\sigma_1 - \sigma_3)$ for axisymmetrical conditions. For all three K applied, the specimen contracts in the radial direction, and dilates in the circumferential direction (Fig. 4.6b). The largest volumetric and radial strain rate was observed when K = 0.50. Slightly larger radial, circumferential and volumetric strain rates were observed when K = 0.47 compared to when K = 0.45. Given the relatively lower strain rates observed when K = 0.47, a different clean sand specimen was anisotropically consolidated with only K = 0.47 (Fig. 4.6c and Fig. 4.6d). During the anisotropic consolidation with K = 0.47, radial and horizontal strains reached up to +0.17 % and -0.10 %, respectively, for the clean sand specimen. Although these strains were close to zero, an additional test was conducted on a clean sand specimen anisotropically consolidated with K = 0.43 (Fig. 4.6e and Fig. 4.6f) to see if the maximum radial strain can be reduced compared to the one generated during the anisotropic consolidation with K = 0.47 (Fig. 4.6c and Fig. 4.6d). During the anisotropic consolidation to p' = 100 kPa with K = 0.43, maximum radial and horizontal strains induced are +0.12 % and -0.10 %, respectively, for the clean sand specimen with D_R = 48 %. Anisotropic consolidation to p' = 100 kPa with K = 0.43 as in Fig. 4.6e and Fig. 4.6f simulates K_0 conditions more closely than anisotropic consolidation to p' = 100 kPa with K = 0.47 as in Fig. 4.6c and Fig. 4.6d. Further decrease in K is expected to increase the horizontal strain. Therefore, anisotropic consolidation to p' = 100 kPa with K = 0.43 was considered sufficiently close to simulating K_o conditions. An example of the stress path followed during anisotropic consolidation to p' = 100 kPa with K = 0.43 (K_0 – consolidation) is given in Fig. 4.7a. The stress path shown in Fig. 4.7a is applied on both clean and NP silty sand (FC = 15%) specimens. Stress components applied to achieve the stress path in Fig. 4.7a are given in Fig. 4.7b. Increase in axial stress is larger than the increase in radial and circumferential stresses, and the predominant loading is in the vertical direction. The radial and circumferential stresses are increased at the same rate and by the same magnitude. Strains generated during the anisotropic consolidation of clean and NP silty sand specimens (D_R = 40% for the clean sand and D_R = 41% for the NP silty sand at the end of saturation) are shown in Fig. 4.7c and Fig.4.7d, respectively. During anisotropic consolidation, the NP silty sand experiences axial strain as large as 1 % (D_R = 40 %), while the clean sand (D_R = 41 %) undergoes only 0.4 % axial strain. The maximum radial strain measured for the clean and NP silty sand specimens are 0.1 %, and -0.1 %, respectively, at the end of anisotropic consolidation (Figs. 4.7c and 4.7d). Even though, the signs of radial strains measured are different for clean and NP silty sands, the magnitudes of the strains are close to zero. The maximum circumferential strains measured during the consolidation of clean and NP silty sand specimens are -0.1 % and -0.25 %, respectively. The magnitude of the circumferential strain becomes slightly larger when FC is increased to 15 %. For the NP silty sand specimens, maximum strains induced in the radial and circumferential directions are -0.1 % and -0.25 %, respectively. Fig. 4.7c and Fig. 4.7d show the strain response of one clean sand and one

NP silty sand specimens during the anisotropic consolidation. In this study, 32 clean sand and 16 NP silty sand specimens were subjected to the same stress path during the anisotropic consolidation. Maximum strains observed excluding the creep strains for these specimens are given in Table 4.3 and Table 4.4 for clean and NP silty sand specimens, respectively. Maximum strains induced including the effect of creep are given in Table 4.5 and Table 4.6. The following analysis of strains is valid for the strains before the creep stage. The variations of axial, radial, circumferential and volumetric strains for different tests are also provided in Figs. 4.8 and 4.9 for clean and NP silty sand specimens, respectively. The average axial strain (0.98 %) experienced by NP silty sand specimens (Fig. 4.8) is larger than the median axial strain (0.34 % before creep) experienced by clean sand specimens (Fig. 4.9). Furthermore, NP silty sand specimens underwent slightly larger volumetric strain (average volumetric strain = 0.61 %) than clean sand specimens did (average volumetric strain = 0.38 %). Only two clean sand specimens out of 32 experienced a radial strain larger than 0.2 % (Table 4.4). The maximum radial strain measured for clean sand specimens was 0.31 % (Table 4.4). The average radial strain for the clean sand specimens was 0.15 % before the creep. Radial strain for NP silty sand specimens ranged between -0.02 % and -0.20 %. Except for one clean sand specimen (circumferential strain = 0.33 %), 31 clean sand specimens experienced a circumferential strain between -0.06 % and -0.20 %, and the average circumferential strain was -0.10 % for all of the clean sand specimens. For the NP silty sand specimens, all but two specimens experienced a circumferential strain between -0.19 % and -0.34 % (Table 4.4). The average circumferential strain for NP silty sand specimens is -0.27 %.

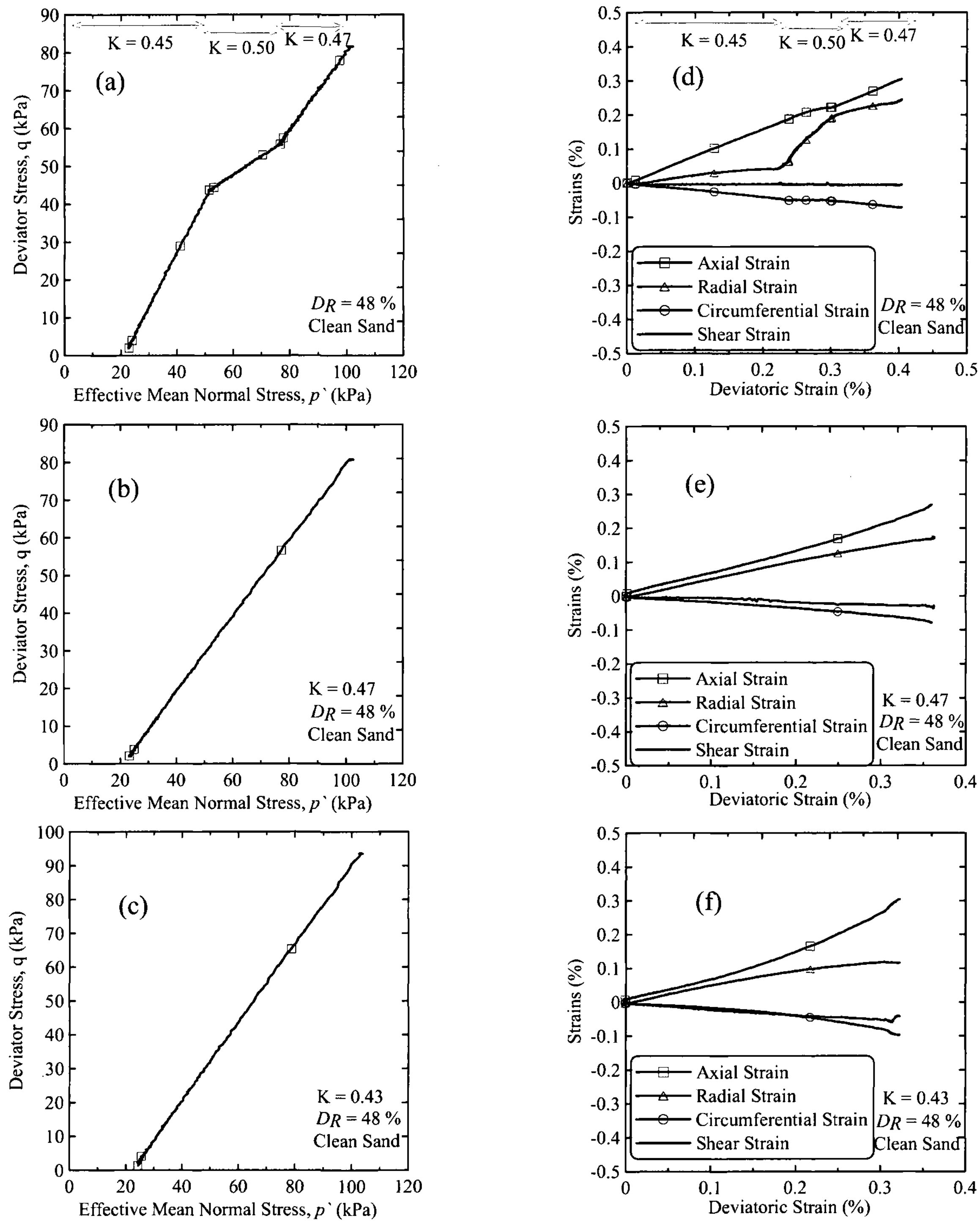

Figure 4.6. Stress paths and strain response during the anisotropic consolidation of three tests stress paths for (a) varying K, (b) $K = 0.47$, (c) $K = 0.43$, strain response for (d) varying K, (e) $K = 0.47$, and (f) $K = 0.43$.

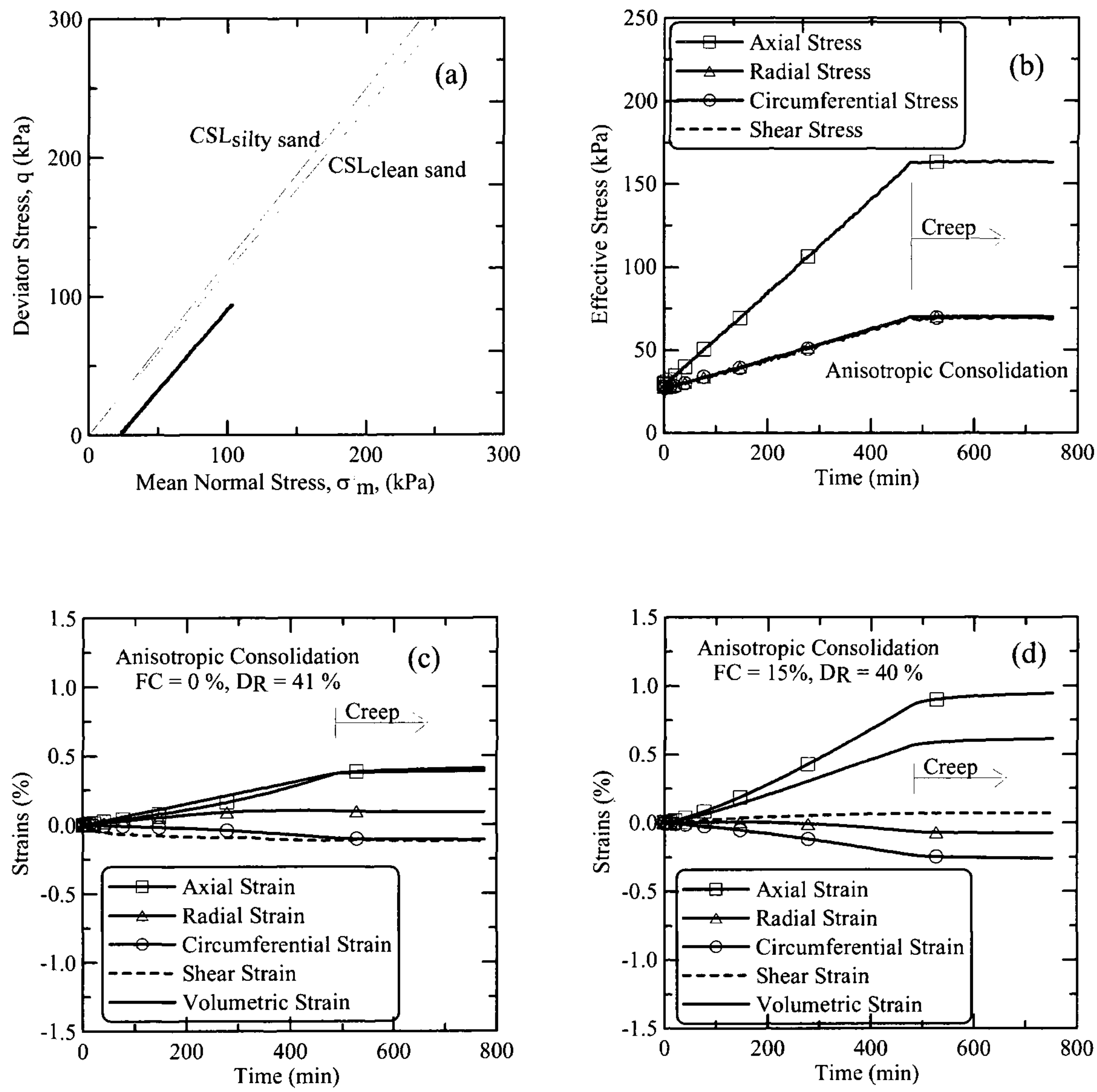

Figure 4.7. Anisotropic consolidation stage (a) stress path followed, (b) stresses applied in radial coordinates, (c) strain response of clean sand, and (d) strain response of NP silty sand.

Table 4.3. Strains measured during anisotropic consolidation of 32 clean sand specimens before the creep stage

Test No	**D_R* (%)**	**ε_a (%)**	**ε_r (%)**	**ε_θ (%)**	**ε_p (%)**
Clean Sand 1	40	0.25	0.17	-0.07	0.35
Clean Sand 2	46	0.27	0.12	-0.08	0.30
Clean Sand 3	50	0.54	0.08	-0.16	0.46
Clean Sand 4	39	0.42	0.18	-0.13	0.47
Clean Sand 5	40	0.40	0.09	-0.10	0.39
Clean Sand 6	38	0.38	0.09	-0.10	0.37
Clean Sand 7	52	0.30	0.16	-0.08	0.38
Clean Sand 8	47	0.44	0.08	-0.13	0.39
Clean Sand 9	51	0.24	0.16	-0.07	0.33
Clean Sand 10	37	0.59	0.03	-0.17	0.44
Clean Sand 11	37	0.35	0.12	-0.09	0.38
Clean Sand 12	46	0.31	0.14	-0.10	0.35
Clean Sand 13	44	0.67	0.31	-0.30	0.68
Clean Sand 14	46	0.24	0.17	-0.08	0.33
Clean Sand 15	40	0.36	0.10	-0.10	0.37
Clean Sand 16	47	0.35	0.13	-0.08	0.40
Clean Sand 17	42	0.30	0.14	-0.09	0.36
Clean Sand 18	41	0.30	0.18	-0.11	0.38
Clean Sand 19	46	0.30	0.16	-0.09	0.37
Clean Sand 20	49	0.25	0.14	-0.07	0.33
Clean Sand 21	41	0.31	0.15	-0.10	0.37
Clean Sand 22	54	0.41	0.15	-0.14	0.42
Clean Sand 23	43	0.26	0.17	-0.07	0.35
Clean Sand 24	51	0.37	0.12	-0.09	0.39
Clean Sand 25	49	0.21	0.16	-0.05	0.32
Clean Sand 26	49	0.25	0.15	-0.06	0.34
Clean Sand 27	52	0.26	0.30	-0.10	0.46
Clean Sand 28	42	0.32	0.15	-0.09	0.38
Clean Sand 29	49	0.26	0.15	-0.07	0.34
Clean Sand 30	42	0.31	0.13	-0.10	0.34
Clean Sand 31	45	0.28	0.14	-0.07	0.34
Clean Sand 32	44	0.32	0.14	-0.09	0.37

* Relative density after the reconstitution

ε_z = axial strain, ε_r = radial strain, ε_θ = circumferential strain, ε_p = volumetric strain

Table 4.4. Strains measured during anisotropic consolidation of 16 NP silty sand specimens before the creep stage

			Maximum Strains Measured			
Test No	**D_R* (%)**	**FC (%)**	**ε_a (%)**	**ε_r (%)**	**ε_θ (%)**	**ε_p (%)**
NP Silty Sand 1	54	15	0.74	-0.02	-0.21	0.51
NP Silty Sand 2	55	15	0.82	-0.05	-0.21	0.56
NP Silty Sand 3	54	15	0.68	-0.05	-0.19	0.44
NP Silty Sand 4	53	14	0.83	-0.16	-0.24	0.43
NP Silty Sand 5	39	16	0.86	-0.06	-0.24	0.57
NP Silty Sand 6	48	13	1.23	-0.14	-0.34	0.77
NP Silty Sand 7	48	14	0.86	-0.06	-0.24	0.57
NP Silty Sand 8	47	11	0.91	-0.09	-0.22	0.60
NP Silty Sand 9	43	14	1.01	-0.13	-0.31	0.58
NP Silty Sand 10	36	13	0.88	-0.10	-0.24	0.54
NP Silty Sand 11	35	13	1.21	-0.20	-0.32	0.70
NP Silty Sand 12	46	12	1.05	-0.08	-0.31	0.67
NP Silty Sand 13	47	13	0.88	-0.10	-0.27	0.51
NP Silty Sand 14	59	14	0.89	-0.12	-0.23	0.54
NP Silty Sand 15	41	13	0.87	-0.08	-0.24	0.56
NP Silty Sand 16	34	13	0.86	-0.10	-0.26	0.50
MEAN =	47	14	0.98	-0.1	-0.27	0.61
COV (%) =	16	9	14	41	15	15
* Relative density after the reconstitution, D_R						
ε_z = axial strain, ε_r = radial strain, ε_θ = circumferential strain, ε_p = volumetric strain						

Table 4.5. Strains measured during anisotropic consolidation of 32 clean sand specimens after the creep stage

		Maximum Strains Measured			
Test No	**D_R* (%)**	**ε_a (%)**	**ε_r (%)**	**ε_θ (%)**	**ε_v (%)**
Clean Sand 1	40	0.29	0.17	-0.11	0.36
Clean Sand 2	46	0.30	0.12	-0.10	0.32
Clean Sand 3	50	0.57	0.08	-0.17	0.48
Clean Sand 4	39	0.48	0.24	-0.17	0.55
Clean Sand 5	40	0.45	0.09	-0.12	0.42
Clean Sand 6	38	0.45	0.11	-0.12	0.44
Clean Sand 7	52	0.33	0.17	-0.09	0.41
Clean Sand 8	47	0.48	0.07	-0.14	0.41
Clean Sand 9	51	0.26	0.17	-0.08	0.35
Clean Sand 10	37	0.66	0.01	-0.20	0.47
Clean Sand 11	37	0.40	0.11	-0.11	0.40
Clean Sand 12	46	0.34	0.13	-0.11	0.36
Clean Sand 13	44	0.73	0.32	-0.33	0.72
Clean Sand 14	46	0.27	0.16	-0.09	0.34
Clean Sand 15	40	0.41	0.09	-0.11	0.39
Clean Sand 16	47	0.40	0.14	-0.10	0.44
Clean Sand 17	42	0.34	0.14	-0.10	0.37
Clean Sand 18	41	0.33	0.17	-0.12	0.38
Clean Sand 19	46	0.33	0.17	-0.11	0.39
Clean Sand 20	49	0.28	0.13	-0.08	0.34
Clean Sand 21	41	0.33	0.17	-0.12	0.38
Clean Sand 22	54	0.46	0.16	-0.17	0.45
Clean Sand 23	43	0.28	0.18	-0.08	0.37
Clean Sand 24	51	0.41	0.11	-0.11	0.41
Clean Sand 25	49	0.23	0.16	-0.06	0.34
Clean Sand 26	49	0.28	0.15	-0.07	0.35
Clean Sand 27	52	0.28	0.31	-0.11	0.48
Clean Sand 28	42	0.36	0.14	-0.10	0.40
Clean Sand 29	49	0.29	0.15	-0.08	0.36
Clean Sand 30	42	0.35	0.12	-0.11	0.36
Clean Sand 31	45	0.31	0.13	-0.08	0.36
Clean Sand 32	44	0.38	0.13	-0.11	0.39

* Relative density after the reconstitution

ε_z = axial strain, ε_r = radial strain, ε_θ = circumferential strain, ε_p = volumetric strain

Table 4.6. Strains measured during anisotropic consolidation of 32 clean sand specimens after the creep stage

			Maximum Strains Measured			
Test No	**D_R* (%)**	**FC (%)**	**ε_a (%)**	**ε_r (%)**	**ε_θ (%)**	**ε_p (%)**
NP Silty Sand 1	54	15	0.83	-0.02	-0.24	0.58
NP Silty Sand 2	55	15	0.95	-0.05	-0.25	0.65
NP Silty Sand 3	54	15	0.76	-0.06	-0.22	0.48
NP Silty Sand 4	53	14	0.86	-0.18	-0.25	0.44
NP Silty Sand 5	39	16	0.94	-0.07	-0.26	0.61
NP Silty Sand 6	48	13	1.36	-0.16	-0.37	0.84
NP Silty Sand 7	48	14	0.94	-0.07	-0.26	0.62
NP Silty Sand 8	47	11	0.99	-0.1	-0.24	0.65
NP Silty Sand 9	43	14	1.13	-0.14	-0.34	0.65
NP Silty Sand 10	36	13	0.97	-0.11	-0.27	0.6
NP Silty Sand 11	35	13	0.97	-0.11	-0.26	0.59
NP Silty Sand 12	46	12	1.16	-0.1	-0.34	0.73
NP Silty Sand 13	47	13	0.95	-0.11	-0.29	0.56
NP Silty Sand 14	59	14	0.97	-0.13	-0.25	0.59
NP Silty Sand 15	41	13	0.96	-0.09	-0.27	0.6
NP Silty Sand 16	34	13	0.95	-0.11	-0.29	0.56
MEAN =	47	14	0.98	-0.1	-0.27	0.61
COV (%) =	16	9	14	-41	-15	15
* Relative density after the reconstitution, D_R						
ε_z = axial strain, ε_r = radial strain, ε_θ = circumferential strain, ε_p = volumetric strain						

Rolo (2003) conducted anisotropic consolidation (K_0 conditions) defined as the stress state change from p'= 70 kPa to p' = 93 kPa with pure axial loading and then, increase of q to 150 kPa and p' to 200 kPa with K = 0.5 on four different HC Ham river sand specimens with 15 % Kaolin clay (average void ratio = 0.564). Observed maximum radial ranged between -0.1 % and 0.1 %, while the maximum circumferential strain ranged between -0.05 % and 0.15 %. Rolo (2003) considered the magnitudes of these strains close enough to zero indicating K_0 conditions.

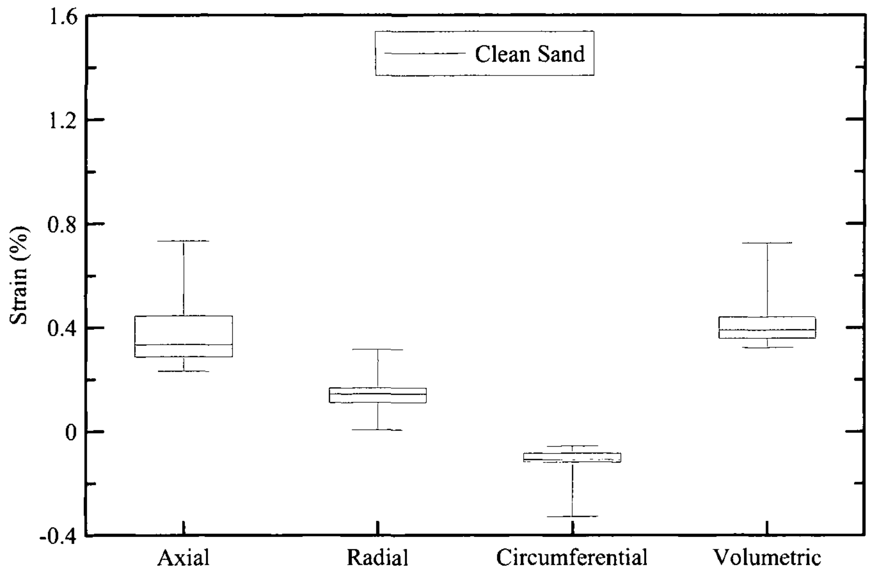

Figure 4.8. Variation of maximum strains measured during anisotropic consolidation of 32 clean sand specimens

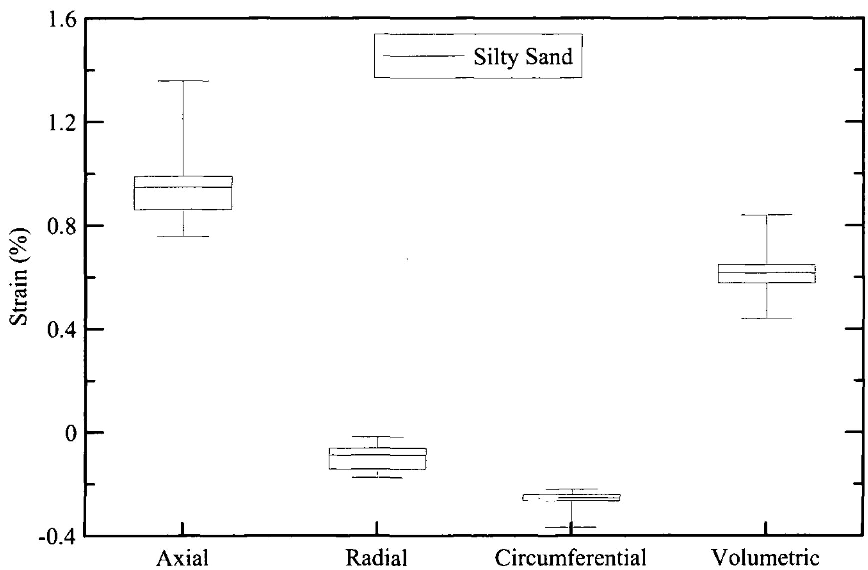

Figure 4.9. Variation of maximum strains measured during anisotropic consolidation of 16 NP silty sand specimens

In this study, the measured average radial and circumferential strains for the clean and NP silty sand specimens (FC = 15 %) fall in the range observed by Rolo (2003) even though the materials used are quite different. In both studies, magnitudes of radial and circumferential strains measured for clean and NP silty sand specimens may be considered close to zero for practical purposes, and, thus, the anisotropic consolidation conducted closely simulates the K_0 conditions without introducing any physical constraints in the horizontal plane of the specimens.

The final stress state of the specimen after K_0 consolidation is close to the critical state line (CSL) on p' - q plane, where the CSL corresponds to a critical state friction angle of 29.5° for clean sands, and 34.4° for NP silty sands (Carraro 2004). Even though the stress path approaches the CSL, there is no sign of instability in the specimen behavior, and the deformations are small. However, Vaid and Chern (1985) mentioned that sand specimens may be stable in drained conditions around the CSL, but a small disturbance in undrained conditions would trigger flow deformations.

The deviatoric stress – strain response of 32 clean sand and 16 NP silty Ottawa sand specimens during anisotropic consolidation are given in Figs 4.10 and 4.11, respectively. 30 out of 32 the clean sand specimens experienced ε_q between 0.4 % and 0.6 %, while 13 out of 16 NP silty sand specimens experienced ε_q between 0.9 % and 1.2 %. Fig. 4.10 and 4.11 show good repeatability for both clean and NP silty sand specimens. The secant stiffness of the clean sand is larger the secant stiffness of NP silty sand. Furthermore the secant stiffness of clean sand is almost constant, while that of the NP silty sand degrades during anisotropic consolidation.

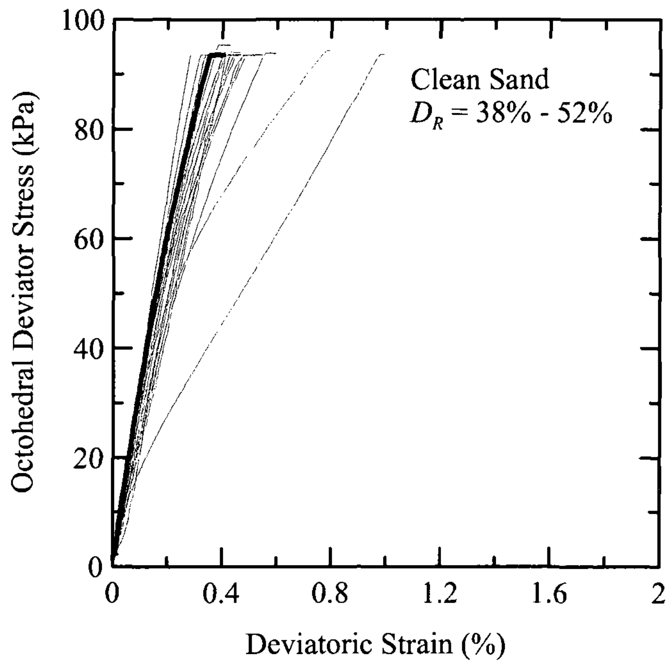

Figure 4.10. Deviatoric stress-strain behavior of clean sand during anisotropic consolidation.

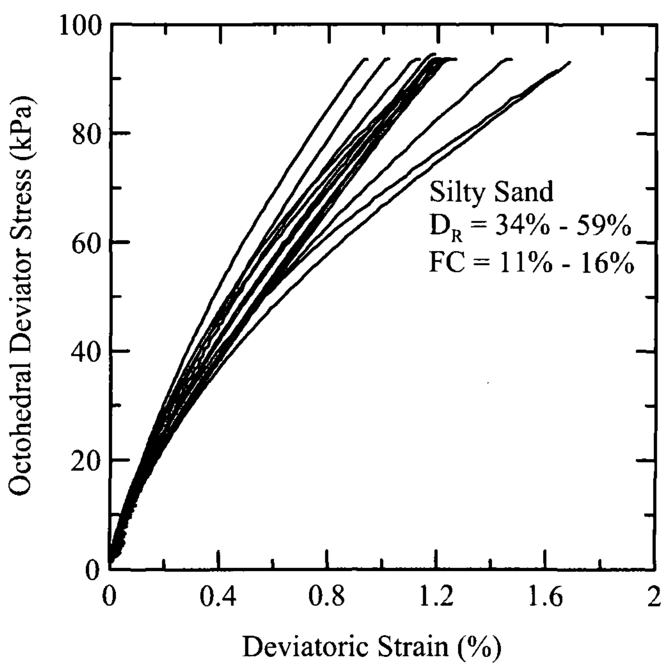

Figure 4.11. Deviatoric stress-strain behavior of NP silty sand during anisotropic consolidation.

4.3.3 Effect of Major Principal Stress Rotation on Drained Behavior of Ottawa Sand with and without NP Silt

Following the anisotropic consolidation, the major principal stress was rotated at constant p', K, σ_1, σ_2, and σ_3 (Fig. 4.12). According to Eq. 2.14, in order to increase α, (1) the shear stress may be increased, (2) circumferential stress may be increased, or (3) the axial stress may be decreased. In this study, all of these stress changes were conducted at the same time (Fig. 4.12) to increase α linearly as a function of time as shown in Fig. 4.12a and Fig. 4.12b. Radial stress was not changed during the major principal stress rotation. Fig.4.12 shows the stresses applied on clean and NP silty sand specimens during α increase to 30° and 60°. The major principal stress rotation to 60° required larger decrease in the axial stress and increase in the circumferential stress while keeping the shear stress increase around the same compared to the stress components applied to achieve 30° rotation. Moreover, all three principal stress magnitudes were constant during α increase to 30° and 60° (Fig. 4.12c).

Exactly the same stress changes were imposed on clean and silty sand specimens during the rotation of the major principal stress, which allows comparison of their strain responses for a given D_R.

Stress paths associated with geotechnical applications typically involve change in both the magnitude and direction of principal stresses. Part of this study was conducted without allowing any changes in the magnitudes of the principal stresses to characterize the effect of major principal stress rotation alone. In other words, during the rotation of the major principal stress, no change in the stress path on p'- q plane was allowed.

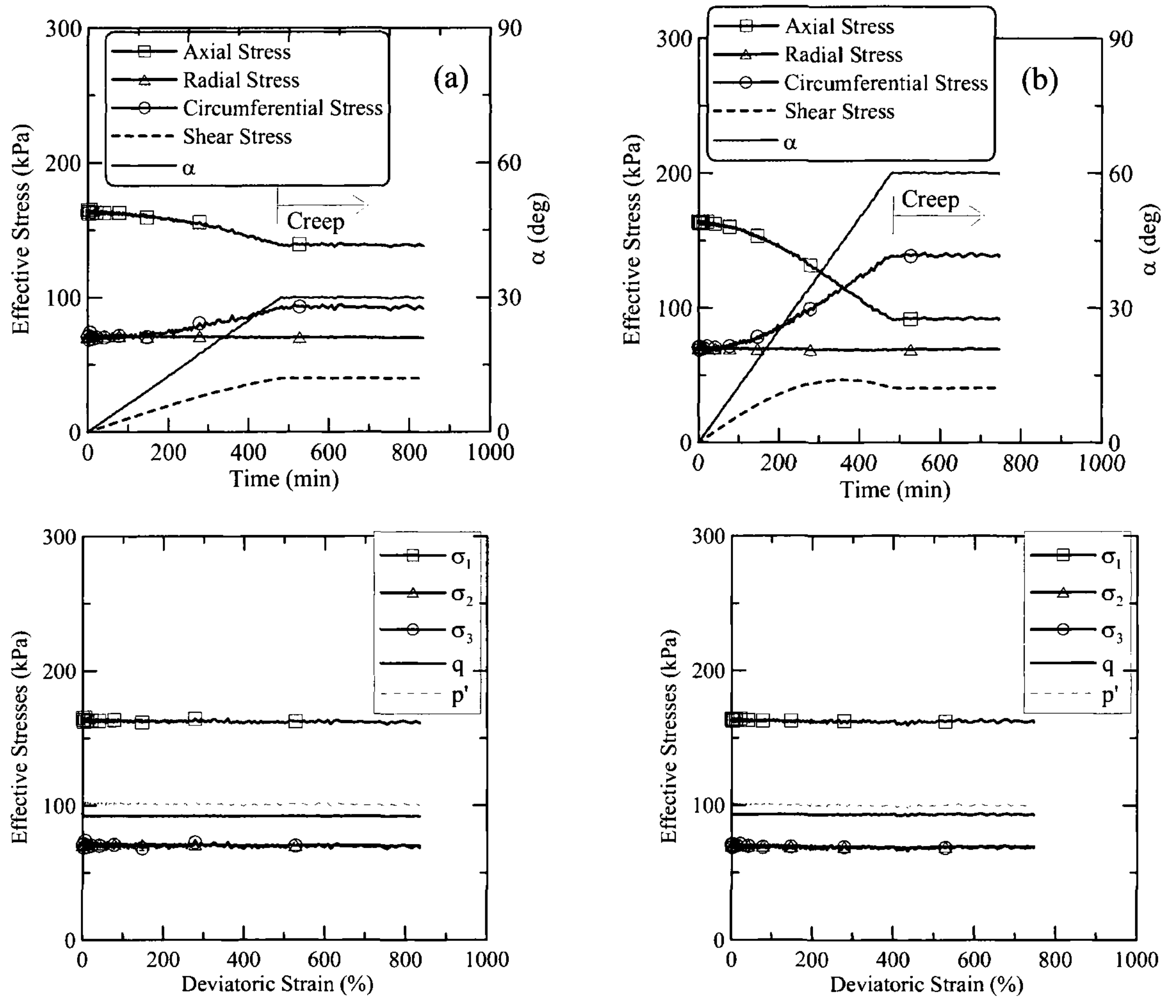

Figure 4.12. (a) Basic stress components, (b) principal stresses to rotate α by 30°, and (c) basic stress components, (d) principal stresses to rotate α by 60°.

Strains induced in clean and silty sand specimens due to α increase to 30° (three tests for each soil type) and 60° (three tests for each soil type) are shown in Fig. 4.13 and Fig. 4.14. The final axial strain induced by α increase to 30° was less than 0.4 % for both clean and NP silty sand specimens (Figs. 4.14a and 4.14d), where D_R shown are at the end of anisotropic consolidation. When α was rotated by 60° clean sand specimens experienced an average maximum axial strain of 0.5 % (Fig. 4.13a), while the NP silty sand specimens underwent negligible axial strain (Fig. 4.13a). During α rotation to 60°, both clean and NP silty sand specimens initially contracted, and, then dilated in the vertical direction. This may be due to the large reduction in the axial stress to achieve α = 60°. The change in behavior from contraction to dilation occured approximately when α = 45°. In other words, specimens showed contractive behavior up to α = 45°, and, then, dilative behavior when α > 45°.

Clean sand specimens experienced negligible radial strains while increasing α to 30°, and radial strain of about -0.5 % while increasing α to 60°. The radial strain experienced by the NP silty sand was negligible when α was increased to 30° or 60°. The rotation of the major principal stress was conducted without changing the radial stress. Therefore, the small or negligible radial strain observed during the rotation of the principal stress is in agreement with the stresses applied.

The circumferential strain development during the rotation of the major principal stress is shown in Fig. 4.13c and Fig. 4.13f for clean and silty sand specimens, respectively. While the circumferential stress was increased to increase α by 30°, negligible circumferential strains developed in clean and NP silty sand specimens. However, as α was further increased to 60°, clean sand specimens experienced a circumferential strain between 0.5 % and 0.9 %, while NP silty sand specimens experienced a circumferential strain between 0.6 % and 0.8 %. The HC specimen wall diameter decreased while their height increased during this process.

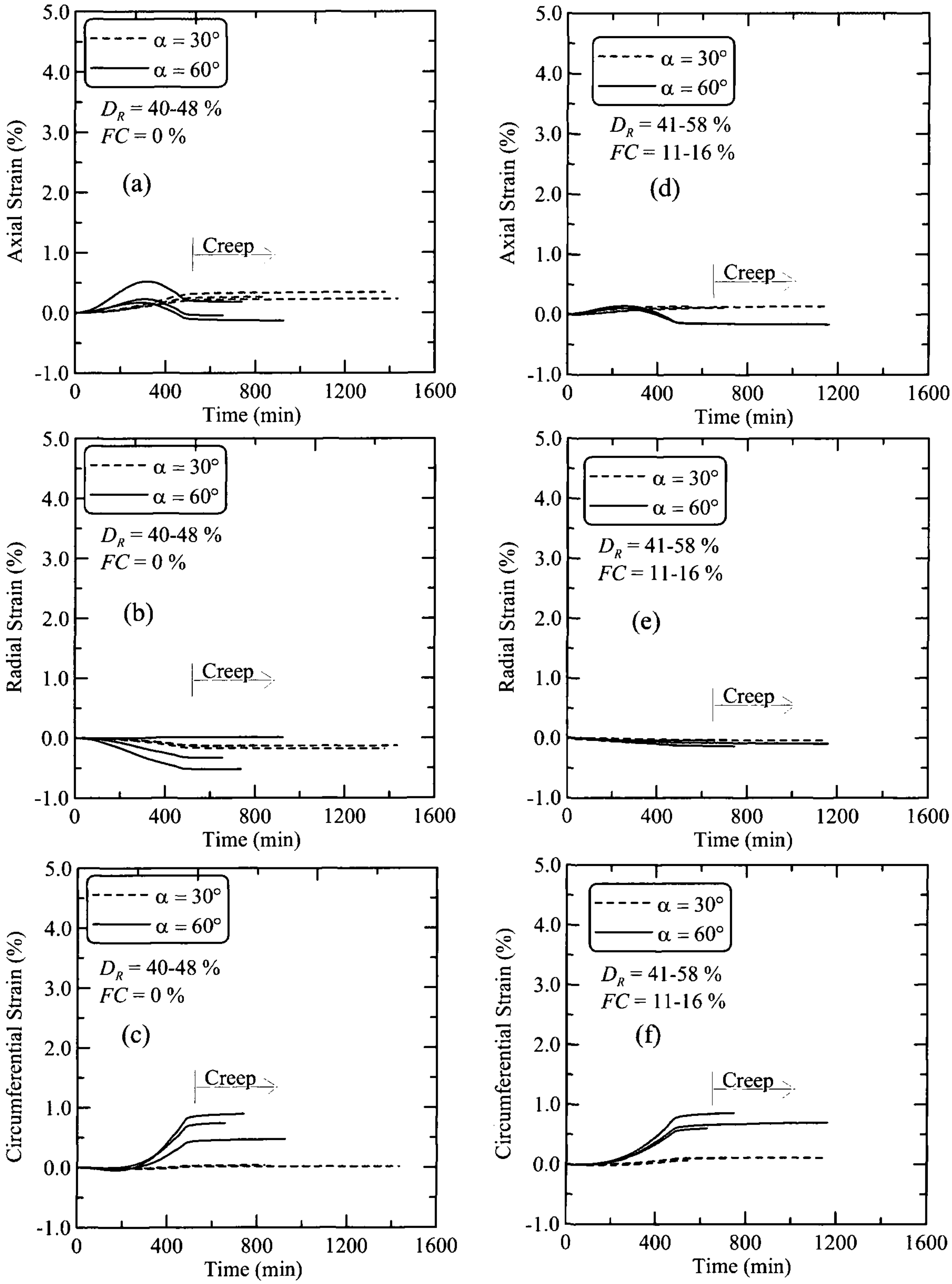

Figure 4.13 (a) Axial, (b) radial, (c) circumferential strains induced in clean sand specimens, (d) axial, (e) radial, (f) circumferential strains induced in silty sand specimens during the major principal stress rotation.

Fig. 4.14a and Fig. 4.14c show the shear strain behavior of clean and NP silty sand specimens, respectively, when subjected to 30° and 60° major principal stress rotation. When α was increased to 30°, the shear strain observed (including the creep) was between 1.2 % and 1.6 % for the clean sand, and 0.9 % for the NP silty sand. When α was increased to 60°, clean sand specimens experience shear strains between 2.6 % and 4.8 % and silty sand specimens experience between 1.9 % and 2.4 %. The predominant strain component during α increase to both 30° and 60° is the shear strain. The volumetric strains induced due to α increase by 30° were between 0.1 % and 0.2 % for both clean and NP silty sand specimens. Increase in α to 60° resulted in volumetric strains between 0.4 % and 0.6 % for the clean sand, and between 0.5 % and 0.6 % for the NP silty sand.

The shear strain experienced by the silty sand specimens was less than what was experienced by the clean sand specimens for both 30° and 60° increase in α. This can be due to two factors, (1) fabric difference, or (2) relative density difference between clean and silty sand specimens. As mentioned in Section 4.3.2, prior to the major principal stress rotation, silty sand specimens underwent larger axial strains during anisotropic consolidation than clean sand specimens. The generated strain during anisotropic consolidation naturally has an impact on the relative density at the end of the consolidation

After the specimen reconstitution, average relative densities for the clean and NP silty sand specimens considered here were 41 % and 45 %, respectively. Anisotropic consolidation increased the average relative density of the clean sand specimens to 44 %, and the average relative density of the silty sand specimens to 50 %. Even though this relative density difference is relatively small, the shear strain behaviors of clean and NP silty sands are compared in Fig. 4.15 to completely eliminate the effect of D_R.

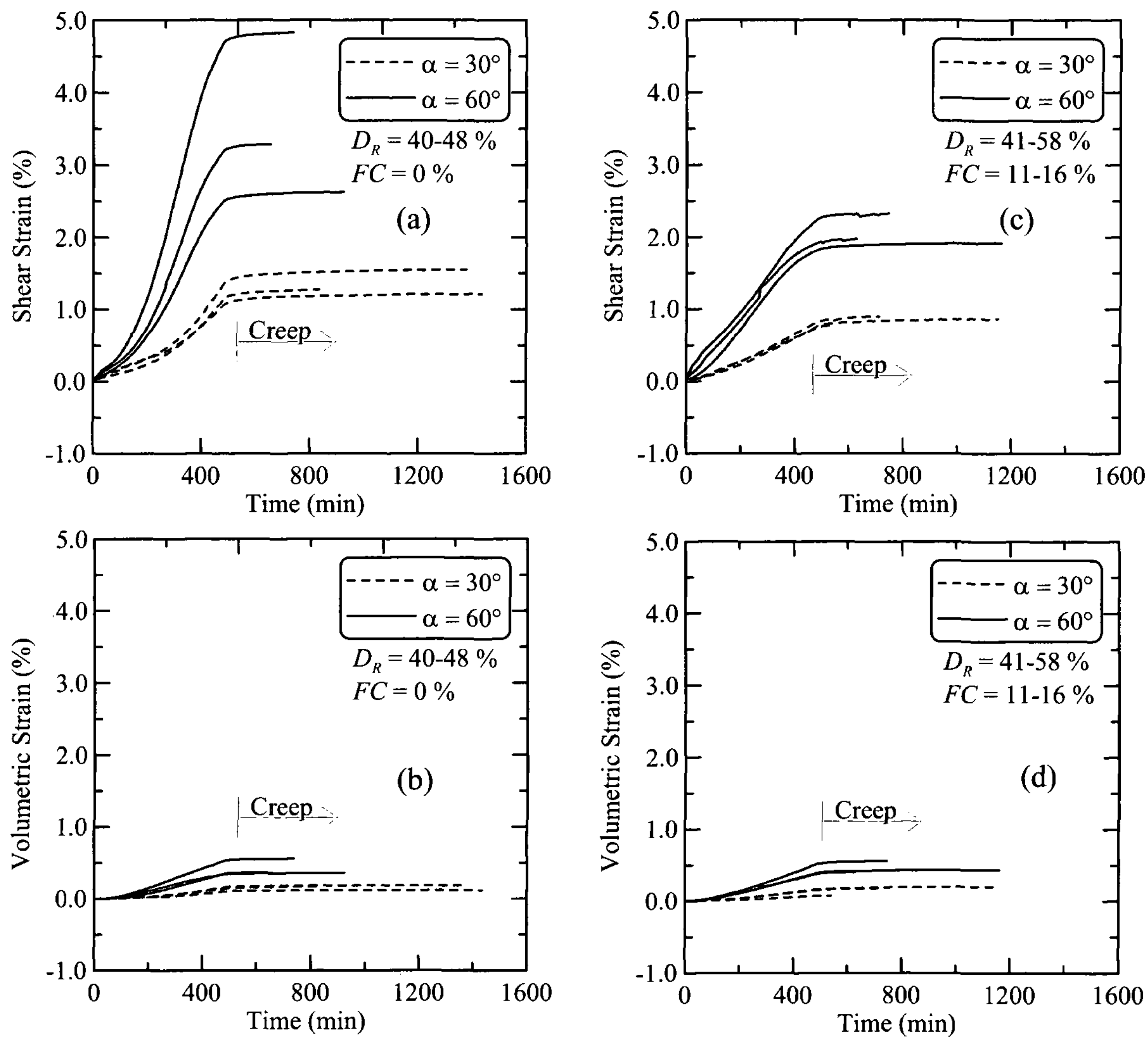

Figure 4.14. (a) Shear, (b) volumetric strains induced in clean sand specimens, (c) shear, (d) volumetric strains induced in NP silty sand specimens during the major principal stress rotation.

For the similar D_R at the beginning of the principal stress rotation, clean sand specimen still experienced larger shear and circumferential strains than silty sand specimen did for both 30° and 60° increase in α. Therefore, the difference between the behaviors of clean and silty sand specimens given in Figs. 4.13, 4.14, 4.15 may be primarily attributed to the fabric difference between clean and silty sand.

Figs. 4.13 through 4.15 indicate that sand specimens with or without fines may be sheared significantly due solely to the drained principal stress rotation even if the magnitudes of principal stresses remain constant.

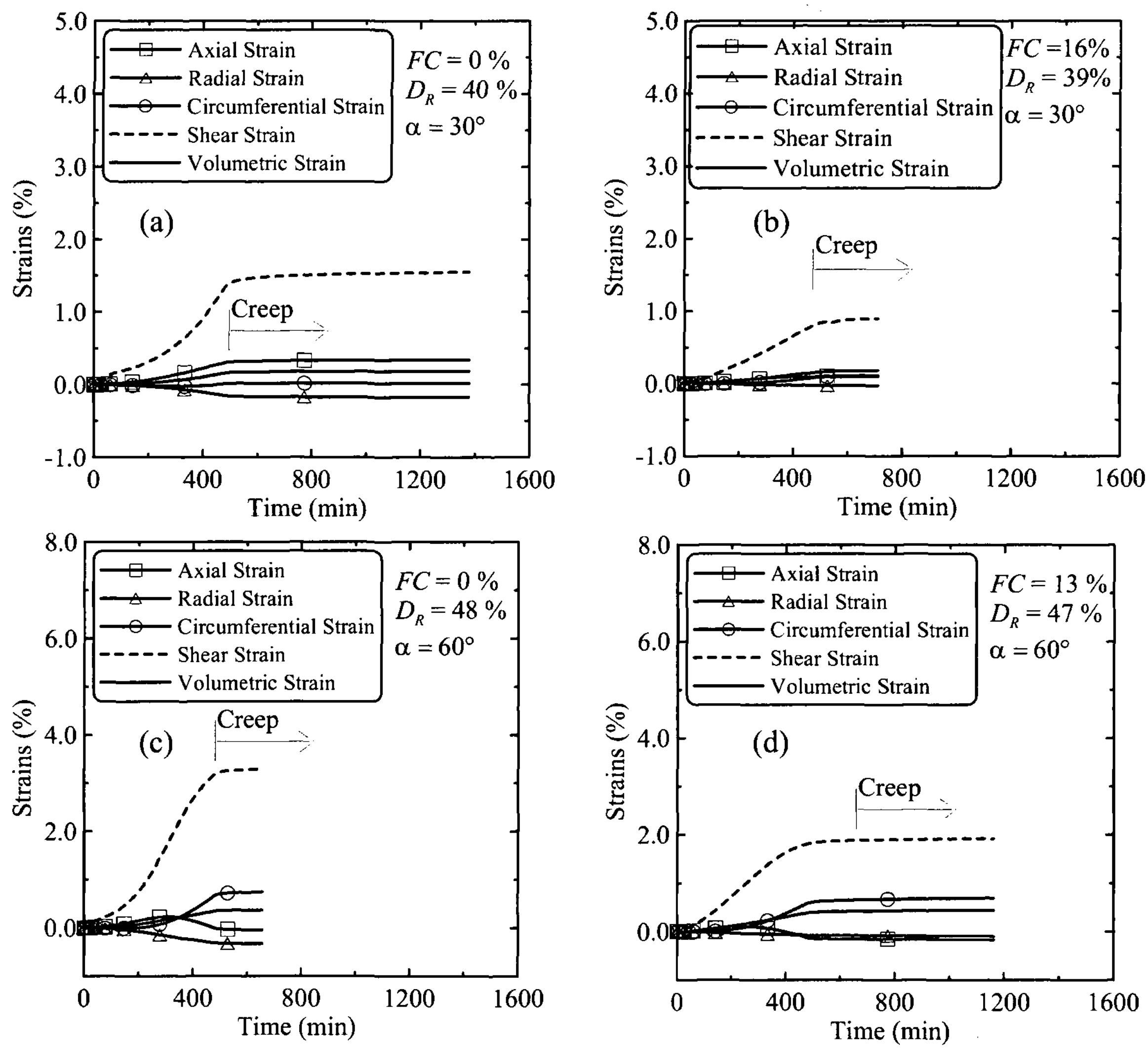

Figure 4.15. Strain response of (a) clean sand, (b) silty sand during α rotation to 30°, (c) clean sand, and (d) silty sand during α rotation to 60°.

Shear stress – shear strain behaviors of clean and NP silty sand specimens during drained principal stress rotation to 30° or 60° are given in Fig. 4.16.

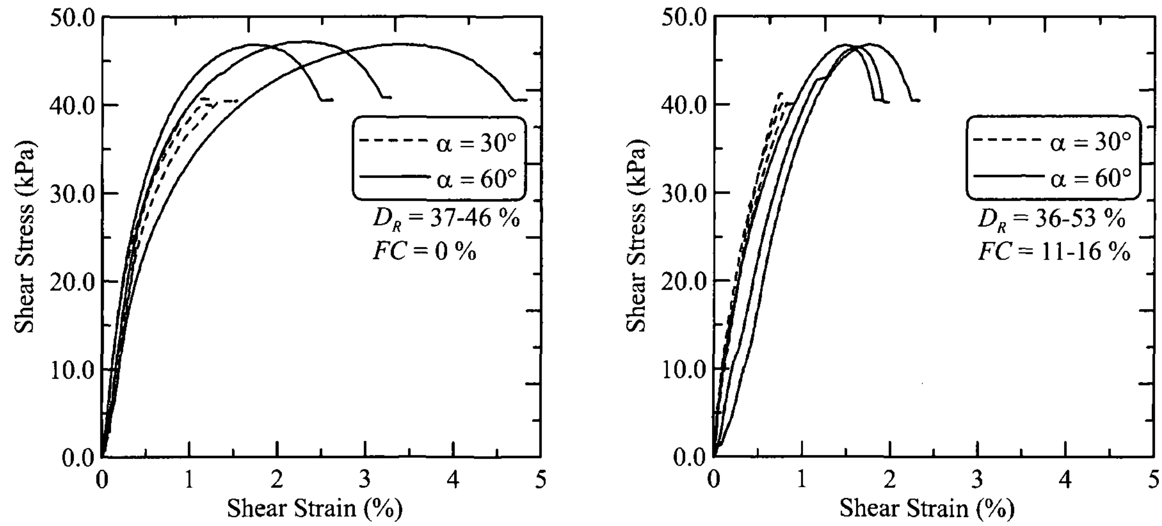

Figure 4.16. Shear stress – strain behavior of (a) clean sand, and (b) NP silty sand during drained α increase to 30° or 60°.

During drained increase in α to 30°, both clean and silty sand specimens had similar initial secant modulus up to 0.5 % shear strain. However during the increase in α to 60°, the initial secant modulus of the clean sand was larger than that of the silty sand. Furthermore, both clean and NP silty sands experienced stiffness degradation throughout the principal stress rotation.

4.3.4 Effect of b Change on Drained Behavior of Ottawa Sand with and without NP Silt

At constant p' and $\alpha = 0°$, b was increased from 0 to 0.5 or 0.8 to analyze its effect on the drained behavior of K_0-consolidated Ottawa sand specimens with and without NP silt. The typical stresses applied to achieve b = 0.5 and b = 0.8 are shown in Fig. 4.17a and Fig. 4.17c, respectively.

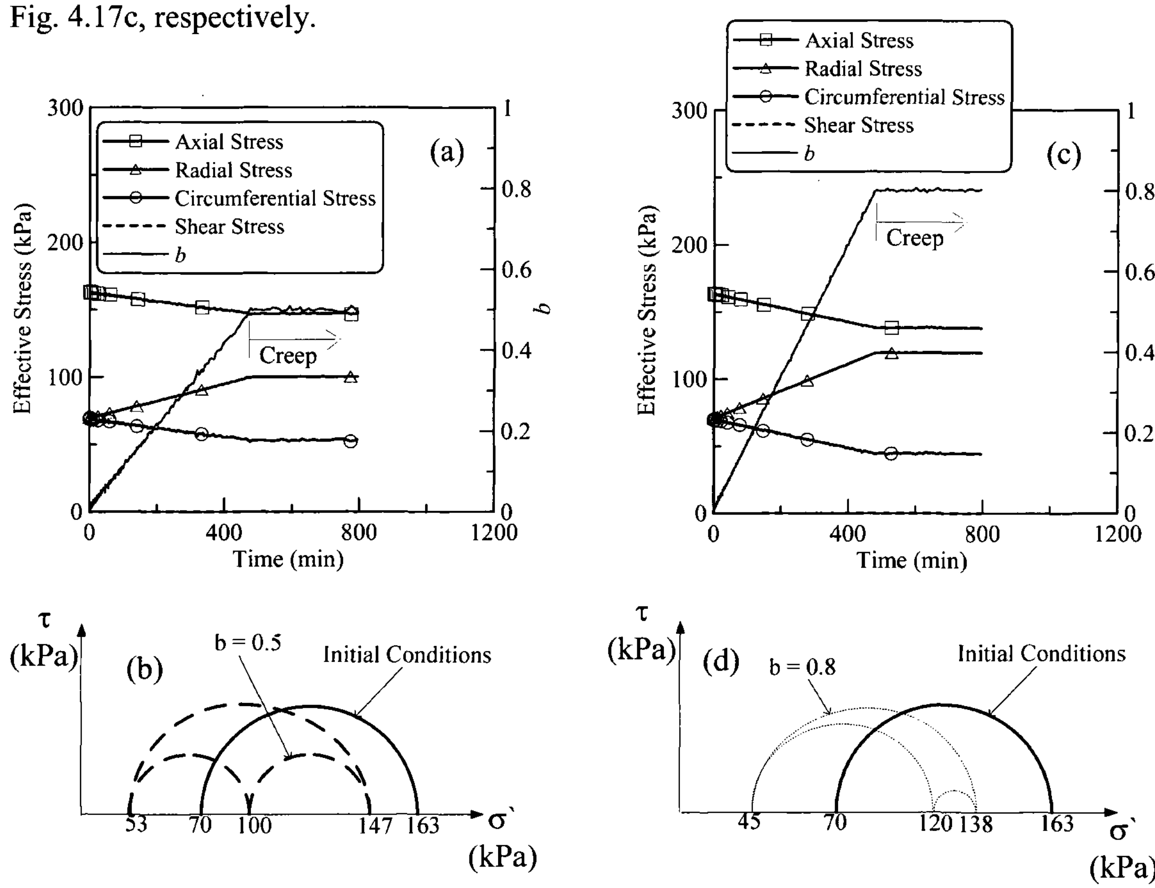

Figure 4.17. For the drained increase to b = 0.5 (a) stresses applied, (b) initial and final Mohr's circles, and for the drained increase to b = 0.8 (c) stresses applied, (d) initial and final Mohr's circles

Shown in Fig.4.17 are the Mohr's circles at the beginning and end of the b increase. Mohr's circles shift left due to b increase, and the amount of shift is proportional to the b

magnitude. Stresses at the beginning and end the end of b increase show that (σ_1 - σ_3) is maintained constant during b increase.

An increase in b was achieved by simultaneously (1) reducing the axial and circumferential stresses, and (2) increasing the radial stress. Even though increasing only the radial stress may have sufficed to increase b, the axial and circumferential stresses were also reduced along with the increase in the radial stress to increase b at constant p'. No shear stress changes were applied to the specimens at this stage. Therefore, the axial, radial and circumferential effective stresses were the major, intermediate and minor effective stresses, respectively. The amount of reduction in axial and circumferential stresses and the increase in radial stress were proportional to the target b magnitude to be achieved. In other words, increasing b to 0.8 required larger axial and radial stress drops along with a larger radial stress increase compared to the stress changes required to increase b to 0.5. Unlike the α increase stage, the principal stresses were not kept constant while b was increased to the target value, since b increase requires incrementing the intermediate principal stress. However, as mentioned previously, p' was kept constant.

Fig. 4.18 and 4.19 illustrate the strain responses of clean and NP silty Ottawa sand specimens when to the stress changes shown in Fig. 4.17. In these figures, each α and b combination is represented with three test results. Relative densities for clean and NP silty sand specimens at the end of anisotropic consolidation were in the range of 41-54 % and 42-64 %, respectively. The fines content for NP silty sand specimens was between 12 % and 14 %. In the following discussion, the strains reported refer to the end of the stress increments rather than the end of the creep period. Increasing b to 0.5 or 0.8 did not cause any axial or shear strains to either clean sand or NP silty sand. Similarly, increasing b to

0.5 generated negligible circumferential strains in both clean sand and silty sand. However, further increase in b to 0.8 resulted in about -0.3 % circumferential strain and this magnitude was similar for both clean and NP silty sand. The expansion in the circumferential direction was in agreement with the reduction in the circumferential stress required to increase b (Fig 4.17). Increasing b to 0.5 induced about 0.2 % of radial strain in clean sand, while it induced about 0.3 % of radial strain in silty sand. Further increase in b to 0.8 increased the radial strain to 0.4 % and 0.6 % in clean and silty sands, respectively. The volumetric strains observed in clean and silty sands during b increase to 0.5 and 0.8 were between 0.1 % and 0.3 %. Increase in b to 0.8 induced slightly larger volumetric strain than increasing b to 0.5. The volumetric strain developed during b increase was much smaller than the volumetric strains generated during K_0 consolidation.

Increasing b to 0.5 resulted in an average deviatoric strain of 0.3 % and 0.4 % for clean and silty sands, respectively. Further increase of b to 0.8 increased the level of deviatoric strains to the average values of 0.6 % and 0.8 % for clean and silty sands, respectively.

The largest elementary strain generated due to b increase was in the radial direction, which was attributed to the increase in the radial stress required to increase σ_2' to its target value. The larger stress increment applied to increase b was in the radial direction or in the horizontal plane. However, the magnitudes of the radial and circumferential strains observed due to this loading were very similar for both clean and silty sand specimens. This suggests that clean and silty sand may have similar fabrics on the horizontal plane, at the end of anisotropic consolidation.

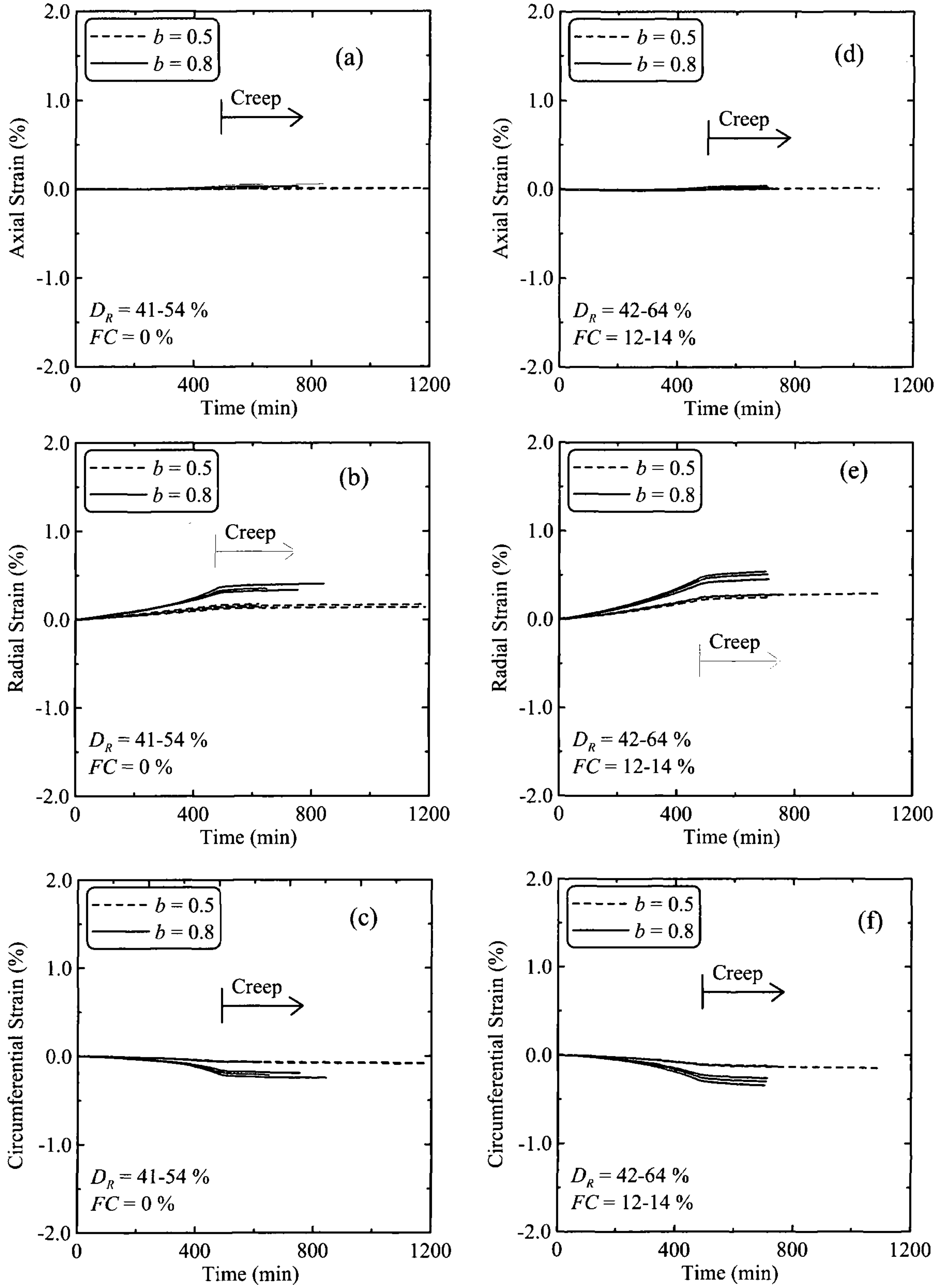

Figure 4.18. (a) Axial, (b) radial, (c) circumferential strains induced in clean sand specimens, (d) axial, (e) radial, and (f) circumferential strains induced in silty sand specimens during b increase to 0.5 and 0.8.

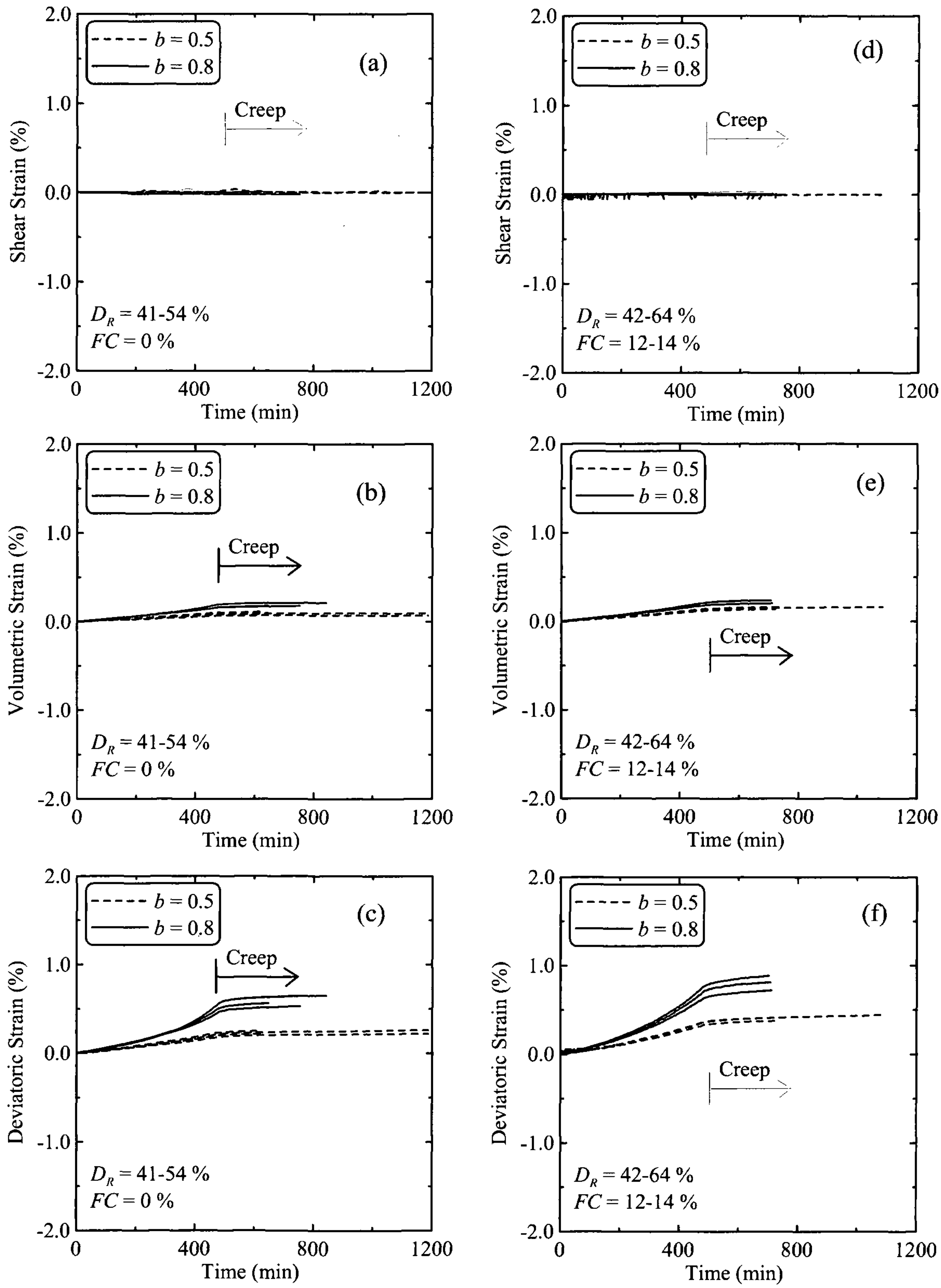

Figure 4.19. (a) Shear, (b) volumetric, (c) deviatoric strains induced in clean sand specimens, (d) shear, (e) volumetric, and (f) deviatoric strains induced in silty sand specimens during *b* increase to 0.5 and 0.8.

The maximum change in relative density during the b increase stage was limited to 2 % for both clean and silty sand specimens.

The magnitudes of the volumetric or deviatoric strains induced during b increase were less than those observed during anisotropic consolidation or principal stress rotation stages. In other words, increasing the relative magnitude of σ_2 (with respect to $\sigma_1'$and σ_3') at constant p' in drained conditions did not result in significant volumetric and deviatoric strain generation in both clean and silty sands. Furthermore, the process of increasing σ_2' appears to have developed plain strain conditions with all relevant deformation having developed on the horizontal plane.

4.3.5 Effect of Simultaneous Principal Stress Rotation and *b* Increase on the Drained Behavior of Ottawa Sand with and without NP Silt

In previous sections, the effects of systematic α and b increases on the drained behavior of clean or NP silty Ottawa sands were discussed separately. Increasing α at constant p' and q under drained conditions was shown to induce large shear strains. However, increasing b at constant p' and q resulted in large radial strains. In this section, the effect of increasing α and b simultaneously on the drained response of clean sands is discussed. Based on the findings from sections 4.3.3 and 4.3.4, the effect of simultaneous increases of α and b on the drained response is expected to be similar for clean sand and NP silty sand.

The effect of simultaneously increasing α and b on the drained behavior of clean Ottawa sand was investigated by linearly increasing both α (to 30° or 60°) and b (to 0.5 or 0.8) at constant p' in 8 h. The typical stress changes applied in radial coordinates or principal directions to achieve these boundary conditions are given in Fig. 4.20 and Fig. 4.21, respectively. Increases in shear and radial stresses, and decrease in axial stress are common for all α and b combinations shown in Fig. 4.20. The circumferential stress was not significantly changed to increase α to 30° and b to 0.5 or 0.8. However, the circumferential stress was increased to increase α to 60° and b to 0.5 or 0.8. The principal stress magnitudes were kept constant during major principal stress rotation. However, the principal stress magnitudes were no longer constant when α and b were changed at the same time (Fig. 4.21). The major and minor principal stress magnitudes decreased, while the intermediate principal stress increased to achieve the target α and b. Stress changes such as shown in Fig. 4.20 and 4.21 result in a linear increase of both α and b, as shown in Fig. 4.22.

Shown in Fig. 4.23 and 4.24 are the strain responses of the clean and NP silty sand specimens subjected to the stress paths depicted in Fig. 4.20 and 4.21, where three lines for each α and b combination stand for three tests. The relative density at the end of anisotropic consolidation for the specimens analyzed in Fig. 4.23 and 4.24 ranges between 44 % and 56 %.

Negligible axial and circumferential strains developed when α was increased to 30°, and b is increased to 0.5 or 0.8. On the other hand, when α was increased to 60° and b was increased to 0.5 or 0.8, an average axial strain of approximately -1 % (extensional) developed in clean sand specimens. This axial strain development is attributed to the effect of increasing α to 60°, since increasing b alone was shown to induce negligible axial strains (Fig. 4.18a).

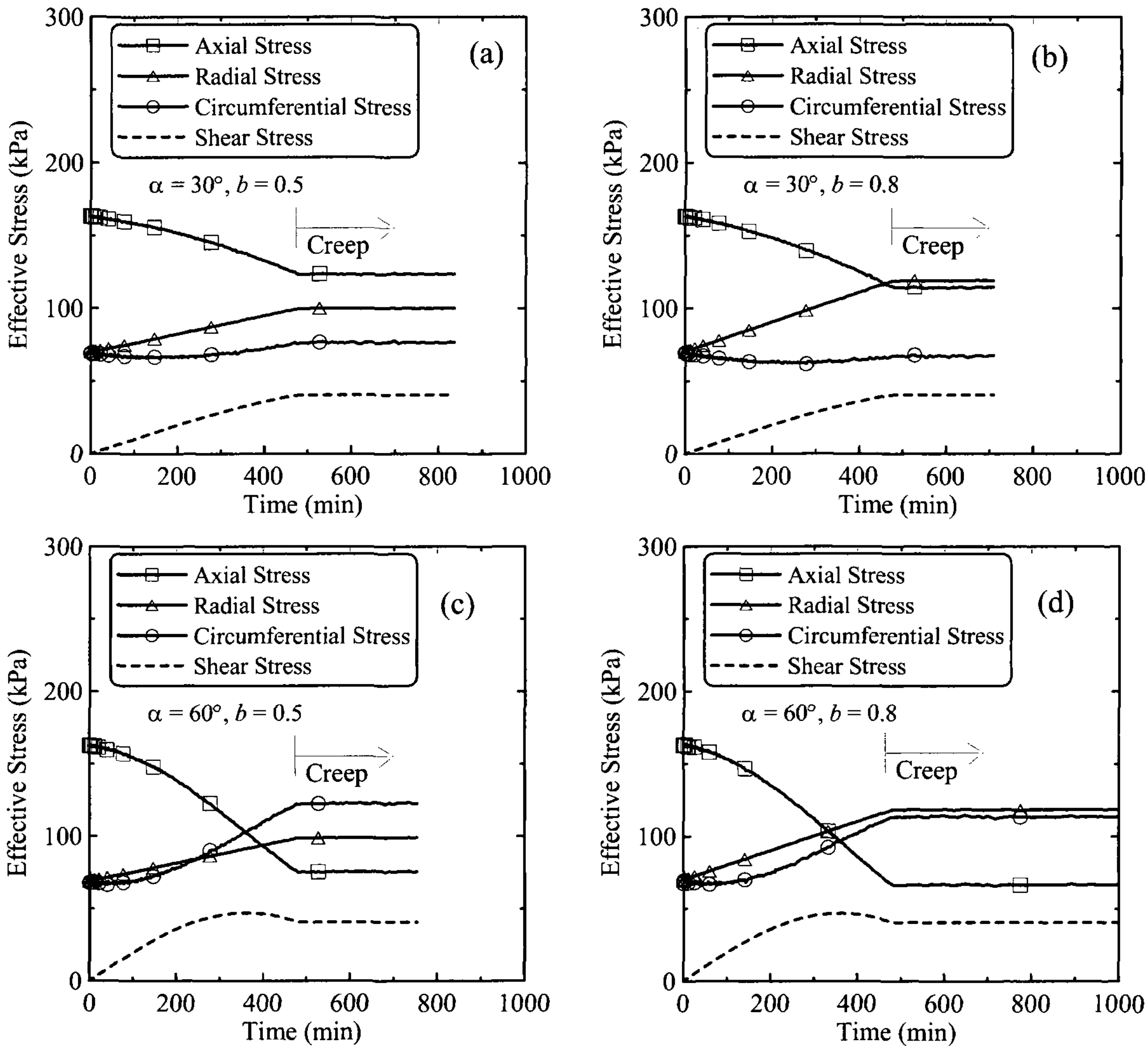

Figure 4.20 Typical stresses applied in radial coordinates to achieve (a) $\alpha = 30°$ and b = 0.5, (b) $\alpha = 60°$ and b = 0.5, (c) $\alpha = 30°$ and b = 0.8, and (d) $\alpha = 60°$ and b = 0.8.

For the same boundary conditions of α increase to 60° and b increase to 0.5 or 0.8, the average circumferential strain was again close to 1 % (compressional). When b was increased with α = 0°, the average circumferential strain was about -0.5 % (extensional) (Figure 4.18c and 4.18f). However, when α increased to 60° with b = 0, an average circumferential strain of about 0.7 % (compressional) was induced (Fig. 4.13c). Therefore, it appears that the effect of α dominates when α and b changes are applied together, based on the circumferential strain response of clean sand. When $b = 0$, increase in α to 30° was shown to induce negligible radial strain, whereas increase to 60° was shown to result in -0.5 % (extensional) radial strain. Increase in b to 0.5 or 0.8 when α = 0° resulted in average radial strains of 0.2 % and 0.5 % (compressional), respectively. Thus, the radial strain response shown in Fig. 4.23b and 4.23e appears to be primarily controlled by b changes.

Increase in α requires application of shear stresses, unlike increase in b. Thus, shear strains developed when α was increased to 30° or 60°, and the effect of b on the shear strain development was negligible (Figs. 4.14a and 4.19a). The shear strain responses in Figs. 4.24a show that an increase in b to 0.5 combined with an increase in α to 30° resulted in average of 1.2 % shear strain, whereas increase in α to 60° resulted in an average shear strain of 5.3 %. The actual variation of shear strain from 4.5 % to 6.5 % for three specimens subjected to α increase to 60° and b increase to 0.5 (Fig. 4.24a) is attributed to the relative density difference among specimens. The specimens that experienced the largest and lowest shear strains had D_R = 45 % and D_R = 55 %, respectively. This relative density difference also impacts the deviatoric strain response shown in Fig. 4.24c. Increasing b to 0.8 resulted in an average shear strain of 1.8 % with α = 30°, whereas increasing b to 0.8 and α to 60° induced about 5.3 % average shear strain (Fig. 4.24d). The actual shear strain variation between 4.2 % and 6.6 % for three specimens subjected to the same stress path of α increase to 60° and b increase to 0.8 cannot be explained by the relative density difference, since these three specimens did not follow the trend of denser specimens experiencing less shear strain. The difference in shear strain response may be attributed to the possible non-uniformities that may have been induced during the specimen preparation in the specimen with D_R = 48% (the one experiencing 6.6 % shear strain during α and b increase), since the other two specimens experienced relatively similar shear strains of 3 % and 4.2 %.

Based on the typical shear strain response of clean sand, the effect of α appears to dominate the overall response during simultaneous changes in α and b. Furthermore, the shear strains observed in clean sand specimens for any α and b combination was larger than any other individual strain component. This suggests that, the shear stresses required to increase α induced the largest deformations in the clean sand specimens despite the level of b used in the tests.

Volumetric strains due to increases in α and b did not exceed 1 %, and the effect of increasing α from 30° to 60° or changing b from 0.5 to 0.8 did not significantly impact the amount of volumetric strain experienced by the clean sand specimens (Figs. 4.24b and 4.24e).

The deviatoric strain magnitudes shown in (Fig. 4.24c and 4.24f) are very close to the shear strain magnitudes in observed (Fig. 4.24a and 4.24d), indicating that for the α and b combinations applied, the largest strain component is the shear strain for the clean sand specimens. Furthermore, the shear or deviatoric strain response is predominantly controlled by the increase in α rather than b. Loading due to geotechnical structures such as foundations or embankments typically induce α and b that are both greater than zero (except below the centerline). Furthermore, the loading due to these structures is expected to take place in drained conditions if the soil underneath is highly permeable sand. The analysis of such loading cases requires consideration of α induced along with q and p', since the sand behavior was shown to significantly depend on α increase regardless of whether b is increased along with α or not (Figs. 4.24a and 4.24d). Therefore conducting a simple drained triaxial test for the soil elements below these structures may not be realistic, since this type of testing cannot take into account the effect of α.

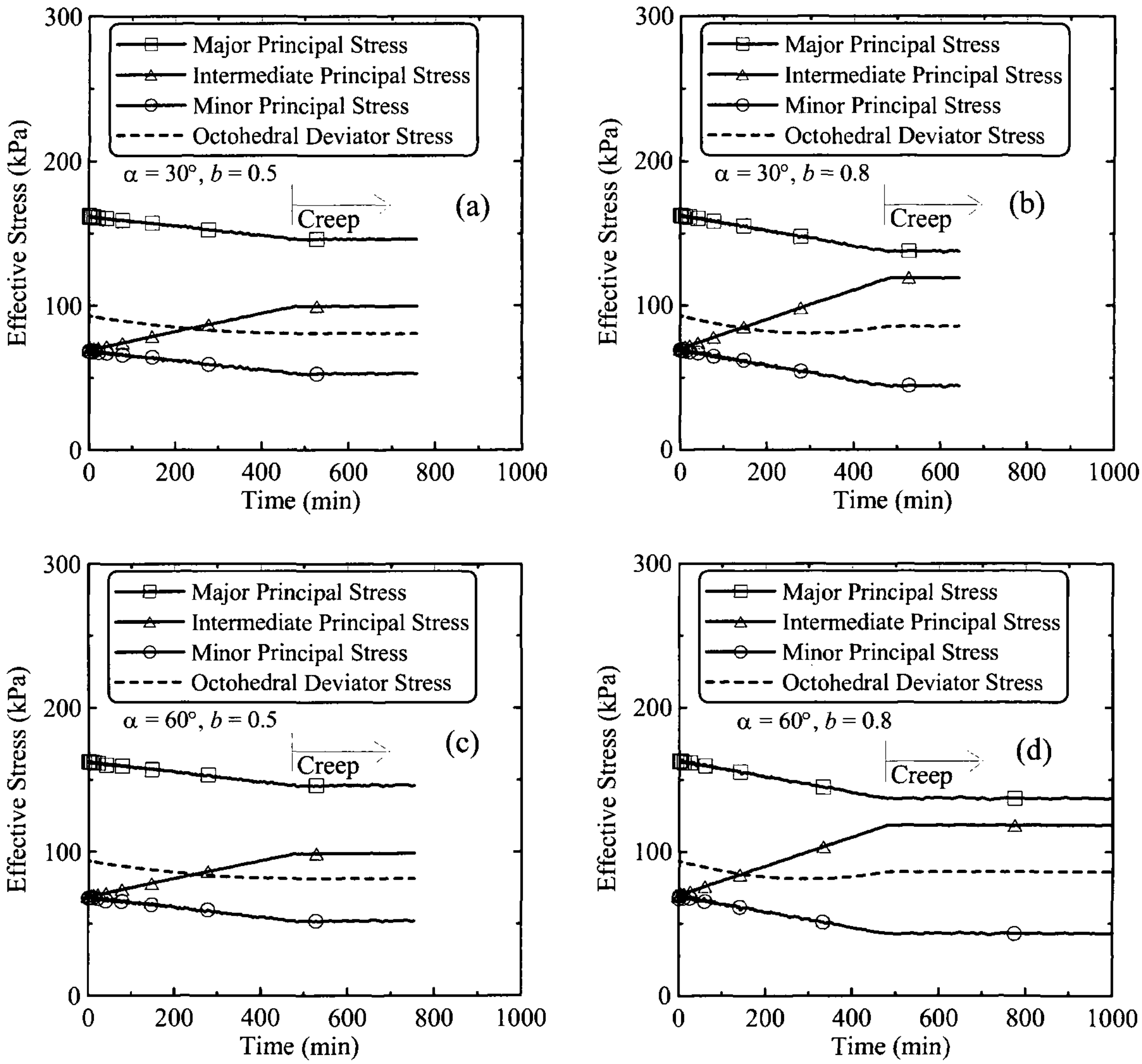

Figure 4.21 Typical principal stresses applied to achieve (a) $\alpha = 30°$ and $b = 0.5$, (b) $\alpha = 30°$ and $b = 0.8$, (c) $\alpha = 60°$ and $b = 0.5$, and (d) $\alpha = 60°$ and $b = 0.8$.

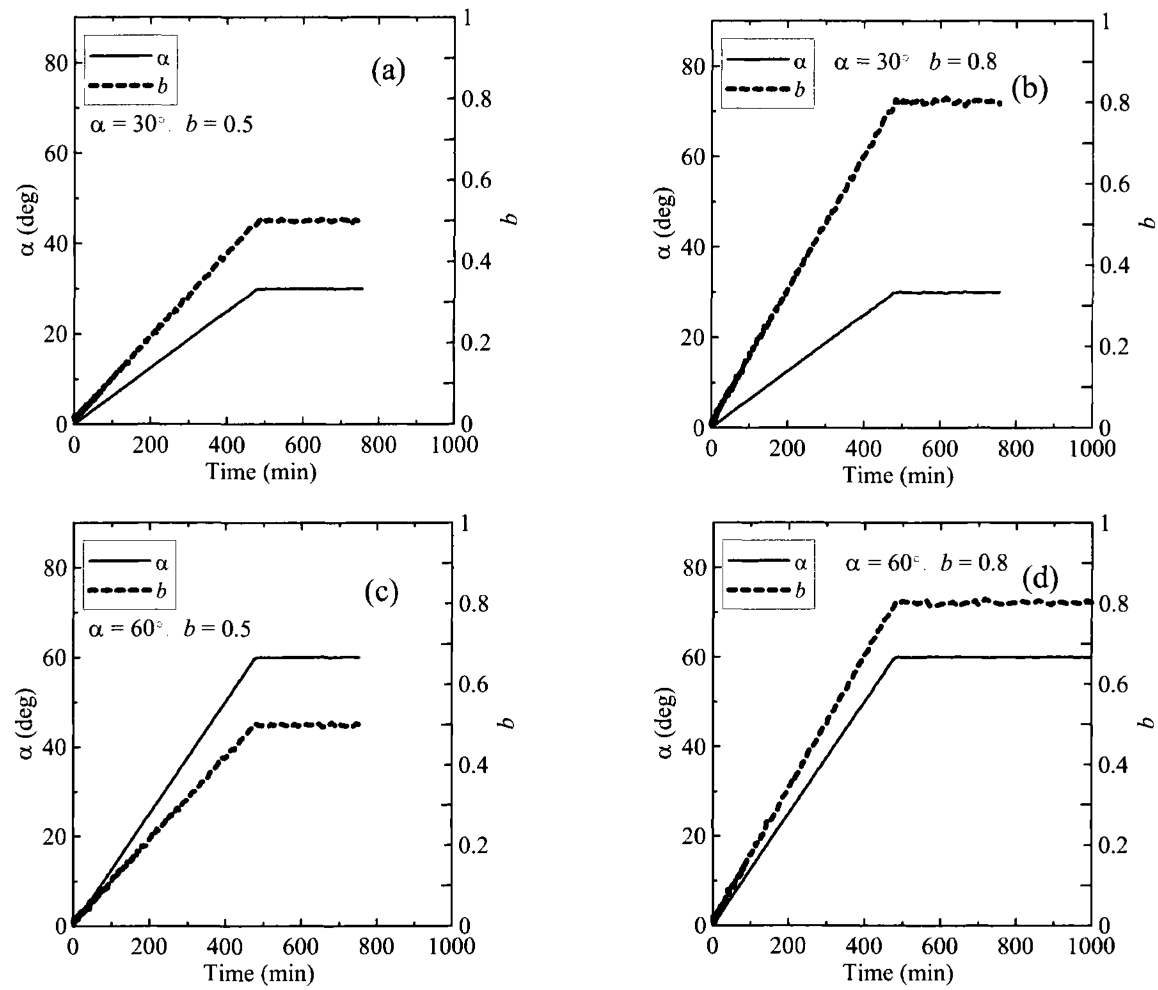

Figure 4.22. Variation of α and b as a function of time (a) $\alpha = 30°$ and $b = 0.5$, (b) $\alpha = 30°$ and $b = 0.8$, (c) $\alpha = 60°$ and $b = 0.5$, and (d) $\alpha = 60°$ and $b = 0.8$.

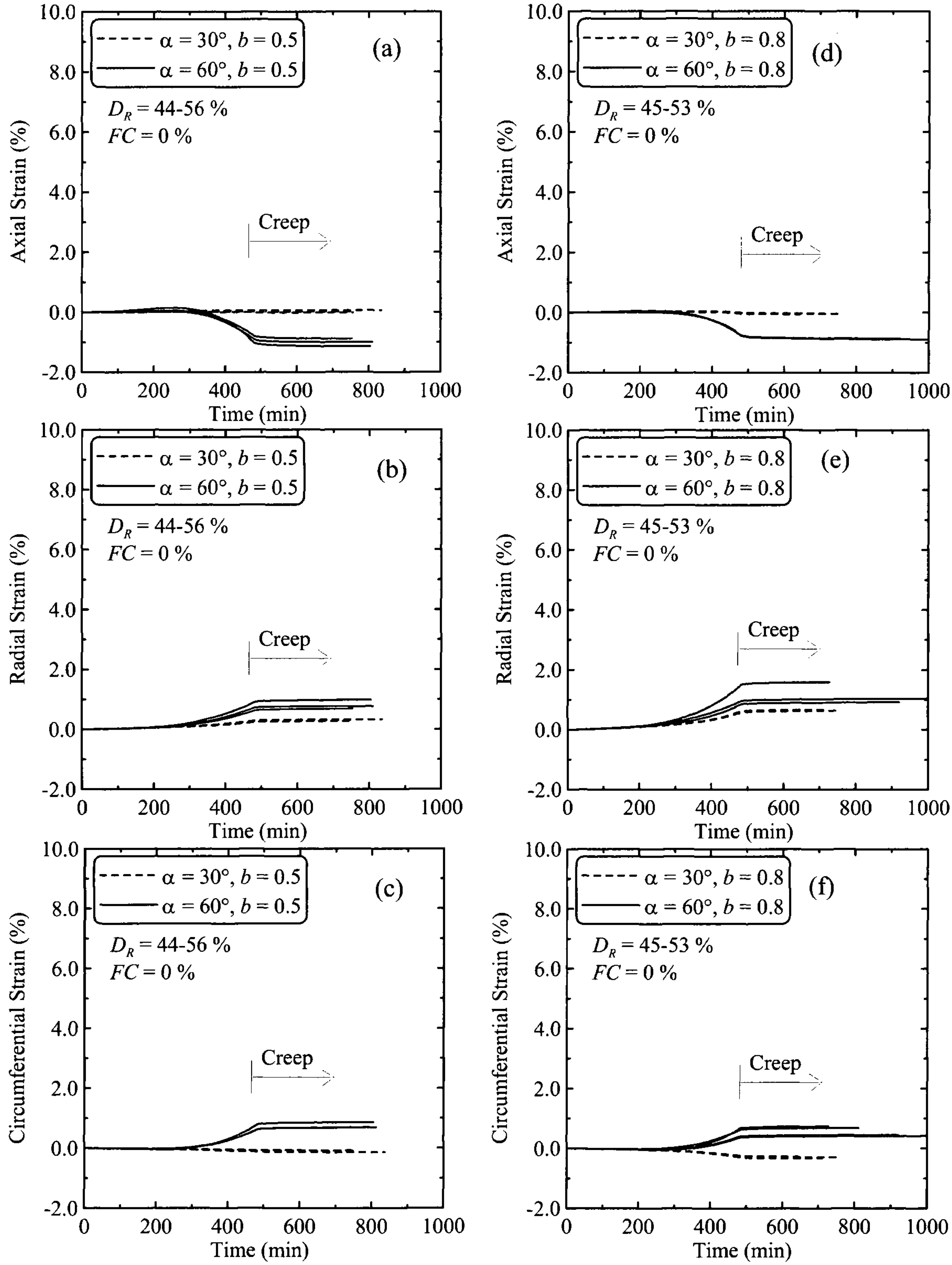

Figure 4.23. (a) Axial, (b) radial, (c) circumferential strains induced during b increase to 0.5 and α increase to 30° or 60°, (d) axial, (e) radial, and (f) circumferential strains induced during b increase to 0.8 and α increase to 30° or 60°.

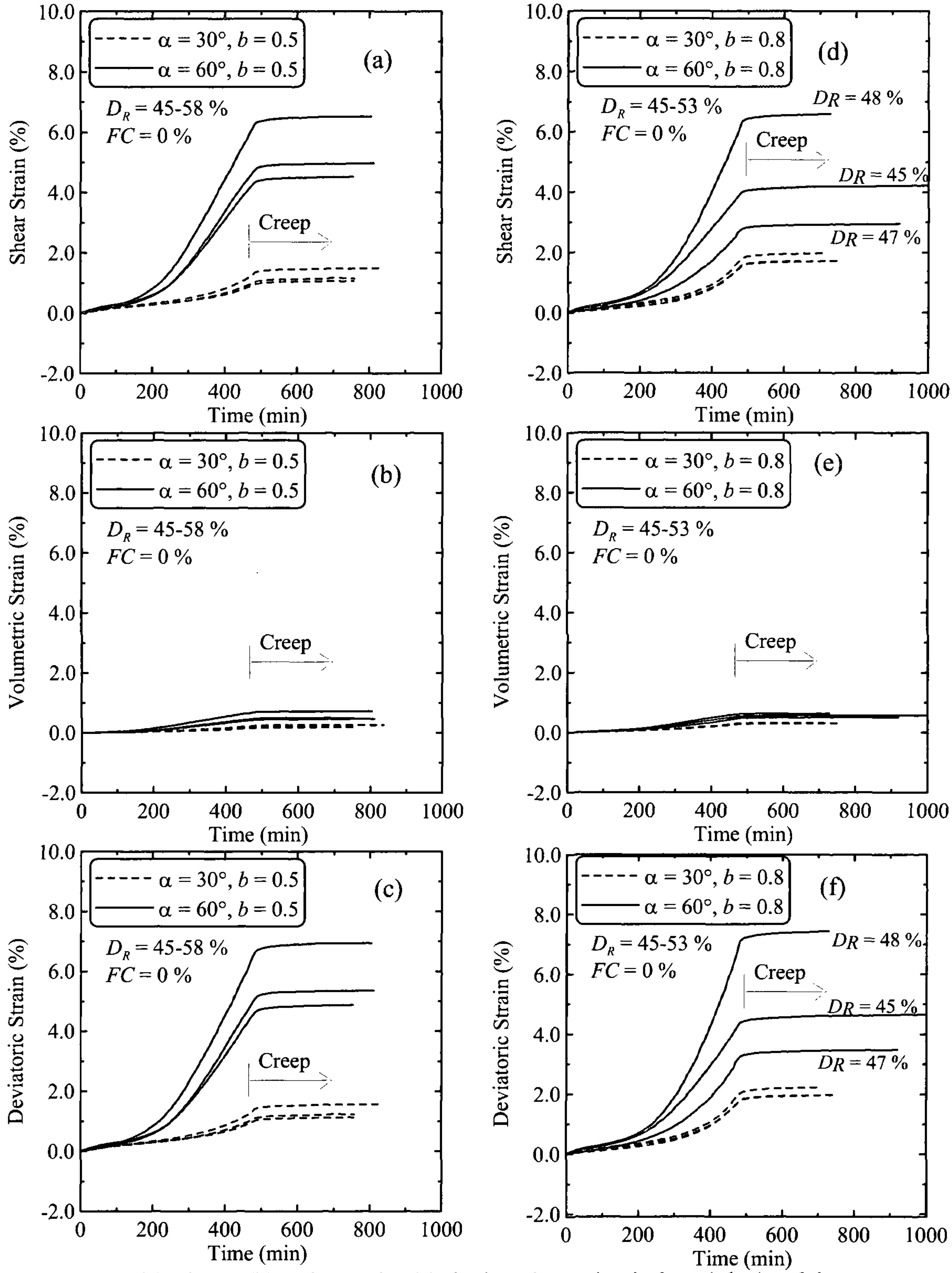

Figure 4.24. (a) Shear, (b) volumetric, (c) deviatoric strains induced during b increase to 0.5 and α increase to 30° or 60°, (d) shear, (e) volumetric, and (f) deviatoric strains induced during b increase to 0.8 and α increase to 30° or 60°.

4.3.5 Creep Response of Ottawa Sand with and without NP Silt

As discussed in the experimental program (section 3), the specimens were allowed to creep at the end of anisotropic consolidation and α and/or b change stages until the change in volumetric strain $\Delta\varepsilon_p$ was less than 0.05 % per day. The creep rate for each stage was defined as the ratio of the total volumetric strain due to creep measured after the target stress conditions were achieved for a given stage to the total volumetric strain experienced by the specimen during the original stage duration (Zdravkovic and Jardine 2001). Average creep rates for the clean and NP silty Ottawa sand specimens are given in Table 4.5 and Table 4.6, respectively, for the various drained testing stages performed. No correlation between the creep rates and relative density was found, and the relatively large COVs reported in Tables 4.5 and 4.6 cannot be explained based on the variation in the relative density of the specimens alone.

Table 4.5. Creep rates for clean Ottawa sand specimens for various drained stages.

CLEAN SAND	Creep Rate			
	Average	COV*	Minimum	Maximum
STAGE	(%)	(%)	(%)	(%)
Anisotropic Consolidation	6	56	1	15
$\alpha = 30°, b = 0$	17	17	14	20
$\alpha = 60°, b = 0$	5	6	5	5
$\alpha = 0°, b = 0.5$	7	19	5	7
$\alpha = 0°, b = 0.8$	8	33	5	9
$\alpha = 30°, b = 0.5$	11	12	10	12
$\alpha = 30°, b = 0.8$	7	12	6	8
$\alpha = 60°, b = 0.5$	5	15	4	5
$\alpha = 60°, b = 0.8$	5	31	3	6

*COV = (standard deviation / average)*100

Table 4.6 Creep rates for NP silty Ottawa sand specimens for various drained stages.

SILTY SAND	Creep Rate			
	Average	COV*	Minimum	Maximum
STAGE	(%)	(%)	(%)	(%)
Anisotropic Consolidation	9	22	7	14
$\alpha = 30°, b = 0$	16	31	11	21
$\alpha = 60°, b = 0$	9	22	8	12
$\alpha = 0°, b = 0.5$	15	20	13	19
$\alpha = 0°, b = 0.8$	13	8	11	13

*COV = (standard deviation / average)*100

According to Tables 4.5 and 4.6, the NP silty Ottawa sand typically exhibited higher creep than clean Ottawa sand during anisotropic consolidation and α and/or b stages. Drained major principal stress rotation with α increasing from 0° to 30° induced the largest creep rates regardless of the accompanied b change. Conversely, α increase from 0° to 60° resulted in the lowest creep rates. No trend regarding the effect of increasing b from 0.5 to 0.8 on the creep rates can be discerned from Tables 4.5 and 4.6. However, increasing b to 0.5 or 0.8 induced larger creep rates than those observed during anisotropic consolidation for both sands, but particularly in the case of the NP silty Ottawa sand.

Zdravkovic and Jardine (2001) conducted K_0 consolidation on dense silt (D_R = 88%) followed by drained major principal stress rotation. They also increased b while keeping σ_1 and p' constant. They reported an average creep rate of 10 % during K_0 consolidation, which is similar to the rate measured for the NP silty Ottawa sand tested in this study. They reported an average creep rate of 35 % for principal stress rotation stage at constant p'. However, this creep rate was the average of creep rates observed for various tests with different α, and, thus, may not be compared directly with the results given in Table 4.5 or 4.6. They also concluded that increasing α and *b* caused more creep than K_0 consolidation.

The average creep rate for the drained major principal stress rotation stages (α increase to 30° or 60°) carried out in this study with $b = 0$ was 11 % for the clean Ottawa sand and 13 % for the NP silty Ottawa sand. Both of these creep rates are larger than the average creep rates measured for these materials during K_0 consolidation. Similarly, the average creep rate for the *b* increase stage (*b* increase from 0 to either 0.5 or 0.8) with α = 0° was 7 % for the clean sand and 14 % for the NP silty sand. Again, both sands experienced more creep during the *b* increase stage than during K_0 consolidation. Therefore, the average creep rates observed when α or *b* were increased in drained conditions at constant p' are larger than the creep rates observed during K_0 consolidation for both sands, which is consistent with the observations made by Zdravkovic and Jardine (2001) for the nonplastic silt tested in their study.

4.3.6 Undrained Cyclic Response Under Axisymmetric Conditions

Sand specimens with and without NP silt were prepared using the SD technique. The uniformity and repeatability of the SD specimens were evaluated and discussed in section 4.2.

Following BP saturation, the specimens were anisotropically consolidated following approximately K_0 conditions (section 4.3.2). Then, major principal stress rotation and/or b changes were imposed at constant p' and q (sections 4.3.3 to 4.3.5). Finally, an additional undrained cyclic loading stage was conducted to evaluate the undrained cyclic behavior of the HC specimens of clean and NP silty Ottawa sands subjected to various levels of α and b. A summary of the imposed stress conditions and specimen relative densities after each sub-stage is provided in Table 4.1 for clean Ottawa sand specimens and in Table 4.2 for NP silty Ottawa sand specimens.

Ishihara (1983) conducted a 2-D seismic analysis on an embankment loaded with a real earthquake acceleration history and showed that, at various locations inside the embankment, the deviator stress (= σ_z - σ_θ in Eq. 2.14) and the shear stress ($\tau_{z\theta}$ in Eq. 2.14) act on soil elements in such a way that the amount of principal stress rotation, α, is constant during the earthquake loading. According to this observation, α, b, and p induced prior to the undrained cyclic loading stage were maintained constant during undrained cyclic loading to evaluate the effects of pre-shear α and b on the cyclic resistance of Ottawa sand with and without NP silt. This approach is similar to the systematic approach followed by Sivathayalan and Vaid (2002), who investigated the effect of pre-shear α and b on the monotonic undrained behavior of clean Fraser River sand.

Undrained cyclic loading during conventional axisymmetric (triaxial) tests typically involves sinusoidal variation of the maximum shear stress ($\Delta\tau_{max} = (\sigma_1 - \sigma_3)/2$) applied to a plane inclined at 45° to the horizontal. The magnitude of the shear stress applied during cyclic loading is typically reported as a cyclic stress ratio *CSR* = Δq / p′ or $CSR = \Delta\tau_{max} / p$ where Δq (deviator stress difference induced during undrained cyclic loading), $\Delta\tau_{max}$ and p' are defined in section 2.6.2. The Δq / p′ ratio represents the three dimensional, generalized stress state, and, thus, is more appropriate than the $\Delta\tau_{max} / p'$ ratio to evaluate the effect of σ_2. Correlations between these two ratios are given in Table 4.7 as a function of *b* based on Eq. 2.40.

Table 4.7. Correlations between the two *CSR* ratios

b	**Δq / p′**
0.0	2.00 $\Delta\tau_{max} / p'$
0.5	1.73 $\Delta\tau_{max} / p'$
0.8	1.83 $\Delta\tau_{max} / p'$
1.0	2.00 $\Delta\tau_{max} / p'$

Since $\Delta\tau_{max}$ ignores the effect of σ_2, it cannot be used as a fundamental stress parameter to evaluate the distortional response of soils. Thus, any additional references to *CSR* in this text refer to the three dimensional ratio Δq / p′ applied during cyclic loading, where Δq is the deviator stress change applied during cyclic loading, and p' is the mean effective stress prior to undrained cyclic loading.

At the end of anisotropic consolidation prior to undrained cyclic loading, the stress state may be close to the *UIL*. Since undrained cyclic loading leads to the accumulation of positive excess pore pressure for most specimens tested (loose to medium dense) and shifts the stress path to the left towards the *UIL* and *CSL*, the *UIL* may be reached quickly and flow deformation may be rapidly triggered causing specimen instability (Undrained instability state *UIL*). Therefore, the *CSR* magnitude plays an important role on how quickly the *UIL* may be reached. If the *CSR* is large, the stress path may reach the *UIL* before the cyclic stress path reaches Point B in Fig. 3.8 in the very first loading cycle.

As mentioned before, prior to undrained cyclic loading, the specimens were subjected to (1) BP saturation, (2) anisotropic consolidation, and (3) α and/or b increase. As shown in section 4.3.3, the average initial relative densities of clean and NP silty Ottawa sands are similar. However, anisotropic consolidation induces a relatively larger increase in the relative density of the NP silty Ottawa sand specimens (average increase of 6 %) compared to the increase imparted to the clean sand specimens (average increase of 2 %). The final relative densities of the specimens prior to undrained cyclic loading and at the end of all other previous testing stages are provided in Fig. 4.25a, and Fig. 4.25b for the clean and NP silty sand specimens, respectively. At the end of α and/or b increase stage, the average relative density is 49 % for clean sand specimens, and 53 % for NP silty sand specimens. This difference stems from the larger relative density change induced in the NP silty sand specimens compared to that induced in the clean sand specimens during anisotropic consolidation, as mentioned previously. Both the clean and NP silty sand specimens were reconstituted to similar relative densities by adjusting the tapping patterns applied during specimen preparation. The change in relative density developed during anisotropic consolidation, however, was difficult to control for clean or NP silty sands. Since the cyclic response of sandy soils is influenced by relative density (Polito and Martin 2003, Carraro et al. 2003) among many other factors, the relative density effect was taken into account while making comparisons between the cyclic resistances of the clean and NP silty sand specimens under different stress states.

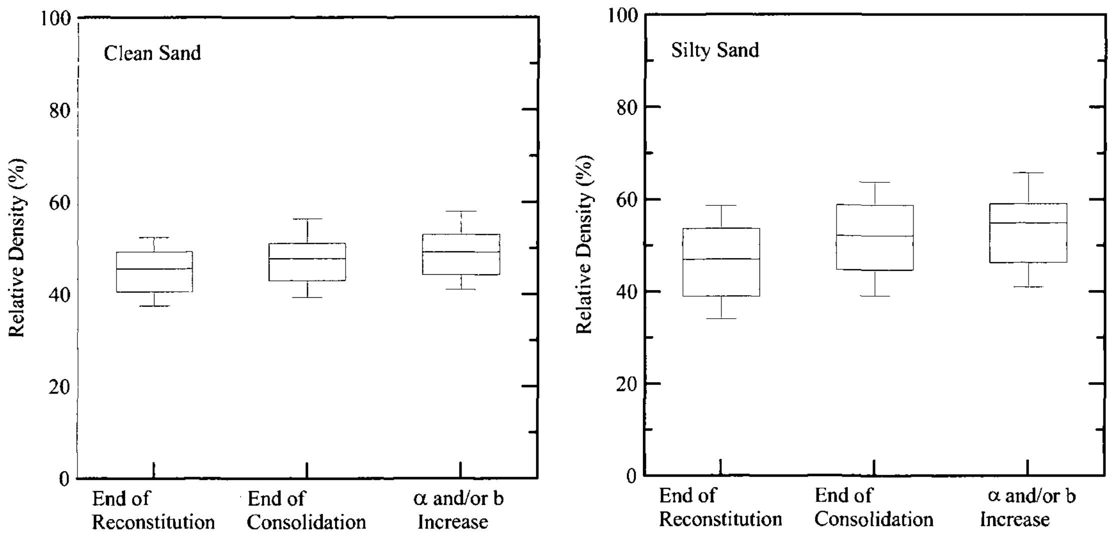

Figure 4.25. Relative density variations at different testing stages for (a) clean Ottawa sand specimens, and (b) NP silty Ottawa sand specimens.

4.3.6.1 Excess Pore Pressure, Deviatoric and Axial Strain Responses

The axial and deviatovic strains and excess pore pressure responses for the clean and NP silty Ottawa sand specimens subjected to undrained cyclic loading with $\alpha = b = 0$ and under various *CSR* levels are given in Fig. 4.26 and Fig. 4.27, respectively.

Deformations in clean Ottawa sand become large in the very first loading cycle for $CSR \geq 0.20$ (Fig. 4.26), in agreement with the onset of instability shown in Fig. 4.31, as it will be discussed later. The following should be considered while evaluating the amount of the excess pore pressure or strains induced undrained instability from the perspective of critical state soil mechanics: (1) full consideration of the soil behavior at the moment of undrained instability requires considering the inertia forces (Uthayakumar and Vaid 1998), and (2) the control of the actuators is a difficult task to perform during *UI*. However, for the specimens tested the excess pore pressure generated did not exceed the initial p', i.e., p' did not become zero during undrained cyclic loading as it is typically observed for anisotropic consolidated specimens (Vaid and Chern 1985). Furthermore, as soon as *UI* takes place, clean sand specimens start exhibiting dilative behavior after phase transformation (*PTS*). In other words, the excess pore pressure starts decreasing and the rate of strain generation becomes much lower than that observed during UI (Fig. 4.26). This type of behavior cannot be classified as either classical flow liquefaction or cyclic mobility. The deviatoric strain response of clean sands observed in this study when $\alpha = b = 0$ is similar to the behavior described as limited liquefaction followed by cyclic mobility (Fig. 4.28) by Vaid and Chern (1985). When subjected to $CSR = 0.14$, the clean sand experienced UI in two cycles after which large axial strain developed quickly. The excess pore pressure did not become equal to p' at the UI state (Fig. 4.26) preventing the specimens from undergoing full liquefaction ($p' = 0$). This is similar to what Vaid and Chern (1985) suggested for undrained cyclic loading with no shear-stress reversal. However, even if p' may never become equal to zero, large strains (ε_z between 2% and 4%) still develop due to limited liquefaction followed by cyclic mobility (Fig. 4.28). When *CSR* was reduced to 0.10, the sand specimen did not experience *UI*, and exhibited a steady strain and pore pressure build up, which is typical of classical cyclic mobility behavior.

The NP silty sand specimen sheared with $CSR = 0.30$ experienced an excess pore pressure build up as large as the initial p' during the first two loading cycles (Fig. 4.27a). The resulting deformation due to this excess pore pressure generation reached about 15 %

axial strain (contraction). At this strain level, the displacement limit of the *HC* vertical actuator was exceeded, and further deformation (contraction) could not take place.

Comparing the excess pore pressure and axial strain responses of the NP silty sand with those of the clean sand tested under the same *CSR* = 0.30 (Fig. 4.26a), it can be seen that the *NP* silty sand temporarily undergoes full liquefaction whereas both specimens exhibit limited liquefaction followed by the cyclic mobility in the long run. When *CSR* is reduced to 0.20, both clean sand and NP silty sand experience limited liquefaction followed by cyclic mobility (Fig. 4.27b) with the excess pore pressure never exceeding the initial p' level prior to undrained cyclic loading. The corresponding excess pore pressure and axial strain reached during *UI* was about 50 kPa and 8 % for the NP silty sand specimen, and about 60 kPa and 3.5 % for the clean sand specimen. However, it should be noted that the clean sand specimen is looser (D_R = 42 %) than its silty sand counterpart (D_R = 59 %), thus *UI* might have caused even larger excess pore pressure build up and axial strain if the silty specimen were as loose as the clean sand like in the case for *CSR*=0.3. Further decrease in *CSR* to 0.10 prevents the NP silty sand and clean sand specimens from undergoing UI, and cyclic mobility is observed (Figs. 4.26c and 4.27c) for both materials.

4.3.6.2 Generalized Strain Response

The generalized strain responses of the clean and NP silty Ottawa sand specimens are provided in Fig. 4.26 and Fig. 4.27, respectively. Fig. 4.26 and 4.27 also include the excess pore pressure response, which follow the trends of strains (sudden increase in strain corresponds to sudden increase in excess pore pressure etc.). In Fig. 4.27a, all strain components experienced by the NP silty sand specimen sheared with *CSR* = 0.30

tapered off after two cycles due to the limits of the actuators being reached at that moment. This large deformation is associated with the mobilization of a large excess pore pressure equal to the initial p' (full liquefaction). Both clean and NP silty sand specimens experienced contraction in the axial direction and extension in both radial and circumferential directions, regardless of the *CSR* applied, during axisymmetric undrained cyclic loading.

The radial strain was equal to the circumferential strain during axisymmetric undrained cyclic loading for both clean and NP silty sand specimens, as expected. The maximum radial and circumferential strains extension observed were about -8% for both clean and *NP* silty sands for $CSR \leq 0.30$.

For both sands the predominant strain component was the axial strain, with the actual ε_z values ranging from of 2.5 % to 7 % for clean sand, and from 4 % to 15 % for NP silty sand when *CSR* is between 0.10 and 0.30.

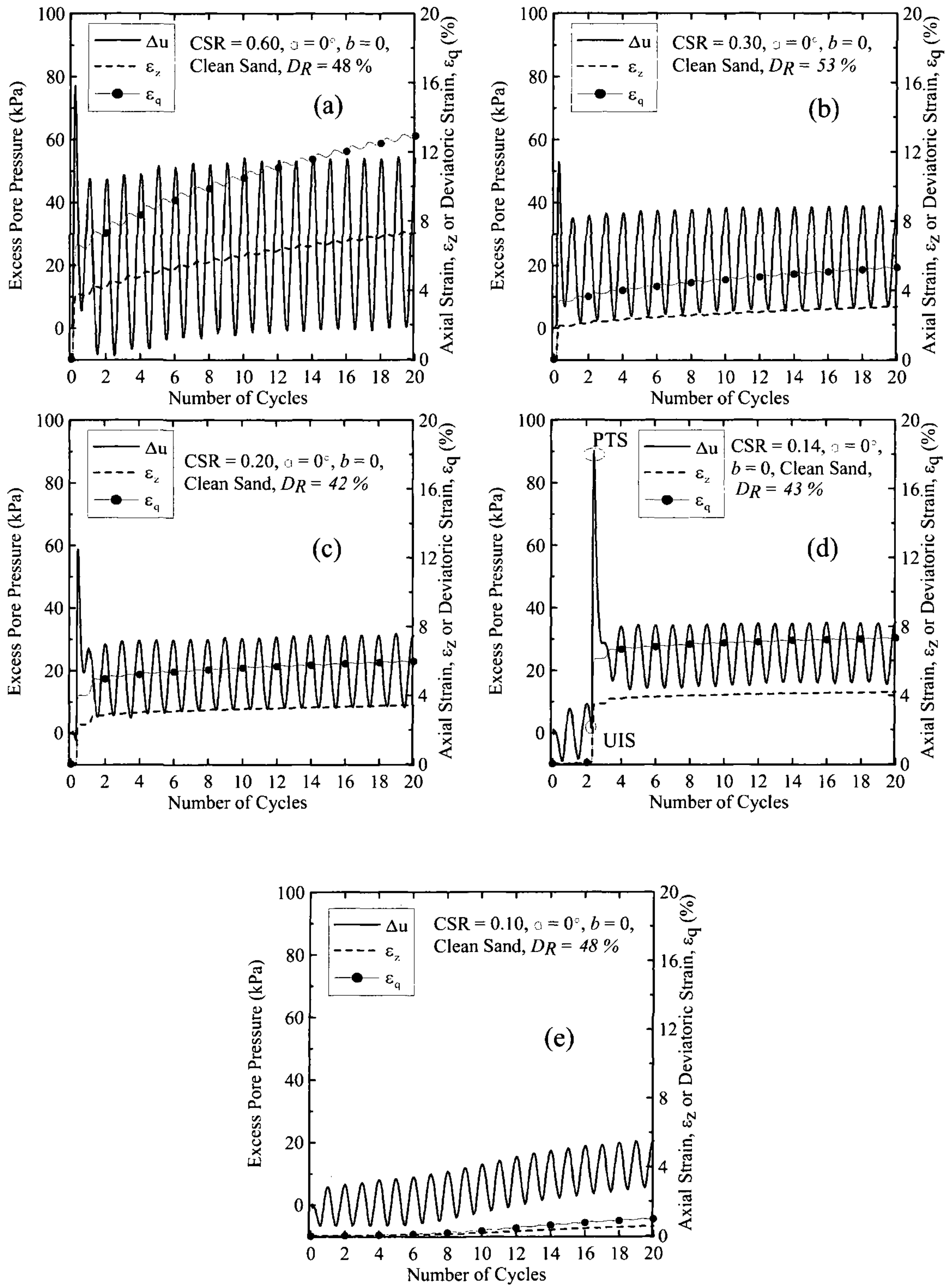

Figure 4.26. Excess pore pressure, deviatoric and axial strain responses of clean sand specimens under undrained cyclic loading with $\alpha = b = 0$ for (a) $CSR = 0.60$, (b) $CSR = 0.30$, (c) $CSR = 0.20$, (d) $CSR = 0.14$, and (e) $CSR = 0.10$.

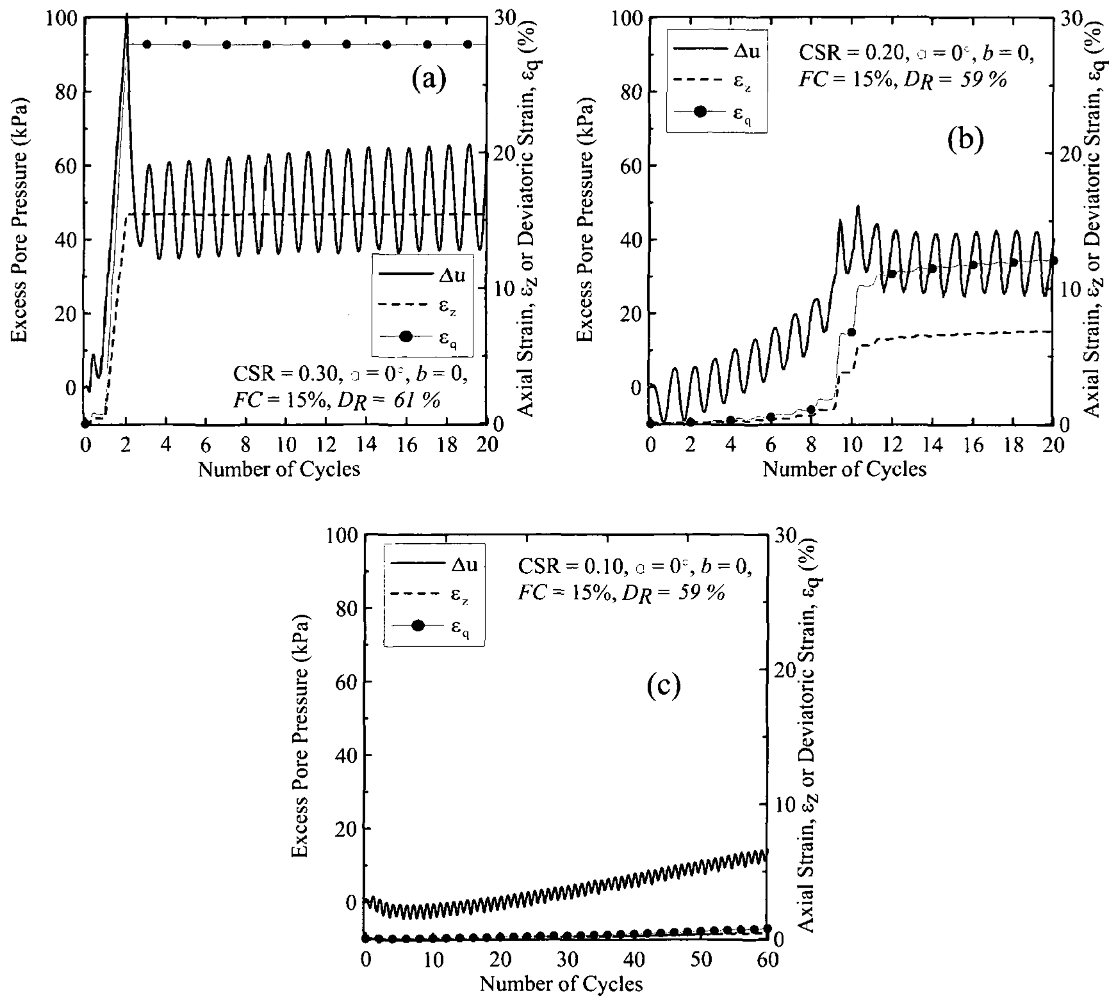

Figure 4.27. Excess pore pressure, deviatoric and axial strain responses of NP silty sand specimens under undrained cyclic loading with $\alpha = b = 0$ for (a) $CSR = 0.30$, (b) $CSR = 0.20$, (c) $CSR = 0.10$.

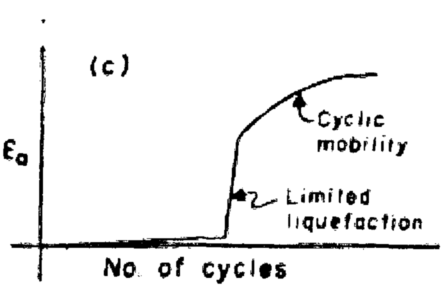

Figure 4.28. Limited liquefaction followed by cyclic mobility (Vaid and Chern 1985)

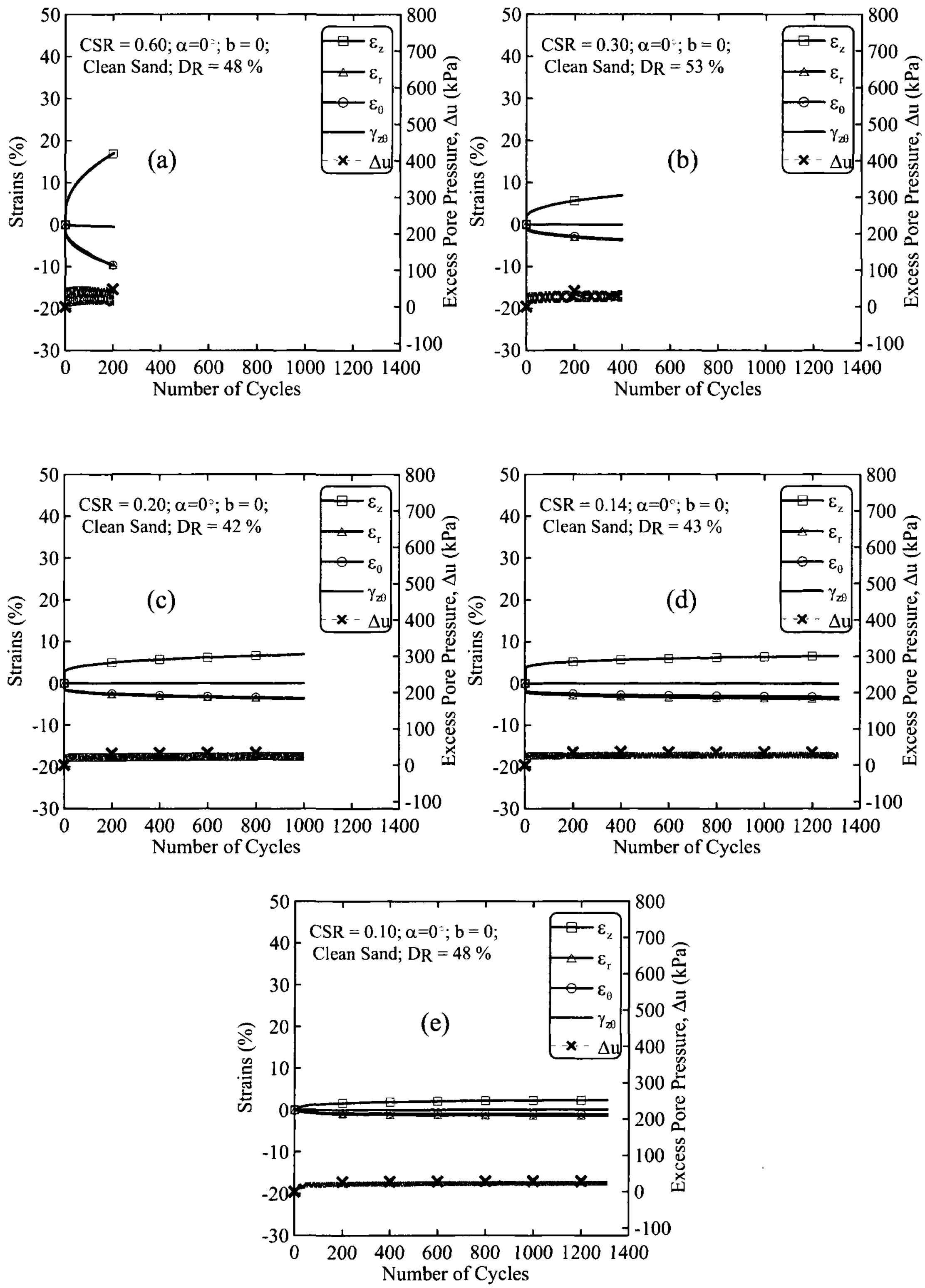

Figure 4.29. Generalized strain and excess pore pressure responses of clean sand specimens under undrained cyclic loading with $\alpha = b = 0$ for (a) $CSR = 0.60$, (b) $CSR = 0.30$, (c) $CSR = 0.20$, (d) $CSR = 0.14$, and (e) $CSR = 0.10$.

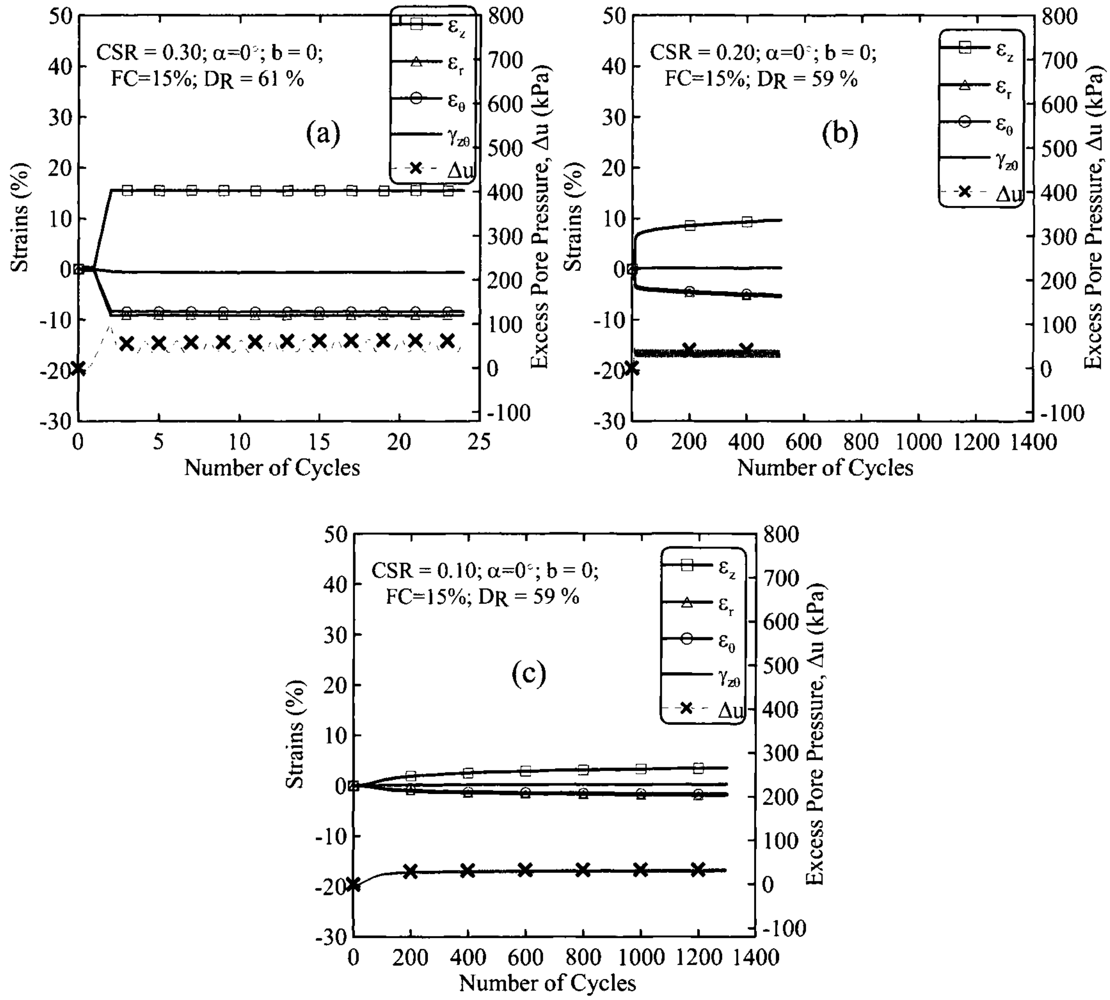

Figure 4.30. Strain and excess pore pressure responses of NP silty sand specimens under undrained cyclic loading with $\alpha = b = 0$ for (a) $CSR = 0.30$, (b) $CSR = 0.20$, (c) $CSR = 0.10$.

Given the strain responses mobilized for both sands under similar *CSR*, the NP silty sand systematically exhibits a weaker response than clean sand. This pattern was observed also for the same materials tested in a conventional triaxial device following isotropic consolidation (Carraro et al. 2003), despite the *NP* silty sands tested in the present study being consistently denser than their clean sand counterparts. Regardless of the strain component considered, the typical deformation pattern resembles that induced by limited flow liquefaction (or UI) followed by cyclic mobility for $CSR \geq 0.14$ for clean sand and for $CSR \geq 0.20$ for NP silty sand. When $CSR = 0.10$, both clean sand and NP silty sand showed cyclic mobility regardless of the strain component considered, with the NP silty sand always presenting relatively larger strains in spite of being denser than the clean sand.

4.3.6.3 Stress Paths and Undrained Instability

The effective stress paths shown in Fig.4.31 indicate that upon reaching the *UIS* in $q - p'$ space, the clean sand specimens experience a temporary undrained instability response and develop positive excess pore pressures between 50 and 90 kPa in less than one cycle, which decreases p' significantly for $CSR \geq 0.14$ (Fig. 4.31a, 4.31b, 4.31c, and 4.31d). Undrained instability (UI) was taken as the moment after which the excess pore pressure deviates significantly from the common trend expected for a given CSR within the same cycle (see Fig. 4.26d). UI usually lasted much less than the cyclic loading period used (= 1s). Following UI, clean sand specimens underwent phase transformation and exhibited dilative behavior resulting in a reduction in the excess pore pressure, and, thus, p' increased. During UI, the pore pressure increases take place within about 0.02 s to 0.04 s before the sudden strain build-up is observed, indicating that the pore pressure increases result in the softening of the specimen. The high-speed DA system used allowed capturing this behavior. For practical purposes, the pore pressure increases can be claimed to happen at the same time as the strains build up. When $CSR \geq 0.20$, UI is observed during the first loading cycle, whereas the specimen sheared with $CSR = 0.14$ experienced *UI* after the second cycle. When *CSR* is reduced to 0.10, clean sand did not experience *UI*. The onset of *UI* took place at a stress state slightly below the *CSL* for clean sand specimens (Carraro 2004, Murthy et al. 2007) tested under axisymmetric monotonic loading.

The effective stress paths for the undrained cyclic loading of the NP silty sand specimens with $\alpha = 0°$ and $b = 0$ on are shown in Fig. 4.32. To clearly identify the onset of *UI*, only data during the cycle when *UI* is observed is shown in Figs. 4.32a and 4.32b. For example, Fig. 4.32a shows only the stress path during the second cycle when *UI* is observed. The *NP* silty sand specimens experienced *UI* when *CSR* > 0.10. The number of cycles required to reach *UI* reduces as *CSR* increases (Fig. 4.27). When *CSR* = 0.30, only two loading cycles were required to cause about 100 kPa excess pore pressure generation decreasing p' to about 0 kPa. When *CSR1* = 0.20 (Fig.4.32b), the stress path does not indicate any significant sudden excess pore pressure build up to 9 cycles of loading. However, during the 9th cycle, about 30 kPa of excess pore pressure is generated in half a second (the time elapsed between each data point in Fig. 4.32 is 0.02 sec), clearly indicating that the NP silty sand fabric is collapsing at that point. Fig. 4.32c shows the stable response of the specimen cyclically sheared with *CSR* = 0.10, and $\alpha = 0°$ and $b = 0$.

4.3.6.4 Liquefaction Resistance Curves

Various levels of *CSR* were used to investigate the undrained cyclic behavior of clean and NP silty Ottawa sand specimens when $\alpha = 0°$ and $b = 0$. The liquefaction resistance curves for both soils are given in Fig. 4.33 for strain-based liquefaction critera ($\varepsilon_q = 2.5$ % in Fig. 4.33a, $\varepsilon_q = 5.0$ % in Fig. 4.33b, and $\varepsilon_q = 8.75$ % or $\varepsilon_z = 5$ % in Fig. 4.33c). Tests conducted in thus study had a maximum of 1300 loading cycles.

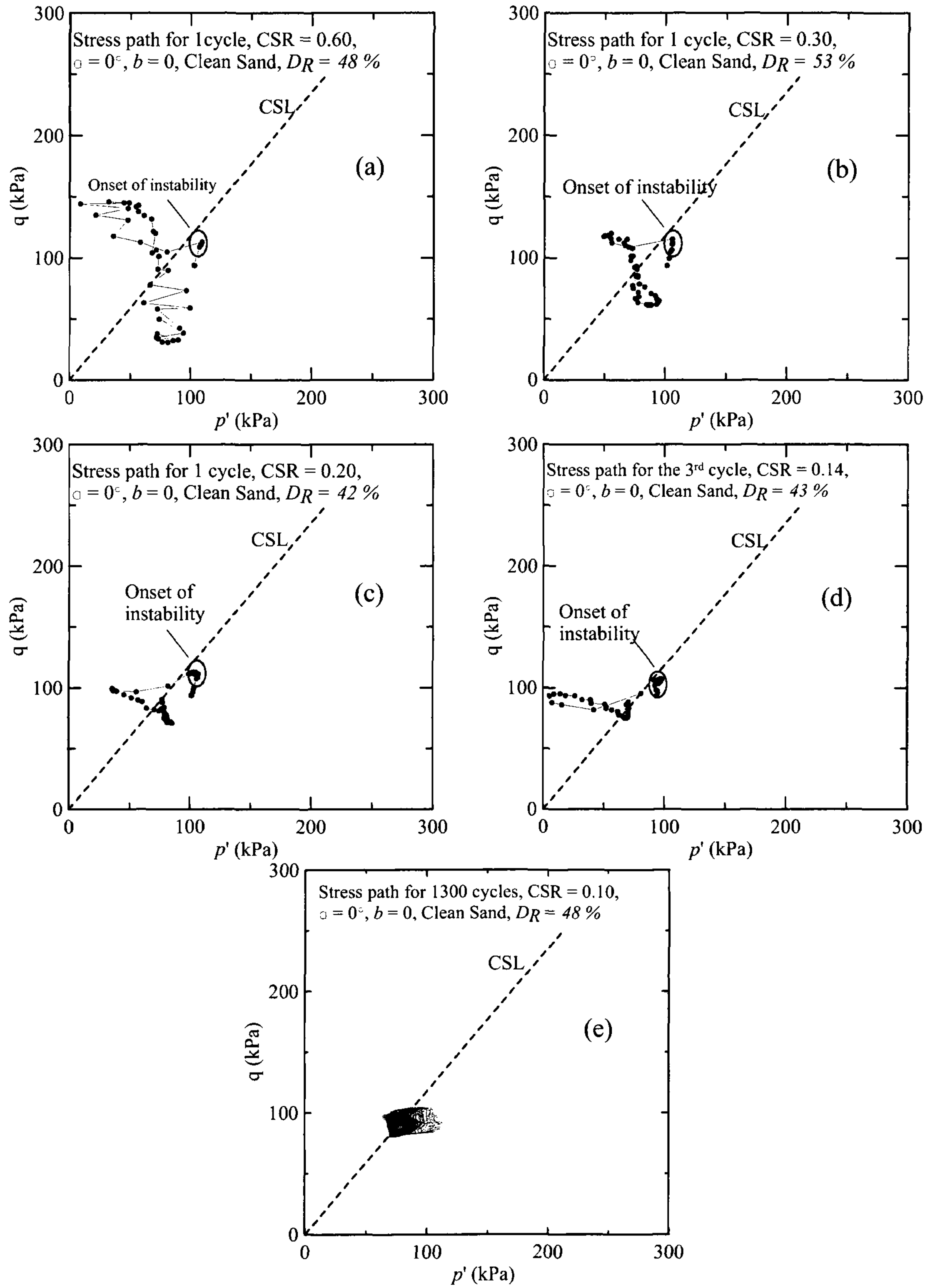

Figure 4.32. Effective stress paths for the undrained cyclic loading of clean sand specimens under $\alpha = b = 0$ (a) $CSR = 0.60$, (b) $CSR = 0.30$, (c) $CSR = 0.20$, (d) $CSR = 0.14$, and (e) $CSR = 0.10$.

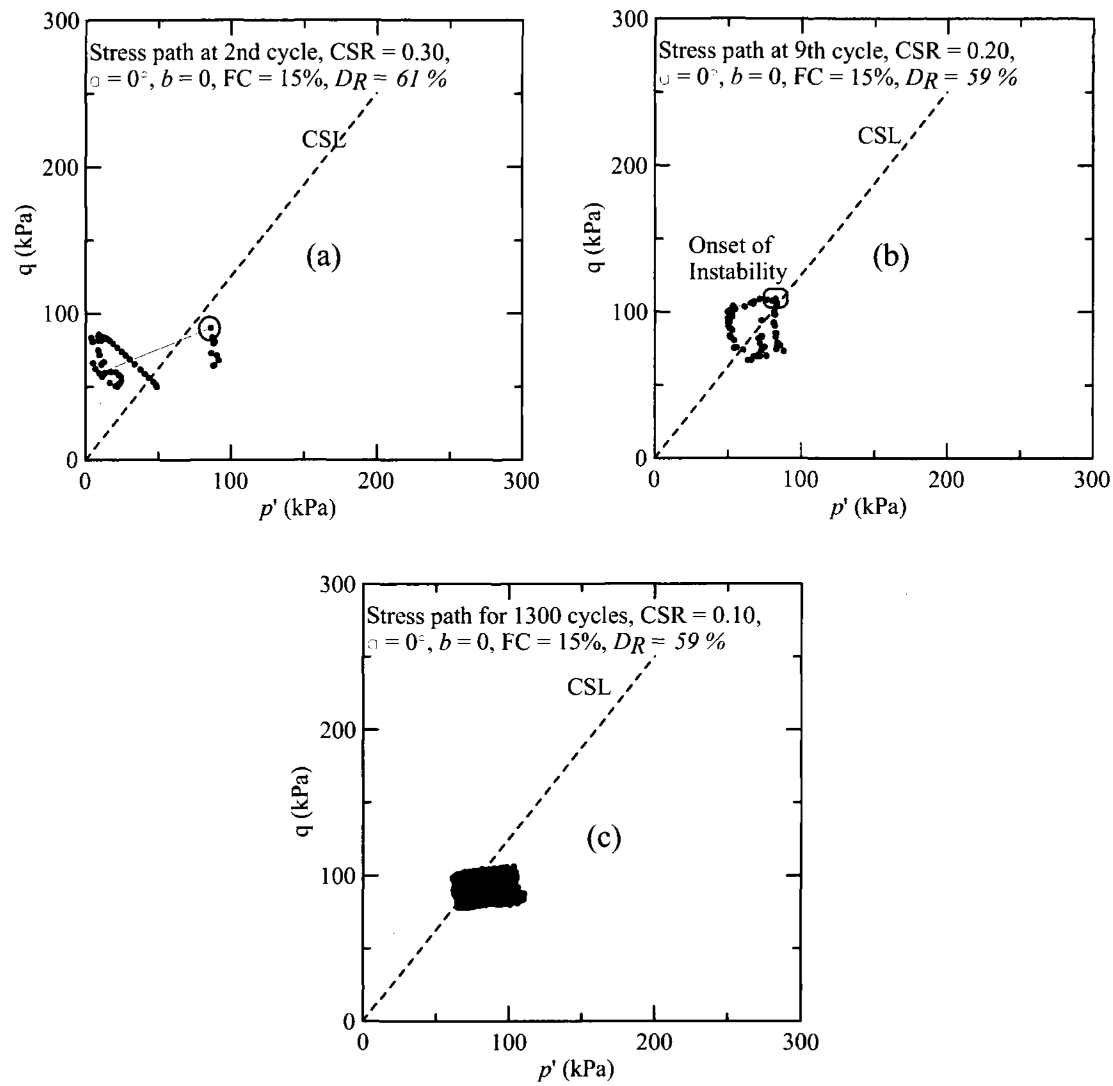

Figure 4.32. Effective stress paths for the undrained cyclic loading of NP silty sand specimens under $\alpha = b = 0$ (a) $CSR = 0.30$, (b) $CSR = 0.20$, (c) $CSR = 0.10$.

If the specimen did not develop the deviatoric strain defined as the liquefaction criterion, the number of cycles that would take to reach the liquefaction criterion was extrapolated by fitting a best fit curve on the deviatoric strain response of the specimen. The curve fit was placed on the last portion of the deviatoric strain response curve where no sudden increases took place.

Fig. 4.33a indicates that the NP silty Ottawa sand has a higher liquefaction resistance than clean sand if $\varepsilon_q = 2.5$ % was used as the liquefaction criterion. When the liquefaction criterion was $\varepsilon_q = 5.0$ %, both clean and NP silty sands had similar liquefaction resistances. The deviatoric strain is 1.75 times the axial strain during axisymmetric undrained cyclic loading with $\alpha = 0°$ and $b = 0$. Therefore, $\varepsilon_q = 2.5$ % and $\varepsilon_q = 5.0$ % correspond to $\varepsilon_z = 1.4$ % and $\varepsilon_z = 2.9$ %, respectively. The axisymmetric liquefaction criterion has been commonly defined as 5 % double amplitude axial strain (Castro 1975, Ishihara 1993), which corresponds to ε_q of 8.75 %. The liquefaction resistance curves for clean and NP silty sands for the liquefaction criterion of $\varepsilon_z = 5.0$ % or $\varepsilon_q = 8.75$ % are given in Fig. 4.33c., where NP silty sand showed a weaker response than clean sand. Fig 4.33 shows that NP silty sand may have lower, similar, or higher liquefaction resistance than clean sand depending on the selected liquefaction criterion. Thus, comparison of the liquefaction resistances of clean sand and NP silty sand depends significantly on the liquefaction criterion used in analysis. According to the commonly used liquefaction criterion of $\varepsilon_z = 5.0$ % or $\varepsilon_q = 8.75$ %, for the undrained cyclic triaxial testing, NP silty sand has lower liquefaction resistance than clean sand, which is in agreement with the findings of Carraro (2004) and Carraro et al. (2003) for the same materials subjected to undrained cyclic triaxial testing on isotropically consolidated specimens.

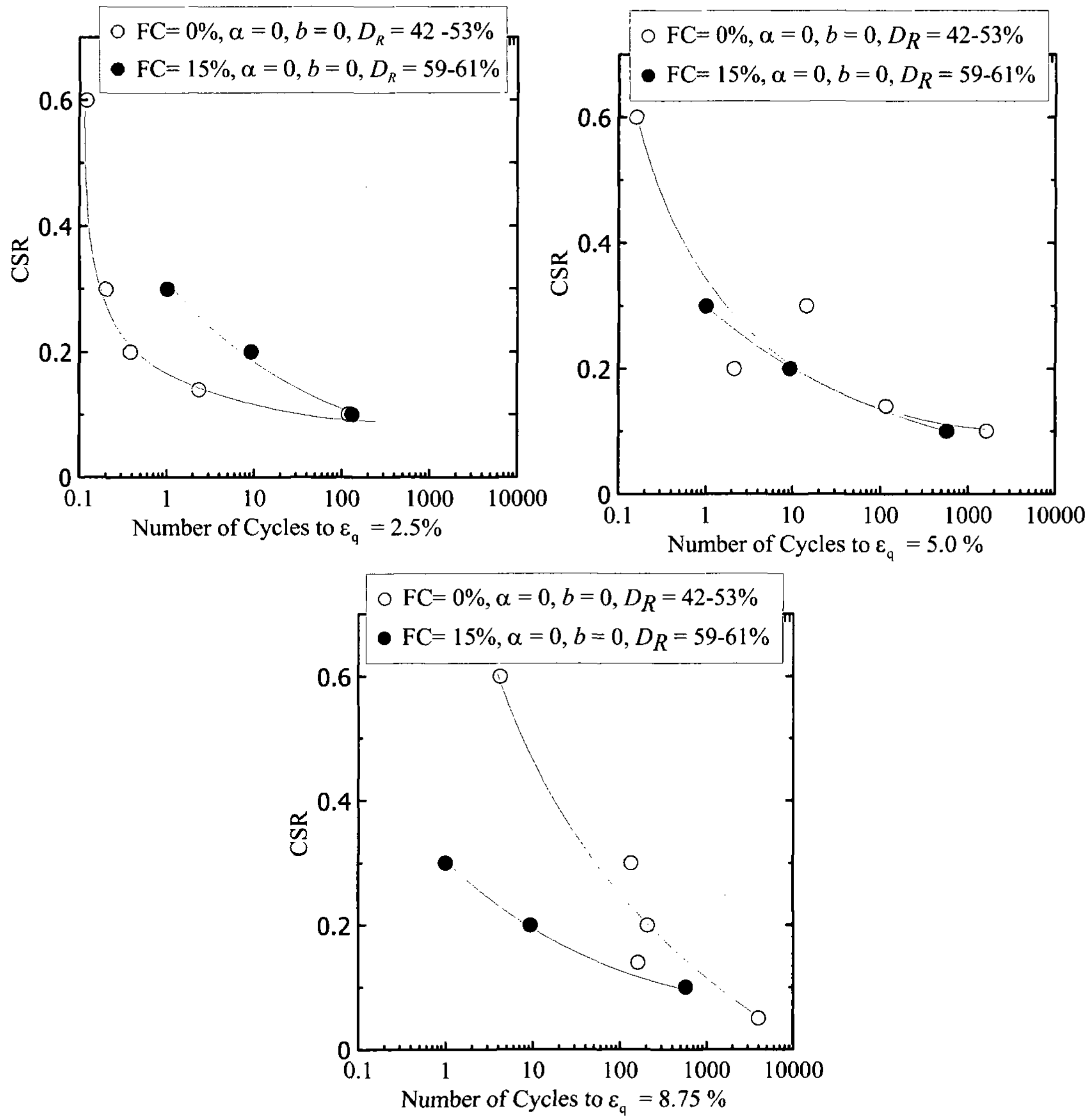

Figure 4.33. Axisymmetric liquefaction resistance curves for anisotropically consolidated clean and NP silty Ottawa sands. Failure defined as (a) ε_q = 2.5 %, and (b) ε_q = 5 %, and (c) ε_q = 8.75 % or ε_z = 5 %.

4.3.7 Effect of Major Principal Stress Rotation on the Undrained Cyclic Response of Ottawa Sand with and without NP Silt

The effect of α on the undrained cyclic response and liquefaction resistance of Ottawa sand with and without NP silt was investigated through a series of undrained cyclic loading tests with $\alpha = 0°$, $30°$ or $60°$. In these tests, α was kept constant during undrained cyclic loading. All tests were conducted at the same initial p' (=100 kPa), and the D_R range prior to the cyclic stage was 41 - 50 % for the clean sand specimens and 43 - 60 % for the NP silty sand specimens. The FC of the NP silty sand was between 11 and 16 % (one specimen had FC = 11 %, the rest had FC between 13 and 16 %) as shown in Table 4.2.

4.3.7.1 Excess Pore Pressure and Deviatoric Strain Responses

The excess pore pressure and deviatoric strain responses of the clean and NP silty Ottawa sands subjected to undrained cyclic loading with $\alpha = 30°$ or $60°$ are given in Fig. 4.34 and Fig. 4.35, respectively. The clean sand specimens subjected to undrained cyclic loading with *CSR* varying between 0.06 and 0.10 at $\alpha = 30°$ developed large excess pore pressure (40 – 70 kPa) during UI. When α was rotated to 60° prior to undrained cyclic loading, the excess pore pressure did not exceed 25 kPa for *CSR* ranging from 0.06 to 0.10. Thus, the increase in α from 30° to 60° reduced the maximum induced excess pore pressure induced during undrained cyclic loading. However, a lower number of cycles is needed to develop large ε_q than in the case when $\alpha = 30°$. When *CSR* = 0.10, UI was observed for the specimen subjected to undrained cyclic loading with $\alpha = 30°$ and $b = 0$ (Fig. 4.31a) at about 3-4 cycles. Unlike the stress path for undrained cyclic loading with $\alpha = 30°$ and $b = 0$, the stress path for the undrained cyclic loading with $\alpha = 60°$ and $b = 0$

showed UI for a lower excess pore pressure at a lower number of cycles (Fig. 4.34b). However, the deviatoric strain for this specimen reached up to 12 % after 3 loading cycles (Fig. 4.34b) a value slightly higher than that developed for the $\alpha = 30°$, $b = 0$ case. Further decrease in *CSR* to 0.06 during undrained cyclic loading of clean sand also resulted in limited flow liquefaction followed by cyclic mobility (UI was observed) for both $\alpha = 30°$ and $\alpha = 60°$.

The NP Ottawa silty sand specimen subjected to the undrained cyclic loading with $CSR = 0.30$ and $\alpha = 30°$ experienced large deviatoric strain ($\varepsilon_q > 10\%$) after one cycle and could not sustain any more loading resulting in the loss of control. Similarly, when $CSR = 0.20$ and $\alpha = 60°$, the excess pore pressure response of the NP silty sand specimen indicated failure in three cycles after which the testing control was lost due to excessive actuator movement. These two specimens did not experience an excess pore pressure equal to the initial $p' = 100$ kPa. Yet, they experienced very large strains and could not resist further loading indicating the collapse of the fabric. Even though, flow liquefaction may be defined as the state when the excess pore pressure equals the initial p', which is usually accompanied with large strains, these two specimens may also be considered to have experienced flow liquefaction since the sand fabric collapsed and did never recover from it due to excessive deformations. Decreasing *CSR* to 0.24 or 0.20 while keeping $\alpha = 30°$ did not change the overall UI behavior of the NP silty sand. The only difference is that the number of cycles to UI increased as *CSR* decreased. On the other hand, the NP silty sand specimen subjected to $CSR = 0.14$ and $\alpha = 60°$ experienced UI after 32 cycles resulting in an excess pore pressure of 60 kPa and 30 % deviatoric strain development (limited liquefaction followed by cyclic mobility). Further reducing *CSR* to 0.10 when α

= 60° causes a cyclic mobility type of behavior for the NP silty sand specimen with no obvious UI developing during cyclic loading.

4.3.7.2 Generalized Strain Response

The strain response of clean sand during cyclic shearing with α = 30° or 60° is shown in Fig. 4.36. As the major principal stress rotates from the vertical, the predominant strain component becomes the shear strain. The primary contraction observed in the axial direction when α = 0° or 30° turns into extension when α is increased to 60°. The extensional response in radial and circumferential directions, when α = 0° or 30°, turns into a contractive response as α is increased to 60°. The clean sand specimen subjected to undrained cyclic loading with α = 30° and *CSR* = 0.10 experienced large increase in excess pore pressure (by about 55 kPa. in Fig. 4.34a), shear and axial strains (8 % and 2.5 %, respectively) at UI (Fig. 4.34 and 4.36). However, as α increased to 60°, the excess pore pressure increase of 25 kPa at UI was not as significant as that observed for α = 30°, but the strain response of the specimen loaded with α = 60° still showed temporary collapse of the fabric (8 % deviatoric strain induced in one cycle). Furthermore, when α = 60° during the undrained cyclic loading, the excess pore pressure decreased significantly before increasing at UI, which may be due to the fact that failure takes place during the first part of the first cycle, which is associated with decrease in q. This dilative behavior may be observed in Fig. 4.36d, where sand specimen subjected to undrained cyclic loading with α = 60° experienced extension in the axial direction while being twisted (sheared) around the vertical axis.

As mentioned before, prior to the undrained cyclic loading, the specimens were subjected to major principal stress rotation under drained conditions, and the fabric induced during this stage is expected to influence the behavior observed during the subsequent undrained cyclic loading. The basic strain components for the clean Ottawa sand as a function of the principal stress rotation are given in Fig. 4.37. For specimens with similar D_R, drained principal stress rotation to 60° induced much larger shear strain (about 5 %) than rotation to 30° (about 1.5 %). Furthermore, during the 60° rotation, the axial strain increased up to α = 45° and, then, started decreasing. When α was 60°, the induced axial strain was close to zero, and the behavior of the specimen in the axial direction was dilative. On the other hand, the specimen subjected to 30° rotation under drained conditions exhibited steady contraction in the axial direction. The contractive fabric induced in the axial direction prior to undrained cyclic loading with α = 30° may explain the sudden collapsible behavior (UI) and the large excess pore pressure generated during subsequent undrained cyclic loading. The dilative fabric induced in the axial direction prior to and during undrained cyclic loading with α = 60° may explain the relatively lower excess pore pressure build up at UI compared to α = 30° case. However, the specimen cyclically loaded with α = 60° still exhibited weaker response and lower number of loading cycles was needed to reach a certain deviatoric strain threshold.

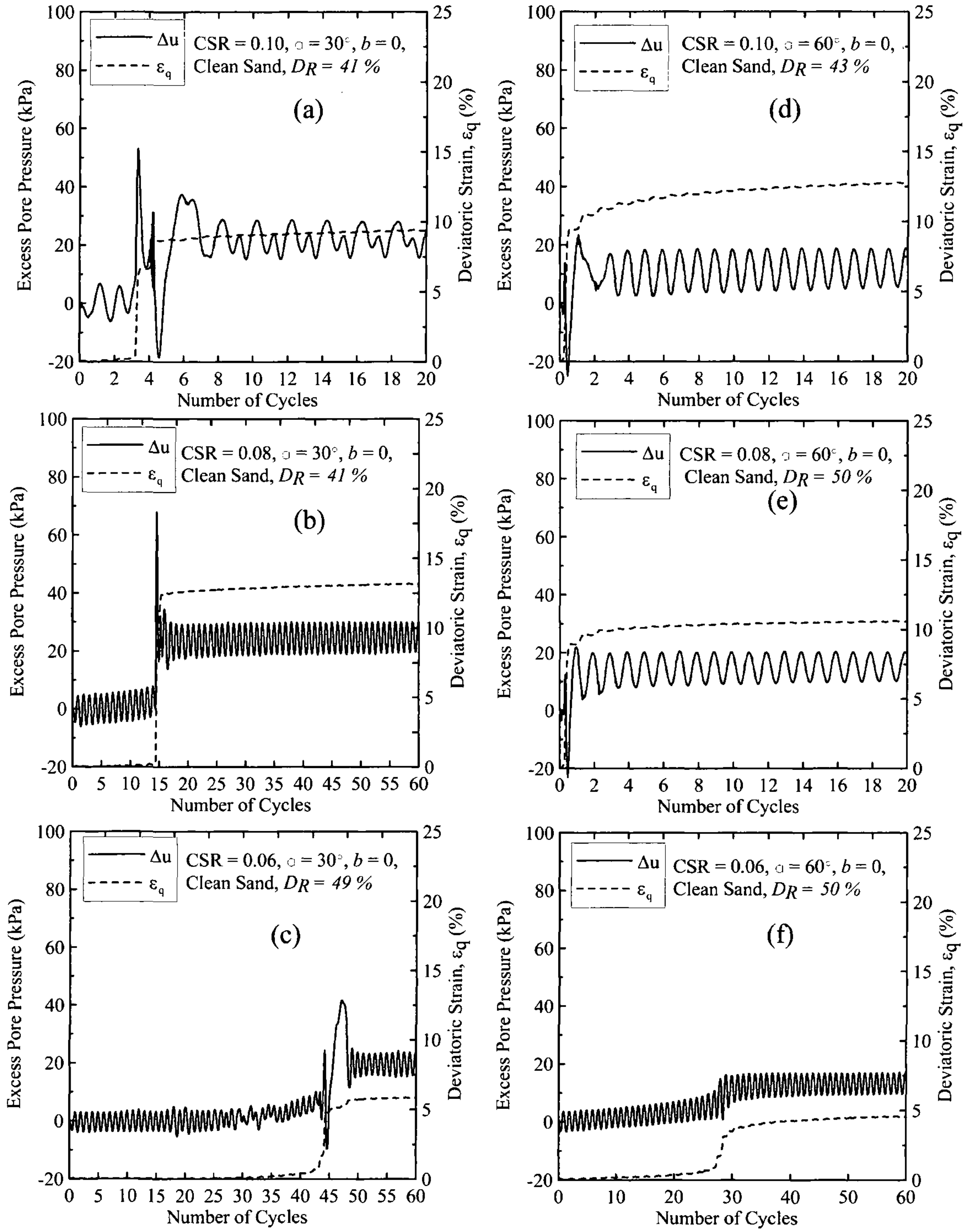

Figure 4.34. Pore pressure and deviatoric strain responses for clean sand specimens cyclically sheared with $b = 0$ and (a) α = 30° at $CSR = 0.10$, (b) α = 30° at $CSR = 0.08$, (c) α = 30° at $CSR = 0.06$, (d) α = 60° at $CSR = 0.10$, (e) α = 60° at $CSR = 0.08$, and (f) α = 30° at $CSR = 0.06$.

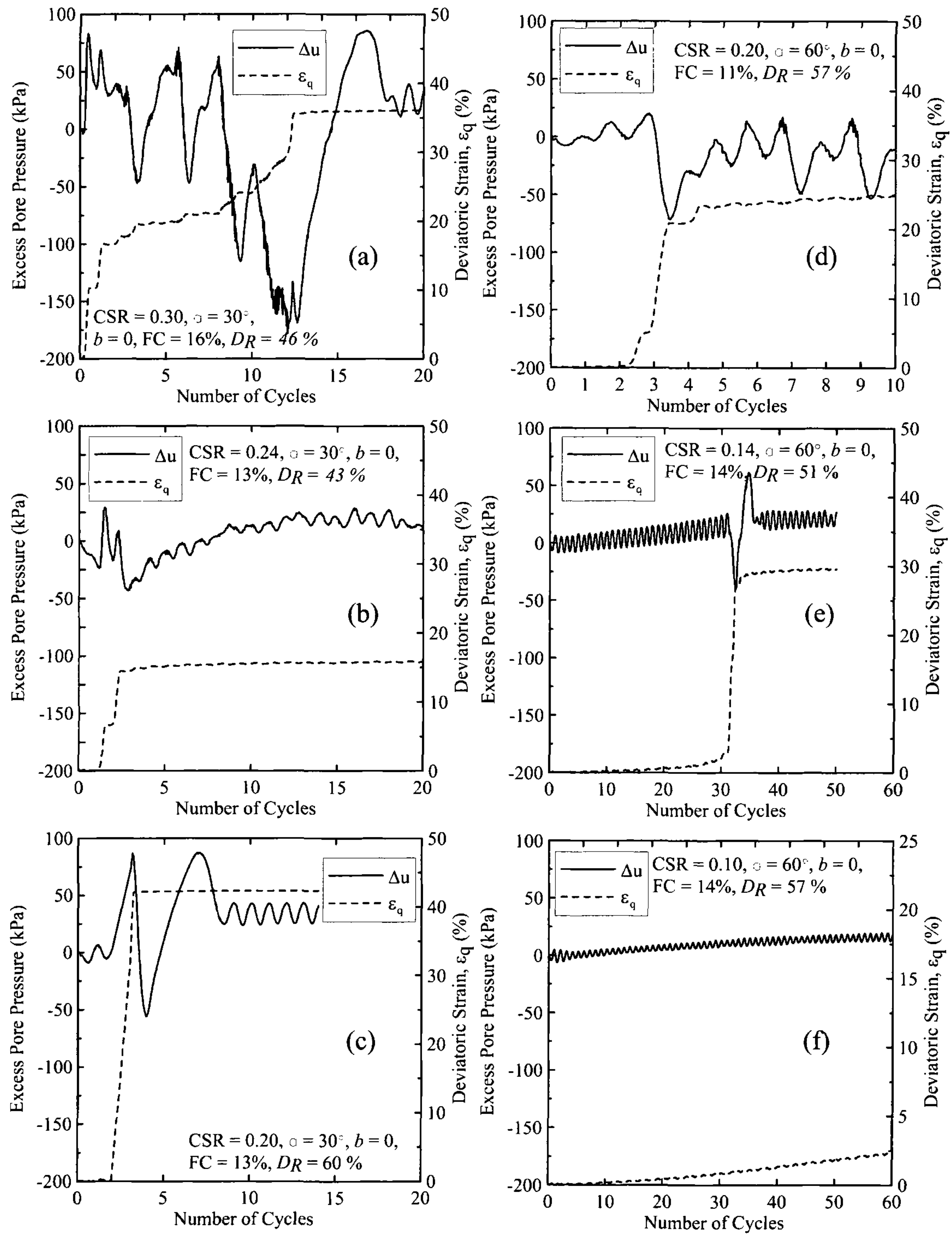

Figure 4.35. Pore pressure and deviatoric strain responses for NP silty sand specimens cyclically sheared with $b = 0$ and (a) $\alpha = 30°$ at $CSR = 0.30$, (b) $\alpha = 30°$ at $CSR = 0.24$, (c) $\alpha = 30°$ at $CSR = 0.20$, (d) $\alpha = 60°$ at $CSR = 0.20$, (e) $\alpha = 60°$ at $CSR = 0.14$, and (f) $\alpha = 30°$ at $CSR = 0.10$.

compared to the number of cycles needed for the specimen cyclically sheared with α = 30°. This weaker response may be attributed to the significant pre-shearing that takes place during drained principal stress rotation to 60° and the direction of the loading during undrained cyclic loading.

The generalized strain and excess pore pressure responses of the NP silty sand specimens subjected to cyclic shearing with α = 30° or α = 60° are given in Fig. 4.38. The predominant strain component was the shear strain (between 18 % and 33 %) for 0.20 < *CSR* < 0.30 and α = 30° or 60° applied. When α = 30°, the NP silty sand specimens experienced contraction in the axial direction. However, as α is increased to 60°, extension was observed in the axial direction. When α = 30° and 0.20 < *CSR* < 0.30, the radial and circumferential strains were extensional in nature and their magnitudes were similar with the maximum of less than 10 %. However, with the increase in α to 60, the maximum radial or circumferential strain was less than 2.5 % (in contraction) for *CSR* = 0.20, while the shear and axial strains were 30 % and - 5 % (in extension), respectively.

Figs. 4.36 and 4.38 also include the excess pore pressure response of the sand specimens along with their strain response. When UI occured, the sand specimens experienced large strain and excess pore pressure increases at nearly the same time.

4.3.7.3 Stress Paths and Undrained Instability

The effective stress paths for clean and NP silty Ottawa sand specimens cyclically sheared with α > 0°, and *b* = 0 are given in Fig. 4.39 and Fig. 4.40, respectively.

When *CSR* = 0.10, α = 30° and *b* = 0, UI as defined in section 4.3.6 was evident during the fourth loading cycle for the clean sand specimen (Fig. 4.39a). Unlike the

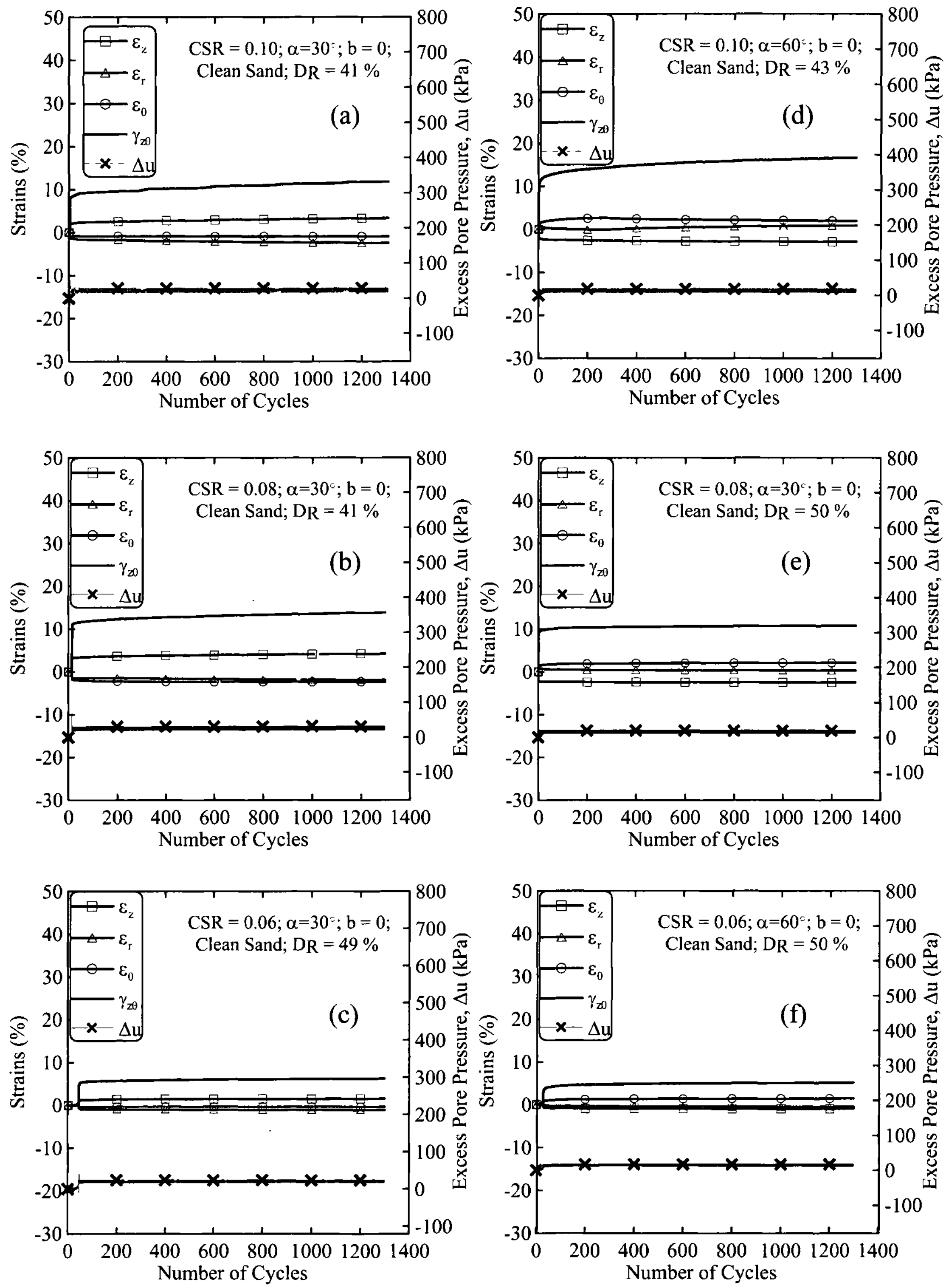

Figure 4.36. Generalized strain and excess pore pressure responses of clean sand specimens cyclically sheared with $b = 0$ and (a) $\alpha = 30°$ at $CSR = 0.10$, (b) $\alpha = 30°$ at $CSR = 0.08$, (c) $\alpha = 30°$ at $CSR = 0.06$, (d) $\alpha = 60°$ at $CSR = 0.10$, (e) $\alpha = 60°$ at $CSR = 0.08$, and (f) $\alpha = 30°$ at $CSR = 0.06$.

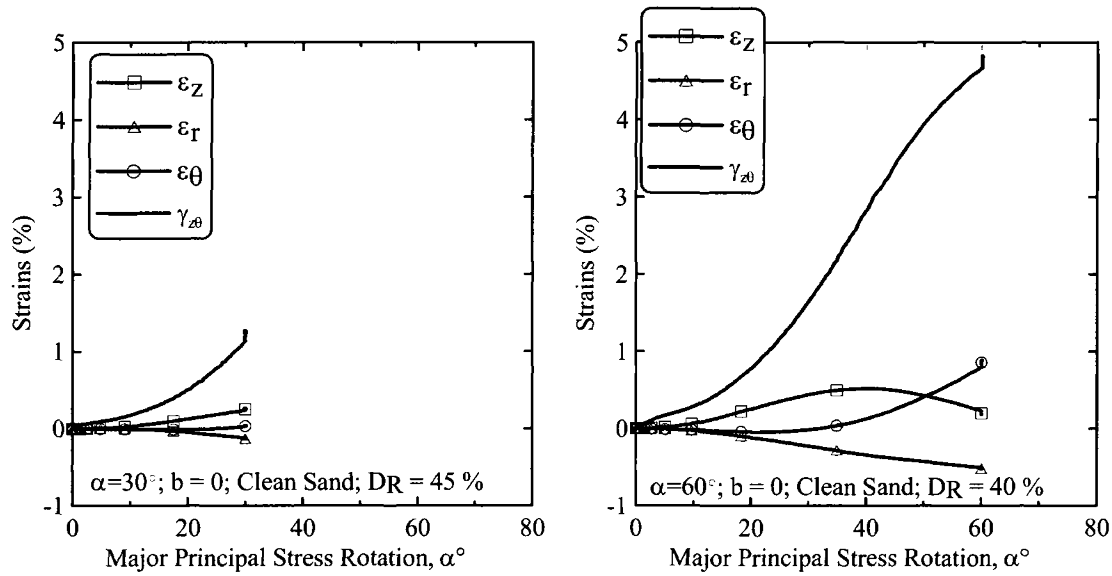

Figure 4.37. Strain response of sand specimens subjected to drained principal stress rotation to (a) α = 30°, and (b) α = 60°.

undrained cyclic loading with α = 30° and *CSR* = 0.10, the stress path for the undrained cyclic loading with α = 60° and b = 0 did not show instability in terms of large excessive pore pressure build up (Fig. 4.38b). As *CSR* was reduced to 0.08 or 0.06, the clean sand specimens still experienced UI when cyclically sheared with α = 30° or 60°. However, the number of loading cycles to reach UI increased as *CSR* decreased as expected.

The NP silty Ottawa sand when subjected to undrained cyclic loading with both α = 30° (0.20 < *CSR* < 0.30) and α = 60° (0.10 < *CSR* < 0.20) experienced UI. Only the specimen subjected to α = 60° and *CSR* = 0.10 did not experience UI. As *CSR* was decreased, the number of cycles to reach UI increased as expected. The *CSR* range applied to clean sand specimens was 0.06 – 0.10, whereas the silty sands were subjected to higher *CSR* range between 0.10 and 0.30. As mentioned in section 4.3.6, the *CSR* magnitude is expected to impact the instability observed. Therefore, the instability behavior of clean and silty sand could only be compared when *CSR* = 0.10 and α = 60°

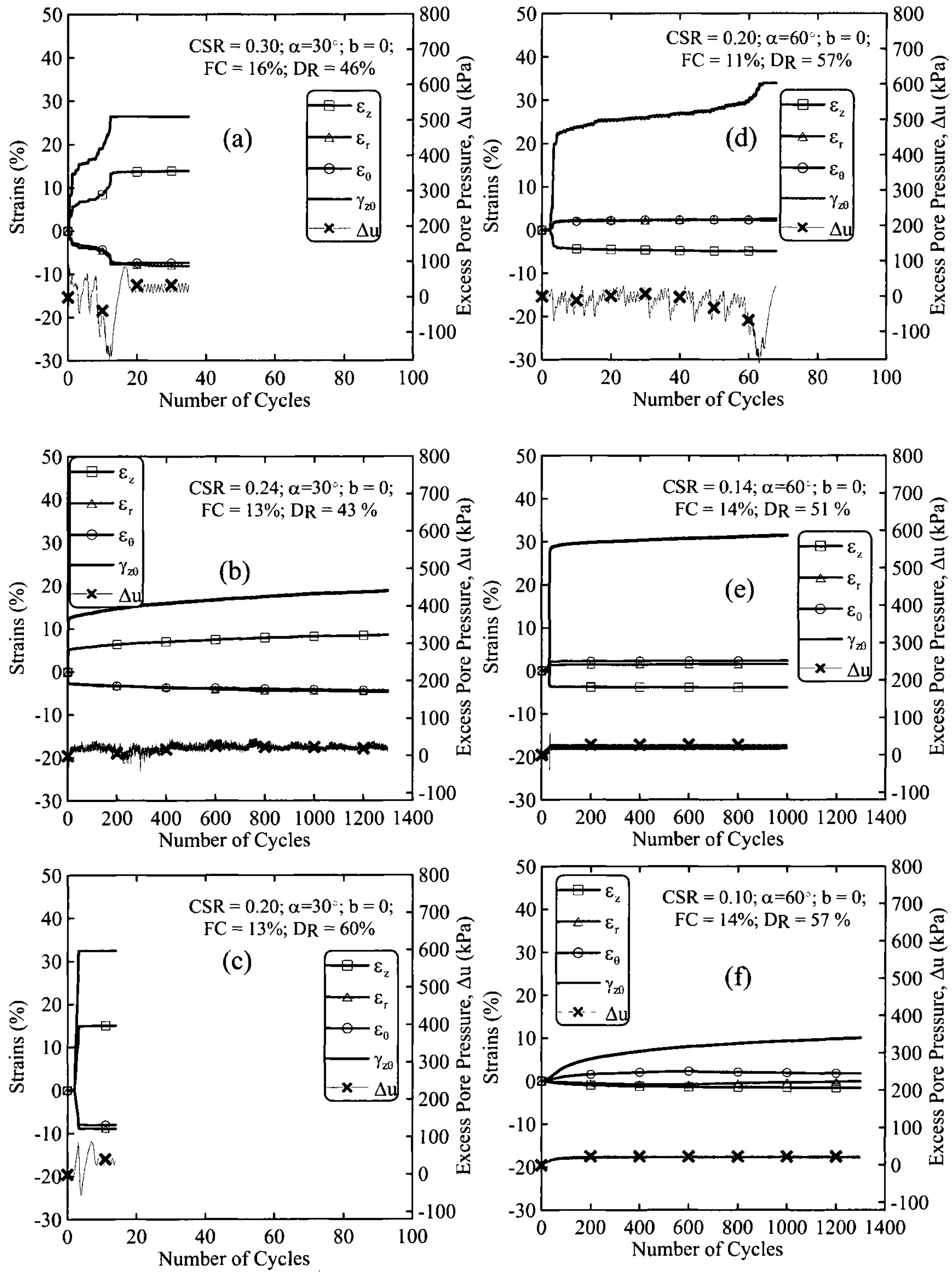

Figure 4.38. Generalized strain and excess pore pressures responses of NP silty sand specimens cyclically sheared with $b = 0$ and (a) $\alpha = 30°$ at $CSR = 0.30$, (b) $\alpha = 30°$ at $CSR = 0.24$, (c) $\alpha = 30°$ at $CSR = 0.20$, (d) $\alpha = 60°$ at $CSR = 0.20$, (e) $\alpha = 60°$ at $CSR = 0.14$, and (f) $\alpha = 30°$ at $CSR = 0.10$.

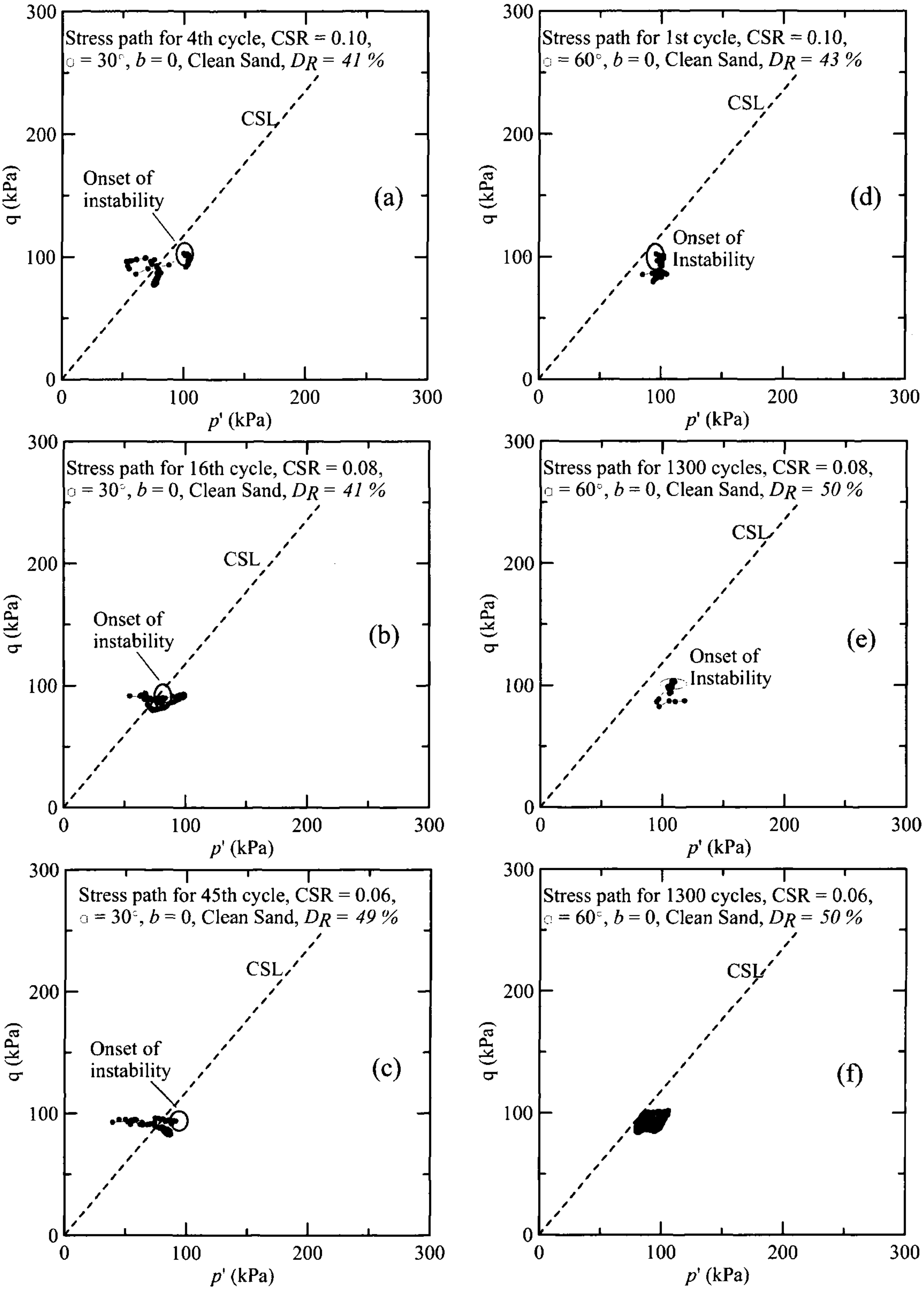

Figure 4.39. Effective stress paths for clean sand specimens cyclically sheared with $b = 0$ and (a) α = 30° at CSR = 0.10, (b) α = 30° at CSR = 0.08, (c) α = 30° at CSR = 0.06, (d) = 60° at CSR = 0.10, (e) α = 60° at CSR = 0.08, and (f) α = 30° at CSR = 0.06.

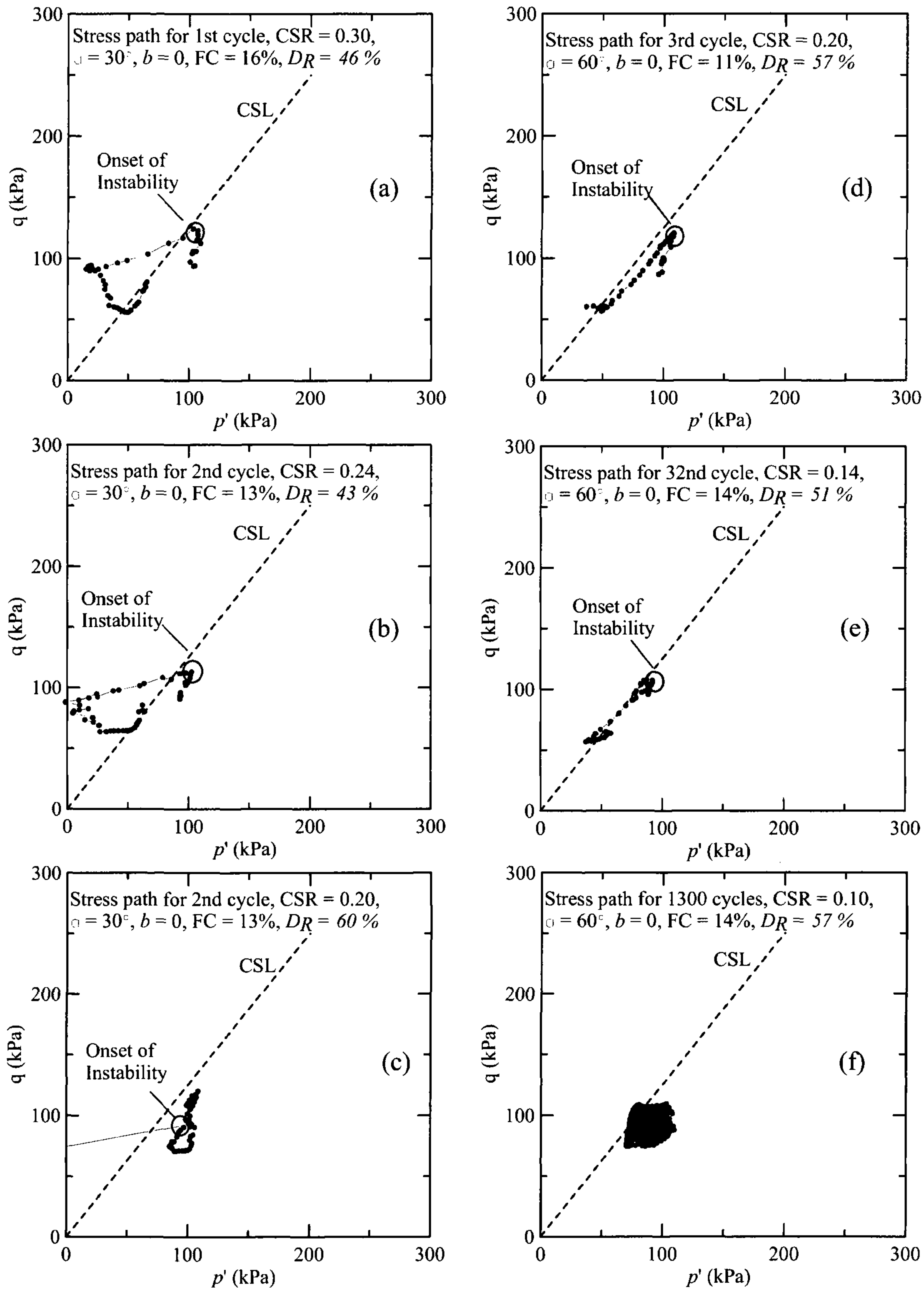

Figure 4.40. Effective stress paths for silty sand specimens cyclically sheared with $b = 0$ and (a) α = 30° at *CSR* = 0.30, (b) α = 30° at *CSR* = 0.24, (c) α = 30° at *CSR* = 0.20, (d) α = 60° at *CSR* = 0.20, (e) α = 60° at *CSR* = 0.14, and (f) α = 30° at *CSR* = 0.10.

which did not induce UI in NP silty sand (Fig. 4.39f), but did induce UI in the clean sand specimen during the 1st cycle (Fig. 4.40f).

4.3.7.4 Liquefaction Resistance Curves

The effect of drained α rotation on the liquefaction resistance of clean and NP silty Ottawa sands are given in Fig. 4.41, where each data point represents the number of cycles required to induce ε_q = 2.5 %, 5.0 %, or 8.75 % for a given *CSR*. Increasing α from 0° to 30° significantly reduces the liquefaction resistance of clean Ottawa sand for all three liquefaction criteria (Fig. 4.41a, 4.41b, and 4.41c). However, the reduction is more pronounced if the liquefaction criterion is ε_q = 8.75 %. The liquefaction resistance of NP silty Ottawa sand also is reduced by the increase in α from 0° to 30°. The reduction in the liquefaction resistance of NP silty Ottawa sand is not as significant as the reduction in the liquefaction resistance of clean Ottawa sand when α is increased from 0° to 30°.

Increasing α from 30° to 60°, induces further reduction in the liquefaction resistance of clean sand. However, the decrease in liquefaction resistance of the clean Ottawa sand is more pronounced when α is increased from 0° to 30° compared to the decrease observed when α is increased from 30° to 60°.

Increasing α from 30° to 60° does not cause large reduction in the liquefaction resistance of NP silty sand. Furthermore, the change in the strain-based liquefaction criterion does not impact the liquefaction resistance curves for NP silty sand as it does for their clean sand counterparts.

The variation of *CRR* as a function of α is as given in Fig. 4.42a and 4.42b for clean and NP silty Ottawa sands, respectively, where *CRR* is defined as the *CSR* required to reach one of the aforementioned strain-based liquefaction criteria at 20 cycles. Every

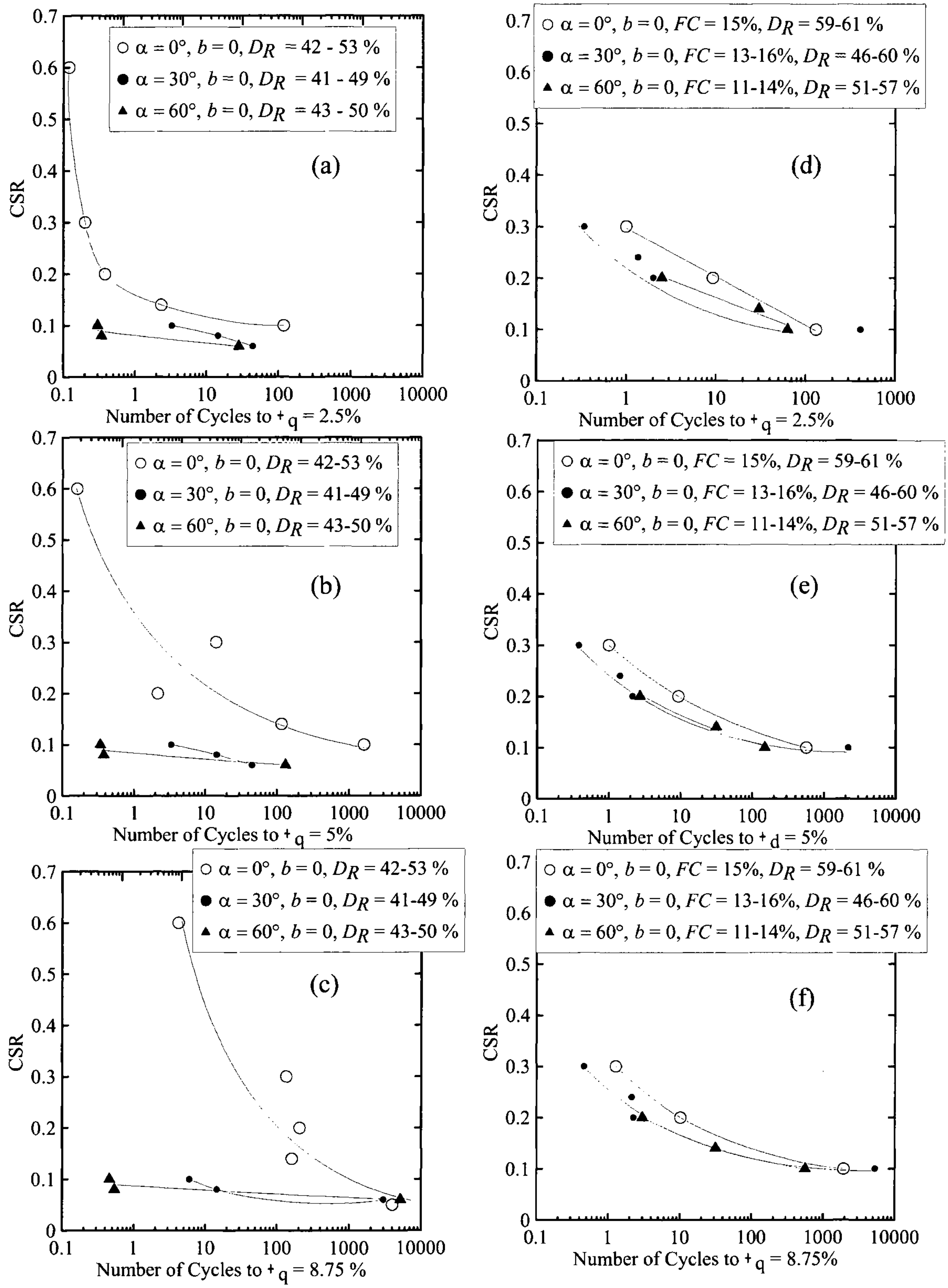

Figure 4.41. Liquefaction resistance curves for clean sand at (a) ε_q = 2.5 %, (b) ε_q = 5 %, (c) ε_q = 8.75 %, and for silty sand at (d) ε_q = 2.5 %, (e) ε_q = 5.0 %, and (f) ε_q = 8.75 % when b = 0 and α = 0, 30 or 60°.

CRR shown in Fig. 4.42 is normalized by the *CRR* determined for α = 0° and *b* = 0 axisymmetric case for the same ε_q criterion. According to Fig. 4.42a, *CRR* of clean sand decrease as much as 80 % when *α* is increased to 30° if the liquefaction criterion is ε_q = 8.75 %. Increasing *α* from 30° to 60° does not have a significant additional effect on *CRR*. The NP silty sand does not experience as significant a reduction in *CRR* as the clean sand does when *α* is increased to 30°. However, a reduction in *CRR* of as much as 20 % may take place for the NP silty sand if *α* is increased from 0° to 30° or 60° with ε_q = 8.75 %. Increasing *α* from 30° to 60° does not cause a significant additional reduction in *CRR* except when the liquefaction criterion is ε_q = 5 % (even this reduction is not more than 5 %). Unlike the clean sand, the largest drop in *CRR* as α is increased takes place if the liquefaction criterion is ε_q = 2.5 %.

In summary, increase in *α* to 30° reduces the *CRR* of clean sand as much as 80 %, while only 20 % change in *CRR* is observed for NP silty sand. Increasing *α* from 30° to 60° does not significantly impact the *CRR* of clean or NP silty sand.

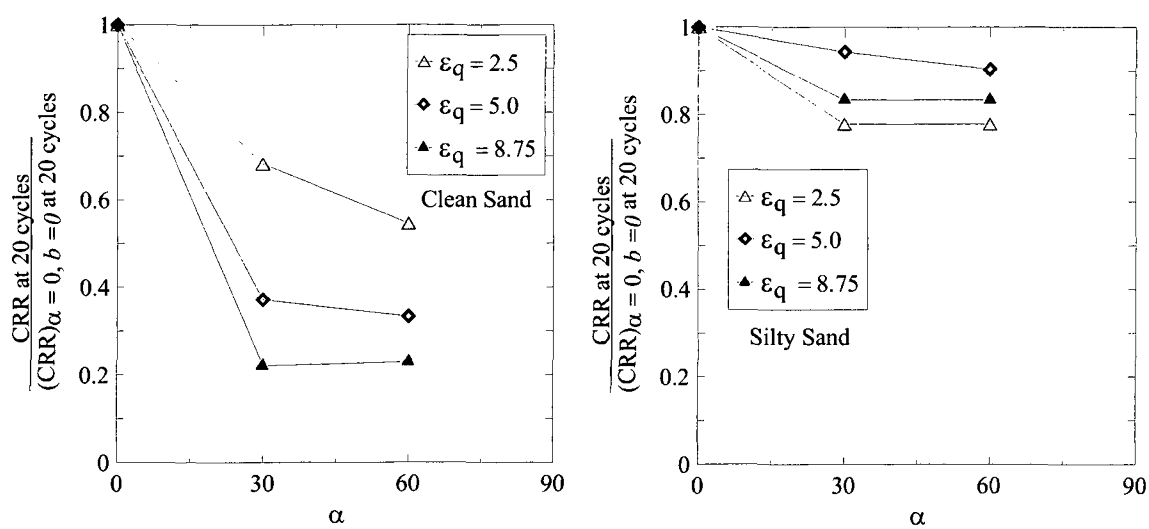

Figure 4.42. Normalized *CRR* as a function of *α* for (a) clean sand, and (b) silty sand.

Results shown in Figs. 4.36, 4.37, 4.38, 4.41 and 4.42 indicate that the fabric of Ottawa sand with and without NP silty sand is substantially anisotropic based on its undrained cyclic response. As the major principal stress rotates from the vertical towards the horizontal direction, the sand exhibits weaker cyclic response. However, the effect of principal stress rotation is less significant if the Ottawa sand contains NP silt (FC = 11 - 15%). This is attributed to change in the fabric of the clean sand by the addition of NP silt. The anisotropic behavior may be suppressed with the addition NP silt.

This finding implies that K_0 consolidated loose to medium dense alluvial sand deposits that are prone to drained principal stress rotation due to the nature of the applied loads prior to an earthquake are likely to exhibit a weaker response and experience large strains even under small disturbances (CSR < 0.10). Furthermore, liquefaction events associated with these soil deposits may take very fast due to UI. These deposits may or may not exhibit stable behavior after undergoing large deformations depending upon the amount major principal stress rotation induced, the scale of the shaking (CSR), the fines content, and the soil state (D_R and p').

4.3.8 Effect of *b* on the Undrained Cyclic Response of Ottawa Sand with and without NP Silt

The effect of *b* on the undrained cyclic response and liquefaction resistance of clean and NP Ottawa silty sands was studied by conducting a series of undrained cyclic loading tests where *b* was kept constant at 0, 0.5 or 0.8 with $\alpha = 0°$ and $p' = 100$ kPa. The relative density range prior to undrained cyclic loading for the clean and NP silty sand specimens were 41 % - 55 % and 43 % – 66 %, respectively. The FC of the NP silty sand specimens ranged between 12 % and 14 %.

4.3.8.1 Excess Pore Pressure and Deviatoric Strain Responses

The excess pore pressure and deviatoric strain responses of the specimens subjected to undrained cyclic loading sheared with $\alpha = 0°$ and $b > 0$ are given in Fig. 4.43 and Fig. 4.44 for clean and NP silty Ottawa sands, respectively. Only one clean sand specimen (Fig. 4.43a) subjected to undrained cyclic loading with $b = 0.5$, $\alpha = 0°$ and $CSR = 0.52$ exhibited temporary UI with sudden increase in the deviatoric strain (8 %) and excess pore pressure (100 kPa) in the first loading cycle. This test had to be terminated due to axial strain limits of the apparatus being reached after 400 cycles. Similarly, one of the NP silty sand specimens subjected to undrained cyclic loading with $CSR = 0.17$ and $b = 0.5$ exhibited a large but temporary increase in excess pore pressure of 110 kPa, but this moment lasted less than two seconds and the excess pore pressure decreased back to 40 kPa. Momentarily, p' dropped below zero, but the specimen did not fail completely, although ε_q during UI reached 17 %. The behavior of both clean and NP Ottawa silty sand specimens that experienced UI (Figs. 4.43a and 4.44b) resembled flow liquefaction followed by the cyclic mobility and maybe associated with the loosest D_R tested. The rest of the clean and NP silty sands exhibited cyclic mobility.

The clean sand specimen subjected to undrained cyclic loading with CSR = 0.55, b = 0.8 and silty sand specimens subjected to undrained cyclic loading with (1) CSR = 0.26 and b = 0.5, (2) CSR = 0.46 and b = 0.8, and (3) CSR = 0.28 and b = 0.8 experienced a distinct peak and, then, a drop in the excess pore pressure, even though they did not exhibit UI, as defined previously. In these cases, the peak excess pore pressure was not attained in a short time period, causing UI. This behavior suggests that both the clean and NP silty sand fabric has the potential to experience UI but the occurrence of UI would be dependent on the level of CSR and D_R of the specimen.

4.3.8.2 Generalized Strain Response

The strain and excess pore pressure responses of clean and NP silty sands during undrained cyclic loading for various b and α = 0° are shown in Figs. 4.45 and 4.46, respectively. When b = 0.5 or 0.8, both clean and NP silty sand specimens experienced extension in the circumferential direction. With the increase in CSR, both clean and NP silty sands experienced increasingly larger circumferential strain. After 400 cycles (since one of the tests had only 400 cycles of loading) of undrained cyclic loading with b = 0.5 for CSR varying between 0.09 and 0.52, the circumferential strain measured varied between 0.2 % and 7 % (extensional) for the clean sand specimens. When b was increased to 0.8, the extensional circumferential strain range increased up to 0.5 % to 10 % after 400 cycles of undrained cyclic loading with CSR between 0.07 and 0.39. Circumferential strains for the NP silty sand varied between 2 % to 10 % (extension)

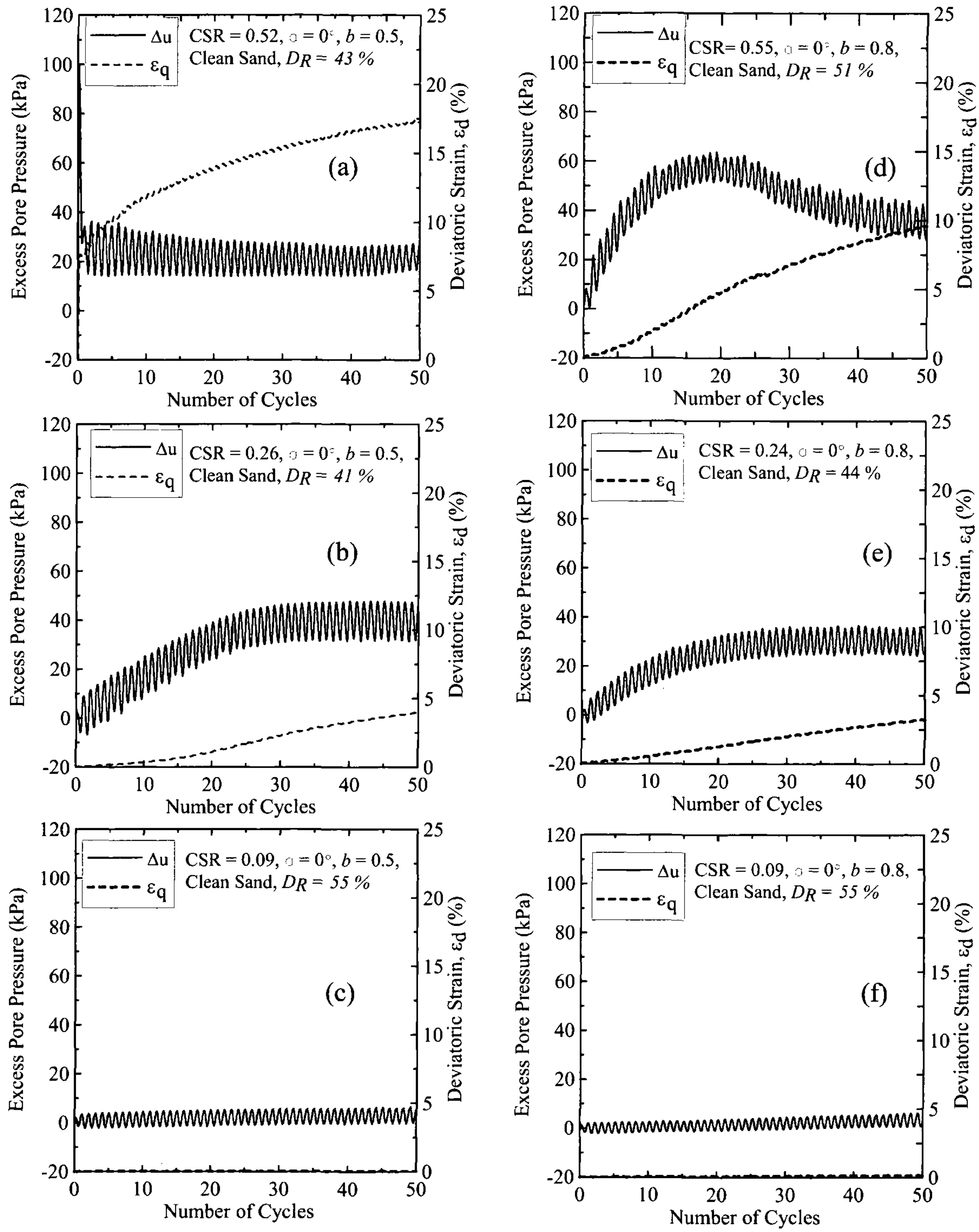

Figure 4.43. Excess pore pressure and deviatoric strain responses of the clean sand specimens cyclically sheared with $\alpha = 0°$ and $b = 0.5$ for (a) $CSR = 0.52$, (b) $CSR = 0.26$, (c) $CSR = 0.09$ and = 0.8 at (d) $CSR = 0.55$, (e) $CSR = 0.24$, (f) $CSR = 0.09$.

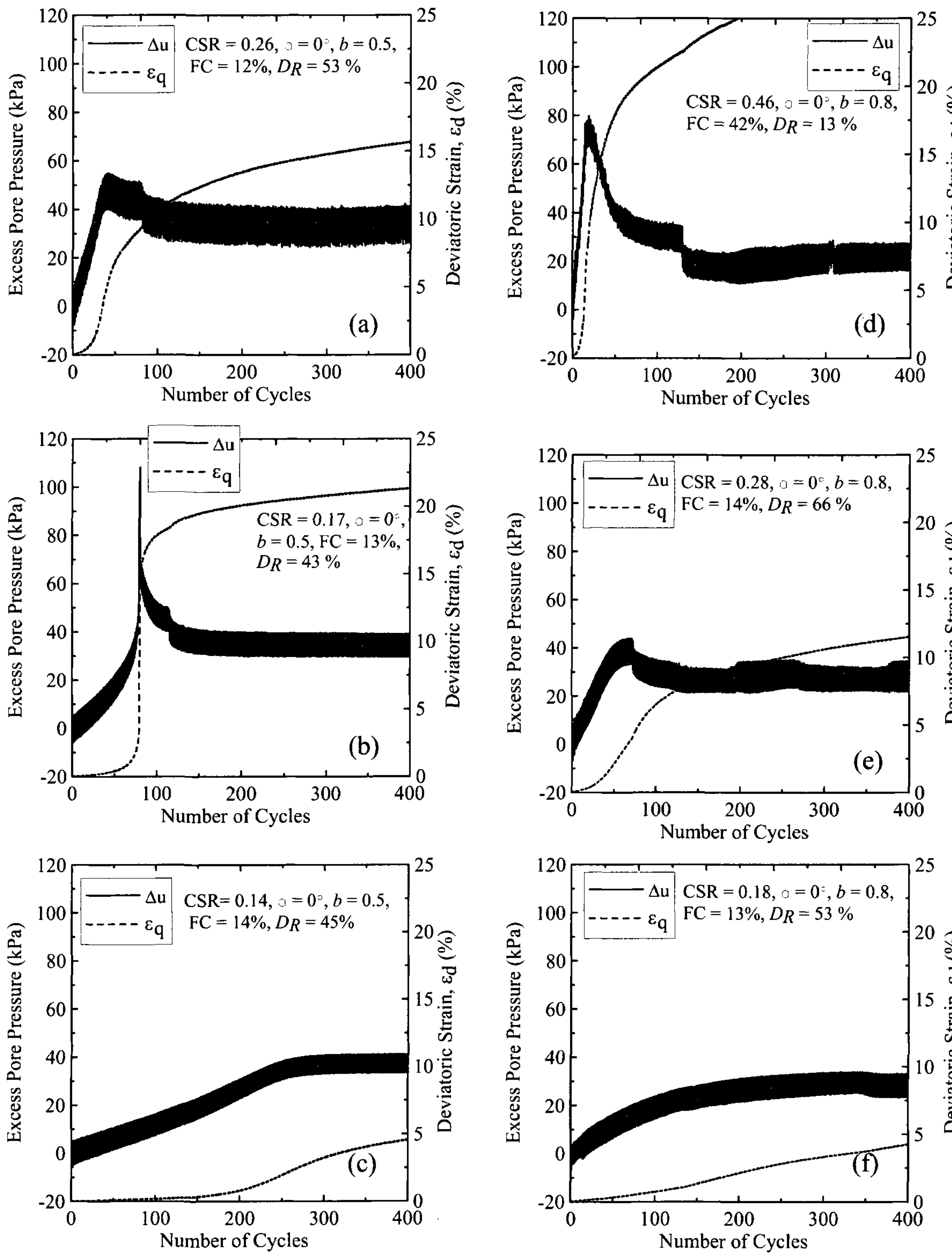

Figure 4.44. Excess pore pressure and deviatoric strain responses of the NP silty sand specimens cyclically sheared with α = 0 and b = 0.5 for (a) *CSR* = 0.26, (b) *CSR* = 0.17, (c) *CSR* = 0.14 and b = 0.8 at (d) *CSR* = 0.46, (e) *CSR* = 0.28, (f) *CSR* = 0.18.

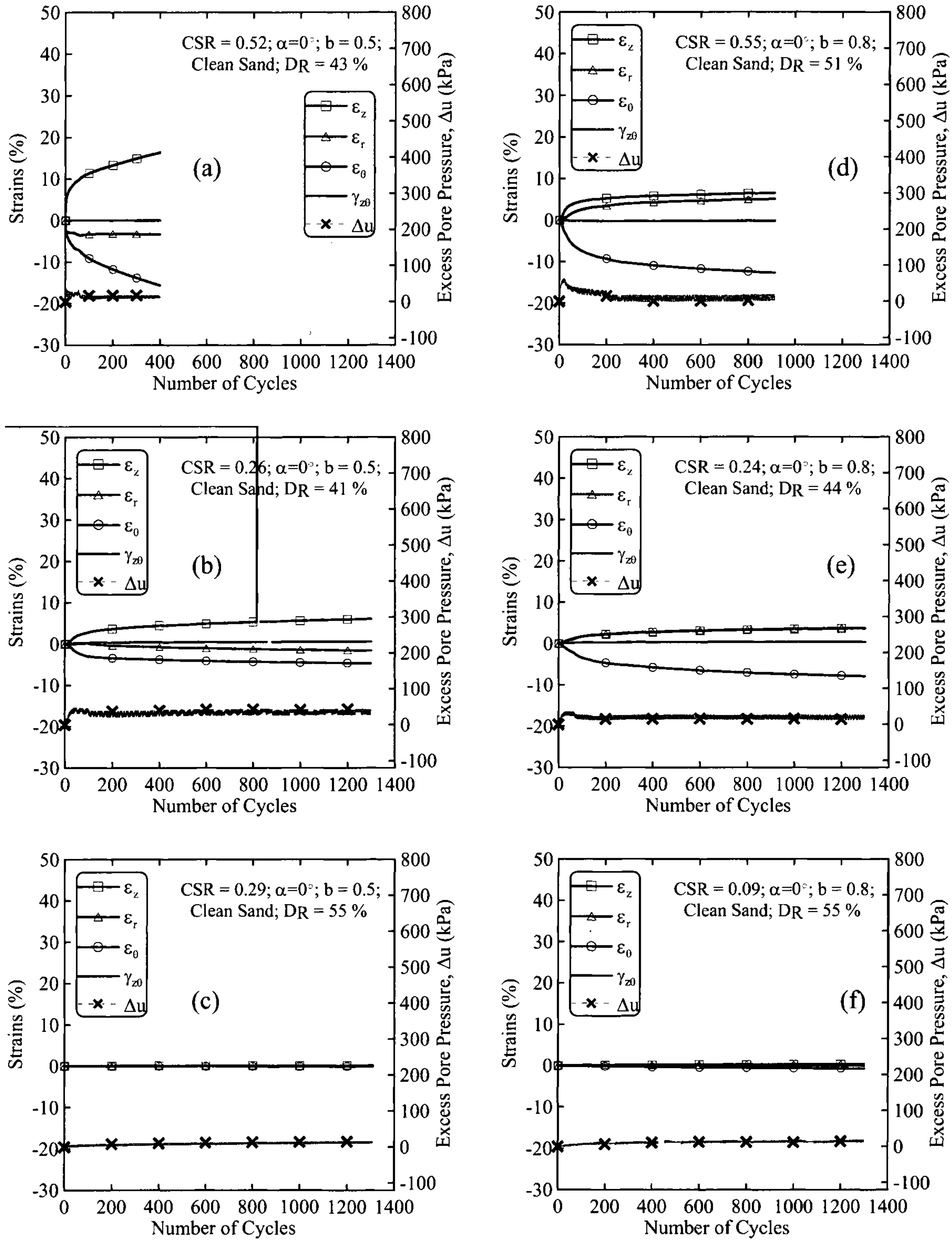

Figure 4.45 Generalized strain responses of the clean sand specimens cyclically sheared with α = 0 and b = 0.5 at (a) *CSR* = 0.52, (b) *CSR* = 0.26, (c) *CSR* = 0.09 and b = 0.8 at (d) *CSR* = 0.55, (e) *CSR* = 0.24, (f) *CSR* = 0.09.

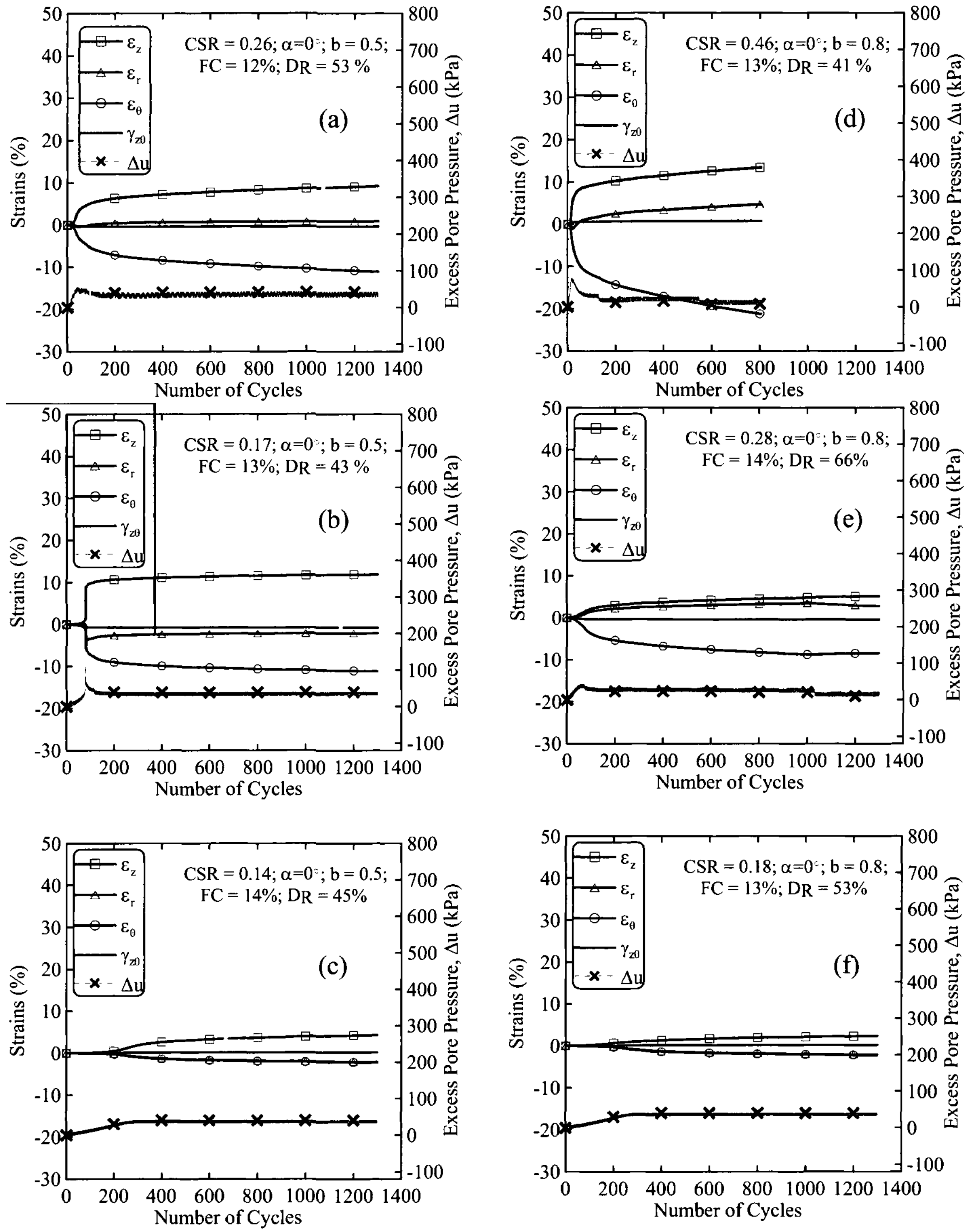

Figure 4.46. Generalized strain response of silty sand specimens cyclically sheared with α = 0 and b = 0.5 at (a) *CSR* = 0.26, (b) *CSR* = 0.17, (c) *CSR* = 0.14 and b = 0.8 at (d) *CSR* = 0.46, (e) *CSR* = 0.28, (f) *CSR* = 0.18.

when $b = 0.5$ and *CSR* between 0.14 and 0.26, and between 2 % and 17 % (extension) when $b = 0.8$ and *CSR* between 0.13 and 0.32.

Unlike the circumferential strain response, increases in b applied prior to undrained cyclic loading typically decreased the axial strain mobilized during undrained cyclic loading. When $b = 0.5$ during undrained cyclic loading, the clean sand specimens experienced axial strains between 0.2 % and 16 % for *CSR* between 0.09 and 0.52. When $b = 0.8$, the axial strain induced on the clean sand specimens varied between 0.2 % and 6 % for *CSR* between 0.07 and 0.39. Similarly, when $b = 0.5$ for *CSR* between 0.14 and 0.26, axial strain experienced by the NP silty sand was between 3 % and 10 %. Increasing b to 0.8 and applying *CSR* between 0.18 and 0.46, axial strain experienced by the silty sand specimens ranged between 1 % and 11 %. The total range of axial strain observed when $b = 0.5$ and $b = 0.8$ did not necessarily show the reduction in the axial strain due to increase in b. This is attributed to the *CSR* difference between the two cases. Comparison of axial strains shown in Fig. 4.45b and Fig. 4.45d or Fig. 4.46c and Fig. 4.46f; however, shows the reduction in axial strain due to increase in b for similar *CSR*.

The primary strain response in the radial direction was contractive when $b = 0$ and 0.5 and, then, turned into extension when $b = 0.8$ for both sands. The largest radial strains for the *CSR* ranges applied were 3 % (compression) and 2 % (compression) for clean and NP silty Ottawa sands, respectively, when $b = 0.5$. However, when b was increased to 0.8, the largest radial strains for the *CSR* ranges applied were 5 % (extension) and 3 % (extension) for clean and NP silty Ottawa sands,respectively.

The deformation patterns shown in Fig. 4.45 and 4.46 indicate that, when subjected to undrained cyclic loading with $b > 0$ and $\alpha = 0°$, the clean and silty sand specimens compress in the axial direction and bulges out in the horizontal plane (Fig. 4.47). In this type of deformation, the radial strain stands for the change in the specimen wall thickness, which is the least amount of strain measured. However, large axial and circumferential (diameter change) strains may be observed.

The excess pore pressure responses and deformation patterns shown in Fig. 4.45 and 4.46 are related. When UI takes place and the excess pore pressure increases abruptly, the strains also build up in abruptly. Conversely, if the excess pore pressure increases steadily, strains also increase steadily.

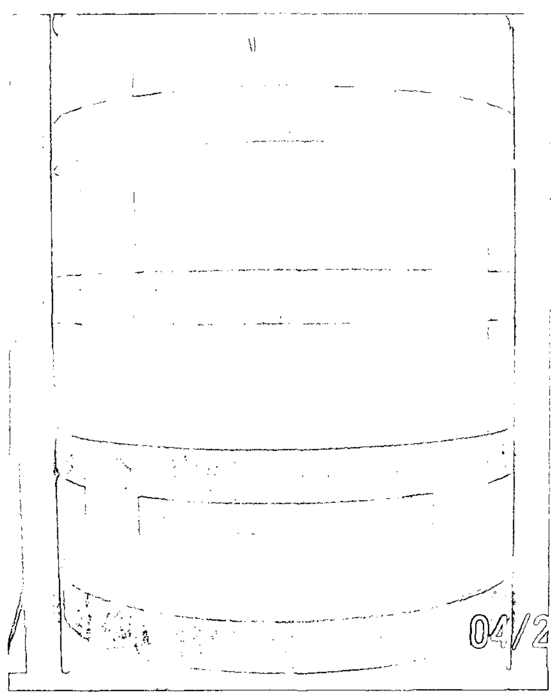

Figure 4.47. Typical deformation pattern of clean sand specimens subjected to undrained cyclic loading with $\alpha = 0°$, $b = 0.5$ and $CSR = 0.49$.

4.3.8.3 Stress Paths and Undrained Instability

The effective stress paths for the clean and NP silty Ottawa sand specimens subjected to undrained cyclic loading for various *CSR* with $b > 0$ are given in Fig 4.48 and Fig. 4.49, respectively. The effective stress paths (Fig. 4.48) for cyclic tests with $\alpha = 0°$ and $b > 0$ show that only one clean sand specimen experienced UI due to high $CSR = 0.52$ and low $D_R = 43$ % (Fig. 4.49a). Similarly, only two NP silty sand specimens experienced UI (Fig. 4.46b and 4.46d). Except for these three specimens, all other clean and silty sand specimens subjected to undrained cyclic loading with $\alpha = 0°$ and $b > 0$ exhibited a relatively steady increase in excess pore pressure and, thus, corresponding decrease in p' (cyclic mobility). Figs. 4.48 and 4.49 also show that almost all effective stress paths with large *CSR* exceed the axisymmetric CSL (not temporarily), which suggests that additional bounding surfaces may control the soil behavior for b and may lie above the CSL for $\alpha = 0°$ and $b = 0$. However, the CSL line shown in p'- q plane is established for axisymmetric testing conditions and may not reflect accurately the three dimensional stress conditions for tests with $b > 0$. Some researchers claimed that the slope of the CSL may be smaller with the increase in b (Uthayakumar and Vaid 1997). The data shown in Fig. 4.48 and 4.49 does not support such behavior. Further research is needed to explore the effect of σ_2 on the undrained response of sands.

4.3.8.4 Liquefaction Resistance Curves

The effect of b on the liquefaction resistance of clean and NP silty sand is depicted in Fig. 4.50. The liquefaction resistances were determined according to the liquefaction criteria of $\varepsilon_q = 2.5$ %, 5.0 %, or 8.75 %. For both clean and silty sands, the liquefaction resistance curve for $b = 0$ lies below the liquefaction resistance curves for $b = 0.5$ and $b =$

0.8. This suggests that increasing *b* to 0.5 or 0.8 increases the number of cycles to reach liquefaction criteria. The liquefaction resistance curves of clean sand for $b = 0$ and $b = 0.5$ are more apart from each other compared to the relative locations of the liquefaction resistance curves for $b = 0.5$ and $b = 0.8$. The liquefaction resistance curves of clean sand when $b > 0$ merge closer to the curve for $b = 0$ as the deviatoric strain required for the liquefaction criterion increases. However, the relative locations of the liquefaction resistance curves for the NP silty sands for various *b* are not significantly impacted by the liquefaction criterion, again, suggesting a less anisotropic fabric than their clean sand counterparts.

The variation of the liquefaction resistance (*CRR*) as a function of *b* is given in Fig. 4.51. The liquefaction resistance (*CRR*) is defined as the *CSR* required to reach the liquefaction criterion in 20 loading cycles, and was determined using the liquefaction curves given in Fig. 4.50. In Fig. 4.51, the *CRR* for each *b* was normalized by the corresponding *CRR* for $\alpha = 0°$ and $b = 0$ case in order to see the effect of *b* compared to the axisymmetric case.

Increases in *b* to 0.5 or 0.8 increase the normalized *CRR* for both clean and silty sand regardless of the liquefaction criterion used. However, the amount of *CRR* increase as a function of *b* depends on the liquefaction criterion for the clean sand. If $\varepsilon_q = 8.75$ %, the *CRR* gain with the increase in *b* is less than that observed for the liquefaction criterion of $\varepsilon_q = 2.5$ % or $\varepsilon_q = 5.0$ %. For silty sand, increases in *CRR* as a function of *b* is not significantly impacted by the liquefaction criterion. Increase in *b* to 0.5 increases the *CRR* by 1.5 – 2.9 times for clean sand, and 1.5 – 1.6 times for silty sand. Further increase in *b*

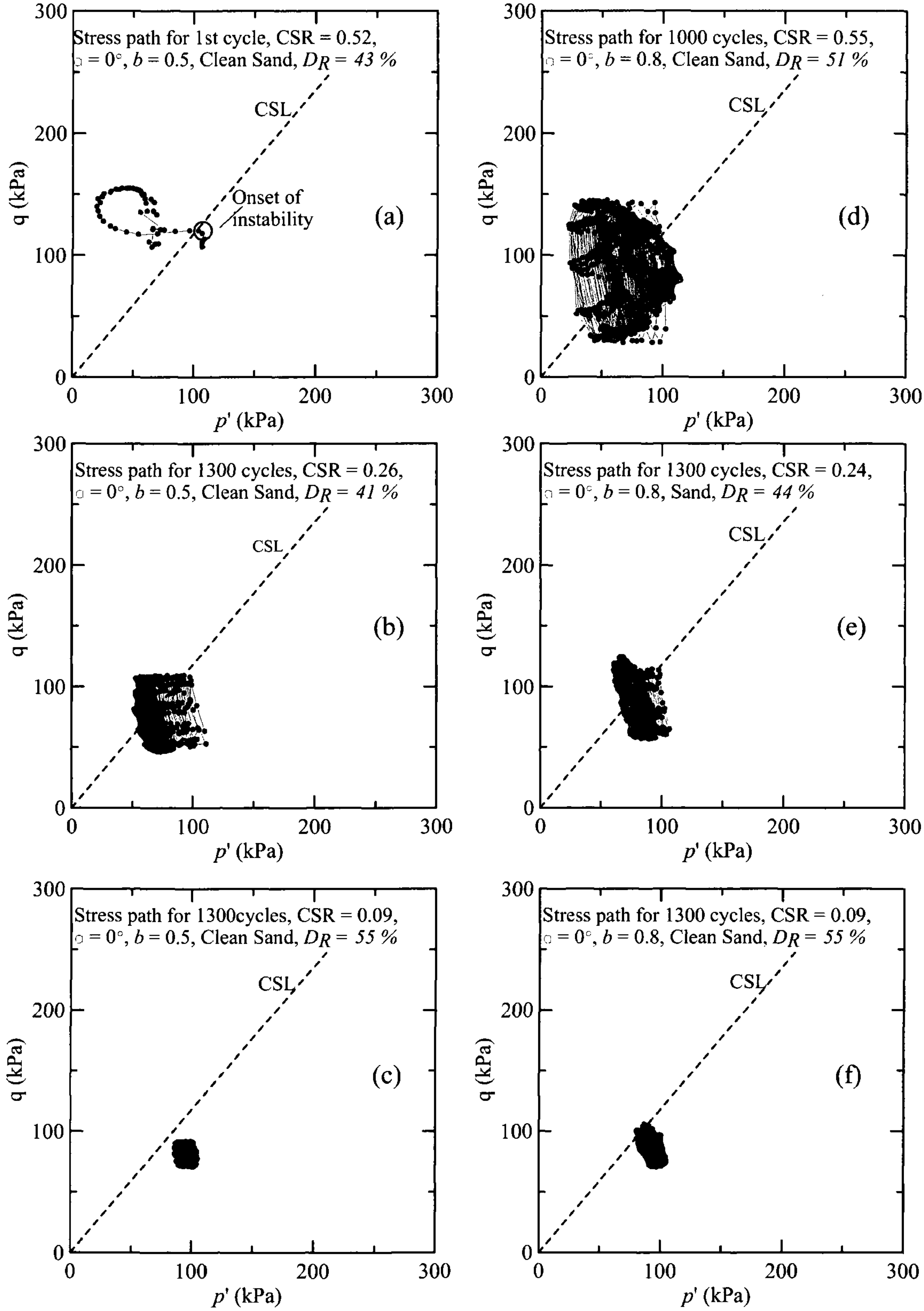

Figure 4.48. Effective stress paths for the clean sand specimens cyclically sheared with α = 0 and b = 0.5 at (a) *CSR1* = 0.52, (b) *CSR1* = 0.26, (c) *CSR1* = 0.09 and b = 0.8 at (d) *CSR1* = 0.55, (e) *CSR1* = 0.24, (f) *CSR1* = 0.09.

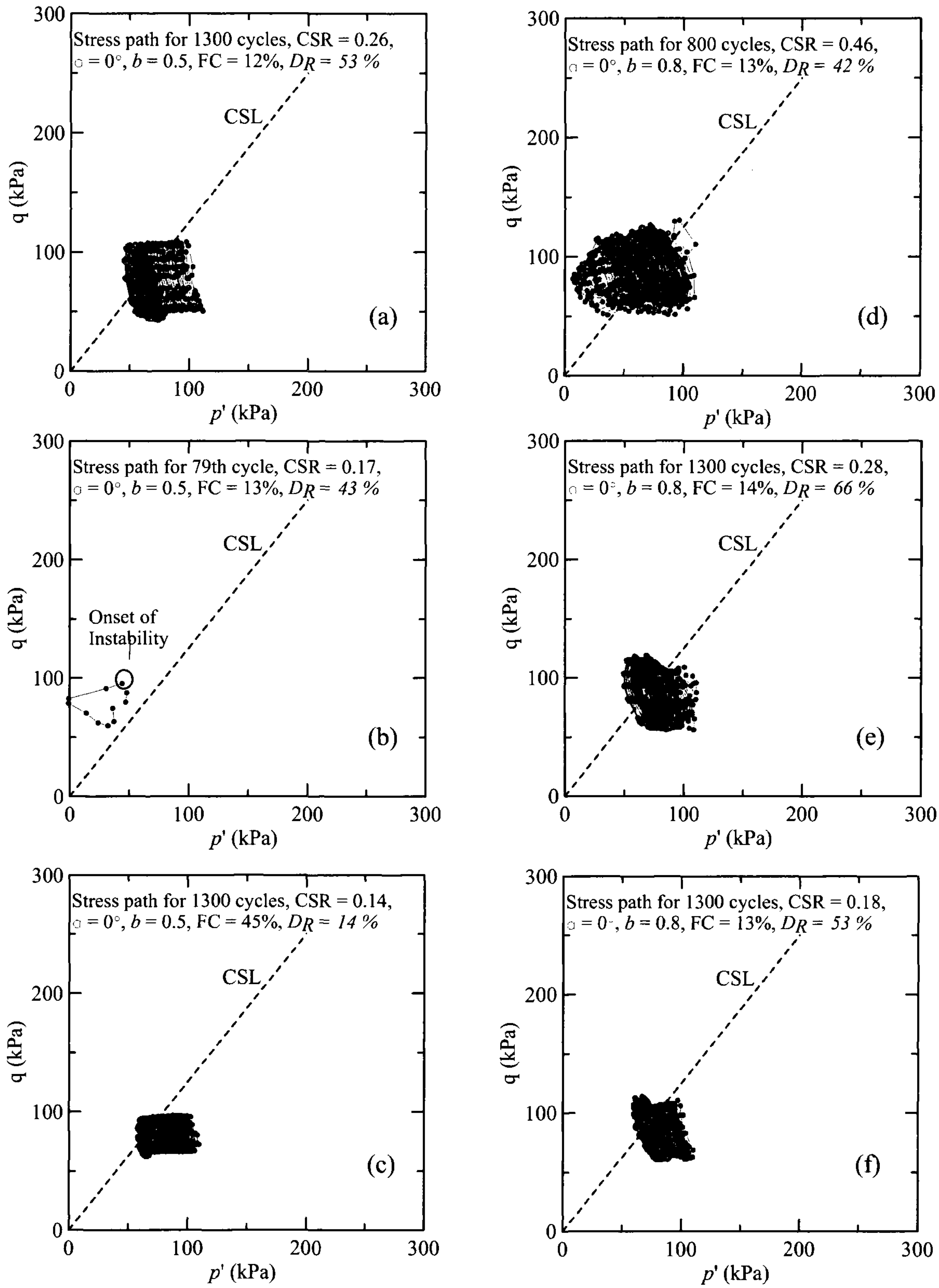

Figure 4.49. Effective stress paths for the NP silty sand specimens cyclically sheared with α = 0 and b = 0.5 at (a) *CSR1* = 0.26, (b) *CSR1* = 0.17, (c) *CSR1* = 0.14 and b = 0.8 at (d) *CSR1* = 0.46, (e) *CSR1* = 0.28, (f) *CSR1* = 0.18.

to 0.8 increases the *CRR* of clean and silty sand by 2.0 – 3.8 times and 2.4 – 2.7 times, respectively. The range for *CRR* increase due to b increase is larger for clean sand, since the liquefaction response of clean sand depends on more on liquefaction criterion than silty sand.

Results depicted in Fig. 4.50 and 4.51 show that the liquefaction resistance of the clean or NP silty sand is increased with the increase in b. Bolton (1986) mentioned that plane strain strength is above the axisymmetric strength for sands, which implies that when b is increased to 0.3 – 0.5 at $\alpha = 0°$ (plane strain conditions) the resulting monotonic strength is larger than the strength observed for $b = 0$ and $\alpha = 0$. The corollary of this would be relatively less liquefaction resistance obtained from cyclic triaxial tests when $\alpha = 0°$ and $b = 0$ compared to the in situ plane strain conditions with $b > 0$. Therefore a liquefaction design based on cyclic triaxial test results may be more conservative considering the plane strain conditions observed in the field. The findings shown in Fig. 4.50 and 4.51 confirm this conclusion. However, the results shown in Fig. 4.50 and 4.51 are valid for $\alpha = 0°$, and may not be true when $\alpha > 0°$. The implications of having both α and b greater than zero will be discussed in section 4.3.9.

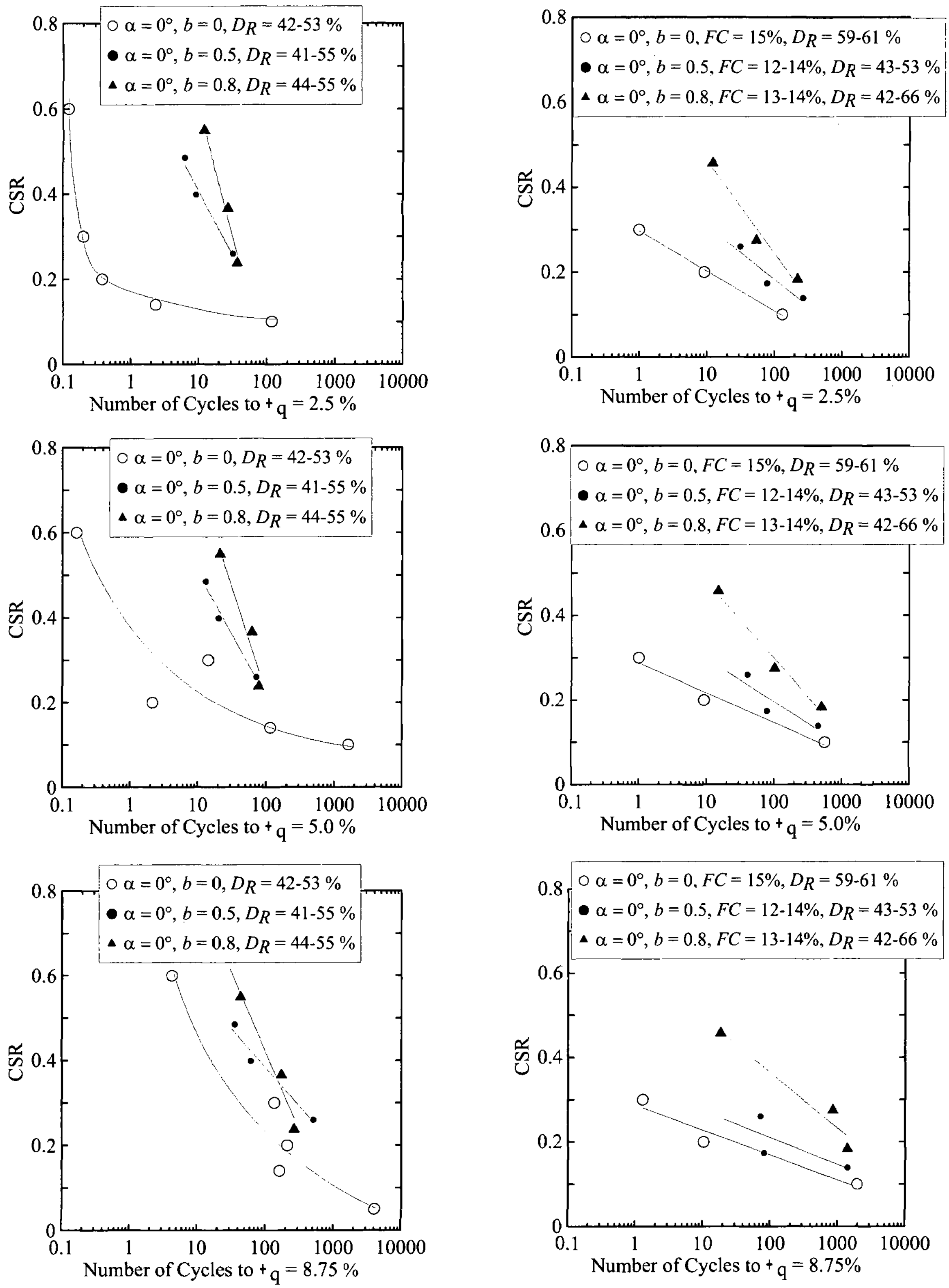

Figure 4.50. Liquefaction resistance curves for clean sand at (a) ε_q = 2.5 %, (b) ε_q = 5 %, (c) ε_q = 8.75 %, and for silty sand at (d) ε_q = 2.5 %, (e) ε_q = 5.0 %, and (f) ε_q = 8.75 % when α = 0° and b = 0, 0.5 or 0.8.

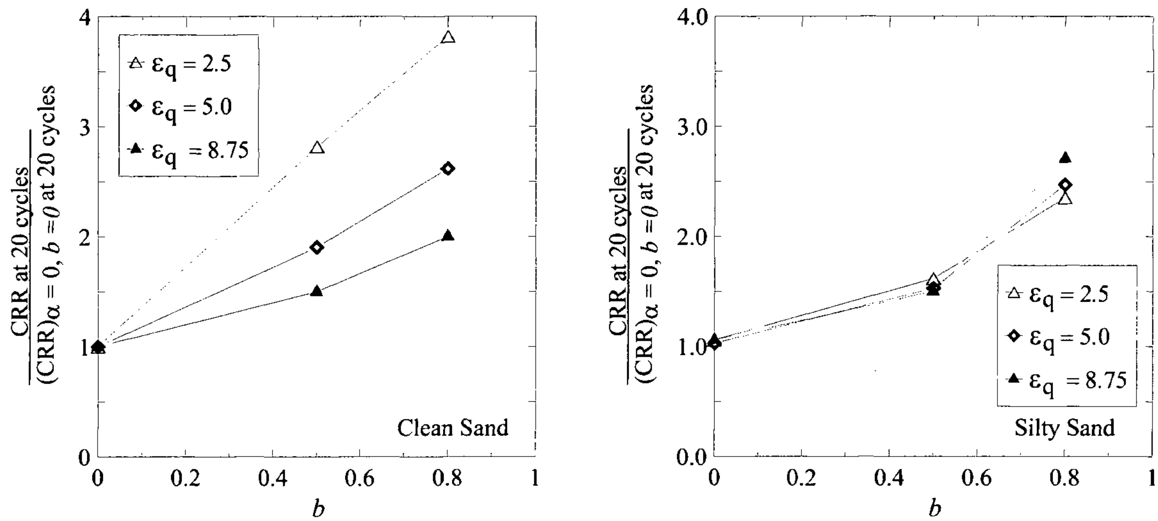

Figure 4.51. Normalized *CRR* as a function of *b* for (a) clean sand, and (b) silty sand.

4.3.9 Effect of Simultaneous Major Principal Stress Rotation and *b* Increase on the Undrained Cyclic Response of Clean Ottawa Sand

Increase in α from 0° to either 30° or 60° was shown to reduce the liquefaction resistance of clean Ottawa sand (Fig. 4.33), whereas increase in *b* was shown to increase the liquefaction resistance of clean Ottawa sand (Fig. 4.47). The combined effect of α and *b* on the liquefaction resistance of the clean Ottawa sand was investigated by conducting twelve cyclic shear tests where both α and *b* were greater than zero and maintained constant throughout the undrained cyclic loading. The D_R range for the specimens tested at this stage was between 45 % and 58 %. The response of four specimens subjected to undrained cyclic loading with similar *CSR* are analyzed in this section, as keeping *CSR* constant allows comparison of the relative effects of α and *b* on the undrained cyclic response. However, results from all twelve tests were used to analyze the relative effects of α and *b* on the liquefaction resistance of Ottawa sand.

4.3.9.1 Excess Pore Pressure and Deviatoric Strain Responses

The clean Ottawa sand specimen subjected to undrained cyclic loading with α = 30°, *b* = 0.5 and *CSR* = 0.10 experienced UI after five cycles and developed an excess pore pressure of 44 kPa in less than one cycle (Fig. 4.52a). This large pore pressure build up induced a 5.5 % deviatoric strain. The deviatoric strain response is in accordance with the limited flow liquefaction followed by cyclic mobility, which was also observed for the specimen subjected to undrained cyclic loading with α = 30°, *b* = 0, and *CSR* = 0.10. However, the specimen tested under *b* = 0 developed UI after 3 cycles. The difference in number of cycles to reach UI between these two specimens may be due to the relative density difference or the effect of *b*. The specimen tested under *b* = 0 and α = 30° (D_R =

41 %) reached UI after three cycles and developed an excess pore pressure of about 55 kPa, while the specimen tested under $b = 0.5$ and $\alpha = 30°$ ($D_R = 58$ %) experienced UI after five cycles and developed about 45 kPa. Since both D_R and b difference between these two specimens may cause the discrepancy in number of cycles to reach UI and the amount of excess pore pressure generated at UI, a conclusion regarding the effect of b is difficult to make. However, increasing b to 0.5 when $\alpha = 30°$ and $CSR = 0.10$ definitely did not eliminate the UI even when combined with the relatively larger D_R. Further increase in b to 0.8 at $\alpha = 30°$ and $CSR = 0.09$ eliminated UI in the specimen response, which was characterized by cyclic mobility (Fig. 4.52b).

When $\alpha = 60°$, the excess pore pressure did not exceed 10 kPa for $b = 0.5$ and $CSR = 0.09$ (Fig. 4.52c), and 20 kPa for $b = 0.8$ and $CSR = 0.09$ (Fig. 4.52d). However, both of these specimens experienced UI and large sudden increases in the deviatoric strain during the first few cycles after which the deviatoric strain increased steadily. For similar $CSR = 0.10$, the corresponding clean sand specimen ($D_R = 43$ %) subjected to undrained cyclic loading with $\alpha = 60°$ and $b = 0$ exhibited the same behavior in terms of UI and sudden deviatoric strain development during the first loading cycle. Consequently, increasing b from 0 ($D_R = 43$ %) to 0.5 ($D_R = 54$ %) or 0.8 ($D_R = 47$ %) when $\alpha = 60°$ does not change the type of the behavior even with the contribution of larger D_R for both cases. The number of cycles to reach UI, however, is slightly increased, which may be due to the effect of b or D_R.

4.3.9.2 Generalized Strain Response

The generalized strain responses of the specimens considered in Fig. 4.52 are given in Fig. 4.53 along with their excess pore pressure response. The predominant strain component for all combinations of α and b was the shear strain during undrained cyclic loading with $\alpha > 0°$ and $b > 0$, which may be primarily attributed to the effect of α. For the specimens shown in Fig. 4.53, the maximum shear strain varied between 5 % and 10 % during undrained cyclic loading and was significantly larger than any other strain component.

Fig. 4.53 also shows that during undrained cyclic loading with $\alpha = 30°$ and $b = 0.5$ or 0.8, the axial strain was close to zero. However, undrained cyclic loading with $\alpha = 60°$ and $b = 0.5$ or 0.8, induced -3 % axial strain (extension). The circumferential strain was around -1 % (extension) during undrained cyclic loading with $\alpha = 30°$ and $b = 0.5$ or 0.8. However, with the increase in α to 60°, the circumferential strain became 1 % (compressional). The magnitude and direction of the circumferential strain seems to be mainly controlled by α. The radial strain was less than 1 % for $\alpha = 30°$ or 60° when $b = 0.5$, and is increased to about 1.3 % when $b = 0.8$ and $\alpha = 30°$ or 60°.

The strain response given in Fig. 4.53 implies that when α and b are greater than zero, the largest strain component is the shear strain, which is primarily induced by α increase. Therefore, the undrained cyclic response of the clean sand is impacted predominantly by α when applied together with $b > 0$.

The excess pore response given in Fig. 4.53 follows the trend observed for shear strain. When there is a sudden increase in shear strain, the excess pore pressure increases accordingly.

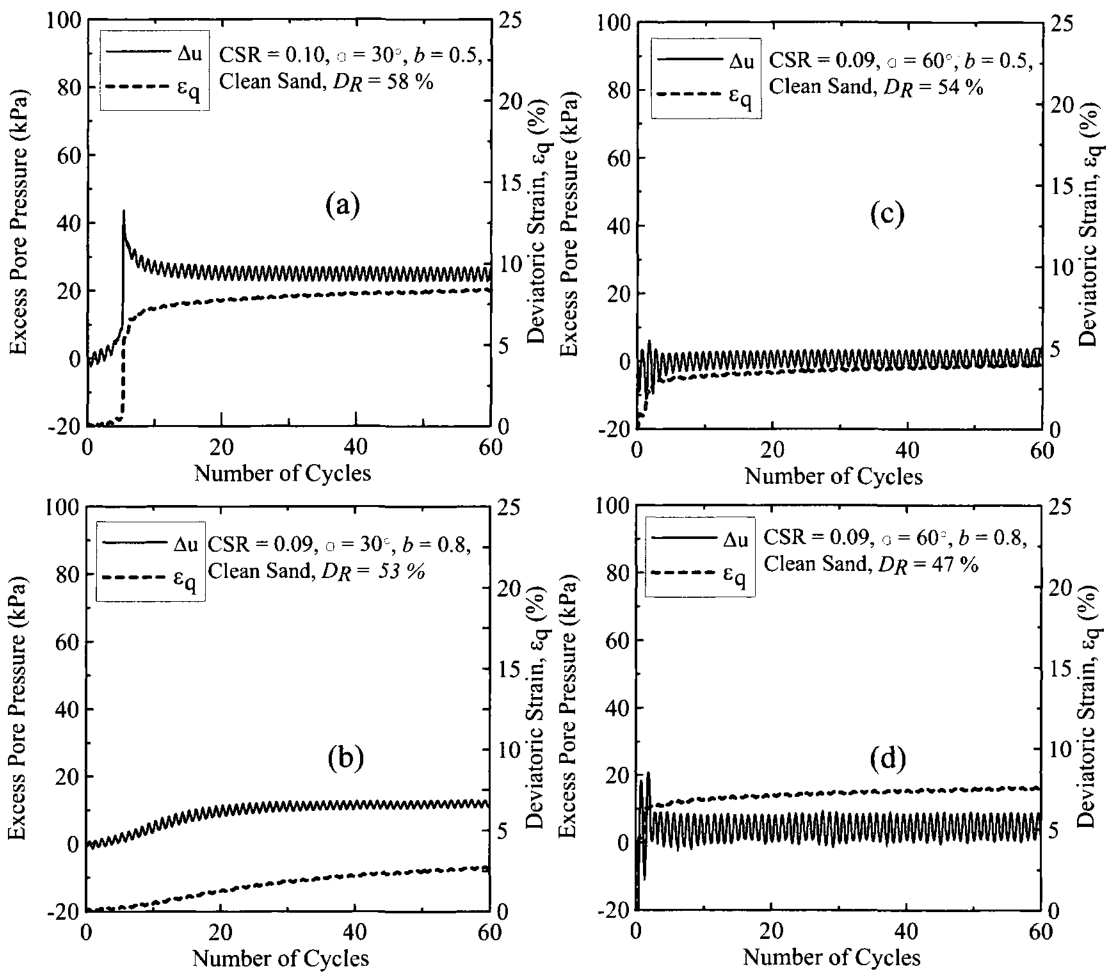

Figure 4.52. Excess pore pressure and deviatoric strain responses of clean Ottawa sand specimens cyclically sheared with (a) $\alpha = 30°$ b = 0.5 CSR = 0.10, (b) $\alpha = 30°$ b = 0.8 CSR = 0.09, (c) $\alpha = 60°$ b = 0.5 CSR = 0.09, (d) $\alpha = 60°$ b = 0.8 CSR = 0.09.

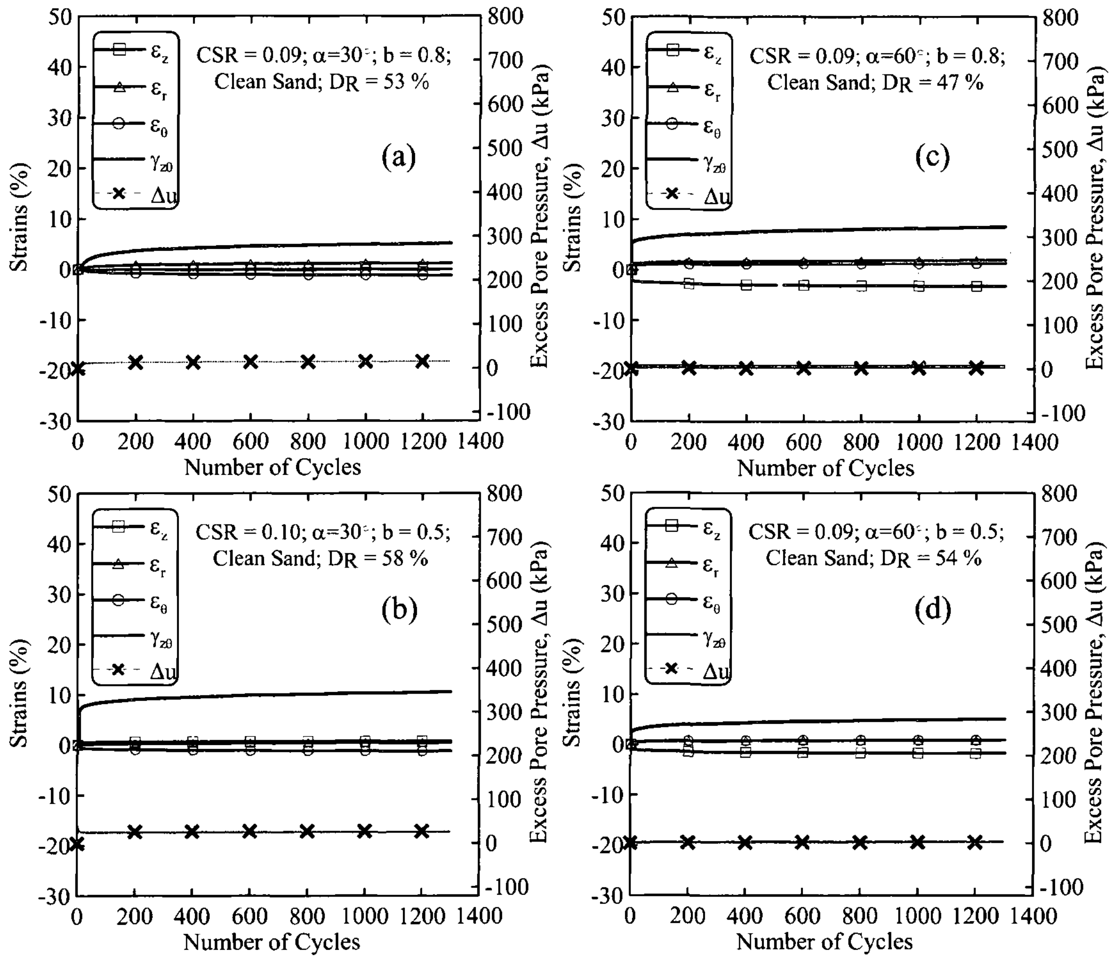

Figure 4.53. Generalized strain and excess pore pressure response of clean Ottawa sand specimens cyclically sheared with (a) $\alpha = 30°$ $b = 0.5$ $CSR = 0.10$, (b) $\alpha = 30°$ $b = 0.8$ $CSR = 0.15$, (c) $\alpha = 60°$ $b = 0.5$ $CSR = 0.09$; (d) $\alpha = 60°$ $b = 0.8$ $CSR = 0.09$.

4.3.9.3 Stress Paths and Undrained Instability

The stress paths for the specimens analyzed in Figs. 4.52 and 4.53 are shown in Fig. 4.54. Data for the rest of the tests confirms the following findings. When $\alpha = 30°$ and $b = 0.5$ ($D_R = 58$ %), instability in the specimen similar to the one described in Fig. 4.39a ($D_R = 41$ %) occured when subjected to undrained cyclic loading with $CSR = 0.10$ even with larger D_R (Fig. 4.54a). Further increase in b to 0.8 ($D_R = 53$ %) eliminated the instability and resulted in cyclic mobility without the development of the sudden large excess pore pressure. For similar, the specimen subjected to $\alpha = 30°$ and $b = 0$ experienced UI (D_R = 41 %), while the specimens subjected to $\alpha = 0°$ and $b = 0.5$ (D_R = 55 %) or 0.8 (D_R = 55 %) did not. Considering the UI observed for $\alpha = 30°$ and $b = 0.5$ (D_R = 58) %, the instability behavior is controlled predominantly by α rather than b when $\alpha = 30°$. When α is increased to 60°, regardless of b, the specimens (D_R = 47 – 54 %) experienced UI when subjected to undrained cyclic loading with $CSR = 0.10$. Again considering that specimens subjected to $CSR = 0.10$ and $b = 0.5$ and 0.8 (D_R = 55 %) did not experience UI, when $\alpha = 60°$, the undrained cyclic response is primarily determined by α.

4.3.9.4 Liquefaction Resistance Curves

The combined effect of α and b on the liquefaction resistance curves of clean sand is shown in Fig. 4.55. Liquefaction criterion of ε_q = 8.75 % is not included in Fig.4.55, since most of the specimens did not reach ε_q = 8.75 at the maximum number of loading cycles of 1300. When the liquefaction criterion is ε_q = 2.5 %, the liquefaction resistance curve for any combination of $\alpha > 0$ and $b > 0$ except $\alpha = 30°$ and $b = 0.5$ plots below the curve for $\alpha = 0°$ and $b = 0$ case (i.e. lower liquefaction resistance). However, the liquefaction resistance curve for $\alpha = 30°$ and $b = 0.5$ (Figs. 4.55a and 4.55b) is still close to the curve for $\alpha = 0°$ and $b = 0$ considering the separation between the curve for $\alpha = 0°$ and $b = 0$, and the curve for $\alpha = 0°$ and $b = 0.5$ (Figs. 4.50a and 4.50b). When the liquefaction criterion is increased to ε_p = 5.0 %, all combinations of $\alpha > 0$ and $b > 0$ have liquefaction resistance curves below the one for $\alpha = 0°$ and $b = 0$. Increasing α to 60° when $b = 0.5$ or 0.8 causes the liquefaction resistance curve to shift down significantly. However, when $\alpha = 30°$ and $b = 0.5$ or 0.8, the liquefaction resistance curve is located relatively close to (compared to $\alpha = 60°$) the curve for $\alpha = 0°$ and $b = 0$. Moreover, when

$\alpha = 60°$, the location of the liquefaction resistance curve is not impacted if b is increased from 0.5 to 0.8. When $\alpha = 30°$, increasing b from 0.5 to 0.8 causes the liquefaction resistance curve upwards (strengthening effect).

Defining the cyclic resistance ratio (*CRR*) as the *CSR* that causes $\varepsilon_q = 2.5$ % or $\varepsilon_q = 5.0$ % at 20 loading cycles, the variation of *CRR* as a function of α and b is given in Fig. 4.56a and Fig 4.56b, respectively. The *CRR* for each test shown in these figures is normalized by the *CRR* determined for the $\alpha = 0°$ and $b = 0$ case. When α is increased from 0° to 60°, *CRR* decreases significantly regardless of b. Furthermore, the effect of b on *CRR* is negligible when applied together with $\alpha = 60°$. For all b, the reduction in *CRR* ratio is more pronounced when α is increased from 0° to 30°, compared to α increase from 30° to 60°. Increase in b does increase the *CRR* when $\alpha = 0°$, while the strengthening effect of b on *CRR* is significantly suppressed for $\alpha > 0°$. When both α and b are greater than zero, the *CRR* ratio decreases. The only exception to this observation is when $\alpha = 30°$ and $b = 0.8$ for the liquefaction criterion of $\varepsilon_q = 2.5$ %, the *CRR* increases by only 10 % compared to *CRR* for $\alpha = 0°$ and $b = 0$ case.

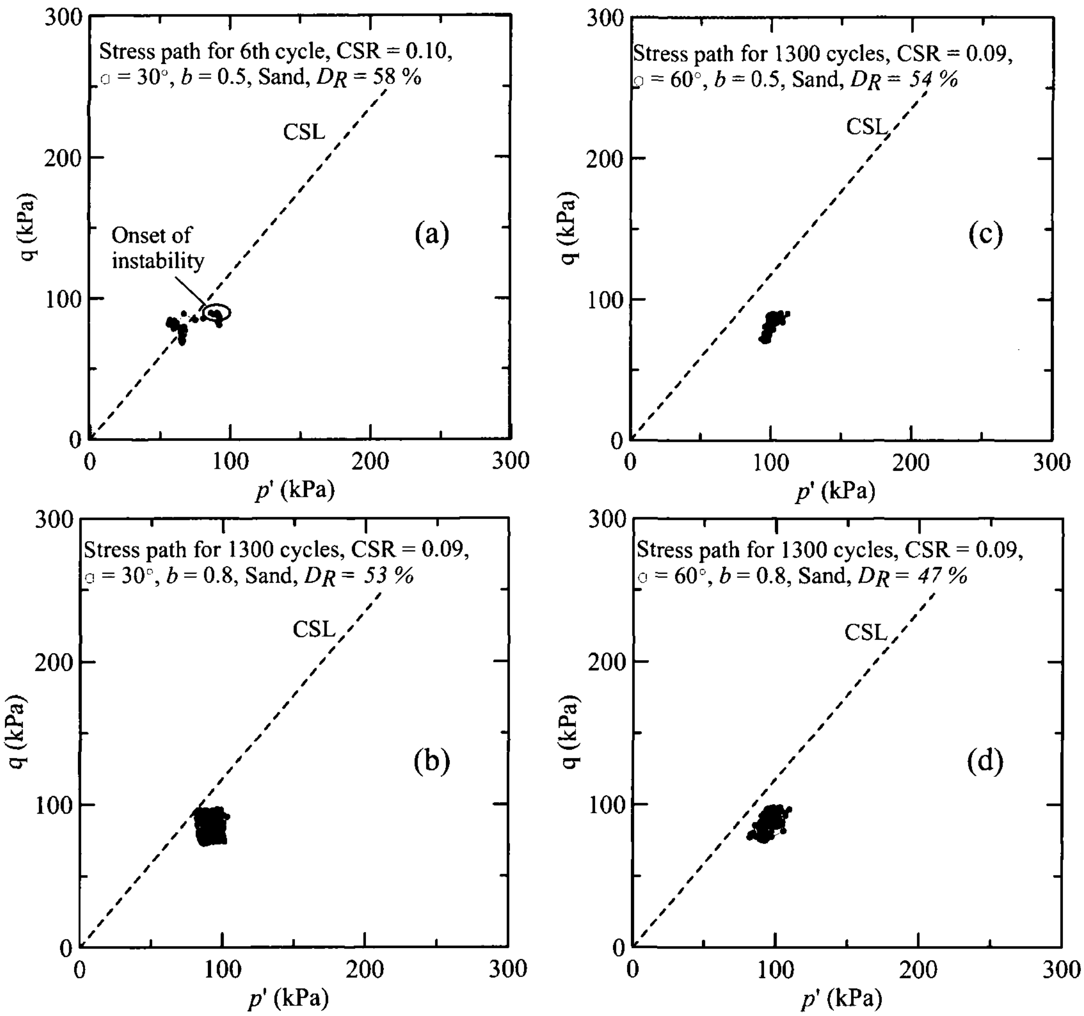

Figure 4.54. Effective stress paths for sand specimens cyclically sh eared with (a) $\alpha = 30°$ b = 0.5 CSR = 0.10, (b) $\alpha = 30°$ b = 0.8 CSR = 0.09, (c) $\alpha = 60°$ b = 0.5 CSR = 0.09, (d) $\alpha = 60°$ b = 0.8 CSR = 0.09.

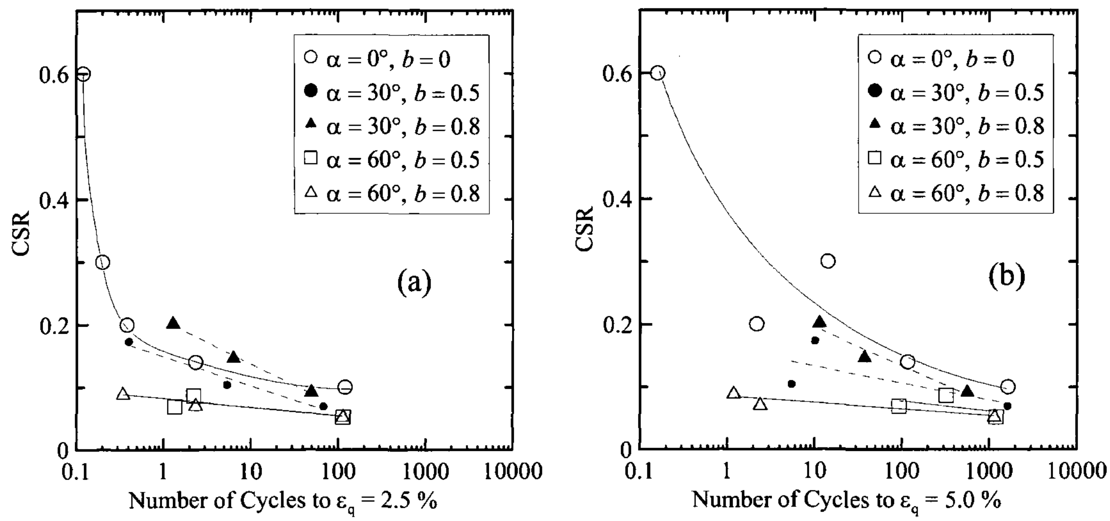

Figure 4.55. Liquefaction resistance curves of clean sand for various *α* and *b* as (a) ε_q = 2.5 %, and (b) ε_q = 5.0 %

Fig. 4 56 shows that when α = 0°, increase in *b* can increase the *CRR* ratio up to 3.8. However, as soon as α is increased to 30° with the simultaneous increase in *b*, the drastic increase in *CRR* due to *b* increase is suppressed, showing the dominant effect of α. When α = 30°, increasing *b* still increases *CRR*, even though the increase is not nearly close the one observed when α = 0°. When α = 60°, the effect of *b* on *CRR* is completely diminished. These findings indicate that when α and *b* are increased simultaneously, the effect on *CRR* is mainly controlled by the magnitude of α.

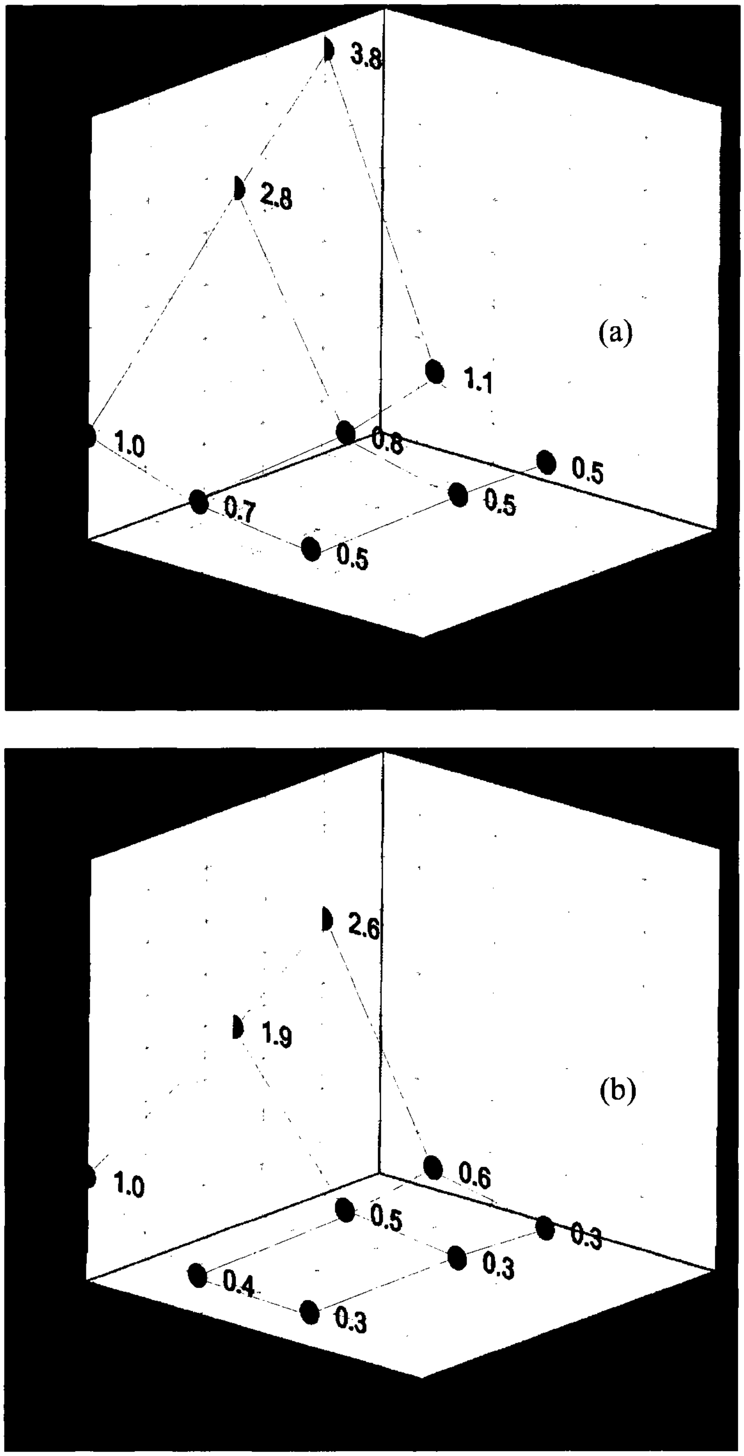

Figure 4.56. Normalized *CRR* as a function of α and b when (a) ε_q= 2.5 %, and (b) ε_q = 5.0 %.

Analyses of stresses induced in the soil elements by foundations (see Fig. 2.17), embankments (Zdravkovic and Jardine 2001), and slopes (Carraro 2009) show that both α and b are typically greater than zero prior to earthquake conditions. Therefore, liquefaction analyses for these cases require considering the effects of α and b together. Conducting a cyclic triaxial tests with $\alpha = 0°$ and $b = 0$ may not always provide a conservative estimate of liquefaction resistance as shown in Fig. 4.53. The effect of α is more drastic than b and when they are both greater than zero, the liquefaction resistance typically decreases compared to $\alpha = 0°$ and $b = 0$ case due to the effect of α. Therefore, b in the range of 0.3 – 0.5 that approximates the plane strain conditions may not provide stronger liquefaction resistance, and the effect of α also should be considered to accurately evaluate the liquefaction resistance and avoid unconservative designs.

5. SUMMARY AND CONCLUSIONS

The effects of drained principal stress rotation and intermediate principal stress coefficient changes on the (1) drained static stress-strain response and (2) undrained cyclic stress-strain response and liquefaction resistance of slurry-deposited clean and NP silty Ottawa sands reconstituted in the laboratory were analyzed in this study using a state-of-the-art dynamic hollow cylinder (HC) apparatus. The main research findings are summarized below.

5.1. SPECIMEN RECONSTITUTION METHOD

In this research, the slurry deposition (SD) method outlined by Carraro and Prezzi (2008) for solid triaxial test specimens was modified to allow reconstitution of HC sand specimens with or without NP silt formed underwater. The uniformity of the reconstituted specimens was studied in terms of both D_R and FC variations across the HC specimen height using a new density gradient mold developed during this study. The maximum local D_R deviations from the average global D_R were about 6 % and 7 % for clean sand (average D_R between 25 % and 35%) and NP silty sand (average D_R between 29 % and 30%) specimens, respectively. The maximum local FC deviation from the average global FC was 0.7 % for the NP silty sand specimens tested. These variations are as good as (or better) than the variations obtained for similar reconstitution methods typically used for solid triaxial specimens (Kuerbis and Vaid 1998, Vaid et al. 1999, Ghionna and Porcino 2006). Additionally, the proposed method allows reconstitution of HC specimens with initial Skempton's pore pressure coefficient B higher than 0.5, thus facilitating back pressure (BP) saturation at BP levels that can be easily achieved in geotechnical laboratories.

5.2. DRAINED RESPONSE OF CLEAN AND NP SILTY OTTAWA SANDS

Slurry-deposited and BP saturated HC specimens of clean and NP silty Ottawa sands were subjected to anisotropic consolidation under nearly K_0 conditions. Then, the major principal stress direction α and/or intermediate principal stress coefficient b were increased to their target values under drained conditions at constant mean effective stress p' and octahedral deviator stress q. The selected values of α used in this study were 0°, 30° or 60°, whereas the selected b values were 0, 0.5 or 0.8. The relative density of the clean and NP silty sands tested ranged between 41 % and 58 % and between 41 % and 66 %, respectively, at the end of drained loading. The average D_R values for all specimens tested were equal to 49 % and 53 % for the clean and NP silty sands, respectively. The FC of the NP silty Ottawa sand tested varied between 11 % and 16 %, with an average FC value of 14 %.

A trial and error procedure was used to determine the principal stress ratio K = 0.43 with which p' is increased to 100 kPa under approximately K_0 conditions (i.e., negligible radial and circumferential strains) during anisotropic consolidation. Anisotropic consolidation to p' = 100 kPa with K = 0.43 resulted in average radial and circumferential strains of 0.15 % and –0.12 %, respectively, for the clean Ottawa sand, and –0.10 % and –0.20 %, respectively, for the NP silty Ottawa sand. The average volumetric strain ε_p at the end of anisotropic consolidation was 0.41 % and 0.61 % for clean and NP silty Ottawa sands, respectively. The stress strain response during anisotropic consolidation is remarkably repeatable for the forty eight HC specimens reconstituted with the proposed method, with most deviatoric strain ε_q values obtained at the end of consolidation ranging from 0.3 % to 0.5 % and 0.9 % to 1.2 % for the clean and NP silty sand specimens, respectively.

Following K_0 consolidation, α and/or b changes were imposed to the HC specimens at constant p' and q under drained conditions. The largest strain component during drained α rotation was the shear strain, as expected. When α was increased to 30° under drained conditions, the shear strain observed was between 1.2 % and 1.6 % for the clean sand, and around 0.9 % for the NP silty sand tested. During additional α increases to 60°, the clean sands experienced shear strains between 2.6 % and 4.8 %, whereas the NP silty sands experienced shear strains between 1.9 % and 2.4 %. Even at constant p' and q, clean and NP silty sands experienced shear strains as large as 2.4% and 4.8 %, respectively, which were solely due to drained principal stress rotation. The largest measured volumetric strain was about 0.6 % for both clean and NP silty sands when α was increased to 30°. Further increase of α to 60° induced maximum volumetric strains of about 0.5 % for the NP silty sand, and 0.6 % for the clean sand.

The largest strain component induced during drained b increase was the radial strain, which may be due to the fact that the intermediate principal stress is equal to the radial stress in HC boundary conditions. Increase in b resulted in larger radial strain (compared to other strain components) development, as expected. However, even when b = 0.8, the maximum radial strain measured was 0.5 % for clean sand and 0.6 % for NP silty sand.

The largest volumetric strain observed during b increase to 0.8 was 0.3 % for both clean NP silty sands. The shear strains induced during b increases were not as large as the shear strains induced during drained principal stress rotation since $\tau_{z\theta}$ is approximately equal to zero during b changes.

During simultaneous increase of both α and b under drained conditions, the shear strain induced in clean sand specimens was larger than any other strain component. This suggests that the shear stresses required to increase α are the primary stress components controlling the largest deformations during this stage, regardless whether b was increased simultaneously with α or not. Induced volumetric strains in clean sand due to increase in α and b did not exceed 1 % for any combination considered, and the effect of increasing α from 30° to 60° or changing b from 0.5 to 0.8 did not significantly impact the amount of volumetric strain experienced by the clean sand specimens.

The drained increase in α and/or b at constant p' and q was shown to induce strains as large as those induced during anisotropic consolidation. Even though the systematic drained analysis conducted during the tests may not be directly related to stress changes experienced by soil elements in the field, which may in some cases involve simultaneous changes of α, b, q and p', the results of this research demonstrate how relevant the effect of changing only α or b may be to the drained behavior of alluvial sand deposits formed under water.

5.3 UNDRAINED CYCLIC RESPONSE OF OTTAWA SAND WITH AND WITHOUT NP SILT

Undrained instability (UI) was observed in many of the tests conducted in this study. Increases in both CSR and α increased the likelihood of UI, whereas increases in b and

D_R led to more stable responses by reducing the likelihood of UI. Most of the specimens that experienced UI exhibited a strain response that resembled limited flow liquefaction followed by cyclic mobility, instead of classical flow liquefaction response. However, for very low levels of *CSR*, UI did not take place and both the strain and excess pore pressure responses of the soil were in accordance with cyclic mobility. For the boundary conditions applied and the D_R range studied, none of the clean sand specimens experienced full liquefaction ($p' = 0$). On the other hand, some NP silty Ottawa sand specimens experienced UI, developing very large deformations that were not followed by a subsequent, steady strain build up.

Strain responses mobilized for both sands under similar *CSR* and $\alpha = 0°$ and $b = 0$ showed that the NP silty sands exhibited a weaker response than their clean sand counterparts. Regardless of the strain component considered, the typical deformation pattern during undrained cyclic loading with $\alpha = 0°$ and $b = 0$ resembled that induced during UI with limited flow liquefaction followed by cyclic mobility for $CSR \geq 0.14$ for clean sand and for $CSR \geq 0.20$ for NP silty sand. When the *CSR* is as low as 0.10, the typical deformation pattern observed was in accordance with cyclic mobility.

During undrained cyclic loading with $\alpha = 0°$ and b = 0, NP silty Ottawa sand has a higher, similar, or lower liquefaction resistance than clean sand if the selected strain-based liquefaction criterion is $\varepsilon_q = 2.5$ %, $\varepsilon_q = 5.0$ % or $\varepsilon_q = 8.75$ %, respectively. Previous studies carried out with undrained cyclic triaxial tests on isotropically consolidated clean and NP silty Ottawa sand (Carraro et al. 2003, Carraro 2004) have shown that for the conventional liquefaction criterion of $\varepsilon_z = 5.0$ % (or $\varepsilon_q = 8.75$ %), the clean Ottawa sand has higher liquefaction resistance than NP silty Ottawa sand for the

FC range considered. Therefore, the findings in this study for the case of $\alpha = 0°$ and $b = 0$ are in agreement with other previous studies established for axisymmetric loading using conventional triaxial protocols. Nevertheless, the liquefaction criterion selected in analyses of liquefaction potential may result in significantly different conclusions, and, thus, should be selected with caution for conditions that diverge from simple axisymmetry.

Increasing α from 0° to 30° at $b = 0$ significantly reduces the liquefaction resistance of clean Ottawa sand for all three liquefaction criteria used. However, the reduction is more pronounced (80 % reduction in *CRR*) if the conventional, axisymmetric liquefaction criterion $\varepsilon_q = 8.75$ % is used. The liquefaction resistance of NP silty Ottawa sand also is reduced by the increase in α from 0° to 30°. The reduction in the liquefaction resistance of NP silty Ottawa sand (20 % reduction in *CRR* when the liquefaction criterion is $\varepsilon_q = 8.75$ %) is not as significant as the reduction in the liquefaction resistance of clean Ottawa sand when α is increased from 0° to 30°. Increasing α from 30° to 60° induces further reduction in the liquefaction resistance of clean sand, yet this reduction is not as pronounced as the reduction observed when α is increased initially from 0° to 30°. Increasing α from 30° to 60° also does not cause large additional reduction in the liquefaction resistance of the NP silty sand. In summary, as the major principal stress rotates from the vertical to the horizontal direction, the sand exhibits a weaker undrained cyclic response. However, the effect of principal stress rotation appears to be less significant if the Ottawa sand contains NP silt (with *FC* = 11 - 15%). This may be attributed to the change in the fabric of the clean sand imparted by the addition of NP silt.

Increases in b from 0 to 0.5 or 0.8 when $\alpha = 0°$ resulted in higher liquefaction resistances for both clean and NP silty Ottawa sands regardless of the liquefaction criterion used. The amount of *CRR* increase seems to depend to a large extent upon the selected liquefaction criterion in the case of the clean Ottawa sand specimens tested. Conversely, the amount of *CRR* increase was not impacted by the liquefaction criterion for the NP silty sand. Increase in b from 0 to 0.5 increases the *CRR* of clean Ottawa sand by 1.5 to 2.9 times, and by 1.5 to 1.6 times for the NP silty sand tested. Further b increases to 0.8 raises the *CRR* of the clean and NP silty Ottawa sands by 2.0 to 3.8 times and by 2.4 to 2.7 times compared to that of $b = 0$ case, respectively. These findings suggest that the approximately plane strain conditions imparted during b changes (with $b = 0.3 - 0.5$) produce higher liquefaction resistance than axisymmetrical conditions with $b = 0$. In other words, undrained cyclic triaxial test may yield conservative liquefaction resistances for situations when the intermediate principal stress is between the major and minor principal stresses. However, this was found to be true only when $\alpha = 0°$.

For the clean Ottawa sand tested, the *CRR* decreases significantly when α is increased from 0° to 60°, regardless of b. Additionally, for all b, the reduction in the *CRR* ratio (defined as the ratio of the *CRR* for the α and b combination considered to the *CRR* for $\alpha = 0°$ and $b = 0$ case) is more pronounced when α is increased from 0° to 30°, compared to α increase from 30° to 60°. Increases in b do increase the *CRR* when $\alpha = 0°$, but the strengthening effect of b on the *CRR* of the sand is significantly suppressed when $\alpha > 0°$. For clean Ottawa sand, the undrained cyclic response is controlled primarily by the magnitude of α when both α and b are greater than zero. Since most geotechnical analyses (e.g. embankments, foundations, slopes etc.) involve stress states where both α

and b may be different than zero, appropriate evaluation of liquefaction potential requires consideration of both α and b, even though the major controlling mechanism might be associated with the mechanical response imparted by the drained rotation of the principal stresses.

6. SUGGESTIONS FOR FUTURE STUDIES

The effect of α or b on the undrained cyclic response of both clean and NP silty Ottawa sand was evaluated separately in this study. The combined effect of $\alpha > 0°$ and $b > 0$ on the liquefaction resistance was studied for only the clean Ottawa sand specimens, since undrained cyclic response of clean sand specimens was impacted more by the changes in α or b compared to that of NP silty sand. However, conducting more undrained cyclic tests with $\alpha > 0°$ and $b > 0$ on the NP silty sand is desirable for the complete understanding of the behavior for two separate sands.

The scope of this study was limited to the cyclic behavior of clean and NP silty Ottawa sands under generalized stress conditions. For a more complete characterization of the undrained instability behavior observed during undrained cyclic loading, monotonic undrained tests for the same generalized stress state variables (α, b, p\` and q) may be conducted. This would allow forming boundary surfaces for the monotonic or cyclic behavior of the sands tested. However, the number of tests required to achieve this task would be well beyond the time allocated for this study.

In this study, the amount of fines in the sand was limited to average of 14 %. Given the less anisotropic fabric observed for NP silty sand, more research may be needed to find the correlation between the anisotropy in undrained cyclic behavior and fines content of Ottawa sand.

A new specimen preparation technique for the reconstitution of sand specimens with fines was developed and evaluated in this study. The application of this method was limited to clean sands and clean sands with non-plastic fines. In a future study, this specimen reconstitution technique can be used to prepare sand specimens with plastic fines, and investigate the monotonic and/or cyclic behavior of these soils under generalized stress conditions.

It is well-know that the relative density impacts the cyclic behavior of sands with or without fines (Polito and Martin, 2002). However, the relative density depends on the methods to determine the limiting void ratios. In this study, the relative densities were determined based on ASTM limiting void ratios to compare the results with the previously published results. However, as shown in this study, the maximum void ratio determination may be more realistic if the slurry deposition based method as proposed by Carraro and Prezzi (2008) is used. The change in the resulting maximum void ratio can influence the relative density by as much as 20 %. Therefore, further development and standardization of the slurry deposition based method to determine the maximum void ratio for sand specimens with fines may be necessary.

7. REFERENCES

Abelev, A.V., Lade, P.V. (2004) "Characterization of Failure in Cross-Anisotropic Soils" *Journal of Engineering Mechanics*, 130(5), 599-606.

Alarcon, A., Chameau, J.L., Leonards, G.A. (1986) "A New Apparatus for Investigating the Stress-Strain Characteristics of Sands" *Geotechnical Testing Journal*, 9(4), 204-212.

Alarcon-Guzman, A., Leonards, G.A., and Chameau, J.L. (1988). "Undrained Monotonic and Cyclic Strength of Sands." *Journal of Geotechnical Engineering*, 114(10), 1089-1109.

Al-Hussaini, M. (1981) "Tensile Properties of Compacted Soils" *Laboratory Shear Strength of Soil, ASTM STP 740, ASCE*, Philadelphia, 207-225.

Altun S., Goktepe, A.B., Akguner, C. (2005). "Cyclic Shear Strength of Silts and Sands Under Cyclic Loading", *Geotechnical Special Publication, n 130-142, Geo-Frontiers 2005*, 1365-1375.

Anderson, W.F., Pyrah, I.C., Pang, L.S., Ali, F.H. (1988) "The Time Dependent Behavior of Normally Consolidated Clay in Thick Hollow Cylinder Tests" *Proceedings, International Conference on Rheology and Soil Mechanics*, Coventry, England, 204-218.

Arnold, M., Mitchell, P.W. (1973) "Sand Deformation in Three-Dimensional Stress State" *Proceeedings, Eighth International Conference on Soil Mechanics and Foundation Engineering*, 1, 11-18.

Arthur, J.R.F, Chua, K.S., Dunstan, T. (1977) "Induced Anisotropy in a Sand" *Geotechnique*, 27(1), 13-30.

Arthur, J.R.F., Chua, K.S., Dunstan, T., Del C., J.I.R (1980). "Principal Stress Rotation: A Missing Parameter", *Journal of the Geotechnical Engineering Division, Proc., ASCE*, 106 (GT4), 419-433

Barden, L., Proctor, D.C. (1971) "The Drained Strength of Granular Material" *Canadian Geotechnical Journal*, 8, 372-383.

Bhatia, S.K., Schwab, J., Finn, W.D.L. (1985). "Influence of Static Shear Stress on the Cyclic Volume Change Behavior of Ottowa Sand.", *Soil Dynamics and Earthquake Engineering, Proceedings of the 2nd International Conference*, Computational Mechanics Ltd, 2.17-2.26

Bhatia, S.K., Scwhab, J., Ishibashi, I. (1985) "Cyclic Simple Shear, Torsional Shear And Triaxial - A Comparative Study" *Advances in the Art of Testing Soils Under Cyclic*

Conditions. Proceedings of a session held in conjunction with the ASCE Convention., Detroit, MI, 232-254.

Bishop, A.W., Green, G.E., Garga, V.K., Andresen, A. and Brown, J.D. (1971) "A New Ring Shear Apparatus and Its Application to the Measurement of Residual Strength" *Geotechnique*, 21(4), 273-328.

Bjerrum, L., Landva, A. (1966) " Direct Simple Shear Tests on Norwegian Quick Clay", *Norges Geotechniske Institutt – Publikasjon; Publication*, n70, 1-20.

Bolton, M.D. (1986) "Strength and Dilatancy of Sands" *Geotechnique*, 36(1), 65-78.

Boulanger, R.W., Seed, R.B. (1995) "Liquefaction of Sand Under Bidirectional Monotonic and Cyclic Loading", Journal of Geotechnical Engineering, 121(12), 870-878

Broms, B.B., Casbarian, A.O (1965) "Effects of Rotation of The Principal Stress Axes and of the Intermediate Principal Stress on the Shear Strength" *Proceedings, Sixth International Conference on Soil Mechanics and Foundation Engineering*, 1, 179-183.

Broms, B.B., Jamal, A.K. (1965) "Analysis of the Triaxial Test-Cohesionless Soils" *Proceedings, Sixth International Conference on Soil Mechanics and Foundation Engineering*, 1, 184-188.

Broms, B.B., Ratnam, M.V. (1963) "Shear Strength of an Anisotropically Consolidated Clay", *Journal of the Soil Mechanics and Foundations Division,* ASCE, 89(SM6), 1-25.

Brown, S.F., Richardson, I.R. (2004). "A Hollow Cylinder Apparatus to Study the Cyclic Loading Behavior of Dry Granular Material", *Advances in Geotechnical Engineering: The Skempton Conference, 2004, Thomas Telford, London*, 369-380

Budhu, M, Britto, A. (1987) " Numerical Analysis of Soils in Simple Shear Devices" *Soils and Foundations*, 27(2), 31-41.

Budhu, M. (1988) "New Simple Shear Apparatus" *Geotechnical Testing Journal*, 11(4), 281-287.

Budhu, M., Arul, B. (1987) "Numerical Analysis of Soils in Simple Shear Devices" *Soils and Foundations*, 27(2), 31-41.

Carraro, J.A.H. (2004) "Mechanical Behavior of Silty and Clayey Sands" PhD Thesis, Purdue University, West Lafayette.

Carraro, J.A.H., Prezzi, M. (2008) "A New Slurry –Based Method of Preparation of Specimens of Sand Containing Fines" *Geotechnical Testing Journal*, 31(1), 1-11.

Casagrande, A. and N. Carillo (1944) "Shear failure of Anisotropic Materials" *Proeedings Boston Soc.. Civil Eng. 31,*74-87.

Casagrande, A (1971) "On Liquefaction Phenomena" *Geotechnique*, 21(3), 197-202

Castro, G. (1975) "Liquefaction and Cyclic Mobility of Saturated Sands", *American Society of Civil Engineers, Journal of Geotechnical Engineering Division*, 101(6), 551-569.

Castro, G., and Poulos, S.J. (1977). "Factors Affecting Liquefaction and Cyclic Mobility." *American Society of Civil Engineers, Journal of the Geotechnical Engineering Division*, 103(6), 501-516.

Chaudhary, S.K., Kuwano, J., Hashimoto, S., Hayano, Y., Nakamura, Y. (2002) "Effects of Initial Fabric and Shearing Direction on Cyclic Deformation Characteristics of Sand" *Soils and Foundations*, 42(1), 147-157.

Chen, J.W. (1988) "Stress Path Effect on Static and Cyclic Behavior of Monterey No. 0/30 Sand" PhD Thesis, University of Colorado, Boulder, CO.

Cheng, R.Y.K. (1981) "Effect of Shearing Strain-Rate on the Undrained Strength of Clay" *Laboratory Shear Strength of Soil, ASTM STP 740, ASCE*, Philadelphia, 243-253.

Cooling, L.F., Smith, D.B. (1936) "The Shearing Resistance of Soils" *Journal of the Institution of Civil Engineers, London*, 3, 333-343

Donaghe, R.T., Gilbert, P.A. (1983) "Cyclic Rotation of Principal Planes to Investigate Liquefaction of Sands" Miscellaneous Paper GL-83-24, US Army Engineer Waterways Experiment Station, Vicksburg, MS.

Drnevich, V.P. (1972) "Undrained Cyclic Shear of Saturated Sand" *Journal of the Soil Mechanics and Foundations Division, ASCE*, 98(SM8), 807-825.

Dusseault, M.B. (1981) "A Versatile Hollow Cylinder Triaxial Device" *Canadian Geotechnial Journal*, 18, 1-7.

Emery, J.J., Finn, W.D.L., Lee, K.W. (1972) "Uniformity of Saturated Sand Specimens" *Evaluation of Relative Density and its Role in Geotechnical Projects Involving Cohesionless Soils,* ASTM Special Technical Publication (STP) 523, 182-194

Esrig, M.I., Bemben, S.M. (1965) "Discussion on Session 2, Division 2" *Proceedings, Sixth International Conference on Soil Mechanics and Foundation Engineering*, 3, 321-323.

Frydman, S., Alpan, I., Zeitlan, J.G.(1971) "Stress-Deformation Behavior of Sand Studied in Hollow Cylinder and Triaxial Apparatus" *Proceedings, Fourth Asian Regional Conference on Soil Mechanics and Foundation Engineering, Bangkok,* 1, 17-23.

Fukushima, S. and Tatsuoka, F. (1982) "Deformation and Strength of Sand in Torsional Simple Shear" *Proceedings, IUTAM Conference on Deformation and Failure of Granular Materials, Delft*, 371-379.

Geuze, E.C.W., Kie, T.T. (1953) " The Mechanical Behavior of Clays" *Proceedings, Second International Congress on Rheology*, Oxford, England, 247-259.

Ghionna, V.N., Porcino, D. (2006). "Liquefaction Resistance of Undisturbed and Reconstituted Samples of a Natural Coarse Sand from Undrained Cyclic Triaxial Tests", *Journal of Geotechnical and Geoenvironmental Engineering*, 132 (2), 194-202

Haythornthwaite, R.M. (1960) "Stress and Strain In Soils" *Proceedings, Second Symposium on Naval Structural Mechanics, Brown University, Rhode Island*, 185-193.

Hight, D.W., Gens, A., Symes, M.J. (1983). "The Development of a New Hollow Cylinder Apparatus for Investigating the Effects of Principal Stress Rotation in Soils", *Geotechnique*, 33 (4), 355-383

Hoeg, K., Dyvik, R., Sandbaekken, G. (2000). "Strength of Undistrubed versus Reconstituted Silt and and Silty Sand Specimens", *Journal of Geotechnical and Geoenvironmental Engineering*, 126 (7), 606-617

Ishibashi, I., Kawamura, M., Bhatia, S.K. (1985) "Torsional Simple Shear Apparatus for Drained and Undrained Cyclic Testing" *Advances in the Art of Testing Soils Under Cyclic Conditions*, Proceedings of a Session Sponsored by the Geotechnical Engineering Division in Conjunction with the ASCE Convention in Detroit, Michigan, October, ed. Vijay Khosla, 51-73.

Ishibashi, I., Sherif, M.A. (1974) "Soil Liquefaction by Torsional Simple Shear Device" *Journal of Geotechnical Engineering Division, ASCE*, 100 (GT8), 871-888.

Ishibashi, I., Sherif, M.A. (1974). "Soil Liquefaction by Torsional Simple Shear Device", *Journal of the Geotechnical Engineering Division, Proc., ASCE.,* 100 (GT8), 871-888

Ishihara, K., Tatsuoka, F., and Yasuda, S. (1975). "Undrained Deformation and Liquefaction of Sand Under Cyclic Stresses." *Soils and Foundations*, 15(1), 29-44.

Ishihara, K., Towhata, I. (1983) "Sand Response to Cyclic Rotation of Principal Stress Directions as Induced by Wave Loads" *Soils and Foundations*, 23(4), 11-26.

Ishihara, K., Yamazaki, A. (1984). "Analysis of Wave-Induced Liquefaction in Seabed Deposits of Sand", *Soils and Foundations*, 24 (3), 85-100

Ishihara, K., Yamazaki, A., Haga, K. (1985) "Liquefaction of K_0-Consolidated Sand Under Cyclic Rotation of Principal Stress Direction with Lateral Constraint." *Soils and Foundations*, 25(4), 63-74.

Ishihara, K., Yasuda, S. (1975) "Sand Liquefaction in Hollow Cyclinder Torsiona Under Irregular Excitation" *Soils and Foundations*, 15(1), 45-59.

Ishihara, K., Yasuda, S. (1975) "Sand Liquefaction in Hollow Cylinder Torsion Under Irregular Excitation." *Soils and Foundations*, 15(1), 45-59.

Kirkpatrick, W.M. (1957) "The Condition of Failure for Sands" *Proceedings, Fourth International Conference on Soil Mechanics and Foundation Engineering*, 1, 172-178

Koester, J.P. (1992). "Cyclic Strength and Pore Pressure Generation Characteristics of Fine-Grained Soils", PhD Thesis, University of Colorado, USA

Kramer, S.L. (1996). *Geotechnical Earthquake Engineering*, Prentice Hall, Upper Saddle River, New Jersey.

Kuerbis, R., Vaid, Y.P. (1988). "Sand Sample Preparation - The Slurry Deposition Method", *Soils and Foundations*, 28(4), 107-118.

Ladd, C.C. (1991) "Stability Evaluation During Staged Construction" *Journal of Geotechnical Engineering*, 117(4), 540-615.

Lade, P.V. (1975) " Torsion Shear Tests on Cohesionless Soil" *Proceedings, Fifth Pan-American Conference on Soil Mechanics and Foundation Engineering*, 1, 117-127.

Lade, P.V. (1981) "Torsion Shear Apparatus for Soil Testing" *Laboratory Shear Strength of Soil, ASTM STP 740, ASCE*, Philedelphia, 145-163.

Lee, K.L., Seed, H.B. (1967) "Cyclic Stress Conditions Causing Liquefaction of Sand", *American Society of Civil Engineers Proceedings, Journal of the Soil Mechanics and Foundations Division*, 93(SM1), 47-70.

Lomise, G.M., Kryzhanovsky, A.L., Vorontsov, E.I. and Goldin, A.L. (1969) "Study on Deformation and Strength of Soils Under Three-Dimensional State of Stress" *Proceedings, Seventh International Conference on Soil Mechanics and Foundation Engineering*, 1, 257-265.

Macky, T.A., Saada, A.S. (1984) "Dynamics of Anisotropic Clays Under Large Strains" *Journal of Geotechnical Engineering*, 110(4), 487-504.
Material." *Soils and Foundations*, 12(1), 17-36.

Miura, K., Miura, S., Toki, S. (1986) "Deformation Behavior of Anisotropic Dense Sand Under Principal Stress Axes Rotation", Soils and Foundation, Vol.26, No.1, pp 36-52.

Miura, S., Toki, S. (1982) "Sample Preparation Method and its Effect on Static and Cyclic Deformation - Strength Properties of Sand" *Soils and Foundations*, 22(1), 61-77.

Mohamad, R., and Dobry, R. (1986). "Undrained Monotonic and Triaxial Strength of Sand" *Journal of Geotechnical Engineering*, 112(10), 941-958

Mulilis, P.J., Seed, B.H., Chan, C.K., Mitchell, J.K., Arulanandan, K. (1977). "Effects of Sample Preparation on Sand Liquefaction", *Journal of the Geotechnical Division*, 103 (GT2), 91-108

Murthy, T.G., Loukidis, D., Carraro, J.A.H., Prezzi, M., Salgado, R. (2007) "Undrained Monotonic Response of Clean and Silty Sands" *Geotechnique*, 57(3), 273-288

Naughton, P.J., O'Kelly, B.C. (2004). "The Induced Anisotropy of Leighton Buzzard Sand", *Advances in Geotechnical Engineering: The Skempton Conference, 2004, Thomas Telford, London*, 556-567

Naughton, P.J., O'Kelly, B.C. (2007) "Stress Non-uniformity in a Hollow Cylinder Torsional Sand Specimen", *Geomechanics and Geoengineering*, 2(2), 117-122.

Norton, F.H. (1938) "An instrument for Measuring Workability of Clays" *Journal of American Ceramic Society*, 21, 33-36

O'Kelly, B.C., Naughton, P.J. (2005). "Development of a New Hollow Cylinder Apparatus for Stress Path Measurements over a Wide Strain Range", *Geotechnical Testing Journal*, 28(4), 345-354.

Oda, M. (1972). "Initial Fabrics and Their Relations to Mechanical Properties of Granular

Oda, M. (1993) "Inherent and Induced Anisotropy in Plasticity Theory of Granular Soils", Mechanics of Granular Materials, Vol.16, No.1-2, pp35-45

Peacock, W.H., Seed, H.B. (1968). "Sand Liquefaction Under Cyclic Loading Simple Shear Conditions". *Journal of the Soil Mechanics and Foundations Division Proceedings of the American Society of Civil Engineers*, SM3, 689-708

Prevost, J., Hoeg, K. (1976) "Reanalysis of Simple Shear Soil Testing" *Canadian Geotechnical Journal*, 13(4), 418-429.

Rolo, R. (2003). "The anisotropic stress-strain-strength behaviour of brittle sediments", PhD Dissertation, University of London, Imperial College of Science, England

Roscoe, K.H. (1953) "An Apparatus for the Application of Simple Shear to Soil Samples" *Proceedings of 3rd International Conference on Soil Mechanics and Foundation Engineering,* 1, 186-191.

Saada, A.S., "Hollow Cylinder Torsional Devices: Their Advantages and Limitations", Advanced Triaxial Testing of Soil and Rock, ASTM STP 977, Robert T. Donaghe, Ronald C. Chaney, and Marshall L. Silver, Eds., American Society for Testing and Materials, Philadelphia, 1988, pp 766-795.

Saada, A.S., Baah, A.K. (1967) "Deformation and Failure of a Cross Anisotropic Clay Under Combine Stress" *Proceedings, Third Pan American Conference on Soil Mechanics and Foundation Engineering,* 1, 67-88.

Saada, A.S., Shook, L.P. (1981) "Behavior of Clays Subjected to Slow Cyclic Loading and Large Strains" *Proceedings, International Conference on Recent Advances in Geotechnical Earthquake Engineering and Soil Dynamics,* St.Louis, 1, 369-376.

Sayao, A., Vaid, Y.P. (1991). "A Critical Assessment of Stress Nonuniformities in Hollow Cylinder Test Specimens", *Soils and Foundations*, 31(1), 60-72.

Sayao, A.S.F., Vaid, Y.P. (1989) " Deformations due to Principal Stress Rotation" *Proceedings of the International Conference on Soil Mechanics and Foundation Engineering*, 1, 107-110.

Seed, H.B., Lee, K. (1966). "Liquefaction of Saturated Sands During Cyclic Loading." *Journal of Soil Mechanics and Foundation Division*, 92(SM6), 105-134.

Seed, H.B., Peacock, W.H. (1971) "Test Procedures for Soil Liquefaction Characteristics" *ASCE Journal of Soil Mechanics Foundations Division*, 97(SM8), 1099-1119.

Shibuya, T., Hight, D.W., Jardine, R.J. (2003) "Four-dimensional Local Boundary Surfaces of an Isotropically Consolidated Loose Sand" *Soils and Foundations*, 43(2), 89-103.

Skempton, A.W. (1954) "Pore-pressure Coefficients A and B", *Geotechnique*, 4(4), 143-147.

Sivathayalan, S., Vaid, Y.P. (2002). "Influence of Generalized Initial State and Principal Stress Rotation on the Undrained Response of Sands", *Canadian Geotechnical Journal*, 39, 63-76.

Sture, S., Budiman, J.S., Ontuna, A.K., Ko, H. (1987) "Directional Shear Cell Experiments on a Dry Cohesionless Soil" *Geotechnical Testing Journal*, 10(2), 71-79.

Suklje, L., Drnovsek, J. (1965) "Investigation of the Tensile Deformability of Soils Using Hollow Cylinders" *Proceedings, Sixth International Conference on Soil Mechanics and Foundation Engineering*, 1, 368-372.

Symes, M.J., Gens, A., Hight, D.W., (1984) "Undrained Anisotropy and Principal Stress Rotation in Saturated Sand" *Geotechnique*, 34(1), 11-27.

Symes, M.J., Hight, D.W., Gens, A. (1982) "Investigating Anisotropy and the Effects of Principal Stress Rotation and of the Intermediate Principal Stress Using a Hollow Cylinder Apparatus" *Proceedings, IUTAM Conference on Deformation and Failure of Granular Materials, Delft*, 441-449.

Talesnick, M., Frydman, S. (1991) "Simple Shear of an Undisturbed Soft Marine Clay in NGI and Torsional Shear Equipment" *Geotechnical testing Journal*, 14(2), 180-194.

Tatsuoka, F., Muramatsu, M., Sasaki, T. (1982) "Cyclic Undrained Stress-Strain Behavior of Dense Sand by Torsional Simple Shear Test" *Soils and Foundations*, 22(2), 55-70.

Tatsuoka, F., Ochi, K., Fujii, S. (1984) "Effect of Sample Preparation Method on Cyclic Undrained Strength of Sand In Triaxial and Torsional Shear Tests" *Bulleting of Earthquake Resistant Structure Research Center*, University of Tokyo, No.17, March, 29-62.

Tatsuoka, F., Ochi, K., Fujii, S., Okamoto, M. (1986). "Cyclic Undrained Triaxial and Torsional Shear Strength of Sands for Different Sample Preparation Methods", *Soils and Foundations*, 26(3), 23-41.

Tatsuoka, F., Sonoda, S., Hara, K., Fukushima, S., Pradhan, T.B.S.(1986a) "Failure and Deformation of Sand in Torsional Shear" *Soils and Foundations*, 26(4), 79-97.

Towhata, I., Ishihara, K. (1985) "Undrained Strength of Sand Undergoing Cyclic Rotation of Principal Stress Axes" *Soils and Foundations*, 25 (2), 135-147.

Tseng, R.J.Y. (1974) "A Study of Liquefaction of Sand By Torsion Shear Test" PhD Thesis, University of Kentucky, Lexington, Kentucky, USA.

Uthayakumar, M., Vaid, Y.P. (1998) "Static Liquefaction of Sands Under Multiaxial Loading" *Canadian Geotechnical Engineering*, 35(2), 273-283.

Vaid, Y.P., and Chern, J.C. (1985). "Cyclic and Monotonic Undrained Response of Saturated Sands." Advances in the Art of Testing Soils Under Cyclic Conditions. Proceedings of a session held in conjunction with the ASCE Convention., Detroit, MI, Engl, 120-147.

Vaid, Y.P., Sayao, A. (1995) "Proportional Loading Behavior of Sand under Multiaxial Stresses", *Soils and Foundations*, 35(3), 23-29.

Vaid, Y.P., Sayao, A., Hou, E., Negussey, D. (1990). "Generalized Stress-Path-Dependant Soil Behavior with a New Hollow Cylinder Torsional Apparatus", *Canadian Geotechnical Journal*, 27, 601-616.

Vaid, Y.P., Sivathayalan, S., Stedman, D. (1999). "Influence of Specimen-Reconstituting Method on the Undrained Response of Sand", *Geotechnical Testing Journal*, 22(3), 187-195.

Whitman, R.V., Luscher, U. (1962) "Basic Experiment into Soil-Structure Interaction" *Journal of the Soil Mechanics and Foundation Division*, ASCE, 88 (SM6), 135-168.

Wijecwickreme, D., Vaid, Y.P. (1991). "Stress Nonuniformities in Hollow Cylinder Torsional Specimens", *Geotechnical Testing Journal*, 14(4), 349-362.

Wu, T.H., Loh, A.K., Malvern, L.E. (1963) "Study of Failure Envelope of Soils" *Journal of the Soil Mechanics and Foundations Division,* ASCE, 89(SM1), 145-179.

Yamamuro, J.A., Wood, F.M. (2004). "Effect of Depositional Method on the Undrained Behavior and Microstructure of Sand with Silt", *Soil Dynamics and Earthquake Engineering*, 24, 751-760.

Yamashita, S., and Toki, S. (1993). "Effect of Fabric Anisotropy of Sand During Rotation of Principal Stress Directions." *Soils and Foundations*, 33(3), 92-104.

Zdravkovic, L (1996). "The stress-strain-strength anisotropy of a granular medium under general stress conditions" PhD Dissertation, University of London, Imperial College of Science, England.

Zdravkovic, L., Jardine, R.J, (1997) "Some Anisotropic Stiffness Characteristics of a Silt Under General Stress Conditions", *Geotechnique*, 47(3), 407-437.

Zdravkovic, L., Jardine, R.J, (2001) "The Effect on Anisotropy of Rotating the Principal Stress Axes During Consolidation", Geotechnique, Vol.51, No.1, 69-83.